University of Reading

Stimuli-Responsive Debondable Adhesives

A thesis submitted in part fulfilment of the degree of Doctor of Philosophy

Tahkur Singh Babra

School of Chemistry, Food and Pharmacy

Supervised by Dr Barnaby Greenland and Professor Wayne Hayes

Sponsored by AWE Plc.

June 2018

Declaration of Original Authorship

I confirm that the research described in this thesis is my own work and that the use of all materials from other sources has been properly and fully acknowledged.

Tahkur Singh Babra

Acknowledgements

First and foremost, I would like to offer my sincerest gratitude to my supervisors, Dr Barny Greenland and Professor Wayne Hayes for giving me this opportunity to carry out my project. Their help, support and guidance over the past four years during my PhD has been invaluable. I am especially thankful to Barny for the weekly meetings, the many hours of correcting my reports and papers, and the invaluable lessons with writing and presenting my work. I would not have got this far without either of you.

At AWE, I would like to thank Dr Colin Warriner and Dr Nick Bazin for their help and support. Special thank goes to Matthew Wood for taking the time to carry out mechanical testing with me and Dr Dario Castiglione for arranging funding. I am thankful to AWE Plc. and EPSRC for co-funding the PhD. I would like to thank Professor Clive Siviour, Akash Trivedi and Marzena Tkaczyk at the Univeristy of Oxford for their help with rheology analysis. A kind thanks goes to Professor Ian Hamley for arranging and helping with SAXS/WAXS analysis.

At the University of Reading, I would like to thank all of the staff members who have provided much help academically and personally over the past years. Specific thanks go to Dr Andrew Russell, Professor Howard Colquhoun, Professor Laurence Harwood, Dr Fred Davis, Dr John McKendrick, Dr Chris Smith and Dr Philippa Cranwell. The staff that keep the department going deserve my thanks, including Gez and Phil in Chemistry stores; Chris, George, Mohammed, Graham and Ben in the teaching labs; Cat Hale in Pharmacy teaching office; Radek, Nick and Pedro in the Chemical Analysis Facilities; Andy, Paul, Gary, Mark and Mike in the workshop; and our health and safety coordinator, Dr Rob Haigh.

I would like to offer my sincerest gratitude to my friends, who its been a pleasure to work, collaborate and socialise with over the past couple of years. Both past and present members of the Greenland, Hayes and Colquhoun groups deserve this gratitude, including Dr Antonio Feula, Dr Flavien Leroux, Dr Aaron Acton, Dr Lewis Hart, Dr Daniel Smith, Dr Ashfaq Afsar, Dr Kelly Melia, Dr Matt Parker, Dr Long Chen, Dr Kate Lim, Dr Mike Budd, Dr Clare Higgins, Dr Ben Baker, Dr Corinne McEwan, Priya Sonkar, Marcus Knappert, Sam Burholt, Sara Salimi, Alex Gavriel, and Adam O'Donnell. A kind thanks goes to my friends James Westwood, Charlotte Marriott, Gagan Singh, Laura Kane and Iain Hopkins. Special thanks go to Jessi Godleman and Hannah Bowden, who have provided me with so much laughter, friendship and support when I needed it most. Finally, I would especially like to thank my best friend and lab partner (even if we were in different labs), Oli Balmford. Whether its sharing our

crazy ideas or solving one another's problems or just having a nice chat over the many coffee and tea breaks, this PhD would not have been the same without you.

Finally, and most importantly, I would like to thank the three most important people in my life. My mum, dad and brother. To my mum and dad, thank you so much for everything you have given me. You have provided me with passion, perseverance, strength, support, and love that kept me going. This PhD could not have been done without either of you by my side. To my brother, Jasraj. Your continual provision of laughter and friendship has always kept me going. You are an excellent chemist, and I look forward to seeing you reach for the stars, to infinity and beyond.

Synopsis

Polymeric adhesives are becoming an increasingly important industrial product. They are routinely used in a wide range of high value and disposable products ranging from bonding large sections of the interior of new cars to wound dressings that replace stiches; from single use packaging to safety critical components in the aeronautical industry. Recently, the introduction of debondable adhesives that break down with an external stimulus has opened up new markets and applications in the adhesive industry. For the first time, components can be securely bonded for the working lifetime of the product, then disassembled on demand to allow for efficient recycling and disposal at the end of the product's usable life-cycle.

The objective of this study was to design and synthesise new, debondable polymeric adhesives that can breakdown or depolymerise in response to an external stimulus, such as chemicals, light or heat. This would ultimately lead to a new class of debond-on-demand adhesive. The work towards this goal is summarised below.

Chapter 2 reports the design, synthesis and evaluation of a fluoride degradable unit which can be incorporated within a linear polyurethane (PU) thermoplastic adhesive. Detailed solution state studies carried out by ^{1}H NMR spectroscopy and gel permeation chromatography before and after depolymerisation confirmed the efficient degradation of the material in response to the addition of fluoride ions. Mechanical strength testing on homogenous films together with rheometric and differential scanning calorimetry studies over multiple heat-cool cycles confirmed the reversibility of the supramolecular network within the PU. Lastly, adhesion testing with different material substrates before and after degradation showed the debond-on-demand nature of this novel material.

Chapter 3 further explores the use of the fluoride degradable unit within two series of linear polyurethanes that vary in chemical structure as part of efforts to increase the adhesive and thermal properties over the polyurethane reported in Chapter 2. The first series of adhesives explores the effect on bonding properties that varying nature of the diisocyanate linkers in the PU has on the adhesive. The second series of adhesives varies by the nature of the soft segment within the PU. It was found that introducing low-melting point crystalline regions into the material results in a polymer that can provide excellent adhesion at lower bonding temperatures (*ca*. 60 °C compared to 120 °C). The thermal response and morphology of the two series of polymers were analysed by variable temperature rheometric analysis, small angle x-ray spectroscopy and wide angle x-ray spectroscopy. Finally, the adhesives were tested at AWE

Aldermaston following international standards at different temperatures before and after degradation with a fluoride source.

Chapters 4 and 5 explore the possibility of producing a fluoride responsive crosslinked material using two different approaches. The first system was a variant of a reactive adhesive which was produced by mixing a trifunctional degradable group with a bis(isocyanate) terminated prepolymer (Chapter 4). Adhesion testing displayed a 28 % strength increase over the linear polymers, and a 55 % strength loss after treatment with fluoride ions. The second method explored the possibility of creating star polymers incorporating the degradable groups at the core. The resulting alcohol terminated branched polymer was then reacted with a commercially available aromatic diisocyanate to form a crosslinked adhesive. Adhesive testing was carried out before and after degradation with fluoride ions showed that fluoride ions could penetrate the crosslinked network resulting in a measurable reduction in bonding strength (approx. 23 %).

Finally, Chapter 6 reports the design and realisation of a novel UV responsive degradable group. Model compound studies were carried out before and after degradation with a UV light source (36 W) using ^{1}H NMR and UV/visible spectroscopies and showed rapid degradation after only 5 minutes irradiation. The UV group was incorporated into a polyurethane adhesive, which also showed rapid degradation in solution on exposure to UV light. The linear PU proved to be an excellent hot melt adhesive for glass substrates (bonds strength = 0.43 MPa), which weakened by up to 86 % after 5 minutes irradiation at 365 nm. However, the mechanism by which debonding occurs in the solid state in still an area of active investigation.

Abbreviations

4,4'-MDI	4,4'-methylene diphenyl diisocyanate
ASTM	American Society for Testing Materials
BDU	Bifunctional degradable unit
br	Broad
CFG	Chemoresponsive functional group
CLP	Crosslinked polymer
d	Doublet
Đ	Polydispersity Index
DMA	Dynamic Mechanical Analysis
DMF	*N,N'*-Dimethylformamide
DMSO-d_6	Dimethyl sulfoxide (deuterated)
DSC	Differential Scanning Calorimetry
DU	Degradable Unit
G' or E'	Storage Modulus
G'' or E''	Loss Modulus
GPC	Gel Permeation Chromatography
Hz	Hertz
IR	Infrared
K_a	Dissociation Constant
Krasol	Krasol HLBH-P 2000
λ	Wavelength
m	Multiplet
m.p.	Melting Point
MS	Mass Spectroscopy
M_n	Number average molecular weight
M_w	Weight average molecular weight
m/z	Mass/charge ratio
NMR	Nuclear magnetic resonance
ONB	*o*-Nitrobenzyl alcohol
ppm	Parts per million
PS	Poly(styrene)
PU	Polyurethane

PTFE	Poly(tetrafluoroethylene)
s	Singlet
SAXS	Small angle X-ray scattering
Stepanpol	Stepanpol PC-205P-30
t	Triplet
TBAB	*tetra*-butylammonium bromide
TBAC	*tetra*-butylammonium chloride
TBAF	*tetra*-butylammonium fluoride
TBAI	*tetra*-butylammonium Iodide
T_c	Crystallisation temperature
TDU	Trifunctional degradable unit
TGA	Thermal gravimetric analysis
T_g	Glass transition temperature
T_m	Melting Temperature
THF	Tetrahydrofuran
UPy	Ureido-pyrimidinone
UTS	Ultimate Tensile Strength
UV	Ultraviolet
UVDU	UV responsive degradable unit
VT	Variable temperature
WAXS	Wide angle X-ray Scattering

Contents

List of Figures

List of Schemes

Chapter 1

Introduction

Polymers make up a significant proportion of the materials that contribute toward modern society, from packaging to automotive vehicles, smart electronics to water purification, drug delivery systems to 2D and 3D printing, and from the clothing we wear daily to the body panels of commercial aeroplanes. This wide range of applications has been made possible by the development of polymers with new chemical structures, architectures and synthetic methods. This thesis focusses on the application of polymeric material as adhesives, which are required in each of the industries mentioned above. Over the past couple of decades, research into optimising polymeric adhesives resulted in different types of adhesives for many different situations. The most common types of adhesives include (i) hot-melt adhesives where adhesion occurs with the polymeric adhesive in the molten state; (ii) pressure sensitive adhesives which require a small amount of force to adhere the substrates; and (iii) reactive adhesives which requires a reaction to occur prior to adhesion. These types of adhesives are now explored in the following sections.

1.1. Adhesives: Commonly used Adhesives and Modes of Adhesion

Adhesives are the oldest of the four joining procedures, with the other three being nuts and bolts, welding and soldering; the latter processes only perfected in the industrial revolution in the 19th century.[1] In nearly all cases, adhesives will not damage or weaken the substrate during application, whereas the other methods of joining will. Different types and methods of applying adhesives have been developed in the past. The history, chemistry and engineering science of adhesives are covered in the accessible and comprehensive book "*Applied Adhesive Bonding: A Practical Guide for Flawless Results*" by Habenicht.[1] The types of adhesives that are most relevant to this project are detailed in the following sections, as well as the methods for mechanical testing used within this project.

1.1.1. Hot Melt Adhesives

Hot melt adhesives are traditional thermoplastics, which become viscous liquids when heated above their viscoelastic transition, the point where the material changes from the solid to liquid

state.[2] Upon cooling to room temperature, the adhesive sets as it solidifies to form the adhered bond. As this viscoelastic transition region is quite narrow, it can be difficult to apply the hot melt adhesive before it cools back to a solid. Therefore, adhesion of two substrates needs to be carried out quickly to avoid wasting the adhesive and damaging the substrate. Commonly, hot melt adhesives are applied at temperatures between 120 °C and 240 °C.[1,2] Different methods of applying hot melt adhesives have been developed to elongate the time that the adhesive is in the liquid state. A common example is seen with a hot glue gun where the adhesive is extruded through a hot nozzle in the melt above its melt point, providing the user with more time to adhere the substrates.[1] Other methods of application of hot melt adhesives include spray application[3,4] and the use of films.[5,6] Different polymer types of hot melt adhesives have been developed, including polyurethanes,[7–9] polyesters[10–12] and polyamides.[13,14]

There are major advantages of hot melt adhesives over pressure sensitive or reactive adhesives.[1] They are solvent free, so no toxic volatiles are released. Hot melt adhesives can be re-melted after adhesion for repair or decommission of the substrates. In comparison to reactive adhesives such as epoxy resins, hot melt adhesives are one-component materials reducing production costs. Finally, even though the short cool time can be a disadvantage, it does allow for rapid rates of adhesion of the substrates, hence increasing the rates of production in industrial applications.

1.1.2. Pressure Sensitive Adhesives

Commonly found on adhesive tapes and labels, these polymeric adhesives are tacky at ambient temperatures.[1,15] They require addition of pressure to ensure a strong adhesion to the substrate. With tapes and labels, the adhesive is either sprayed or rolled to form a continuous sublayer on the substrate (plastics or paper). The strength of the adhesive can be modified by the addition of resins or plasticisers to better suit the application.[16]

Some pressure sensitive adhesives allow for the removal from the substrate by peeling or gentle heating.[1] Most pressure sensitive adhesives do not leave a residue on one of the substrates after removal. For the pressure sensitive adhesives that do leave a residue, the residue can be easily removed with washing. Poly(alkyl acrylates) are commonly used at pressure sensitive adhesives, for example used in 3M's Post-it® Notes.[16–18]

1.1.3. Reactive Adhesives

Reactive adhesives require a reaction to occur prior to adhesion to occur. The reactants show no or little adhesion prior to mixing. Two types of reactive adhesives exist, (i) one-pot and (ii) two-pot reactive adhesives. One-pot adhesives require heat or moisture/air for curing, whereas two-pot adhesives require two physical chemicals for curing with the possible addition of heat.[1] Examples of one-pot reactive adhesives include epoxy resins,[19] polyurethanes,[20] siloxanes[21] and cyanoacrylates. Examples of two-pot adhesives include epoxy resins[19] (epoxy polymer and cross linking amine), polyurethanes[22] (isocyanate reacting with alcohol), siloxanes[21] (reaction with catalyst), and polyacrylates (reaction between alkyl acrylate and a hardening additive).[23] There are disadvantages to using reactive adhesives. Firstly, most of these types of adhesives contain toxic materials which are harmful and can be costly to dispose of if not used. Secondly, for two-pot reactive adhesives, a specific ratio of the two parts are required. If the wrong ratio is used when mixing, then the adhesive may not deliver its optimum performance. In most cases where reactive adhesives are used, a long duration (>6 hours)[1] of cure time may be required before the adhesive reaches its desired strength. Finally, most reactive adhesives form resins which are intractable crosslinked networks, and hence are not reversible by dissolution or melting without damaging the substrates. One major advantage to using reactive adhesives is that high temperatures (>100 °C) are not required which allows these adhesives to be used where the substrate is prone to damage by intense heating.[1] Gentle heating (30 – 40 °C) may be required to reduce curing times.

1.1.4. Solvent Based Adhesives

Adhesives can be transferred to the substrate using a solvent as a carrier. Traditionally, low boiling point (volatile) solvent were used, although there is a move towards using water based solvents to reduce the toxicity of the systems. Solvent based adhesives can be either in (i) a monomeric state, where a reaction must occur during solvent evaporation/removal or (ii) a polymeric state, where adhesion occurs during solvent evaporation/removal.[1] The most well-known example of a monomeric solvent based adhesive is Loctite® Super Glue™ which is based on cyanoacrylates dissolved in methyl ethyl ketone and where the monomers react with moisture in the environment to facilitate curing.[24] An example of polymeric solvent based adhesives is polyvinyl acetate, which is dissolved in water for bonding paper, card and woods.[25] A disadvantage of solvent based adhesives is that if the solvent evaporates in the container because of improper storage, then the adhesive cannot be used and must be disposed of. With

organic solvent based adhesives, most solvents are flammable and must be stored properly. Furthermore, upon evaporation of organic based adhesives, volatile organic compounds are released into the atmosphere which can be hazardous to health.[26] With water based adhesives, the bonding time can be quite long as evaporation of water is slow at ambient temperatures.

1.2. Supramolecular Polymers

Designing adhesives which allow for the efficient disassembly of substrates has been recently introduced into the field of adhesive research and development. This is becoming more important with the increasing shortage in natural materials such as rare metals which is drawing the need to recycle the substrate materials (e.g. electrical components in mobile phones). To facilitate disassembly of composite structures at the end of their life in order to obtain commercially important components for recycling, stimuli-responsive adhesives have been developed. These materials lose their adhesive properties when exposed to an external stimulus. The aspect of having a reversible adhesive that can debond from its substrates with a stimulus is advantageous but including a non-reversible property to the adhesive would allow for the recyclability of the substrates without the need of reactivating the adhesive when the product has reached its "end of life." Both reversible and non-reversible adhesives have been developed in recent years, which respond to stimuli such as heat, light or chemicals.

With reversible adhesives, the use of supramolecular polymers has enveloped the use of traditional polymers. The introduction of supramolecular interactions into polymer networks allowed for the design and synthesis of structurally elegant and sophisticated materials. Supramolecular polymers have become a major research theme in approximately the last 30 years reaching into organic, inorganic and physical chemistries.[27,28] Supramolecular polymers can be defined as "*polymeric arrays of monomeric units that are brought together by reversible and highly directional secondary interactions, resulting in polymeric properties in dilute and concentrated solutions, as well as in the bulk.*"[29] As these interactions can be broken and formed, an association constant (K_a) can be determined by experimental methods such as ^{1}H NMR or UV/visible spectroscopies.[30,31] In solution state studies, K_a has been shown to be as high as 10^6 M^{-1}.[32,33] With solid state supramolecular polymers, the network predominately relies on weaker non-covalent intramolecular interactions which readily assemble and dissemble to form reversible networks (Figure 1.1). These highly dynamic supramolecular polymers not only rely their strong association strengths, but also on reversible switching with an external

stimulus. These interactions are readily allowed to switch 'on' and 'off' with the stimulus, which allows for the polymeric network to strengthen or weaken rapidly.[34]

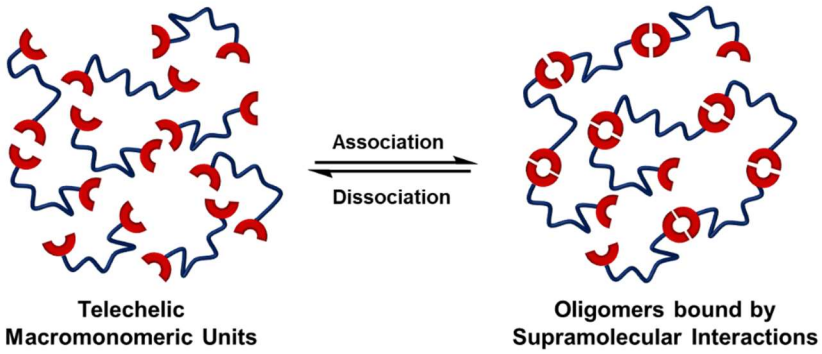

Figure 1.1 *Formation of a supramolecular polymer from low molecular weight monomeric units bound together with highly reversible supramolecular interactions.*

In terms of a stimuli-responsive material, for example a debondable adhesive, the material shows strong adhesion at ambient conditions. When exposed to an external stimulus, the interactions dissociate, breaking the supramolecular network, thereby weakening the material and resulting in adhesive failure. The same stimulus can then be used to increase the strength of the material. In contrast, a stimuli-responsive non-reversible adhesive cannot regain its strength when the network breaks down. (Figure 1.2).

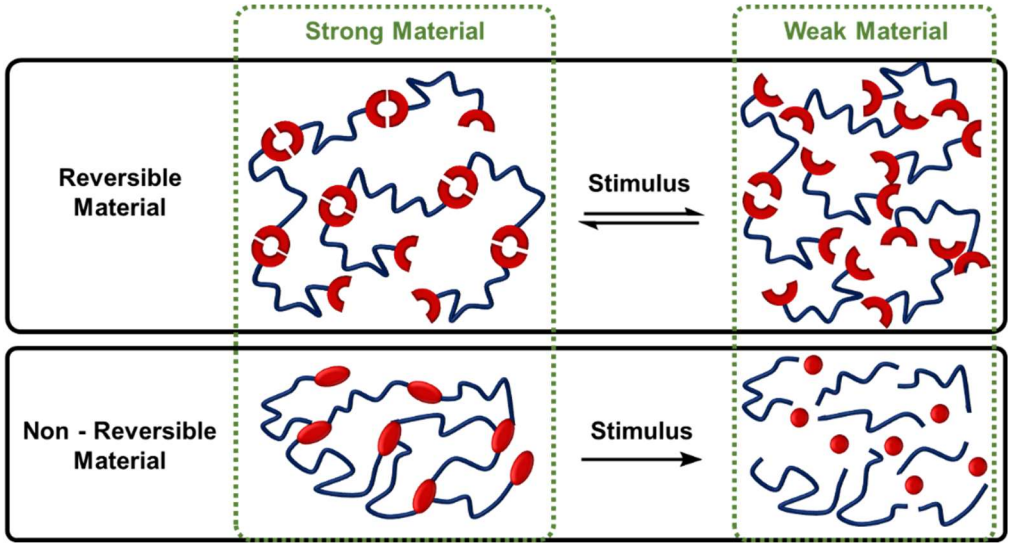

Figure 1.2 *The effect of an external stimuli on the polymer network of a reversible and non-reversible stimuli-responsive polymer.*

The major advantage of reversible stimuli-responsive polymers is that they allow for the recyclability of the material, whereas non-reversible stimuli-responsive polymers produces waste materials that need to be disposed. Owing to this fact, the use of supramolecular polymers containing non-covalent interactions and/or dative covalent interactions has greatly expanded the research into stimuli-responsive materials.

Within the extensive research carried out on supramolecular polymers, hydrogen bonding[35–39] and π-π stacking[40] have shown to be the most robust interactions for functional materials.[41] Other supramolecular interactions include metal-ligand[38,42] and electrostatic[43] interactions which have been researched extensively. Contrasting with non-covalent interactions, reversible dynamic covalent bonds have been used which can also readily break and form with an external stimulus.[44] These modes of interactions have different bonding energies (Table 1.1), and result in a variety of materials with different mechanical properties. These interactions and how they are used in polymeric materials will be explored sequentially in the following sections.

Supramolecular Interaction or Bond	Bond Energy (kJ mol^{-1})
Hydrogen Bond	10 – 65
π-π stacking	0 – 50
Metal – Ligand	0 – 400
Electrostatic	250
Covalent bond	100 – 942

Table 1.1 *Bond energies of supramolecular interactions in comparison to covalent bonds.*[45–47]

1.2.1. Hydrogen bonding in Supramolecular Polymers

Hydrogen bonding supramolecular polymers can be attributed to the discovery of deoxyribonucleic acid (DNA) by Watson and Crick in 1953[48] where the nucleotide base pairs, adenine **1.1** (A), thymine **1.2** (T), cytosine **1.3** (C) and guanine **1.4** (G) are sequenced on the phosphate deoxyribose backbone. The base pairs bond together by hydrogen bonding (A – T, and C – G) (Figure 1.3) to form a helical structure. The hydrogen bonds readily break and reform with another strand during DNA replication.

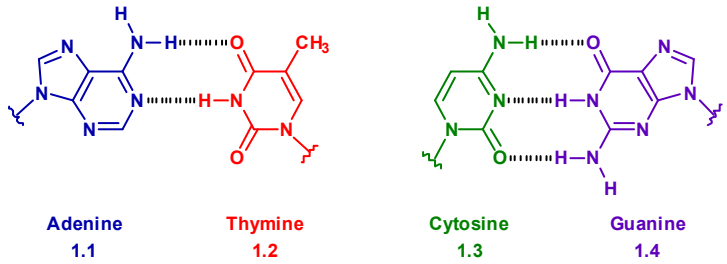

Figure 1.3 *Watson-Crick hydrogen bonding between the DNA base pairs.*

DNA base pairs have been implemented as hydrogen bonding motifs in supramolecular polymer which show thermal reversibility.[49–51] However, the design of novel hydrogen bonding motifs has formed a significant element in the research of supramolecular polymers.[35–39] A notable example of a strongly bound hydrogen bonding motif is the ureido-pyrimidone group

1.5 (UPy) developed by Meijer, Sijbesma and co-workers[32] (Figure 1.4a) which has two hydrogen bonding donors and two hydrogen bonding acceptors that allows UPy to readily bond to itself. Further work on this motif introduced a pairing group, the diamido-naphthyridine[52] **1.6** (Napy) (Figure 1.4b) to enhance the strength of the hydrogen bond. Both groups show thermal reversibility of the hydrogen bonds in supramolecular interactions. The key advantage to using UPy and Napy based materials allows for diblock co-polymer systems. This allows for a range of different properties to be formed from supramolecular polymers.[53,54]

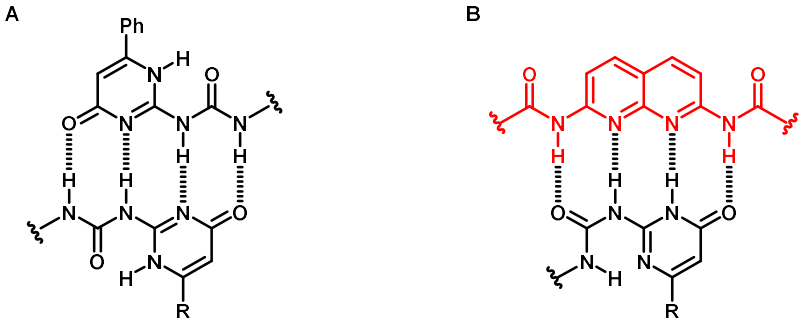

Figure 1.4 *The ureido-pyrimidone (UPy) motif (A) self-assembling with itself by four hydrogen bonds and (B) assembling with the diamido-naphthyridine (Napy) motif.*

Common functional groups seen in hydrogen bonding motifs are urethanes (carbamates) and ureas (carbamides), and their use in polyurethanes or polyureas has been extensively researched in supramolecular polymers.[55] Within the past decade, research into varying the strength of the hydrogen bonding interactions of urethanes/ureas within polyurethanes and polyureas have been explored. Hayes and co-workers reported that using different weakly associating end groups on telechelic macromonomers (Figure 1.5) with different strengths and properties which are dictated by the combination of phase separation and hydrogen bonding.[56–61] For example, utilising the nitro-methoxy functionalised dibenzylamine **1.9** resulted in a material that could heal at 45 °C.[57] In contrast, use of an amine terminated morpholine **1.7** produced a healable material at 37 °C, which could be used as artificial skin.[60]

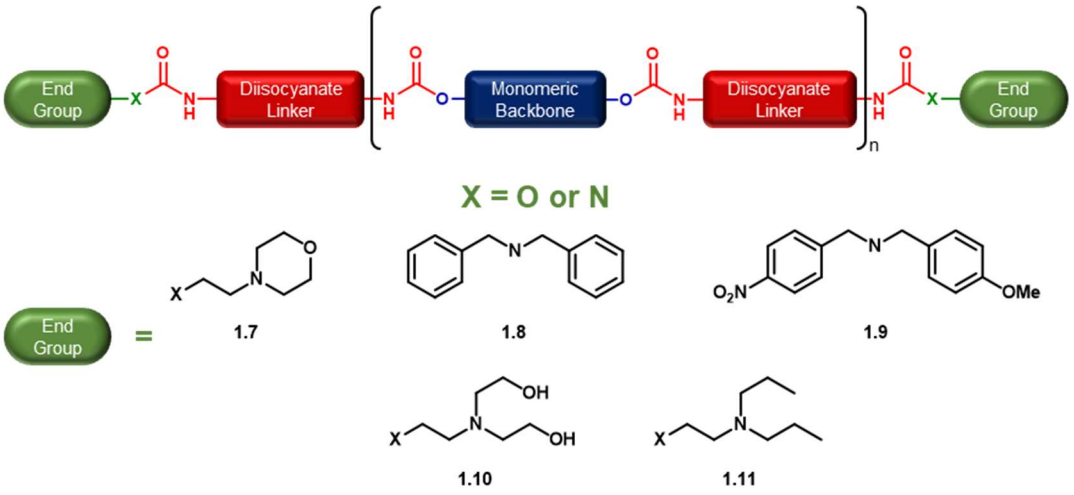

Figure 1.5 *Hydrogen bonded supramolecular polymers with different end groups which provide different chemical and mechanical properties.*

Recently, the introduction of thioureas **1.12** into supramolecular polymers has provided strong materials with reversible properties at room temperature.[62,63] Conventionally, hydrogen bonding from ureas perform linear stacking of the supramolecular polymer. Thioureas show bent stacking (Figure 1.6) which was demonstrated by Aida and co-workers as a glass type material that can be healed at room temperature.[64] This type of material would be highly useful in the technology industry, in particular the mobile phone industry where glass screens are broken every day. A healable glass would reduce production costs and material waste, as spare glass screens do not need to be produced or thrown away after cracking.

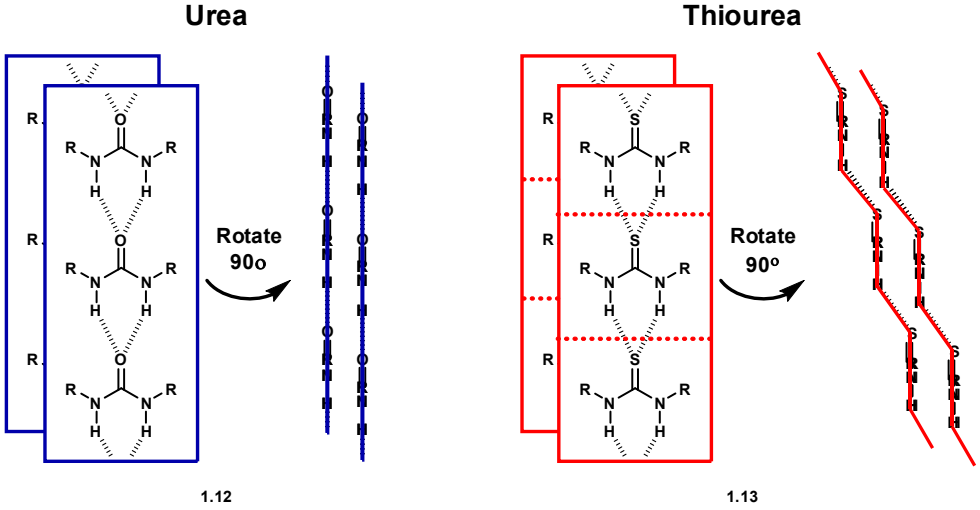

Figure 1.6 *Stacking of thiourea moieties in comparison to urea moieties in hydrogen bonding materials, showing the bent stacking of the thioureas. R = poly(ethylene glycol).*

1.2.2. Aromatic π-π stacking interactions in Supramolecular Polymers

Aromatic π-π stacking interactions in supramolecular polymers have been explored thoroughly throughout the history of supramolecular interactions to create reversible materials with

switchable properties.[40] Strong interactions have been shown using a two-part mixture, one material contains a π-electron poor group and the other contains a π-electron rich group, which together yield a strong reversible polymer.[65] This has been explored by Iverson,[65,66] Stoddart,[67,68] and many others.[69,70] At the University of Reading, within the Colquhoun, Hayes and Greenland groups, the use of the π-electron poor naphthalene diimide and π-electron rich pyrene moieties which interact with each other and have been used for many applications and materials, including the elegantly designed "Roman Handshake" material **1.14** (Figure 1.7a).[71] Examples of materials using the same π-π stacking moieties include thermally healable materials,[72–76] 2D printable inks of different colours,[77] and explosive detectors.[78] Supramolecular crosslinking was also achieved using this method, which is highly reversible in comparison to traditional covalently crosslinked materials.[77]

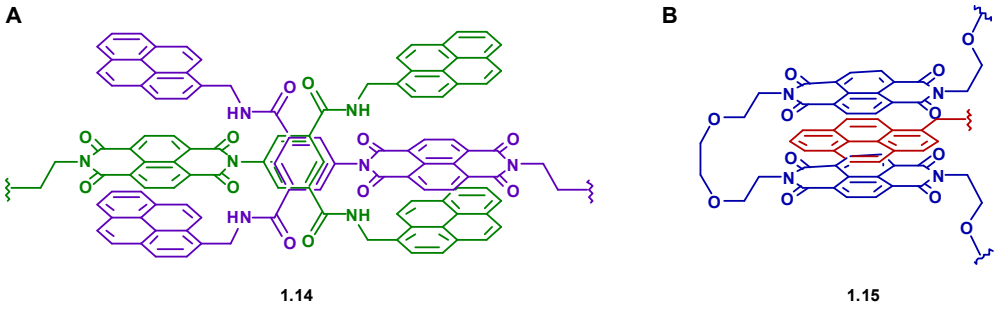

Figure 1.7 *π-π stacking of (A) two tweezer type molecules that self-assemble in a "Roman Handshake" configuration and (B) of the π-electron poor naphthalene diimide (blue) and π-electron rich pyrene (red) moieties used in healable supramolecular polymers.*

1.2.3. Metal-ligand interactions in Supramolecular Polymers

Also known as metallo-supramolecular polymers, these materials offer organic/inorganic properties that are widely required for technological applications where high conductivity is required.[42,43] These materials usually have terminal ligands, which readily dissociate from their counter metal ion when a competitive counter ion or solvent is added to the material (Figure 1.8).[79] Commonly used ligands have either a pyridine and/or pyrrole functional groups, which can bind to metal ions.[80–84] For example, the pyridine/benzimidazole ligand **1.16** that is capable of reversible metal-ligand interaction upon stimulation with UV light. The use of the tridentate ligand terpyridine has been researched extensively as it interacts readily with metal(II) ions such as Fe(II), Zn(II) Co(II) and Cd(II).[79] The wide range of ligands allow for many different materials to be produced and for many new materials to be developed in the future.

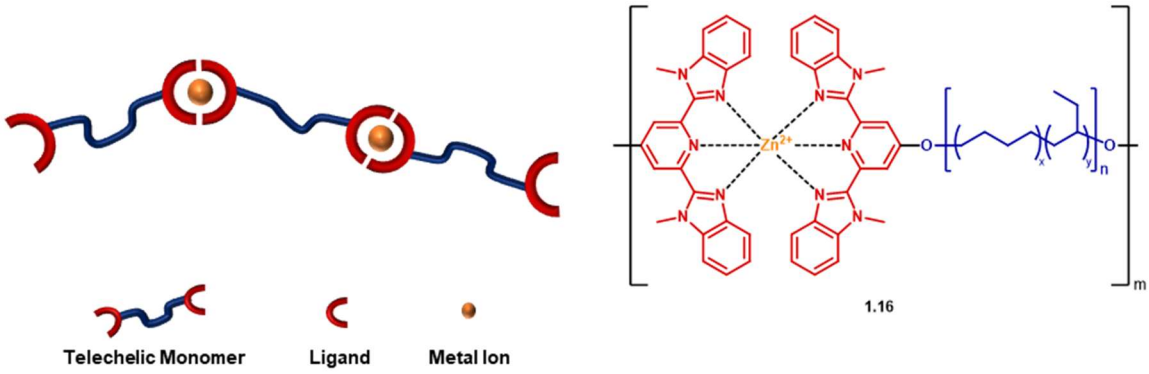

Figure 1.8 *Telechelic macromonomers with terminal ligands that form metal-ligand interactions with a metal ion, as shown by Weder and co-workers.*[85]

1.2.4. Electrostatic interactions in Supramolecular Polymers

Supramolecular polymers containing electrostatic interactions[79,86–89] rely on the coulombic interaction of the opposite charged groups or species, which can readily be changed by varying the nature of the counter ions or functional groups. In most cases, however, the functional groups within the material are charged themselves (e.g. the zwitterion effect of a carboxylic acid and amine which readily interact with each other).[79] Although, ion-ion interactions exhibit the strongest interaction (*ca.* 200 – 300 kJmol^{-1}),[90] dipole-dipole interactions show the most potential with supramolecular polymers as they allow for directional assembly of interactions within the material. This assembly mode was shown by Huang and co-workers (Figure 1.9), where their use of carboxylic acids on a crown-ether **1.17** interacting with a charged bipyridyl unit allows linking through the crown ether ring to form a pH responsive gel.[86,91]

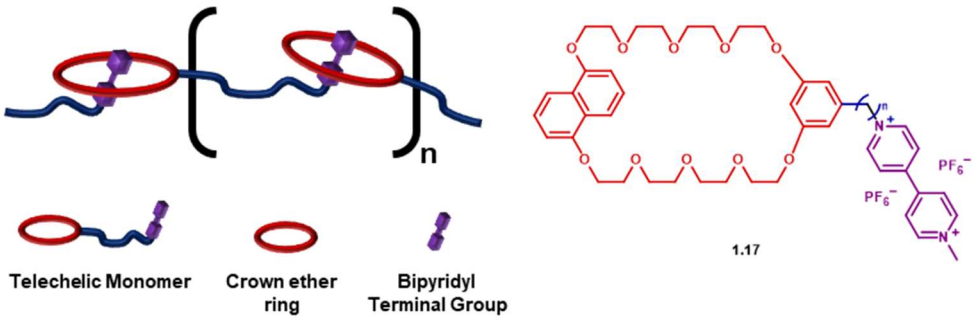

Figure 1.9 *An example of a supramolecular polymer relying on electrostatic interactions, as shown by Huang and co-workers.*[86,91]

1.2.5. Dynamic-covalent bonds in Reversible Polymers

Covalent bonds are much stronger that non-covalent interactions (Table 1.1) and hence are difficult to break. To counter this, dynamic covalent bonds have been developed which are able to reversibly break and form with an external stimulus.[92,93] Dynamic covalent bonds still require

higher energies to change the break/form equilibrium than non-covalent supramolecular interactions, but offer stronger mechanical properties while retaining reversibility.[45–47]

A well-studied dynamic covalent system is the use of the Diels-Alder cyclisation of a furan **1.18** and maleimide **1.19** moieties.[94] These moieties have been shown to cyclise at room temperature[95,96] but require temperatures higher than 60 °C to undergo a retro Diels-Alder cyclisation (Scheme 1.1).[44,97–99]

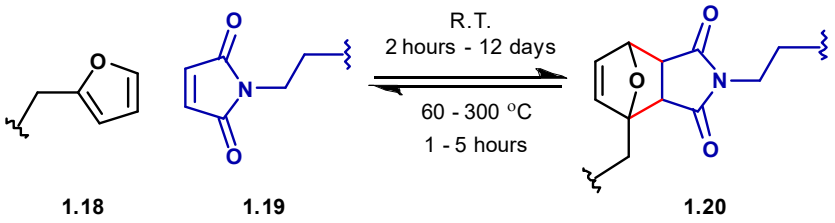

Scheme 1.1 *Cyclisation of the Diels-Alder adducts, furan and maleimide at room temperature and retro Diels-Alder reaction at elevated temperatures. The bonds in red denote the new dative-covalent bonds formed during the cyclisation.*

Another Diels-Alder system formed from the cyclisation of dicyclopentadiene has been reported, which requires elevated temperatures (>170 °C) to dissociate the two adducts allowing for greater thermal stability.[100,101] Similarly, the Diels-Alder cyclisation of cyclopentadiene and pyridine terminated polymers affords a thermally reversible material.[102]

A commonly used photo-induced cyclisation moiety is anthracene **1.21**, which cyclises readily to form a dimer **1.22** at ~365 nm and dissociates to anthracene **1.21** again at ~254 nm (Scheme 1.2).[103,104]

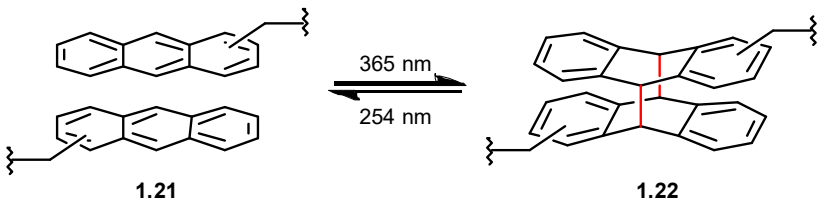

Scheme 1.2 *Reversible dimerisation of Anthracene moieties under UV light. Red bonds show newly formed dynamic covalent bonds.*

In contrast to cyclisation, the use of the reversible disulfide bridges **1.23** (Scheme 1.3a) has been explored. The disulfide bridge is thermally stable under ambient conditions, and is broken by heating or UV light.[105–107] Similarly, alkoxyamines **1.25** work in the same manner (Scheme

1.3b).[108] Conversely, the recent introduction of dative boroxine[109] and boron-nitrogen bonds[110] **1.29** have produced supramolecular polymers that are readily reversible (Scheme 3c).

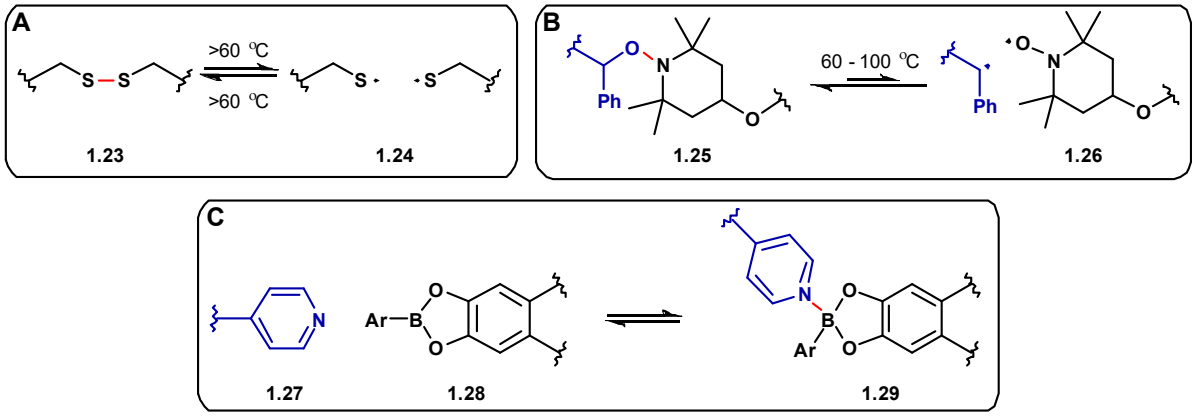

Scheme 1.3 *Reversible dative-covalent bonds of (A) a disulfide bridge, (B) an alkoxyamine bond and (C) a boron-nitrogen bond. Bonds in red indicate the reversible dative-covalent bond.*

Supramolecular interactions allow for reversibility in supramolecular polymers. The use of supramolecular interactions in stimuli-responsive adhesives has increased within the past decade, and examples are now detailed.

1.3. Stimuli – Responsive Adhesives and Materials

Stimuli-responsive polymers change chemically and/or physically when treated with an external stimulus. With stimuli-responsive adhesives, also known as "debond-on-demand adhesives",[111] the polymer network is broken, causing the strength of the adhesive to weaken and allowing the user separate the substrates previously bonded. Two types of stimuli-responsive adhesives exist: (i) reversible adhesives (ii) non-reversible adhesives which change physically and/or chemically but their original properties do not return.

Throughout the development of stimuli-responsive polymers and adhesives, different external stimuli have been explored. The most common stimulus used is heat, which can provide enough energy to break the supramolecular interactions in stimuli-responsive materials.[97,112,113] Furthermore, the introduction of nanocomposites, which absorb heat and reradiate the energy locally, has expanded the research on thermally responsive materials.[114] The recent introduction of graphite and graphene in polymer nanocomposites has resulted in thermally expandable materials to induce debonding.[115,116] Another stimulus used successfully is the use of light to break supramolecular interactions, which has gained greater interest in recent years because of the advancement in technology within the past decade.[103,117] Chemical stimuli have recently shown remarkable results with stimuli-responsive materials, and generally used in conjunction

with either of the two previous stimuli to give multi-stimuli responsive materials.[118,119] An exploration into how these stimuli affect the supramolecular network and they effect the properties of the material are discussed in the following sections.

1.3.1. Thermally Responsive Adhesives and Materials

Thermal stimuli have been used extensively with supramolecular polymers as nearly all of the supramolecular interactions mentioned above respond to thermal treatment. For example, Long and co-workers synthesised a series of UPy functionalised polyacrylates **1.30** which showed adhesion to glass substrates (Figure 1.10a).[120] Higher loadings of the UPy group afforded stronger adhesion. In a similar fashion, Long and co-workers also showed the use of adenine **1.31** and thymine **1.32** functionalised two-pot polyacrylate adhesives (Figure 1.10b).[121,122] These materials showed thermal reversibility of adhesion at 80 °C.

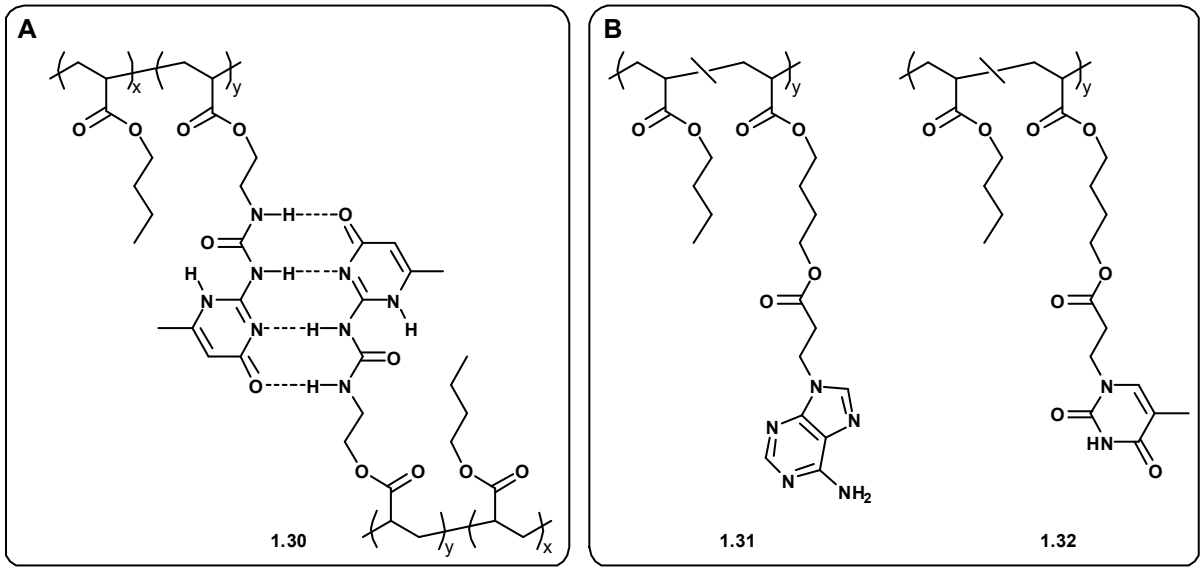

Figure 1.10 *The hydrogen bonded supramolecular adhesives of (A) UPy functionalised and (B) adenine-thymine functionalised polymethacrylate co polymerised with polybutacrylate developed by Long and co-workers.*[121,122]

Hayes and co-workers reported the synthesis of a polyurethane/urea adhesive terminated with morpholine groups **1.7** (Figure 3) that could bind to skin tissue at temperatures as low as 37 °C (skin surface temperature).[60] Similarly, Bosman and co-workers showed the synthesis of a UPy terminated siloxane **1.33** that adhered to glass at 120 °C, and held a 1 kg weight for 24 hours without breaking.[123] The adhesive could be re-adhered at 120 °C and was shown to have the same adhesive properties (Figure 1.11). In both cases, a one-pot synthetic procedure was used to make the telechelic adhesives. This aspect of their generation is highly advantageous for

industrial applications, saving time and money, while keeping the synthesis simple even at large scales.

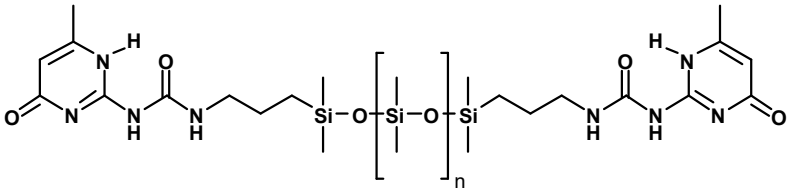

1.33

Figure 1.11 *UPy functionalised polysiloxane used as an adhesive that is thermally reversible at 120 °C.*[123]

Dynamic covalent supramolecular adhesives that are thermally reversible have also been explored. As mentioned previously, the use of the Diels-Alder adducts furan **1.18** and maleimide **1.19** have been used extensively in reversible supramolecular polymers, and in adhesive materials. An example of their use is seen in the work by Aubert,[97] where furfuryl glycidyl ether **1.35** and bisphenylene bismaleimide **1.34** were synthesised and linked together by a Diels-Alder cyclisation before reacting the epoxides with an amine terminated polyether **1.37** to form a thermally reversible epoxy based adhesive (Scheme 1.4).

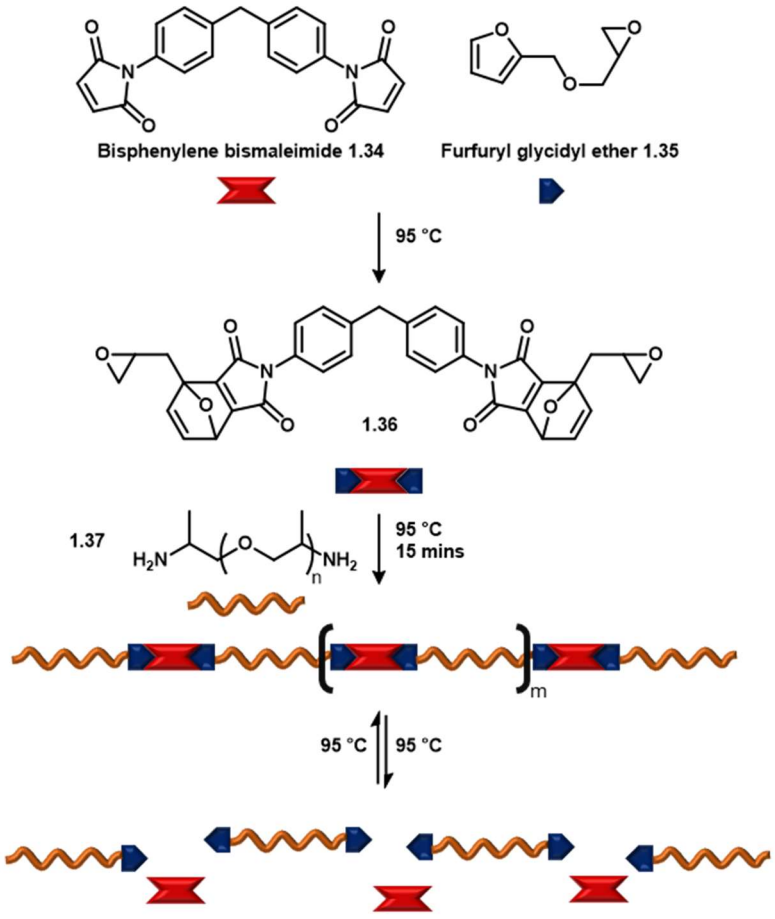

Scheme 1.4 *Thermally reversible adhesive designed by Aubert relying on the Diels-Alder adducts.*[97]

In a similar fashion to Aubert, Fisher and co-workers showed the use of a furfuryl alcohol as a terminal group of a polyester (similar structure to Figure 1.5).[124] This macromonomer was used with the biphenylene bismalemide **1.34** (Scheme 1.4) to produce a series of adhesive polymers of different molecular weights, which shows breaking of the dynamic covalent bond at *ca.* 120 °C and reformation at *ca*. 80 °C. Similar results were seen with polysiloxane based materials by Feng and co-workers with reversible adhesion to glass at 120 °C.[125]

Rowan and co-workers showed the use of a reversible disulfide bridge within the cross-linked polymer network of a co-polyether polyester material.[107] Interestingly, a two-stage adhesion process was evident where the crystalline material was applied to a glass substrate at 80 °C, which disforms the crystalline network of the material to amorphous network with intact disulfide bridges. To enhance the adhesion strength, the sample was heated to 150 °C using a high powered UV light source, which breaks the majority of the disulfide bridges and causes the material to flow into the surface imperfections (Figure 1.12). The second heating stage was also used to debond the glass substrates and could be rebonded by heating the sample again with the high-powered UV light (2000 mW/cm^2). An interesting side property acquired from the breaking and reforming of the disulfide bridges is shape memory. The polymer was adhered between two glass slides, heated until viscous, and the glass slides were twisted before allowing to cool. Reheating the sample allowed the glass slide to return to their original positions, and this process was repeatable thus proving the shape memory effect.

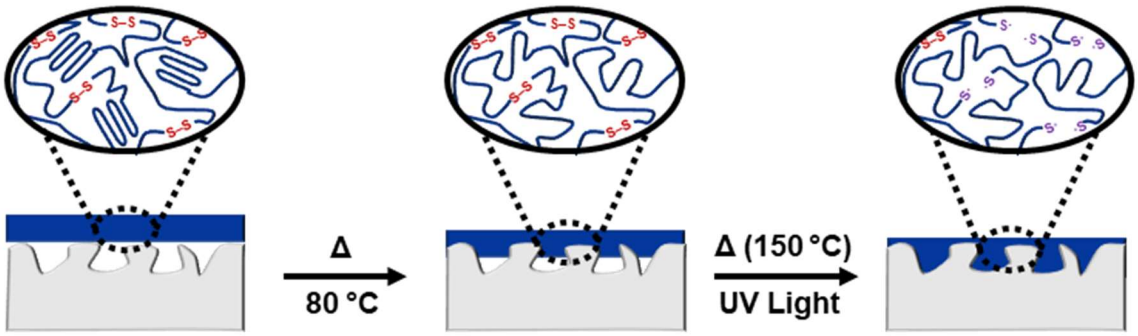

Figure 1.12 *Two stage adhesion of a thermally reversible polymer containing disulfide bonds developed by Rowan and co-workers.*[107] *The material is semi-crystalline at room temperature, and after heating at 80 °C the crystallinity is lost. Further heating at a higher temperature breaks the disulfide bonds, giving stronger adhesion as the viscosity drops allowing complete binding to the substrate.*

Localised thermally bonding adhesives using metal nanoparticle composites have been shown to have quicker bonding times in comparison to traditional heating of the adhesive.[126–129] This method of adhesion is possible by the incorporation of magnetic nanoparticles into the polymer

network, which can be heated by applying a high frequency oscillating magnetic field *via* an induction generator. However, reversing this method to induce debonding has rarely been reported. Bowman and co-workers utilised the Diels-Alder bismaleimide **1.34** (Scheme 1.4) with a trifunctional furan end capped polyether form a reversible cross-linked material imbedded with chromium nanoparticles.[114] Upon treatment with an induction generator, the material exhibited viscous like nature at *ca.* 110 °C within 150 seconds. Ramanujan and co-workers synthesised manganese-zinc-ferrite nanoparticles and imbedded them into a poly(ethylene-co-vinyl acetate) material which showed multiple break-heal cycles without loss of strength.[130] They also showed the use of the material adhered to wire as a healable coating, showing its possible industrial applications. Recently, Greenland and co-workers showed the use of iron nanocomposites imbedded in a supramolecular hydrogen bonded polymer, which showed rapid (<1 min) debonding of glass substrates with an induction generator (Figure 1.13). The material also showed adhesion to metals, woods and plastics.[131]

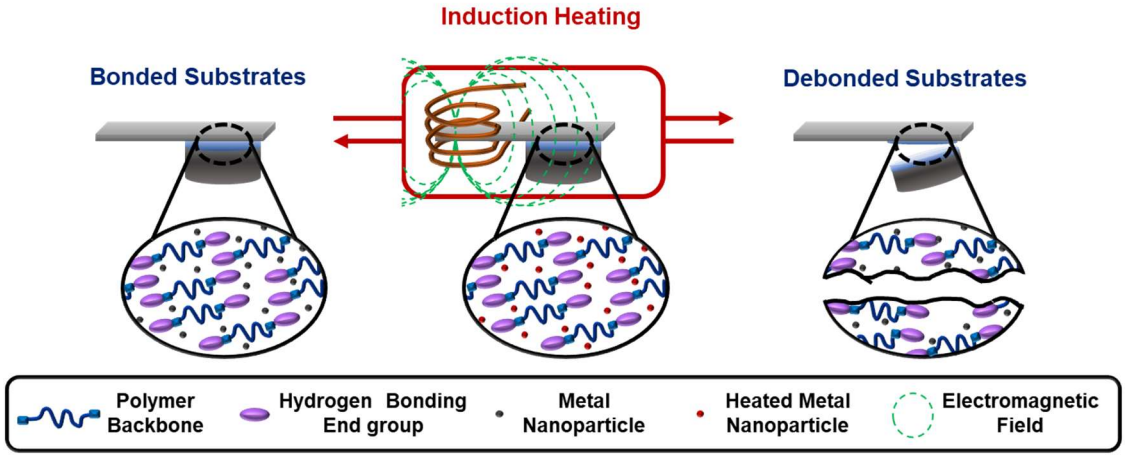

Figure 1.13 *Iron nanocomposite debond-on-demand adhesive developed by Greenland and co-workers.*[131] *The hydrogen bonded supramolecular network falls apart when exposed to an induction generator, which causes localised heating of the iron nanoparticles.*

A simple method for thermal debonding of adhesives is to use thermally expandable particles dispersed into the polymer network. Banea and co-workers used commercially available microcapsules provided by AzkoNobel and embedded them in either in a polyurethane or two-pot epoxy resin; both of which are commercially available adhesives.[116,132] The particles, which contain air, expand when heated to high temperatures (>200 °C) using an induction coil heater. Lower temperatures (100 – 150 °C) could be used, however, debonding time and strength were greater than the when higher temperatures were used. Similarly, Hutchinson and co-workers embedded compressed graphite within polyurethane or epoxy based adhesives.[115] When heated to 235 °C in an oven, the adhesive expanded allowing the bound substrates to fall apart.

One interesting approach to localised heating of debond-on-demand adhesives was shown by Weder and co-workers, where they used a similar telechelic macromonomer shown in Figure 1.5 but with a UPy functionalised polybutadiene that was blended with the UV responsive triazole Tinuvin 326 **1.38** (Figure 1.14).[80] This UV responsive group absorbs light to produce heat, which in turn cause the dissociation of the hydrogen bonds at *ca.* 70 °C.

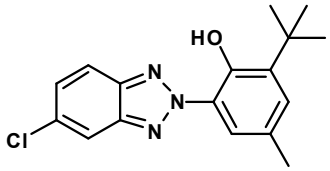

1.38

Figure 1.14 *Tinuvin 326, a UV responsive group that absorbs UV radiation and releases thermal energy for localised debonding of hydrogen bonded supramolecular adhesives.*[80]

The material showed reversible adhesive properties without loss of strength both light induced heating and thermal stimuli. Weder and co-workers extended their work further on this approach, taking a similar material to Long and co-workers[120] (Figure 1.10b) with the addition of a hexamethylene diisocyanate linker to give a polyurethane-urea mix to enhance hydrogen bonding.[133] This material also showed thermal reversibility as an adhesive, both with and without the triazole UV-absorber **1.38**. This interesting and simple approach shows great promise and should produce a variety of light induced thermally responsive adhesives and polymeric materials.

Weder and co-workers also synthesised a benzimidazoyl pyridine ligand as an end group to a hydrogenated polybutadiene telechelic macromonomer **1.39** (Scheme 1.5).[80] When bound to a zinc(II) ion, the macromonomer forms a supramolecular chain extended polymer **1.16**. The ligands show similar structural properties to Tinuvin 326 **1.38**, and when exposed to UV light, the energy is converted to thermal energy which causes dissociation of the metal-ligand interaction. Under standard conditions, the material shows adhesive properties which debonds from its substrates upon exposure to UV light. After removal of the UV light, the metal-ligand interactions reform, and the original strength of the material returns. Kumpfer and Rowan used the same ligand for europium metal-ligand supramolecular polymer for localised heating by UV irradiation.[134]

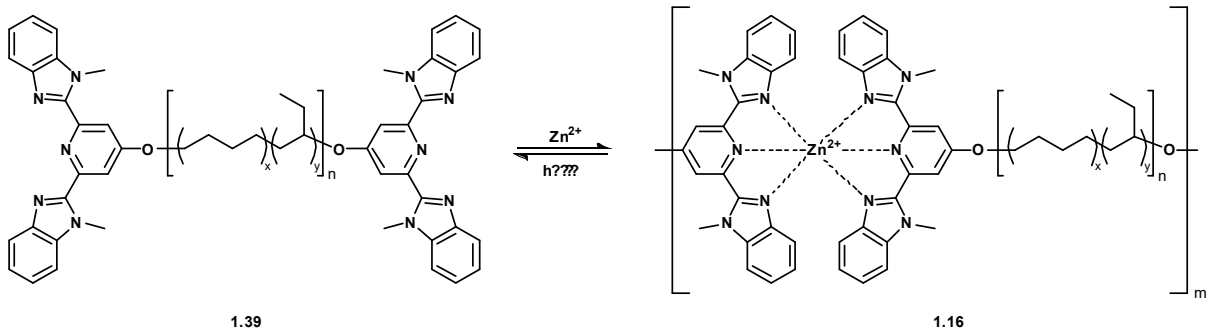

1.39 1.16

Scheme 1.5 *Telechelic macromonomer relying on metal-ligand supramolecular interactions to form debond-on-demand adhesive. The ligands radiate thermal energy when exposed to UV light, which dissociate the metal-ligand interaction, weakening the adhesive material.*[80]

In the examples above, UV light was used as an energy source to heat the samples to induce debonding of the adhesive. The following section explores the use of UV light as a stimulus to induce debonding of adhesives without heating.

1.3.2. Light Responsive Adhesives and Materials

A light responsive material is one that changes physically and/or chemically with a light source without expelling another source of energy. Throughout the history of stimuli-responsive materials, there are common functional groups that appear in light responsive materials. There are two subsections to light or UV responsive adhesives: (i) reversible and (ii) irreversible groups.[135,136]

One commonly used example of a reversible UV responsive functional group are azo-containing motifs. Two different methods of using azo-containing motifs exist that respond to UV light: (i) aromatic azo-containing motifs[135,137–141] which switch between *trans*- to *cis*-stereoisomers and (ii) aliphatic azo-containing motifs[85,141] which break forming molecular nitrogen and radicals. As the bond is breaking in aliphatic azo-containing materials, the material loses strength after irradiation but cannot regain it.

Aromatic azo-containing motifs, or azobenzenes, have been extensively used in UV responsive polymers.[135] Azobenzene derivatives undergo switching of *trans*-isomers to *cis*-isomer which causes a shortening of the overall length of the moiety (Scheme 1.6) from ~9 Å (*trans*-isomer) to ~5.5 Å (*cis*-isomer). The isomerism can be reversed with visible light or thermal stimuli.[135,141]

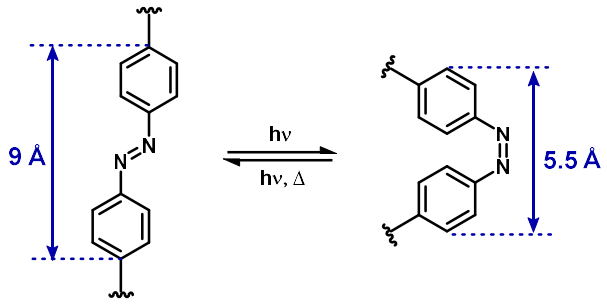

1.40 1.41

Scheme 1.6 *Switching of azobenzene moieties with UV light, which are reversible with visible light or temperature.*

By switching the between the two isomers, the properties of the materials can be reversibly altered. An example of the use of azobenzenes residues in non-adhesive UV responsive materials are seen in shape memory materials. Developed by Kessler and co-workers,[142] this azobenzene containing epoxy resin was folded into a cube using thermal shape programming. On application of a UV light source, the box unfolded and refolded quicker (35 s) than with a thermal stimulus (60 s) and without the need of heating to temperatures above 85 °C. This shows the vast possibilities of using a light stimulus over thermal stimuli.

Recently Staubitz, Gorb and co-workers[143] showed the use of an azobenzene as chain extender with poly(dimethylsiloxane) and bonded the material to a sapphire glass sphere in an atomic force microscope (AFM). Under UV radiation, the polymer showed reversible adhesion to the substrate without loss of strength (0.73 mN (bonded) to 0.27 mN (debonded) to ~0.70 mN (rebonded)). Kihara and co-workers[139,140,144] showed a series of different azobenzene adhesives, some of which turned from solid to liquid when irradiated at a wavelength of 365 nm, before being turned to a solid material again when irradiated at a wavelength of 520 nm allowing the glass substrates to debond from one another. This phase transition allowed for UV curing of the adhesive, which showed adhesion strengths twice as strong as thermal curing.

A reverse approach to debondable adhesives was shown by Harada and co-workers with their azobenzene functionalised glass surface.[145] With the azobenzene groups as the *trans*-isomer, the cyclodextrin based hydrogel adhesive would strongly adhere to the glass substrate. Switching the azobenzene to the *cis*-isomer by UV irradiation meant that the cyclodextrin ring could not bind to the azobenzene groups and hence the hydrogel adhesive does not adhere to the glass surface. This is a reverse approach to debondable adhesives as the surface properties are changed to causes debonding rather than the adhesive itself. The disadvantage to this method is that the surface needed to be functionalised prior to adhesion, and must have reactive groups that will allow for the attachment of the azobenzene groups.

Aliphatic azo containing compounds break down to tertiary carbon-radicals and molecular nitrogen. An example of this has been reported by Weder and co-workers[85] with an organogel based adhesive **1.42**. The poly(vinyl alcohol) organogel was crosslinked with an aliphatic azo group (Scheme 1.7). Upon radiation with UV light, the material depolymerises after 30 seconds as proven with gel inversion tests. Furthermore, when two glass substrates were adhered with the organogel, the sample was able to hold a 200 g weight for over 6 months under ambient temperature and light conditions. This shows that the polymer is only selective to UV light between 320 – 390 nm. The disadvantage to this system is that it is irreversible as nitrogen is evolved, so the adhesive strength cannot be regained in comparison to the azobenzene systems discussed earlier (see Scheme 1.6).

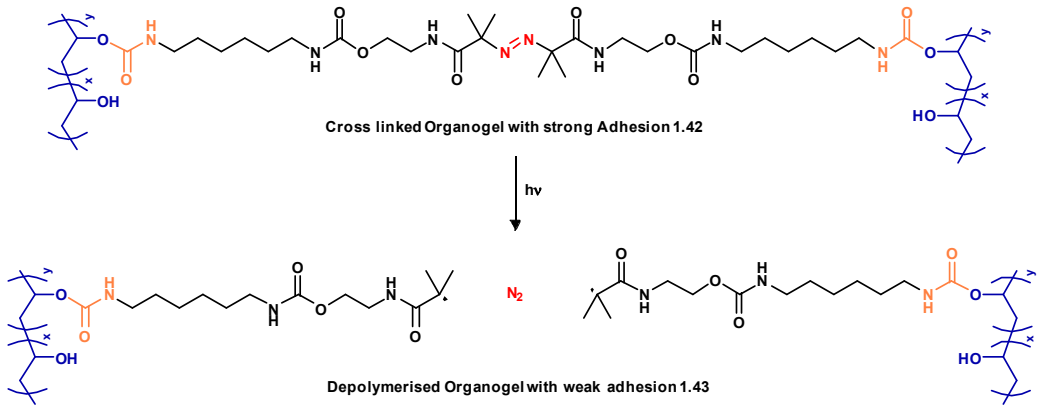

Scheme 1.7 *Irreversible depolymerisation by UV light irradiation of an aliphatic azo containing organogel based adhesive.*[85]

As described previously in Section 1.2.5., employing the use of the dimerisation of anthracene has been extensively researched with reversible materials. Akiyama and co-workers developed a hexavalent anthracene polymer using D-sorbital as the backbone.[103] Upon UV irradiation at 405 nm, the viscous liquid formed a thin film as a result of crosslinking (Figure 1.15). Applying the viscous liquid to glass substrate was aided by the addition of a plasticiser (dibutyl phthalate) to insure a good contact and spread between the two glass substrates. Irradiating the sample with UV light showed strong adhesion at approximately 3 MPa. However, Akiyama stated that as the glass broke just above 3 MPa, it was inconclusive as to how strong the actual adhesive would be. Nevertheless, Akiyama showed that heating to >180 °C broke the anthracene adduct to facilitate debonding of the substrates.

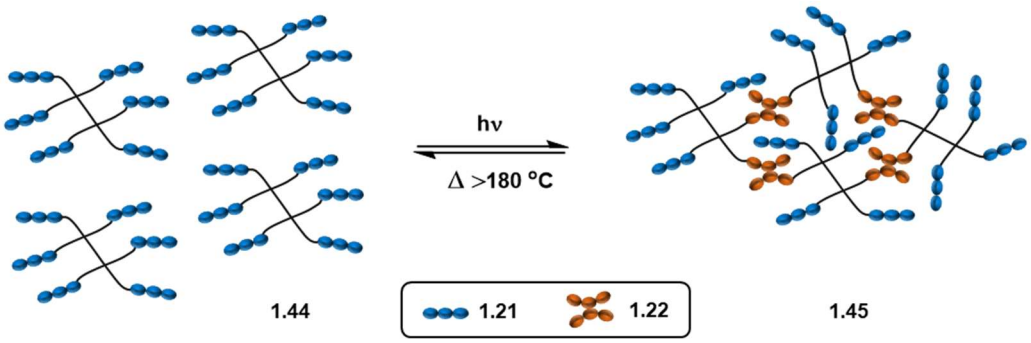

Figure 1.15 *Dimerisation of a hexavalent anthracene based cross linked adhesive.*

Another example of an anthracene functionalised polymethacrylate based adhesive was developed by Chung and co-workers which showed strong adhesion after 60 seconds of UV irradiation.[104] An interesting approach to using anthracene in reversible adhesives was shown by Saito and co-workers[117] who developed a dendritic system with a bent bis-anthracene core **1.45** (Figure 1.16). In comparison to the previous anthracene examples, dimerisation of the anthracene moieties caused debonding by disrupting the polymer network. The pristine material is an organogel with liquid crystalline properties as a result of π-π stacking interactions between the anthracene residues; and therefore, shows strong adhesive properties. A result of this liquid crystallinity is that the polymer must be melted at 70 °C before irradiation with UV light at 365 nm to facilitate dimerisation. Upon UV radiation, the anthracene dimerises and the crystallinity of the polymeric network breaks to form a viscous oil. This, in turn, causes the adhesive to fail and allow the glass substrates to debond. Furthermore, by reversing the dimerisation with high temperatures (160 °C), the polymer regains it liquid crystalline and adhesive properties.

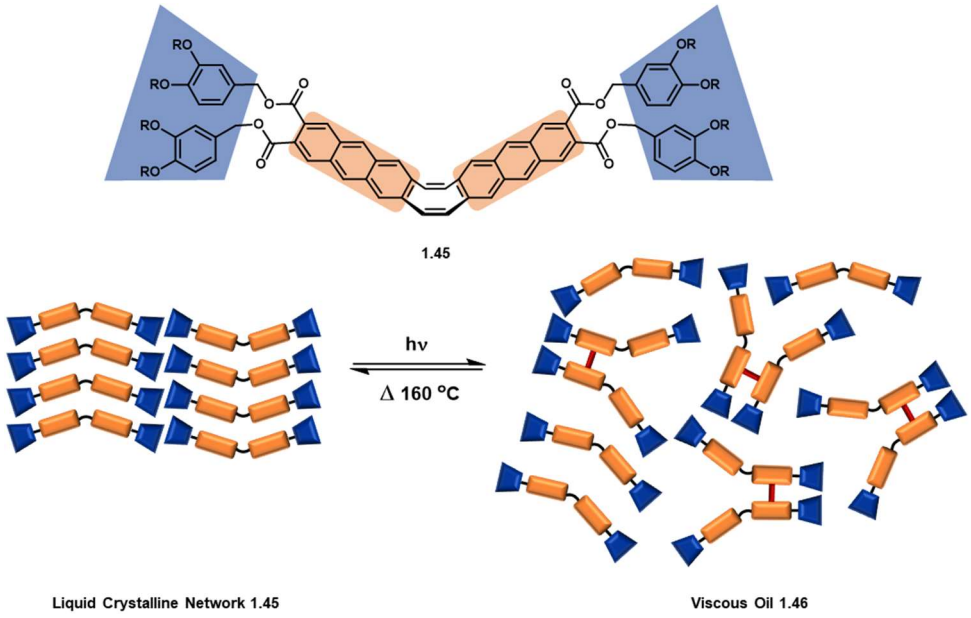

Figure 1.16 *Dimerisation of a bis-anthracene organogel allows for strong adhesion when pristine, and weak adhesion upon irradiation with UV light.*

Another photo-reversible functional group used for reversible polymers are coumarins (**1.47**) which undergo a 2+2 photocycloaddition at ~300 nm and retro-cycloaddition at ~ 290 nm. (Scheme 1.8). An example of coumarins used in reversible adhesives was shown by Love and co-workers who attached the coumarin to a poly(ethyl-co-ethylhexyl)acrylate as terminal groups[16] in a similar fashion to the groups work described in Figure 1.10b.[50,120] The adhesive polymer showed pressure sensitive adhesive properties, which when irradiated with UV produced a cross linked gel. This caused the peel strength of the adhesive to reduce from 1.62 MPa to 0.05 MPa when adhered between a Mylar™ film and silicone release liner.

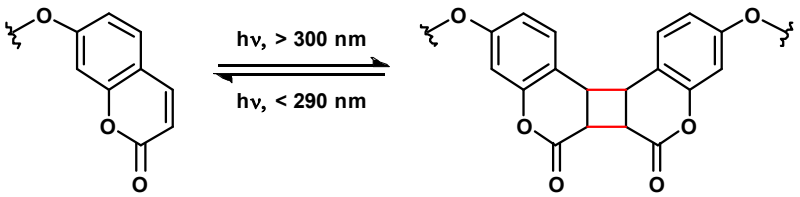

Scheme 1.8 *Reversible dimerisation of coumarin groups used in photo-responsive pressure sensitive adhesives.*

In comparison to the previous examples, light stimuli has been used with photosensitive protecting groups,[146] which in turn have been used as irreversible depolymerisable groups incorporated in polymer backbones. One example of an irreversible depolymerisable group is the use of an *o*-nitrobenzyl (ONB) group **1.49**, which has been incorporated into UV degradable materials since their introduction as a UV cleavable protecting group in 1966 by Barltrop and co-workers.[147] The ONB's undergo hydrogen abstraction from a nitro radical anion **1.50** formed by UV irradiation. The group breaks down to form an *o*-nitroso-benzyl aldehyde **1.53** and releases the hydroxyl terminated substituent (Scheme 1.9).

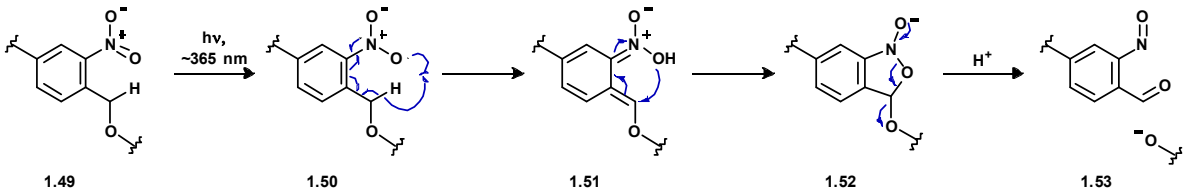

Scheme 1.9 *Mechanism of the degradation of the ONB under irradiation with UV light.*[147]

Examples of materials containing ONB's include microcapsules, sensors, and organic semi-conductors. In terms of adhesives, Long and co-workers incorporated ONB's into a polyester backbone **1.54** (Scheme 1.10).[148] Adhesion of the glass substrates was carried out by solvent removal. In solution state, the supramolecular network is disordered and allowing the solvent to evaporate slowly reorganises the strong network to form an adhesive material. The adhesive showed a drop-in fracture energy from *ca*. 3.4 J/cm^2 to *ca.* 1.6 J/cm^2.

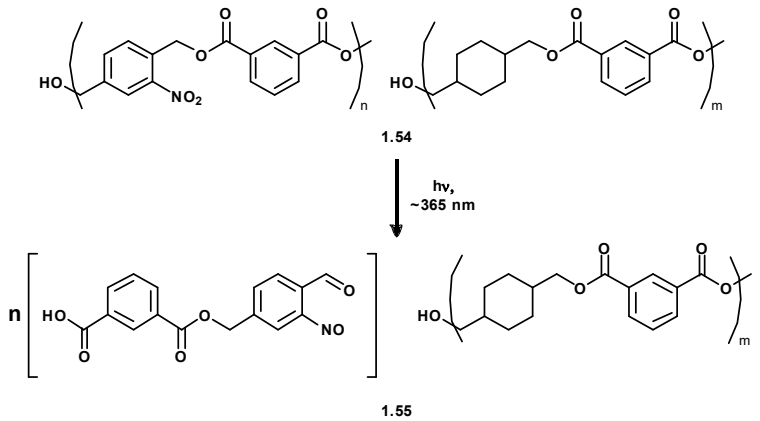

Scheme 1.10 *Depolymerisation of an irreversible UV responsive polyester containing ONB's within the polymer backbone. (B) shows the mechanism of the degradation of ONB with UV light.*[148]

Kim and Chung reported an ONB functionalised methacrylate **1.56** adhesive, in which the ONB group was employed as a cross linker within a polymethacrylate material (Figure 1.17).[149] Adhesion was carried out by addition of water to the polymer paste, which was adhered between two Mylar™ film strips. Adhesion strengths decreased from 341 kPa to 223 kPa after 30 minutes and then to *ca*. 150 kPa after 3 hours.

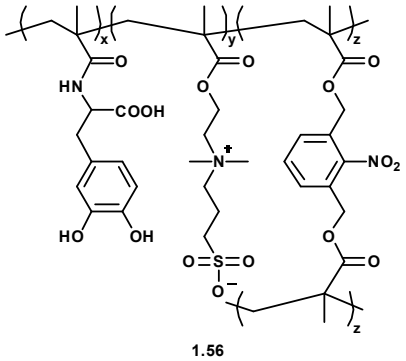

Figure 1.17 *Polymethacrylate based adhesive functionalised with an ONB cross linker for irreversible adhesion.*[149]

1.3.3. Chemoresponsive materials

Chemoresponsive materials which respond to contact with chemicals have existed for many decades, with the most common method of changing the physical properties of the material by changing the pH of a chemoresponsive functional group (CFG).[87,150–152] Altering the pH of the CFG is a reversible reaction and has been shown with reversible adhesives as exemplified below.

Keddie and co-workers reported the use of an acrylic acid pressure sensitive adhesive, which when exposed to basic pH conditions causes the deprotonation of the carboxylic acid.[17] This in turn causes the hydrogen bonding network of the acrylic acid to break down and allows the

adhesive to easily peel away. Lapitsky and Lawrence presented the use of an ionic hydrogel adhesive formed from the ionically cross-linked poly(allylamine) with pyrophosphate and tripolyphosphate.[153] Addition of sodium chloride caused adhesion to glass and Teflon substrates, which could be reversed by the addition of acid.

However, employing the use of a non-reversible CFG within an adhesive has not been extensively researched. Using a non-reversible CFG will allow for the irreversible depolymerisation of the polymeric network, hence allowing for a debondable adhesive. Phillips and co-workers showed the first chemo-responsive debond-on-demand adhesive.[119] They incorporated a *tert*-butyldimethylsilyl (TBS) protecting group (blue, Scheme 1.12) developed by Corey and Venkateswarlu in 1972[154] into a benzyl ether CFG and a benzyl carbonate CFG (Scheme 1.11).

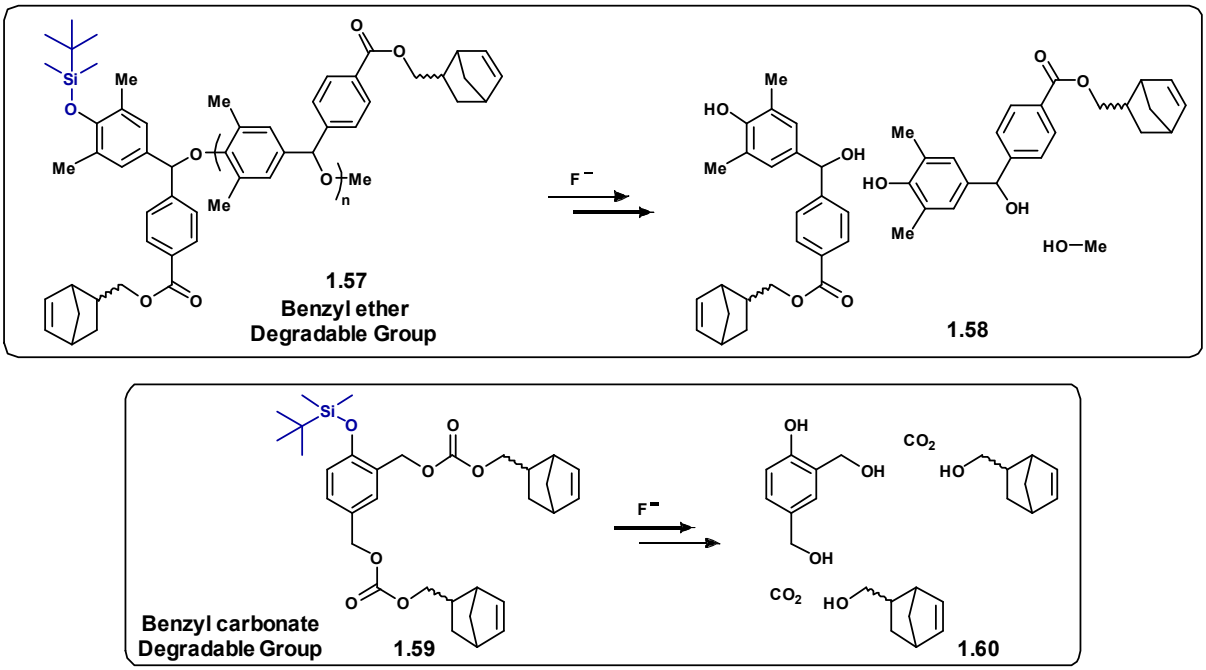

Scheme 1.11 *The two degradable groups designed by Phillips and co-workers which selectively respond to fluoride ions.*[119]

The degradable groups were terminated with norborane rings. When reacted with a norborane terminated ester monomer **1.61** in the presence of Grubbs 2nd catalyst, the monomers cross link to form an adhesive (Figure 1.18).

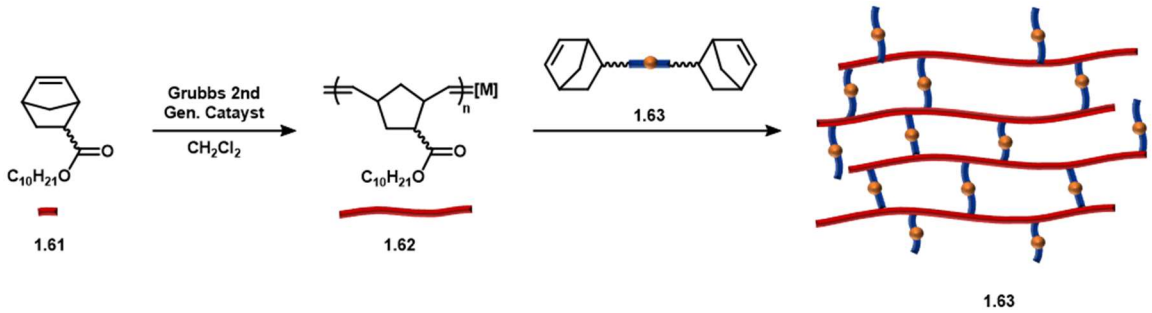

Figure 1.18 *Formation of a fluoride responsive crosslinked adhesive.*

The adhesive can debond from its substrates upon addition of a fluoride source, which cleaves the TBS group to form a phenoxide ion. This in turn causes the intramolecular flow of electrons through the CFG, resulting in the breakdown of the esters or carbonate groups and thereby the crosslinked material. This type of breakdown is called a self-immolative breakdown, and was first developed by Shabat in 2008.[155,156] The adhesive formed from the benzyl ether cross linker showed a reduction in adhesive strength by *ca. 90* % (*ca*. 0.33 MPa to *ca*. 0.03 MPa) after 30 minutes in a fluoride bath. Increasing the value of *n* of the benzyl ether cross linker (Scheme 1.11a) increases the cross-linking density and hence increased the strength of the adhesive. However, there are drawbacks to this system. Firstly, eleven steps were required to make the CFGs **1.57** and **1.59** and hence would be difficult to generate an adhesive based on this technology that is commercially viable. Secondly, although crosslinking increases the adhesive strength of the material, increasing the crosslinking density reduces the permeability of solvent through the material and hence degradation takes longer to reach a debondable state. Finally, as the material must be cross linked for adhesion to occur, the polymer must be made immediately prior to use and hence cannot be stored for later use. On the other hand, the selectivity of the adhesive to fluoride ions only is a desirable property and could lead to a variety of different materials and sensors in the future.

With the different types of adhesives outlined in section 1.1 and the alternative methods of causing debonding described in section 1.3, the following sections explore the common methods of testing the mechanical properties of adhesives.

1.4. Mechanical Testing of Adhesives

When adhesives are tested, the user is seeking to determine the maximum force that can be applied to the adhered substrates before breaking. After breaking the adhesive bond, the tester also notes how the adhesive behaved during breaking; specifically, how the adhesive failed. There are three ways that an adhesive can fail[1,157,158] (Figure 1.19):

(i) *Adhesive failure* - where the adhesive peels away from one of the substrates without leaving any residue;

(ii) *Cohesive failure* - where adhesive has broken completely and left residue on both substrates without any gaps;

(iii) *Both adhesive and cohesive failure* - where the adhesive has broken completely and left residue on both sides with gaps.

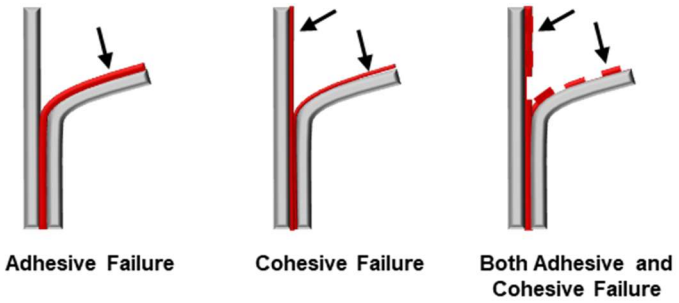

Figure 1.19 *The three different types of failure that occurs to adhesives when broken. Adhesive is shown in red and substrates shown in grey. Arrows indicate where the adhesive remains on the substrates.*[1]

Adhesive failure suggests that the method of curing was imperfect. For example, if a hot melt adhesive was only heated to 80 °C when it should have been heated to 120 °C, adhesion failure occurs. Cohesive failure occurs when the strength of the adhesive material is weaker than the strength of the adhesive bond between the adhesive and substrate. This would be the ideal situation for adhesive testing as this shows excellent adhesion to the substrates and the bond should not fail under normal conditions. Both adhesive and cohesive failure is an improvement on adhesive failure alone as some material has shown proper adhesion; however, improper curing of the adhesive (i.e. correct temperature but curing time was too short) has resulted in reduced performance.

Different methods have been developed for adhesive testing. According to the American Society for Testing Materials (ASTM) database which holds the international standards for mechanical testing, there are 129 different standard procedures developed to test adhesives (as of April 2018).[159] This vast range of different procedures have been developed to counter the vast variety of different applications and different types of adhesives. For example, 27 standards have been developed alone for testing adhesives bonded to wood. Other tests include bonding metals (from copper and aluminium to steel and alloys) and testing the bond strength of liquid and solid adhesives or testing tapes and labels.

Out of the immense variety of procedures for adhesive testing, two tests are commonly used; (i) lap shear[160] and (ii) butt-tensile[161] adhesion testing. Lap shear adhesion tests uses two rectangular substrates of the same size that are overlapped with one another (Figure 1.20) with the adhesive bonded in between. The two substrates are bonded linearly and pulled at a constant rate until the adhesive bond shears. The force required to break the bond is recorded and converted to the lap shear modulus which considers the surface area of the adhered samples.

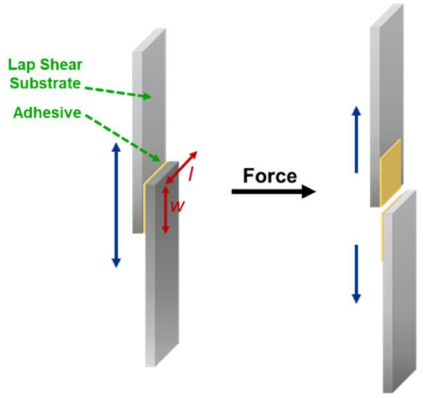

$$Lap\ Shear\ Modulus\ (MPa) = \frac{Force\ at\ break\ of\ adhesive\ bond\ (N)}{cross\ sectional\ area\ l \times w\ (mm^2)}$$

Figure 1.20 *Lap shear adhesive test where two rectangular lap shear substrates are adhered together with an adhesive before being pulled apart by force.*

Butt-tensile adhesion testing takes two cylindrical substrates of the same size and adhered together end-on-end with the adhesive (Figure 1.21). The two substrates are pulled at a constant rate until the bond fails.

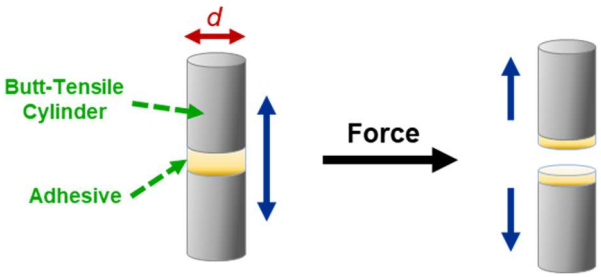

Figure 1.21 *Butt-tensile adhesive test where two cylindrical substrates are adhered together with an adhesive before being pulled apart by force.*

In comparison, the butt-tensile test explores the effect of applying tensile stress on the adhesive; whereas the lap shear test explores the effect of applying shear stress on the adhesive. This is important when testing the adhesive with a substrate material that is stronger. For example, when two pieces of metal are bonded, in a butt-tensile test the adhesive is the weakest point of the sample and failure will occur at the adhesive. However, when two pieces of metal are bonded in a lap shear test, the adhesive and substrates exhibit equal amounts of stress.

Therefore, if the adhesive is stronger than metal substrate, then the metal will break before the adhesive does.

These two methods of adhesive testing are the simplest to carry out yet can provide a significant quantity of data relating to the mechanical properties of the adhesive. Hence, the adhesive polymers designed and produced in this thesis will be tested using these two methods.

1.5. Project Aims

The field of debond-on-demand adhesive has grown extensively over the past decade. Although thermally stimulated debondable adhesives have been extensively studies, they provide the most opportunities when developing reversible debondable adhesives. Therefore, polyurethane networks with thermally reversible supramolecular hydrogen bonding motifs will be used for the backbone of the polymer network.

Although thermal reversibility is a major advantage to debond on demand adhesives, not all industrial cases require reversible adhesives and the need to completely break down the adhesive is required. Therefore, this project focuses on the design and synthesis of a simple degradable groups incorporated into a polyurethane backbone. To ensure our work was suitable for industrial applications, we aimed to complete the following objectives: (i) develop degradable groups that are simple to synthesise on large scales from as little as reactions possible; (ii) ensure quick and efficient depolymerisation rates when incorporated into a polyurethane backbone; (iii) allow for thermal reversibility of the adhesive for debonding-rebonding properties (Chapters 2 and 3).

The crosslinked functionality of the adhesive reported by Phillips and co-workers does provide extra strength to the adhesive.[119] Therefore, keeping with the first two objectives as before, a crosslinking degradable group will be designed. The crosslinking group will first be reacted with an isocyanate terminated pre-polymer to provide a two-pot crosslinked polyurethane adhesive (Chapter 4). The other method would be to use the crosslinking group as a core to ‘grow’ polyester arms from which would have terminal alcohol groups. This star shaped material could then be cross linked with a diisocyanate in a two-pot method to form an adhesive. (Chapters 5).

Finally, using the results of the chemo-responsive degradable group developed in Chapter 2, a novel UV-responsive group will be designed and synthesised, which will allow for the depolymerisation of a linear polyurethane (Chapter 6).

1.6. References

1. G. Habenicht, *Applied Adhesive Bonding: A Practical Guide for Flawless Results*, Wiley-VCH, Germany, 2008.
2. W. Li, L. Bouzidi and S. S. Narine, *Ind. Eng. Chem. Res.*, 2008, **47**, 7524–7532.
3. S. J. Sweeny, *Hot Melt Adheive Spray Dispenser*, US005375766A, 1994.
4. B. J. Boger, *Method and Apparatus For Spraying Hot Melt Adhesive Elongated Fibers in Spiral Patterns by Two or More Side-by-side Spray Devices*, 4815660, 1989.
5. C. A. Iacono and R. E. Miller, *Decoratve Film with Hot Melt Adhesive Layer*, US005981009A, 1999.
6. K. Kawate, S. Ishii and M. P. Perez, *Hot-Melt Adhesive Composition, Heat-Bonding Film Adhesive and Adhereing Method using Hot-Melt Adhesive Composition*, US6265460B1, 2001.
7. E. Orgilés-Calpena, F. Arán-Aís, A. M. Torró-Palau and C. Orgilés-Barceló, *Int. J. Adhes. Adhes.*, 2016, **70**, 218–224.
8. L. Sun, S. Cao, W. Xue, Z. Zeng and W. Zhu, *J. Adhes. Sci. Technol.*, 2016, **30**, 1212–1222.
9. Q. Tang, J. He, R. Yang and Q. Ai, *J. Appl. Polym. Sci.*, 2013, **128**, 2152–2161.
10. H. Jiang, Z. Zheng, W. Song and X. Wang, *J. Appl. Polym. Sci.*, 2008, **108**, 2644–3651.
11. M. Stolt, M. Viljanmaa, A. Södergård and P. Törmälä, *J. Appl. Polym. Sci.*, 2004, **91**, 196–204.
12. W. J. Jackson, T. F. Gray and J. R. Caldwell, *J. Appl. Polym. Sci.*, 1970, **14**, 685–698.
13. F. Chabert, F. Tournilhac, N. Sajot, S. Tenc-Girault and L. Leibler, *Int. J. Adhes. Adhes.*, 2010, **30**, 696–705.
14. Y. Zhou, W. Xue, Z. Zeng, W. Zhu and Z. Li, *J. Adhes. Sci. Technol.*, 2015, **29**, 670–677.
15. S. Sun, M. Li and A. Liu, *Int. J. Adhes. Adhes.*, 2013, **41**, 98–106.
16. S. R. Trenor, T. E. Long and B. J. Love, *J. Adhes.*, 2005, **81**, 213–229.
17. T. Wang, E. Canetta, T. G. Weerakkody, J. L. Keddie and U. Rivas, *ACS Appl. Mater. Interfaces*, 2009, **1**, 631–639.
18. A. I. Everaerts, S. Takeda and P. A. Stark, *Pressure-sensitive adhesives having improved adhesion to acid-rain resistant automotive paints*, US005612136A, 1997.
19. S. J. Shaw, in *Chemistry and Technology of Epoxy Resins*, 1993, pp. 206–255.
20. H. Hess, R. Kopp, G. Grögler, H. Stepanski, G. Arend and H. Tups, *Polyurethane-based one-component reactive adhesives*, US005109096A, 1992.
21. F. De Buyl, *Int. J. Adhes. Adhes.*, 2001, **21**, 411–422.
22. H. Hess, R. Kopp, G. Gröglerl, H. Stepanski, R. Hombach and W. Schäfer, *Polyurethane-based reactive adhesives in which the isocyanate is stabilised by a polyether amine*, US005104959A, 1992.
23. I. Szanka, A. Szanka and J. P. Kennedy, *J. Polym. Sci. Part A Polym. Chem.*, 2015, **53**, 1652–1659.
24. Henkel, Loctite Super Glue Profesional : Technical Data Sheet, http://www.loctiteproducts.com/tds/SG_BOTTLE_PRO_tds.pdf, (accessed 20 August 2018).
25. G. Murray, *Handbook of Materials Selection of Engineering Application*, CRC Press, San Luis Obispo, California, 1st Editio., 1997.
26. O. Wilke, O. Jann and D. Brodner, *Indoor Air*, 2004, **14**, 98–107.
27. J. W. Steed, *Supramolecular Chemistry: From Molecules to Nanomaterials*, Wiley, 2012.
28. J.-M. Lehn, *Reports Prog. Phys.*, 2004, **67**, 249–267.

29. L. Brunsveld, B. J. B. Folmer, E. W. Meijer and R. P. Sijbesma, *Chem. Rev.*, 2001, **101**, 4071–4097.
30. P. Thordarson, *Chem. Soc. Rev.*, 2011, **40**, 1305–1323.
31. D. Brynn Hibbert and P. Thordarson, *Chem. Commun.*, 2016, **52**, 12792–12805.
32. R. P. Sijbesma, F. H. Beijer, L. Brunsveld, B. J. B. Folmer, J. H. K. K. Hirschberg, R. F. M. Lange, J. K. L. Lowe and E. W. Meijer, *Science*, 1997, **278**, 1601–1604.
33. T. Park and S. C. Zimmerman, *J. Am. Chem. Soc.*, 2006, **128**, 11582–11590.
34. F. Tian, D. Jiao, F. Biedermann and O. A. Scherman, *Nat. Commun.*, 2012, **3**, 1–8.
35. G. Armstrong and M. Buggy, *J. Mater. Sci.*, 2005, **40**, 547–559.
36. K. E. Feldman, M. J. Kade, T. F. A. De Greef, E. W. Meijer, E. J. Kramer and C. J. Hawker, *Macromolecules*, 2008, **41**, 4694–4700.
37. S. K. Yang and S. C. Zimmerman, *Isr. J. Chem.*, 2013, **53**, 511–520.
38. L. Voorhaar and R. Hoogenboom, *Chem. Soc. Rev.*, 2016, **45**, 4013–4031.
39. S. Seiffert, *Supramolecular Polymer Networks and Gels*, Springer International Publishing, Switzerland, 2015.
40. W. Hayes and B. W. Greenland, in *Supramolecular Polymer Networks and Gels*, ed. S. Seiffert, Springer International Publishing, Switzerland, 2015, pp. 143–166.
41. T. Aida, E. W. Meijer and S. I. Stupp, *Science*, 2012, **335**, 813–817.
42. P. Wei, X. Yan and F. Huang, *Chem. Soc. Rev.*, 2015, **44**, 815–832.
43. E. Krieg, M. M. C. Bastings, P. Besenius and B. Rybtchinski, *Chem. Rev.*, 2016, **116**, 2414–2477.
44. F. García and M. M. J. Smulders, *J. Polym. Sci. Part A Polym. Chem.*, 2016, **54**, 3551–3577.
45. P. D. Beer, P. A. Gale and D. K. Smith, *Supramolecular Chemistry*, Oxford University Press, Oxford, 1999.
46. F. J. M. Hoeben, P. Jonkheijm, E. W. Meijer and A. P. H. J. Schenning, *Chem. Rev.*, 2005, **105**, 1491–1546.
47. C. F. J. Faul and M. Antonietti, *Adv. Mater.*, 2003, **15**, 673–683.
48. J. D. Watson and D. Crick, Francis, H., *Nature*, 1953, **171**, 737–738.
49. N. Ishikawa, M. Furutani and K. Arimitsu, *ACS Macro Lett.*, 2015, **4**, 741–744.
50. S. Cheng, M. Zhang, N. Dixit, R. B. Moore and T. E. Long, *Macromolecules*, 2012, **45**, 805–812.
51. S. J. Rowan, P. Suwanmala and S. Sivakova, *J. Polym. Sci. Part A Polym. Chem.*, 2003, **41**, 3589–3596.
52. P. S. Corbin and S. C. Zimmerman, *J. Am. Chem. Soc.*, 1998, **120**, 9710–9711.
53. A. J. Wilson, *Soft Matter*, 2007, **3**, 409.
54. K. A. Houton and A. J. Wilson, *Polym. Int.*, 2015, **64**, 165–173.
55. J. Courtois, I. Baroudi, N. Nouvel, E. Degrandi, S. Pensec, G. Ducouret, C. Chanéac, L. Bouteiller and C. Creton, *Adv. Funct. Mater.*, 2010, **20**, 1803–1811.
56. D. H. Merino, A. Feula, K. Melia, A. T. Slark, I. Giannakopoulos, C. R. Siviour, C. P. Buckley, B. W. Greenland, D. Liu, Y. Gan, P. J. Harris, A. M. Chippindale, I. W. Hamley and W. Hayes, *Polymer*, 2016, **107**, 368–378.
57. A. Feula, A. Pethybridge, I. Giannakopoulos, X. Tang, A. Chippindale, C. R. Siviour, C. P. Buckley, I. W. Hamley and W. Hayes, *Macromolecules*, 2015, **48**, 6132–6141.
58. P. J. Woodward, D. Hermida Merino, B. W. Greenland, I. W. Hamley, Z. Light, A. T. Slark and W. Hayes, *Macromolecules*, 2010, **43**, 2512–2517.
59. X. Tang, A. Feula, B. C. Baker, K. Melia, D. Hermida Merino, I. W. Hamley, C. P. Buckley, W. Hayes and C. R. Siviour, *Polymer*, 2017, **133**, 143–150.
60. A. Feula, X. Tang, I. Giannakopoulos, A. M. Chippindale, I. Hamley, F. Greco, C. P. Buckley, C. R. Siviour and W. Hayes, *Chem. Sci.*, 2016, **7**, 4291–4300.

61. L. R. Hart, S. Li, C. Sturgess, R. Wildman, J. R. Jones and W. Hayes, *ACS Appl. Mater. Interfaces*, 2016, **8**, 3115–3122.
62. I. Paraschiv, A. Tomkinson, M. Giesbers, E. J. R. Sudhölter, H. Zuilhof and A. T. M. Marcelis, *Liq. Cryst.*, 2007, **34**, 1029–1038.
63. C. Stefaniu, P. L. Zaffalon, A. Carmine, Q. Verolet, S. Fernandez, T. A. Wesolowski, G. Brezesinski and A. Zumbuehl, *Langmuir*, 2015, **31**, 1296–1302.
64. Y. Yanagisawa, Y. Nan, K. Okuro and T. Aida, *Science*, 2018, **359**, 72–76.
65. C. R. Martinez and B. L. Iverson, *Chem. Sci.*, 2012, **3**, 2191.
66. B. A. Ikkanda and B. L. Iverson, *Chem. Commun.*, 2016, **52**, 7752–7759.
67. L. Fang, M. A. Olson, D. Benítez, E. Tkatchouk, W. A. Goddard III and J. F. Stoddart, *Chem. Soc. Rev.*, 2010, **39**, 17–29.
68. G. Barin, A. Coskun, M. M. G. Fouda and J. F. Stoddart, *Chempluschem*, 2012, **77**, 159–185.
69. T. Nakano, *Polym. J.*, 2010, **42**, 103–123.
70. T. Nakano, *π-Stacked Polymers and Molecules: Theory, Synthesis, and Properties*, Springer Japan, 2014.
71. B. W. Greenland, M. B. Bird, S. Burattini, R. Cramer, R. K. O'Reilly, J. P. Patterson, W. Hayes, C. J. Cardin and H. M. Colquhoun, *Chem. Commun.*, 2013, **49**, 454–456.
72. J. Fox, J. J. Wie, B. W. Greenland, S. Burattini, W. Hayes, H. M. Colquhoun, M. E. MacKay and S. J. Rowan, *J. Am. Chem. Soc.*, 2012, **134**, 5362–5368.
73. L. R. Hart, N. A. Nguyen, J. L. Harries, M. E. Mackay, H. M. Colquhoun and W. Hayes, *Polymer*, 2015, **69**, 293–300.
74. L. R. Hart, J. H. Hunter, N. a. Nguyen, J. L. Harries, B. W. Greenland, M. E. Mackay, H. M. Colquhoun and W. Hayes, *Polym. Chem.*, 2014, **5**, 3680.
75. S. Burattini, B. W. Greenland, W. Hayes, M. E. MacKay, S. J. Rowan and H. M. Colquhoun, *Chem. Mater.*, 2011, **23**, 6–8.
76. S. Burattini, H. M. Colquhoun, B. W. Greenland and W. Hayes, *Faraday Discuss.*, 2009, **143**, 251–264.
77. L. R. Hart, J. L. Harries, B. W. Greenland, H. M. Colquhoun and W. Hayes, *ACS Appl. Mater. Interfaces*, 2015, **7**, 8906–8914.
78. S. Burattini, H. M. Colquhoun, B. W. Greenland, W. Hayes and M. Wade, *Macromol. Rapid Commun.*, 2009, **30**, 459–463.
79. G. Gröger, W. Meyer-Zaika, C. Böttcher, F. Gröhn, C. Ruthard and C. Schmuck, *J. Am. Chem. Soc.*, 2011, **133**, 8961–8971.
80. C. Heinzmann, S. Coulibaly, A. Roulin, G. L. Fiore and C. Weder, *ACS Appl. Mater. Interfaces*, 2014, **6**, 4713–4719.
81. S. J. Rowan and J. B. Beck, *Faraday Discuss.*, 2005, **128**, 43–53.
82. A. Richard, V. Marchi-Artzner, M.-N. Lalloz, M.-J. Brienne, F. Artzner, T. Gulik-Krzywicki, M.-A. Guedeau-Boudeville and J.-M. Lehn, *Proc. Natl. Acad. Sci. U. S. A.*, 2004, **101**, 15279–84.
83. J. B. Beck, J. M. Ineman and S. J. Rowan, *Macromolecules*, 2005, **38**, 5060–5068.
84. P. K. Iyer, J. B. Beck, C. Weder and S. J. Rowan, *Chem. Commun.*, 2005, **1**, 319–21.
85. M. A. Ayer, S. Schrettl, S. Balog, Y. C. Simon and C. Weder, *Soft Matter*, 2017, **13**, 4017–4023.
86. X. Ji, K. Zhu, X. Yan, Y. Ma, J. Li, B. Hu, Y. Yu and F. Huang, *Macromol. Rapid Commun.*, 2012, **33**, 1197–1202.
87. X. Ma and H. Tian, *Acc. Chem. Res.*, 2014, **47**, 1971–1981.
88. X. Lin and M. W. Grinstaff, *Isr. J. Chem.*, 2013, **53**, 498–510.
89. X. Lin, G. Godeau and M. W. Grinstaff, *New J. Chem.*, 2014, **38**, 5186–5189.
90. J. Steed, D. R. Turner and K. Wallace, *Core Concepts in Supramolecular Chemistry and*

Nanochemistry, John Wiley & Sons, Chichester, 1st Ed., 2007.
91. S. Dong, Y. Luo, X. Yan, B. Zheng, X. Ding, Y. Yu, Z. Ma, Q. Zhao and Huang, *Angew. Chem. Int. Ed.*, 2011, **50**, 1905–1909.
92. S. J. Rowan, S. J. Cantrill, G. R. L. Cousins, J. K. M. Sanders and J. F. Stoddart, *Dynamic Covalent Chemistry*, 2002, vol. 41.
93. R. J. Wojtecki, M. A. Meador and S. J. Rowan, *Nat. Mater.*, 2011, **10**, 14–27.
94. N. Roy, B. Bruchmann and J.-M. Lehn, *Chem. Soc. Rev.*, 2015, **44**, 3786–3807.
95. P. A. Pratama, M. Sharifi, A. M. Peterson and G. R. Palmese, *ACS Appl. Mater. Interfaces*, 2013, **5**, 12425–12431.
96. A. M. Peterson, R. E. Jensen and G. R. Palmese, *ACS Appl. Mater. Interfaces*, 2010, **2**, 1141–1149.
97. J. H. Aubert, *J. Adhes.*, 2003, **79**, 609–616.
98. G. Zhang, Q. Zhao, L. Yang, W. Zou, X. Xi and T. Xie, *ACS Macro Lett.*, 2016, **5**, 805–808.
99. A. Fuhrmann, R. Göstl, R. Wendt, J. Kötteritzsch, M. D. Hager, U. S. Schubert, K. Brademann-Jock, A. F. Thünemann, U. Nöchel, M. Behl and S. Hecht, *Nat. Commun.*, , DOI:10.1038/ncomms13623.
100. J. P. Kennedy and K. F. Castner, *J. Polym. Sci. Polym. Chem. Ed.*, 1979, **17**, 2055–2070.
101. E. B. Murphy, E. Bolanos, C. Schaffner-Hamann, F. Wudl, S. R. Nutt and M. L. Auad, *Macromolecules*, 2008, **41**, 5203–5209.
102. A. J. Inglis, L. Nebhani, O. Altintas, F. G. Schmidt and C. Barner-Kowollik, *Macromolecules*, 2010, **43**, 5515–5520.
103. H. Akiyama, Y. Okuyama, T. Fukata and H. Kihara, *J. Adhes.*, 2018, 1–15.
104. T. Harper, R. Slegeris, I. Pramudya and H. Chung, *ACS Appl. Mater. Interfaces*, 2017, **9**, 1830–1839.
105. Y. Xu and D. Chen, *Macromol. Chem. Phys.*, 2016, **217**, 1191–1196.
106. B. T. Michal, C. A. Jaye, E. J. Spencer and S. J. Rowan, *ACS Macro Lett.*, 2013, **2**, 694–699.
107. B. T. Michal, E. J. Spencer and S. J. Rowan, *ACS Appl. Mater. Interfaces*, 2016, **8**, 11041–11049.
108. H. Otsuka, K. Aotani, Y. Higaki, Y. Amamoto and A. Takahara, *Macromolecules*, 2007, **40**, 1429–1434.
109. J. C. Lai, J. F. Mei, X. Y. Jia, C. H. Li, X. Z. You and Z. Bao, *Adv. Mater.*, 2016, 8277–8282.
110. E. Sheepwash, N. Luisier, M. R. Krause, S. Noé, S. Kubik and K. Severin, *Chem. Commun.*, 2012, **48**, 7808.
111. C. Heinzmann, C. Weder and L. M. de Espinosa, *Chem. Soc. Rev.*, 2015, **342**, 342–358.
112. X. Luo, K. E. Lauber and P. T. Mather, *Polymer*, 2010, **51**, 1169–1175.
113. K. Luo, T. Xie and J. Rzayev, *J. Polym. Sci. Part A Polym. Chem.*, 2013, **51**, 4992–4997.
114. B. J. Adzima, C. J. Kloxin and C. N. Bowman, *Adv. Mater.*, 2010, **22**, 2784–2787.
115. N. Pausan, Y. Liu, Y. Lu and A. R. Hutchinson, *J. Adhes.*, 2017, **93**, 791–810.
116. M. D. Banea, L. F. M. Da Silva and R. J. C. Carbas, *Int. J. Adhes. Adhes.*, 2015, **59**, 14–20.
117. S. Saito, S. Nobusue, E. Tsuzaka, C. Yuan, C. Mori, M. Hara, T. Seki, C. Camacho, S. Irle and S. Yamaguchi, *Nat. Commun.*, 2016, **7**, 1–7.
118. W. Seo, S. T. Phillips, T. Pennsyl, V. State, V. Uni, U. V Park and V. Pennsyl, 2010, **16802**, 9234–9235.
119. H. Kim, H. Mohapatra and S. T. Phillips, *Angew. Chemie - Int. Ed.*, 2015, **54**, 13063–13067.
120. K. Yamauchi, J. R. Lizotte and T. E. Long, *Macromolecules*, 2003, **36**, 1083–1088.

121. K. Zhang, M. Aiba, G. B. Fahs, A. G. Hudson, W. D. Chiang, R. B. Moore, M. Ueda and T. E. Long, *Polym. Chem.*, 2015, **6**, 2434–2444.
122. S. Cheng, M. Zhang, N. Dixit, R. B. Moore and T. E. Long, *Macromolecules*, 2012, **45**, 805–812.
123. G. M. L. Van Gemert, J. W. Peeters, S. H. M. Söntjens, H. M. Janssen and A. W. Bosman, *Macromol. Chem. Phys.*, 2012, **213**, 234–242.
124. D. H. Turkenburg, H. van Bracht, B. Funke, M. Schmider, D. Janke and H. R. Fischer, *J. Appl. Polym. Sci.*, 2017, **134**, 1–11.
125. Z. Guo, Y. Zuo and S. Feng, *RSC Adv.*, **6**, 73140–73147.
126. D. Yun, B. Kim, S. T. Oh, G. N. Kim, H. K. Jeon and M. Shon, in *IEEE CEFC 2016 - 17th Biennial Conference on Electromagnetic Field Computation*, 2017, p. 11.
127. D. H. Bae, P. H. Shin, S. T. Kwak, M. J. Moon, M. Y. Shon, S. T. Oh and G. N. Kim, *J. Ind. Eng. Chem.*, 2015, **30**, 92–97.
128. E. A. Riess, A. G. Malofsky, J. P. Barber and D. P. Bauer, *Method of Adhesive Bonding by Induction Heating*, US6849837., 2005.
129. D. E. Novorsky and R. J. Bednarz, *Induction Heating for Adhesive Bonding*, US4749833, 1998.
130. A. S. Ahmed and R. V. Ramanujan, *Sci. Rep.*, 2015, **5**, 1–10.
131. S. Salimi, T. S. Babra, J. Nightingale, W. Hayes and B. W. Greenland, *Induction Heating as an Effiecient Stimulus to Activate a Rebondable Nanocomposite Adhesive*, 2018.
132. M. D. Banea, L. F. M. da Silva, R. J. C. Carbas and S. de Barros, *J. Adhes.*, 2017, **93**, 756–770.
133. C. Heinzmann, U. Salz, N. Moszner, G. L. Fiore and C. Weder, *ACS Appl. Mater. Interfaces*, 2015, **7**, 13395–13404.
134. J. R. Kumpfer and S. J. Rowan, *J. Am. Chem. Soc.*, 2011, **133**, 12866–12874.
135. F. P. Nicoletta, D. Cupelli, P. Formoso, G. de Filpo, V. Colella and A. Gugliuzza, *Membranes*, 2012, **2**, 134–197.
136. P. Wagner and P. Theato, *Polymer*, 2014, 55, 3436–3453.
137. G. Wang, D. Yuan, T. Yuan, J. Dong, N. Feng and G. Han, *J. Polym. Sci. Part A Polym. Chem.*, 2015, **53**, 2768–2775.
138. M. A. Ayer, Y. C. Simon and C. Weder, *Macromolecules*, 2016, **49**, 2917–2927.
139. H. Akiyama, M. Yoshida, H. Kihara, Y. Norikane and R. Azumi, *J. Photopolym. Sci. Technol.*, 2014, **27**, 301–305.
140. H. Akiyama, T. Fukata, A. Yamashita, M. Yoshida and H. Kihara, *J. Adhes.*, 2017, **93**, 823–830.
141. H. Mutlu, C. M. Geiselhart and C. Barner-Kowollik, *Mater. Horizons*, 2018, **5**, 162–183.
142. Y. Li, O. Rios, J. K. Keum, J. Chen and M. R. Kessler, *ACS Appl. Mater. Interfaces*, 2016, **8**, 15750–15757.
143. E. Kizilkan, J. Strueben, A. Staubitz and S. N. Gorb, *Sci. Robot.*, 2017, **2**, eaak9454.
144. H. Akiyama, S. Kanazawa, Y. Okuyama, M. Yoshida, H. Kihara, H. Nagai, Y. Norikane and R. Azumi, *ACS Appl. Mater. Interfaces*, 2014, **6**, 7933–7941.
145. Y. Takashima, T. Sahara, T. Sekine, T. Kakuta, M. Nakahata, M. Otsubo, Y. Kobayashi and A. Harada, *Macromol. Rapid Commun.*, 2014, **35**, 1646–1652.
146. R. S. Givens, P. G. Conrad II, A. L. Yousef and J.-I. Lee, in *CRC Handbook of Organic Photochemistry and Photobiology*, eds. W. Horspool and F. Lenci, CRC Press, USA, 2nd edn., 2003, pp. 694–699.
147. J. A. Barltrop, P. J. Plant and P. Schofield, *Chem. Commun.*, 1966, **22**, 822–823.
148. S. M. June, T. Suga, W. H. Heath, Q. Lin, R. Puligadda, L. Yan, D. Dillard and T. E. Long, *J. Adhes.*, 2013, **89**, 548–558.
149. M. Kim and H. Chung, *Polym. Chem.*, 2017, **8**, 6300–6308.

150. X. Ji, K. Zhu, X. Yan, Y. Ma, J. Li, B. Hu, Y. Yu and F. Huang, *Macromol. Rapid Commun.*, 2012, **33**, 1197–1202.
151. M. K. Nguyen, C. T. Huynh and D. S. Lee, *Polymer*, 2009, **50**, 5205–5210.
152. H.-J. Schneider, *Chemoresponsive Materials: Stimulation by Chemical and Biological Signals*, Royal Society of Chemistry, Cambridge, UK, 1st edn., 2015.
153. P. G. Lawrence and Y. Lapitsky, *Langmuir*, 2015, **31**, 1564–1574.
154. E. J. Corey and A. Venkateswarlu, *J. Am. Chem. Soc.*, 1972, **94**, 6190–6191.
155. A. Sagi, R. Weinstain, N. Karton and D. Shabat, *J. Am. Chem. Soc.*, 2008, **130**, 5434–5435.
156. R. J. Amir, N. Pessah, M. Shamis and D. Shabat, *Angew. Chem. Int. Ed. Engl.*, 2003, **42**, 4494–4499.
157. L. Ernesto Mendoza-Navarro, A. Diaz-Diaz, R. Castañeda-Balderas, S. Hunkeler and R. Noret, *Int. J. Adhes. Adhes.*, 2013, **44**, 36–47.
158. J. P. H. Belnoue and S. R. Hallett, *Int. J. Adhes. Adhes.*, 2016, **68**, 359–368.
159. American Society for Testing Materials, Adhesive Standards, https://www.astm.org/Standards/adhesive-standards.html, (accessed 14 May 2018).
160. American Society for Testing Materials, ASTM D1002-10: Standard Test Method for Apparent Shear Strength of Single-Lap-Joint Adhesively Bonded Metal Specimens by Tension Loading (Metal-to-Metal), https://www.astm.org/Standards/D1002.htm, (accessed 14 May 2018).
161. American Society for Testing Materials, ASTM D2095-96(2015): Standard Test Method for Tensile Strength of Adhesives by Means of Bar and Rod Specimens, https://www.astm.org/Standards/D2095.htm, (accessed 14 May 2018).

Chapter 2

Fluoride Degradable and Thermally Debondable Polyurethane based Adhesive

This chapter has, in part, been published by the author as a research article entitled "Fluoride degradable and thermally debondable polyurethane based adhesive" by T. S. Babra, A. Trivedi, C. N. Warriner, N. Bazin, D. Castiglione, C. Siviour, W. Hayes and B. W. Greenland, Polym. Chem., 2017, 8, 7207-7216."

Note of Contribution: A. Trivedi carried out the rheological (Figure 2.6) and dynamical mechanical analysis (Figure 2.7) at the University of Oxford supervised by Professor C. Siviour. T. S. Babra carried out all other work detailed below. C. N. Warriner, N. Bazin and D. Castiglione were industrial supervisors from AWE Plc. Professor W. Hayes and Dr B. W. Greenland were supervisors at the University of Reading.

Abstract

In this chapter is reported the one-pot, solvent free synthesis of a stimuli-responsive polyurethane (PU) adhesive. The hard domains within the supramolecular PU network contain a silyl protected phenol 'degradable unit' (DU). The DU undergoes rapid decomposition (<30 minutes) upon treatment with fluoride ions which causes depolymerisation of the linear PU adhesive. The mechanism of depolymerisation was investigated in solution using ^{1}H NMR spectroscopy by following the degradation of the polymer in the presence of *tetra*-butylammonium fluoride (TBAF). In the absence of fluoride ions, the material behaves as a typical thermoplastic adhesive, and underwent four adhesion/separation cycles without loss of strength. The fluoride initiated depolymerisation of the PU adhesive in the solution state was verified by GPC analysis, showing reduction in M_n from 26.1 kgmol^{-1} for the pristine PU to 6.2 kgmol^{-1} for the degraded material. Degradation studies on solid samples of the PU which had been immersed in acetone/TBAF solution for 30 minutes exhibited a 91 % reduction in their modulus of toughness (from 27 to 2 MJ m^{-3}). Lap shear adhesion studies showed the fluoride responsive PU was an excellent material to join metallic, plastic, glass and wood surfaces. Pull adhesion tests confirmed that immersing the adhesive in TBAF/Acetone solution resulted in a reduction in strength of up to 40% (from 160 N to 95 N at break) after drying.

2.1. Introduction

Materials with applications as adhesives, sealants and coatings are a vibrant area of polymer chemistry.[1] This scientific interest in this field is driven by the industrial importance of the products which include hot melt adhesives,[2–8] hydrogels,[9–13] epoxy resins[6,14–17] and cross-linked adhesives.[18–20] A more recent addition of this research field is the study of responsive adhesives. These materials are able to debond in response to a stimulus or can exhibit reversible properties which allow for multiple adhesion/separation/adhesion cycles without loss of strength. Responsive adhesives are finding an ever-expanding market, where they replace traditional fabrication methods such as riveting or welding yet permit easy disassembly of the component at the end of its lifecycle. This class of adhesive is becoming increasingly important in order to facilitate more rapid and cost-effective recycling of key components and materials.

The externally controlled temporary reduction in tensile modulus and/or adhesion strength has been demonstrated for various systems, for example, in supramolecular materials or those containing dynamic covalent bonds.[21] This progress in bottom-up material design has facilitated the immergence of new technologies[22,23] across a broad range of disciplines including biomedical applications,[24–27] sensors,[28] healable[29] and damage sensing materials[30] as well as improving product recyclability.[25,31,32]

With respect to reversible adhesive materials, dynamic covalent chemistries[21] have, to date, received the most attention. Typically, these materials break down from high strength to low strength networks on application of a suitable external stimulus (e.g. heat/ light). Removal of that stimulus can lead to a restoration of the pristine properties of the material. This was recently shown by Rowan *et al.* who produced a reversible adhesive harnessing the dynamic nature of the disulfide bond when irradiated with high intensity UV light.[29] Aubert *et al.* produced a debondable epoxide based adhesive which made use of the thermo-reversible (110 °C) formation of the Diels-Alder adduct formed between furan and maleimide precursors.[14] Weder and co-workers synthesised an aliphatic azo containing polymer, which breaks down with either heat or high intensity UV light, weakening the material.[33] Bao and co-workers showed the use of a reversible boroxine bond, which breaks by hydrolysis or force and but can reform by loss of water.[34] (See Chapter 1, section 1.2.5).

A conceptually distinct class of polymeric adhesive that can debond on command are those that contain supramolecular non-covalent interactions which form a reversible network.[35] Thermo-responsive supramolecular adhesives utilising hydrogen bonding[22,36–41] have been

demonstrated, in addition to those that harness metal/ligand interactions which were responsive to both light and heat.[22]

An extra functionality that can be built into these systems is the ability to undergo a permanent reduction in tensile modulus/adhesion strength which persists after the stimulus has been removed. This could be achieved by using a depolymerisable material that undergoes an irreversible reduction in molecular weight leading to a permanent reduction in strength. This was recently demonstrated by Phillips and co-workers who designed an adhesive **2.4** (Scheme 2.1) that degrades on contact with fluoride ions.[42] In this system, fluoride ions caused degradation of an intractable, crosslinked material resulting in a dramatic weakening of the adhesive. There are a couple of disadvantages to this material; first is the 11 synthetic steps required to make this material; and secondly, the adhesive is not thermally reversible as a result of its crosslinking nature.

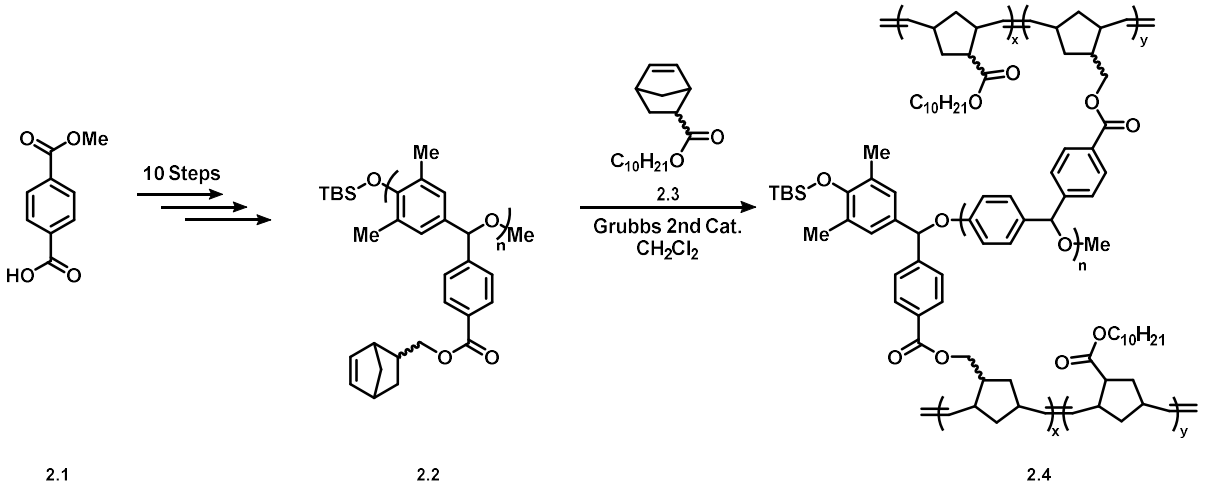

Scheme 2.1 *Synthesis of the fluoride degradable adhesive designed by Philips and co-workers.*

Herein is presented the design and synthesis of a chemo-responsive depolymerisable hot melt adhesive. In contrast to the previous crosslinked fluoride responsive systems (Scheme 2.1), this novel linear polyurethane (PU) behaves like a typical reversible adhesive, undergoing multiple break/re-adhesion cycles without loss of bonding strength (Scheme 2.2). However, the PU also contains multiple fluoride responsive depolymerisable units in the main chain. Contact with fluoride ions results in a permanent reduction in molecular weight and consequently a reduction in the strength of the bond between the components without further application of the stimulus. This approach enables this system to be: i) multi-stimuli responsive, exhibiting reversible adhesive properties in response to heat and permanent loss of adhesion in response to a chemical stimulus and ii) chemo-responsive in nature to permit use in situations where they are thermally sensitive or are not transparent at appropriate wavelengths.

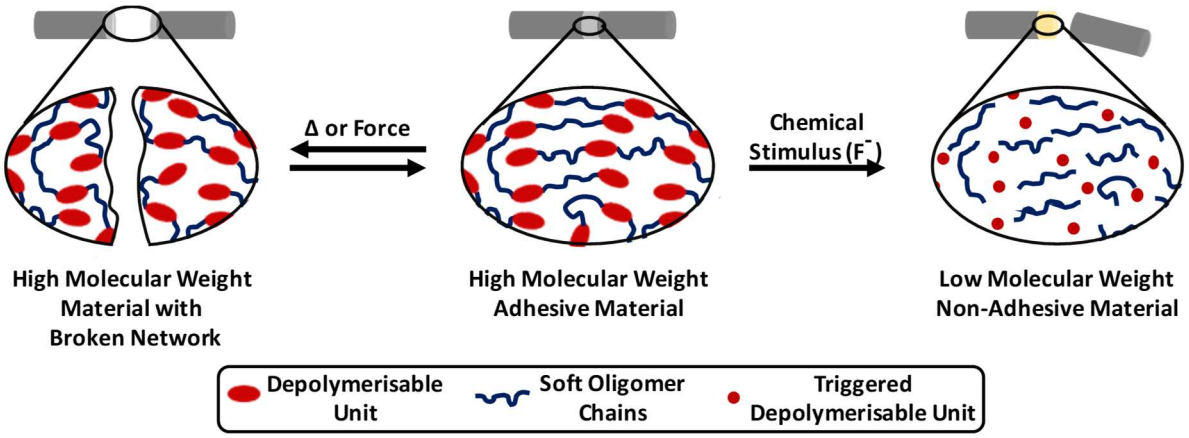

Scheme 2.2 *Schematic showing the rebondable nature of the adhesive in response to elevated temperatures, and complete non-reversible depolymerisation in response to fluoride ions.*

2.2. Results and Discussion

2.2.1. Synthesis of Degradable Unit and Model Compound Testing

Previously, Akkaya and co-workers[43] have shown that *tert*-butyl dimethylsilyl (TBDMS) protected cresol **2.6**, synthesised by a simple two-step process, can be reacted with dioxetane to produce a biscarbonate **2.8**. This species can undergo fluoride initiated degradation of the carbonate functionalities accompanied by loss of CO_2. Shabat and co-workers showed the use of carbamate functionalities as part of an amplified drug release molecule.[44] Inspired by these reports, the degradable unit (DU) **2.6** was synthesised (Scheme 2.3) which was incorporated into a linear PU to result in a degradable system triggered by fluoride anions.

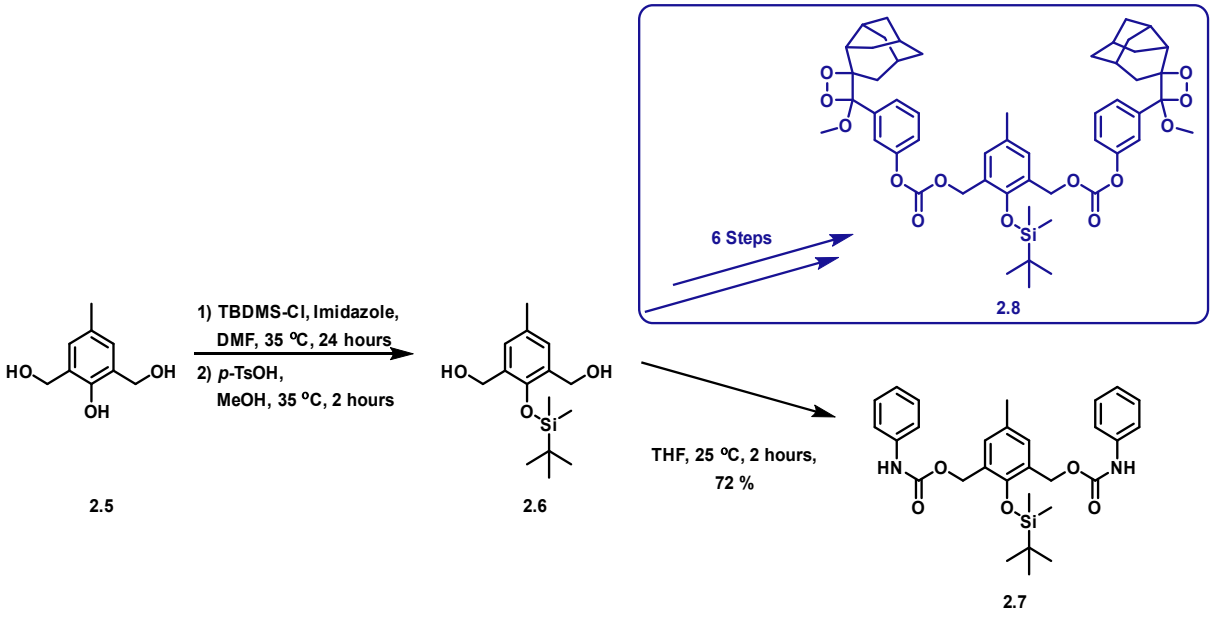

Scheme 2.3 *Synthesis of the degradable unit (**2.6**) and model bisurethane compound (**2.7**).*

Before synthesising polymers and testing complex polyurethane systems, it was first important to demonstrate the selective response of the DU **2.6** to fluoride ions. A model bisurethane compound (**2.7**, Scheme 2.3) was synthesised using phenyl isocyanate end groups. This end group was chosen as it would closely mimic the degradation of the polymer proposed (Scheme 2.7). The proposed mechanism for degradation of **2.7** with fluoride ions is detailed in Scheme 2.4.

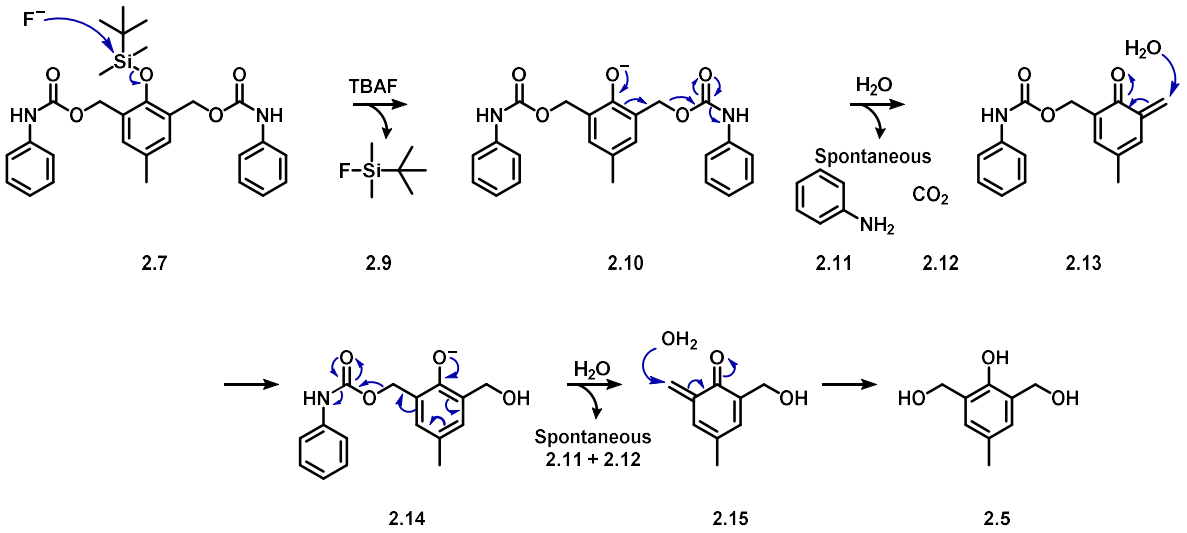

Scheme 2.4 *Proposed mechanism of degradation of DU* ***2.6*** *as part of the model bisurethane model* ***2.7****.*

Degradation of the **2.7** was achieved by the addition of a fluoride source (*tetra*-butylammonium fluoride, TBAF) to a solution of **2.7** in DMSO and followed by ^{1}H NMR spectroscopy (Figure 2.1). Degradation was observed readily by the loss of the singlet resonance signal (7.12 ppm) from the aromatic protons H_A (Scheme 2.5) on the cresol linker **2.7** within one minute of the addition of TBAF (see spectra A and B, Figure 2.1). Spectrum B shows two sets of resonances for two compounds; the first set from complete degradation observed by the appearance of H_I, H_J, and H_K from the released aniline group **2.11b** (a result of the consumption of any water from the TBAF·3H_2O salt and DMSO solvent). The second set of proton resonances is from the released phenyl carbamic acid **2.11a**, which has a short lifetime in aqueous environments. Addition of deuterium oxide was required to drive complete degradation of **2.11a**, resulting in the formation of aniline **2.11b**.

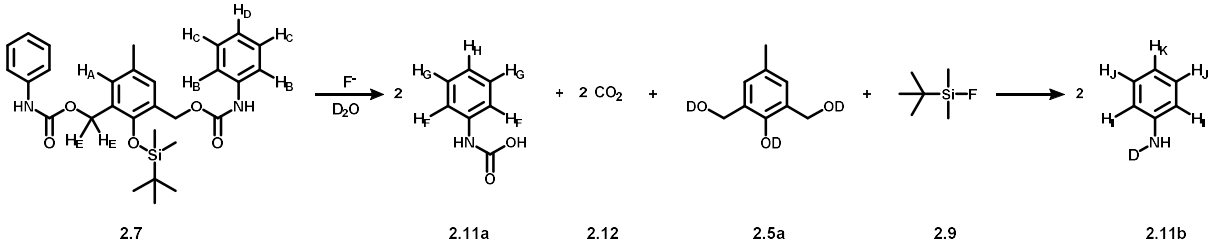

Scheme 2.5 *Proposed degradation of biscarbamate **2.7** upon treatment of fluoride ions, followed by D_2O.*

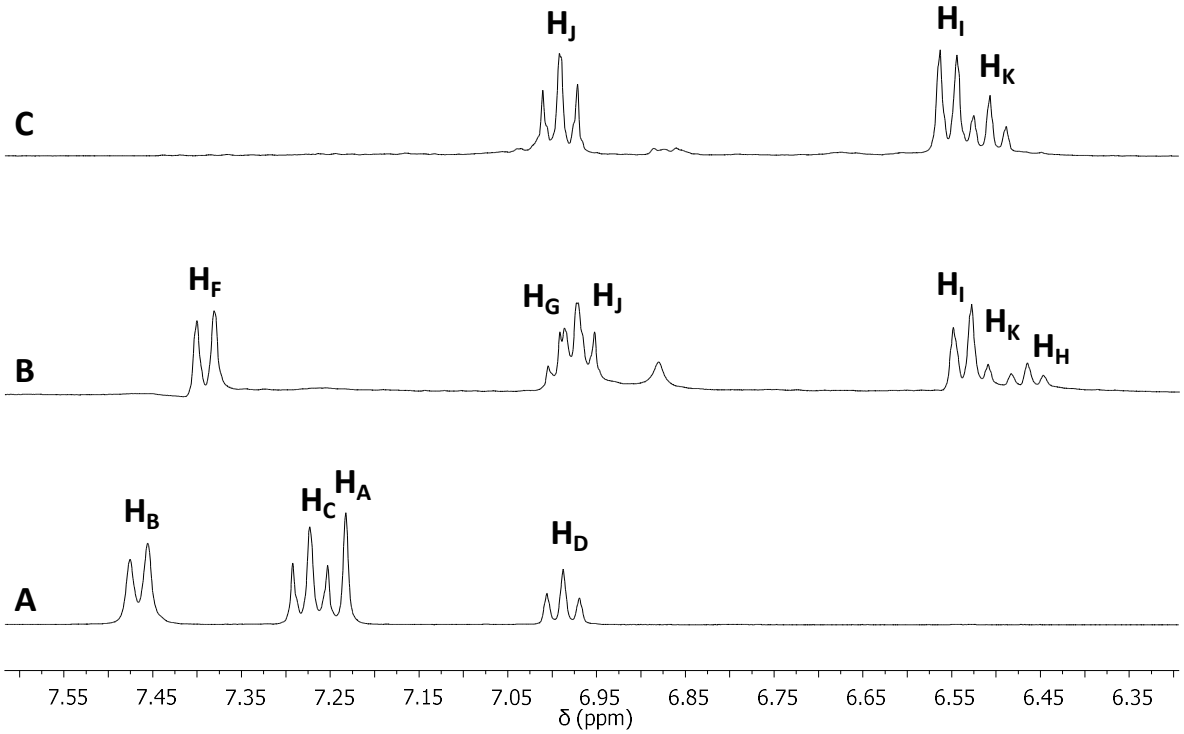

Figure 2.1 *^{1}H NMR spectra showing the two-step degradation of (A) the model compound **2.7** (B) after addition of TBAF, followed by (C) addition of deuterium oxide. (DMSO-d_6, 400 MHz)*

Upon addition of the fluoride ions to the model bisurethane compound **2.7**, a colour change from colourless to yellow was observed (Figure 2.2a). The origin of this colour change was investigated by UV/visible spectroscopy by recording a spectrum of model compound **2.7**, cresol **1**, phenyl isocyanate, TBDMS-Cl and TBAF; as well as a mixture of **2.7** + TBAF and **2.5** + TBAF (Figure 2.2b).

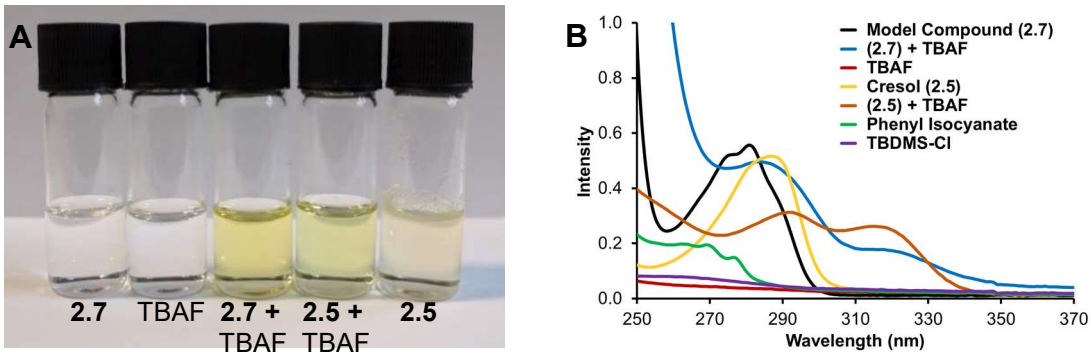

C

	λ_{max} (nm)
Model Bisurethane Compound **2.7**	275, 281
2.7 + TBAF	285, 321
TBAF	-
Cresol **2.5**	287
2.5 + TBAF	292, 317
Phenyl isocyanate	263, 270, 277
TBDMS-Cl	-

Figure 2.2 *(A) Addition of TBAF to model compound (**2.7**) causes a yellow solution to form; which is a result of the formation of cresol interacting with excess TBAF salt. (B) UV-visible spectra of the model compound and its constituents before and after addition of TBAF. (C) λ_{max} values taken from the UV-visible spectra.*

The model compound **2.7**, which is colourless in solution, shows two absorbances at 275 and 281 nm which shift on addition to 285 and 321 nm upon addition of TBAF. The cresol **2.5** solution, which is pale yellow in colour, shows an absorbance maximum at 287 nm. Upon addition of TBAF to cresol **2.5**, the colour changes to a vibrant yellow, similar to that of the model compound **2.7** and TBAF. The absorbances of cresol **2.5** + TBAF are 292 and 317 nm, which are similar to that of model compound **2.7** + TBAF. Therefore, the data shows that on addition of TBAF to model bisurethane compound **2.7**, the breakdown forms the cresol core unit **2.5**, which forms a phenoxide ion in the presence of TBAF to produce a vibrant yellow mixture; evidenced by the similar λ_{max} values. Thus proving the colour change was a result of the formation of cresol **2.5** interacting with TBAF salts and that the production of **2.5** as seen in the proposed mechanism (Scheme 2.3) is correct.

Two experiments were carried out to determine the selectivity of the fluoride ions to the DU **2.6**. The first experiment was to prove that the degradation of the DU **2.6** was a result of a reaction with fluoride ions and not TBAF. The second experiment designed was to show that the fluoride ions were reacting selectively with the silyl protecting group, over the other functional groups in the system.

The model bisurethane compound **2.7** was reacted with different *tetra*-butylammonium halide salts. *Tetra*-butylammonium chloride (TBAC), *tetra*-butylammonium bromide (TBAB) and *tetra*-butylammonium iodide (TBAI) were reacted with **2.7** and compared to the reaction of **2.7** with TBAF. The reactions were monitored by ^{1}H NMR spectroscopy (Figure 2.3). As evident by the ^{1}H NMR spectra and colour change, only the TBAF triggered degradation even after 24 hour exposure to each halide ion, confirming the selectivity to fluoride ions.

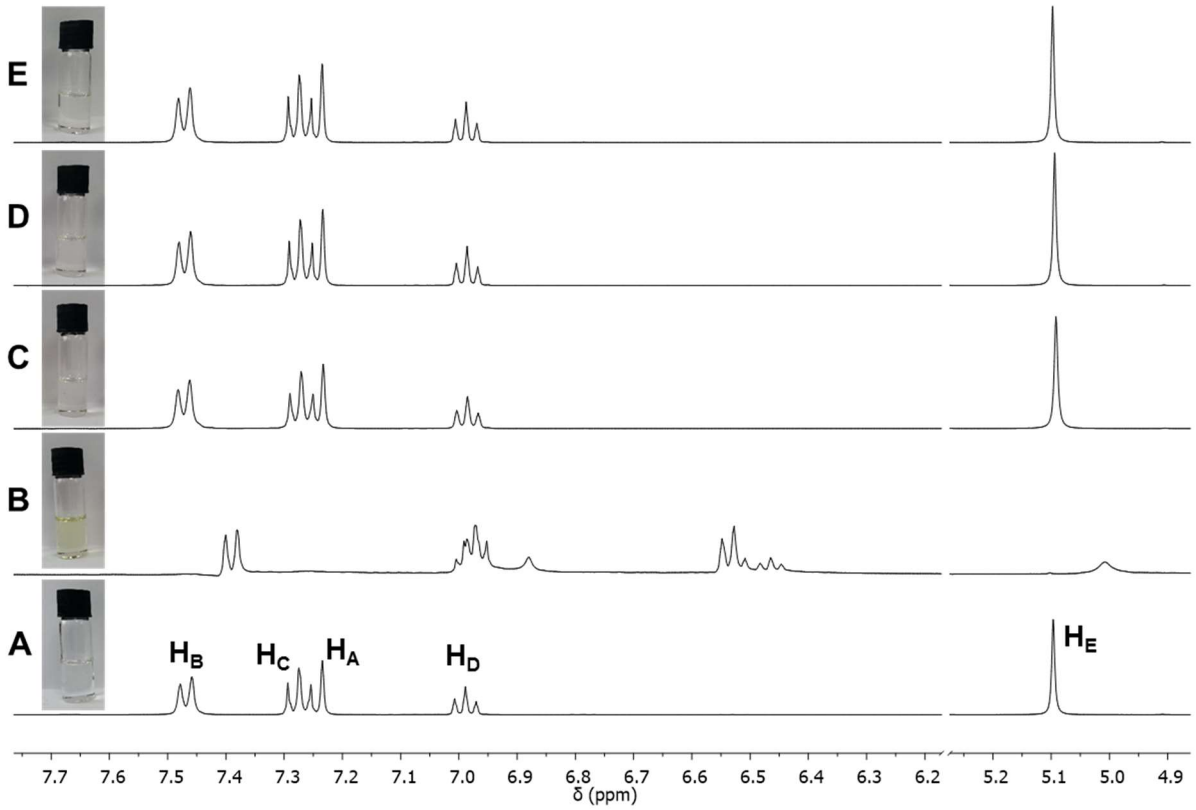

Figure 2.3 *Selectivity of the silyl group to the fluoride ion as determined by ^{1}H NMR spectroscopy. (A)* ***2.7****, (B)* ***2.7*** *+ TBAF, (C)* ***2.7*** *+ TBAC, (D)* ***2.7*** *+ TBAB, and (E)* ***2.7*** *+ TBAI. Photos show colour change from addition of TBAF and not from other tetra-butylammonium salts.*

To further understand the selectivity of fluoride ions to the silyl group of the DU **2.6** and model compound **2.7**, a second degradable unit with a methoxy group **2.16** was synthesised to determine if the cresol linker were affected by the addition of fluoride ions. A model bisurethane compound **2.17** was also synthesised to determine if the carbamate groups or the aniline reporter groups were affected by the addition of fluoride ions (Scheme 2.6).

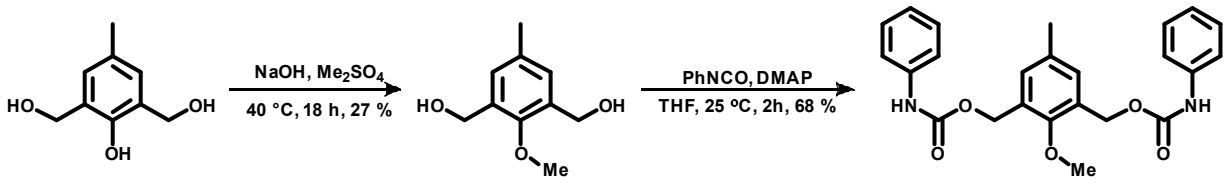

2.5 **2.16** **2.17**

Scheme 2.6 *Synthesis of a methoxy analogue model compound to show that TBAF reacts with the silyl group, not the other functional groups.*

Both the methoxy analogue of the DU **2.16** and model bisurethane compound **2.17** were reacted with TBAF and followed by ^{1}H NMR spectroscopy (Figure 2.4). On addition of TBAF to **2.17** (Figure 2.4a **2.16**, and Figure 2.4b **2.16** + TBAF), no shifts in proton resonances were recorded demonstrating that TBAF does not react with the core cresol group. However, on addition of TBAF to **2.17** (Figure 2.4c pristine, and Figure 2.4d with TBAF), the aromatic resonances shifted and a small loss in intensity/resolution was observed. This is a result of the deprotonation of the urethane proton at 6.71 ppm (Figure 2.4c) by fluoride ions. This does not result in breakdown of the molecule; and hence proves that fluoride ions only affect the silyl group. Further proof that **2.17** did not react with TBAF was determined by mass spectroscopy. Analysis of a sample containing both **2.17** and TBAF revealed mass ions $[M + Na]^{+}$ for 443.1577 Da and 284.1285 Da, respectively (calculated values for. **2.17** = 443.1583 Da and TBAF = 284.4498 Da), and mass ions for degraded materials were not evident.

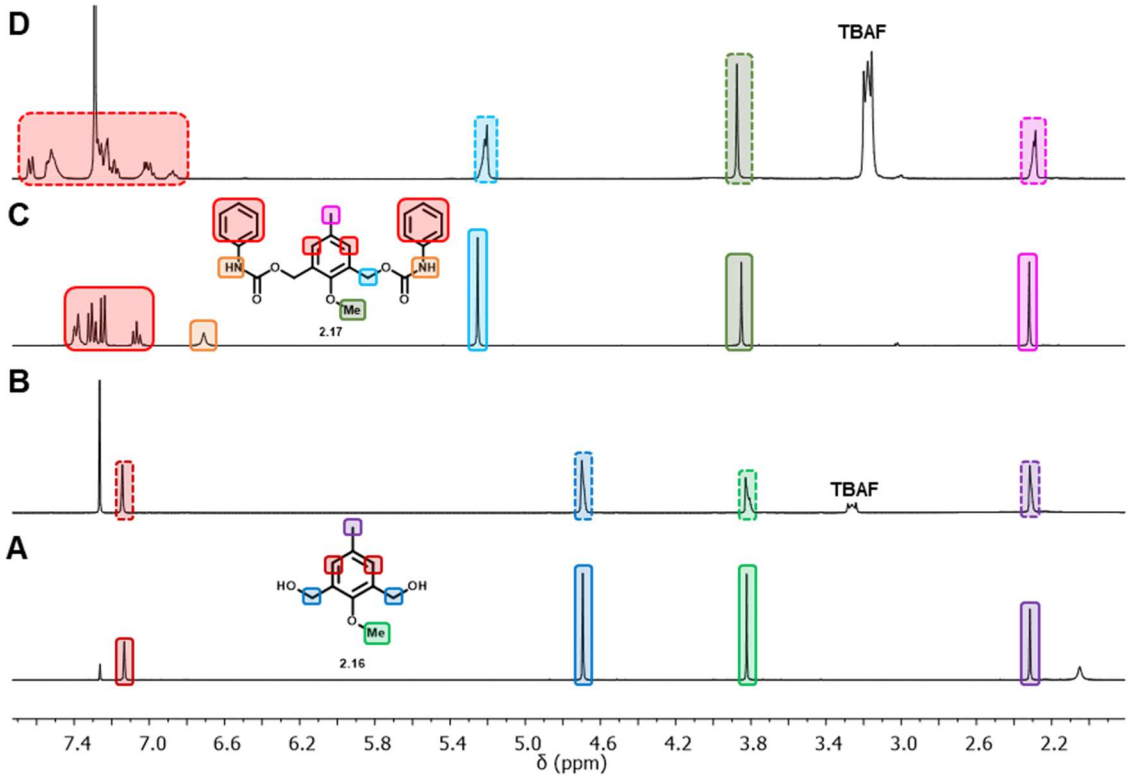

Figure 2.4 *^{1}H NMR spectra representing (A)* ***2.16****, (B)* ***2.16*** *+ TBAF, (C)* ***2.17****, and (D)* ***2.17*** *+ TBAF.*

These experiments demonstrated that degradation of **2.7** was initiated by the selective reaction of fluoride ions with the silyl group and confirmed the suitability of **2.6** as the responsive degradation unit in PU-type polymeric architectures.

2.2.2. Polymer Synthesis

With the synthesis and selective degradation of the novel fluoride selective DU evaluated, attention turned to the synthesis of the responsive PU adhesive. This was synthesised using a one-pot, two step synthesis.[45–47] Initially, an isocyanate terminated pre-polymer **2.20** was produced by addition of methylene diphenyl diisocyanate (4,4'-MDI) **2.19** to Krasol HLBH-P 2000 (Krasol) **2.18** at 80 °C (Scheme 2.7). After 3 hours, the DU **2.6** was added and the temperature increased to 100 °C, (melting point of **2.6** is 93 - 95 °C) and the resulting homogeneous mix stirred until it solidified to give the crude polymer (Scheme 2.7). Purification was achieved by slow precipitation in methanol.

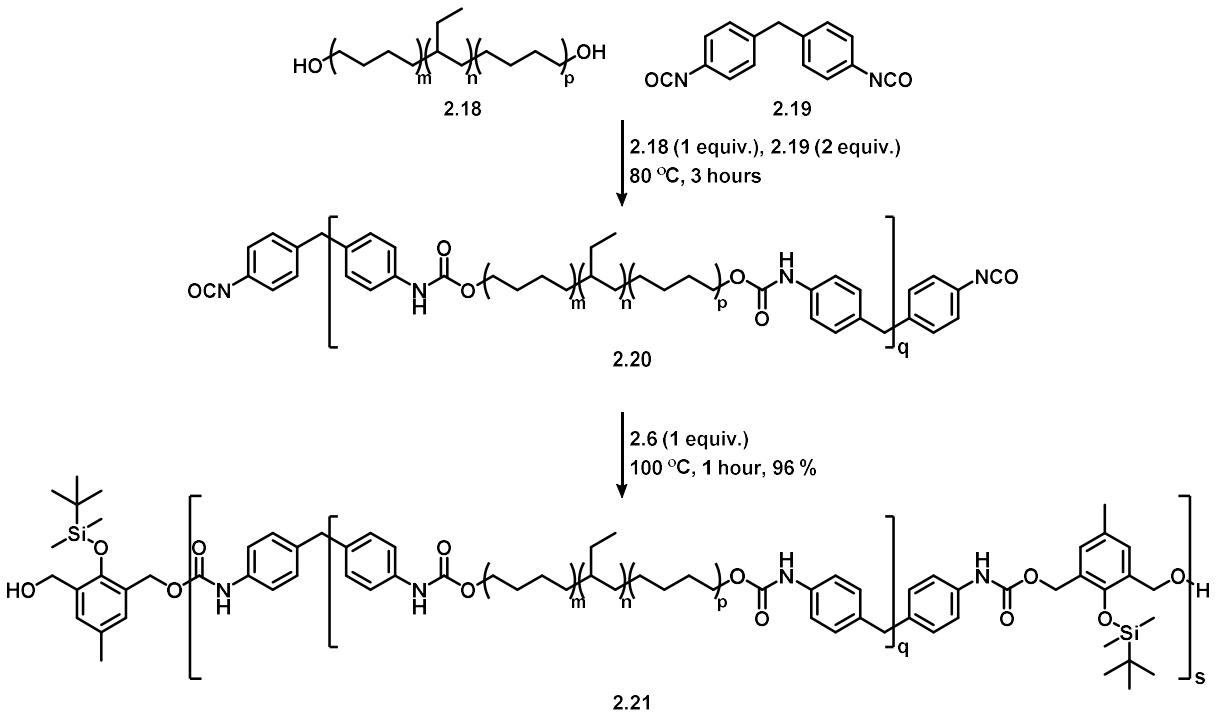

Scheme 2.7 *Solvent free synthesis of the adhesive polymer using Krasol, 4,4'-MDI and the DU (q = 1, 2; s = 19).*

^{1}H NMR spectroscopic analysis showed a shift from 4.7 ppm to 5.2 ppm for the methylene resonance of the DU, indicating formation of the polyurethane. A residual resonance at 4.7 ppm was detected and determined to be the methylene groups at the end of the polymer chains. Using the integrals of the two resonances at 4.7 ppm and 5.2 ppm, the amount of chain extension (denoted as *s*) was determined to be 15 repeat units. GPC analysis of polymer **2.21** revealed

essentially monomodal distribution with M_w 71400 gmol^{-1}, M_n 26100 gmol^{-1} and $Đ$ 2.73, indicating that significant chain extension occurs during the reaction (Krasol **2.18** = M_w 3700 gmol^{-1}, M_n 3300 gmol^{-1}); with s = 19. These values are in broad agreement with Carother's equation (Equation 2.1) (s = $\bar{X}$ = 25) and that any discrepancies could be a result of monomer purity.

$$\bar{X}_n = \frac{1}{1-p}$$

Equation 2.1 *Calculation for the degree of polymerisation for a liner polymer system with two equimolar quantities of monomers. Where* $\bar{X}$ *= degree of polymerisation, p = extent of conversion.*

The thermal properties of the material were studied using differential scanning calorimetry (DSC) and dynamic mechanical analysis. DSC of the polymer showed a glass transition temperature (T_g) at *ca*. -45 °C, which is similar to that of the starting Krasol (T_g *ca*. -46 °C), and is indicative of a phase separated material. The T_g was unaltered over 3 heat/cool cycles showing thermoreversible nature of the material. No polymer melt was seen in the DSC data over the temperature range studied confirming the amorphous nature of the material.

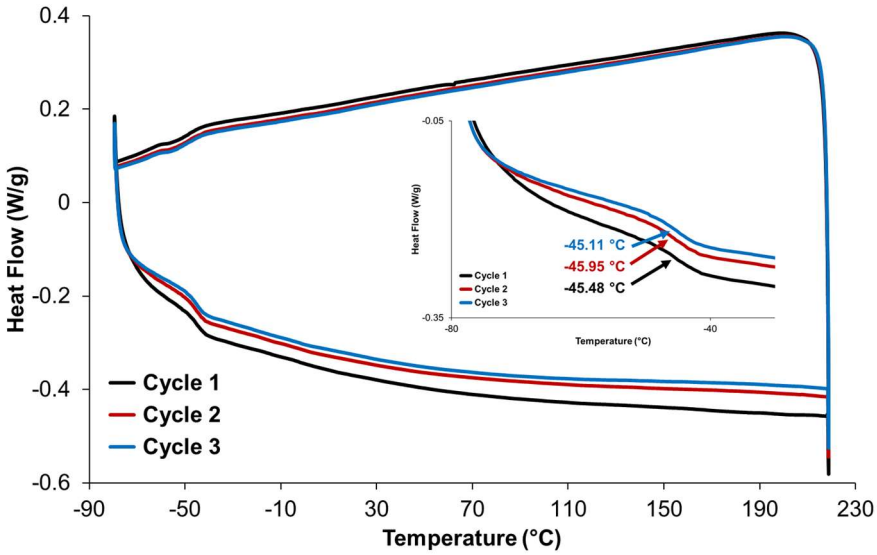

Figure 2.5 *DSC thermogram of the three heat – cool cycles of Polymer* ***2.21****. Insert shows glass transitions from each cycle.*

Polymer **2.21** was subject to dynamic mechanical analysis, DMA (Figure 2.6) and rheological testing (Figure 2.7) by A. Trivedi at the University of Oxford to further investigate the thermomechanical response of the material. In the DMA data, a phase transition was observed at approximately -45 °C, indicating the glass transition temperature and agreeing with the DSC results. A sharp decrease in both storage and loss modulus was observed at temperatures between the T_g and -30 °C, followed by a gradual decrease until specimen failure at 87 °C.

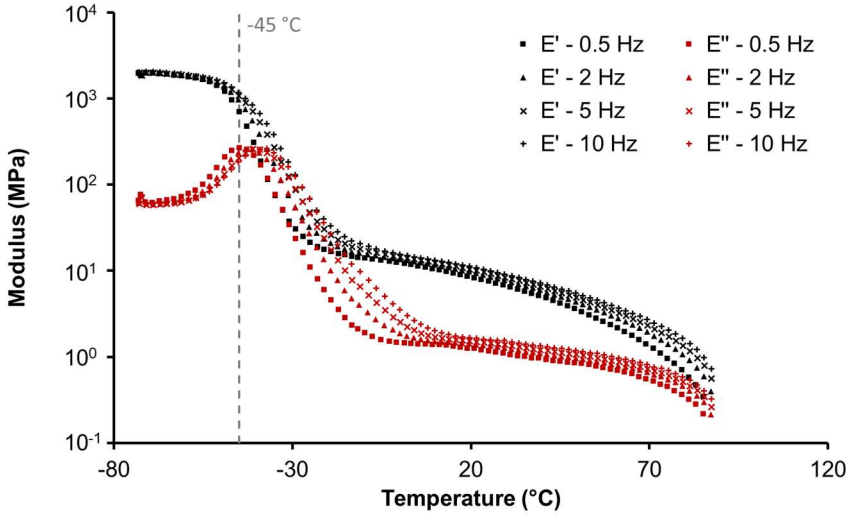

Figure 2.6 *Raw data of storage (E') and loss (E'') moduli superimposed taken at different frequencies, as a function of temperature.*

Rheological data were obtained at temperatures up to 150 °C, with data shown between 110 °C and 150 °C in Figure 2.7. A viscoelastic transition was observed at 128 °C, at the intercept of G' and G''. This remained constant through the three cool-heat cycles. These data clearly show the thermo-reversible nature of the material.

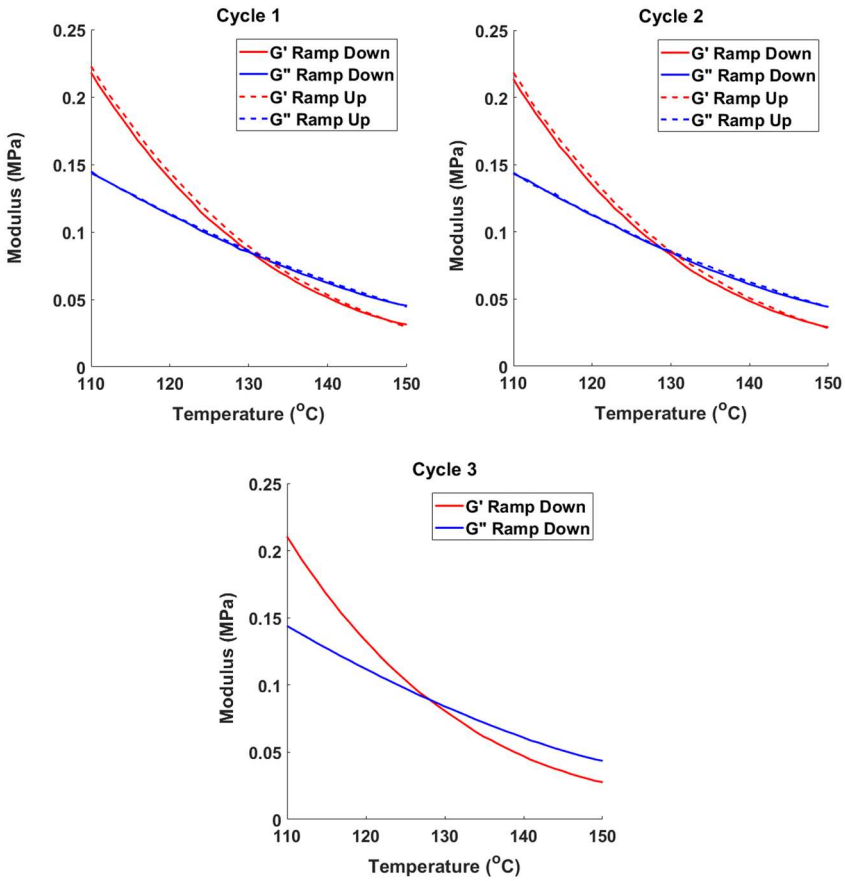

Figure 2.7 *The rheological data of polymer* ***2.21*** *from the three cool-heat cycles, with a cross over at approximately 129 °C throughout all cycles.*

2.2.3. Polymer degradation studies

From analysis of the fluoride initiated degradation studies conducted on a model compound, the proposed scheme for degradation of polymer **2.21** is shown in Scheme 2.8, with mechanistic break down detailed within the box. As previously discussed with the model compound studies, upon addition of fluoride ions, the silyl group would readily cleave to form the *tert*-butyldimethylsilyl fluoride **2.9** and a phenoxide ion, which spontaneously degrades[44] to release carbon dioxide **2.12** and the degraded polymer backbone **2.22**. The quinone reacts with water, provided from the TBAF·3H_2O fluoride salt, to achieve the cresol group **2.5**.

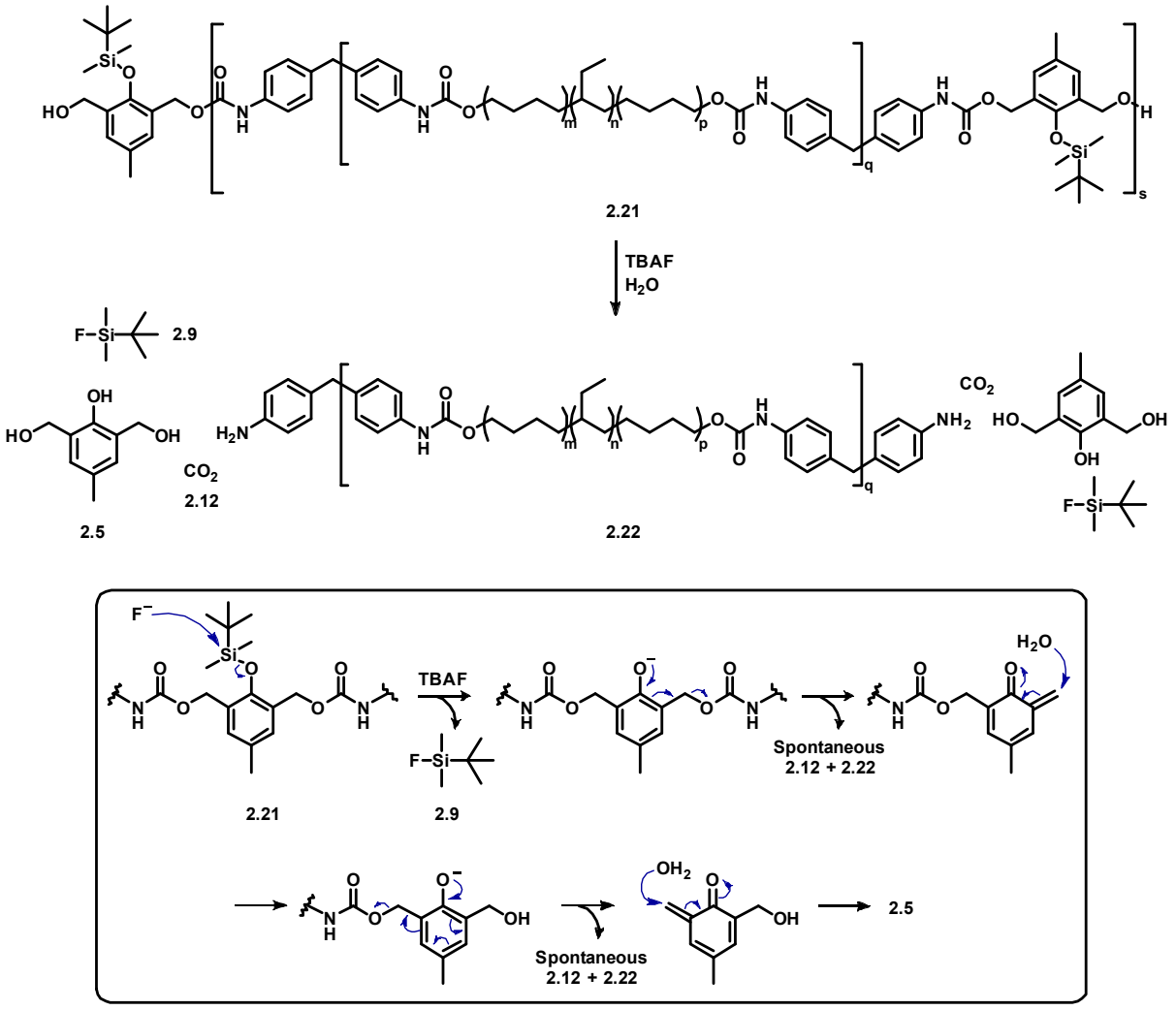

Scheme 2.8 *Depolymerisation of Polymer* ***2.21*** *after TBAF has been applied. Insert shows mechanistic break down of the degradable group within PU* ***2.21****.*

Degradation studies on the polymeric system were conducted initially in the solution state studies by addition of TBAF to a sample of **2.21** in $CDCl_3$ (1:1 molar equivalents of TBAF to degradable unit). The degradation was monitored by ^{1}H NMR spectroscopy. Within 1 minute of exposure to TBAF, the methylene proton resonances at 5.18 ppm and urethane N-H

resonances at 6.60 ppm were not evident in the ^{1}H NMR spectra of the solution of polymer **2.21** indicating rapid and efficient degradation of the polymer (Figure 2.8).

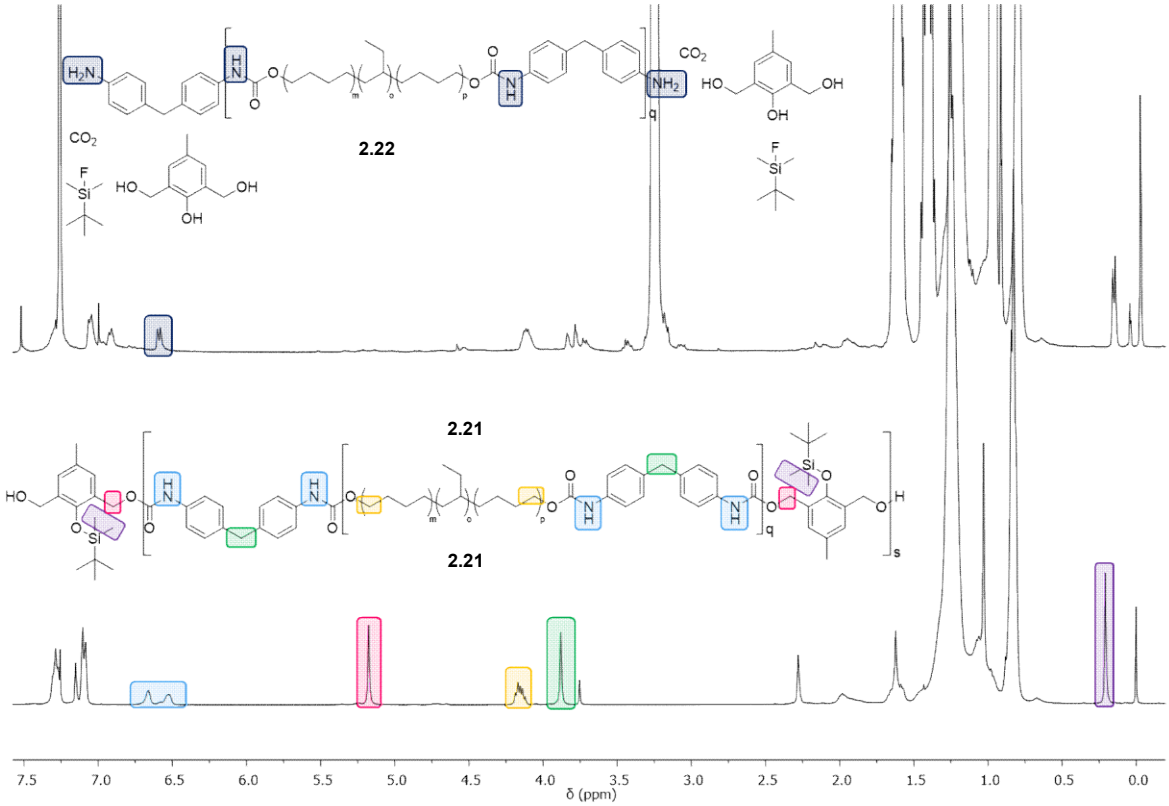

Figure 2.8 *^{1}H NMR spectra showing the degradation of Polymer **2.21** when treated with TBAF. ($CDCl_3$, 400 MHz).*

GPC eluograms of the Krasol **2.18**, polymer **2.21**, and the degraded polymer **2.22** are shown in Figure 2.9. The eluogram for the degraded material is clearly bimodal in nature, however, the overall distribution was calculated to have M_n 6.2 kgmol^{-1} and $Đ$ 1.73 (Figure 2.9, Table 2.1). This drop in molecular weight from polymer **2.21** (M_n = 26.1 kgmol^{-1}, $Đ$ 2.73) confirms the highly efficient fluoride ion initiated degradation of the system. The bimodal appearance of the eluogram of the degraded product has signal maxima at 13 and 3.7 kgmol^{-1}. The lower of the two M_n valued may be compared to the molecular weight of the starting Krasol, (M_n = 3.3 kgmol^{-1}). The persistence of a higher molecular weight fraction in the degraded product M_n = 6.3 kgmol^{-1} can be accounted for by considering uncontrolled nature of the polymerisation (Scheme 2.7). This results in significant chain extension during the synthesis of prepolymer **2.20** (Scheme 2.7), where multiple Krasol units may be connected by 4,4'-MDI residues which are not separated by the DU. Therefore, these Krasol-MDI-Krasol sections are not susceptible to degradation and persist in the molecular weight distribution of the degraded material. Indeed,

from the GPC results, it can be estimated that the value for "*q*" in **2.21** (Scheme 2.7) and **2.22** (Scheme 2.8) is approximately 2.

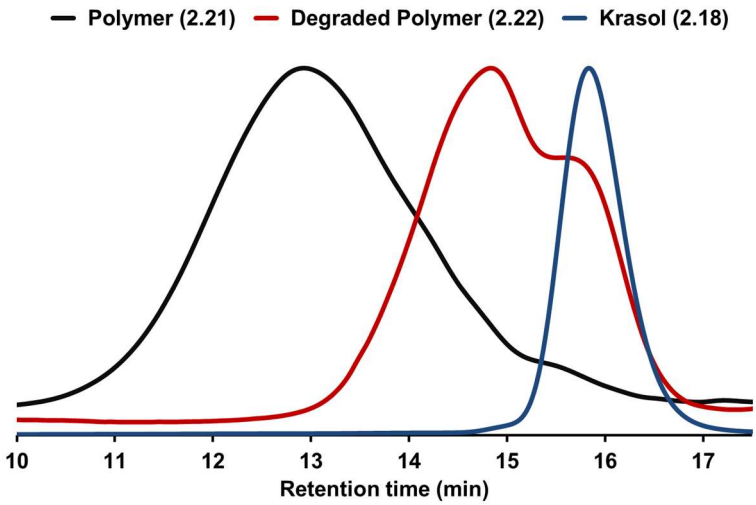

Figure 2.9 *GPC eluograms of polymer (**2.21**), degraded polymer (**2.22**) and the starting Krasol (**2.18**); (THF, PS standards).*

	M_w (gmol^{-1})	M_n (gmol^{-1})	*Đ*
Polymer (2.21)	71400	26100	2.7
Degraded Polymer (2.22)	10000	6200	1.7
Krasol (2.18)	3700	3300	1.1

Table 2.1 *Molecular weight estimation from the GPC chromatographs for polymer (**2.21**), degraded polymer (**2.22**) and Krasol (**2.18**); (THF, PS standards).*

2.2.4. Solid state mechanical testing and degradation studies

Attention then moved on to mechanical testing of polymer **2.21** which could be cast readily into large (15 × 15 cm) homogeneous films (Figure 2.10).

Figure 2.10 *Polymer film (15 × 15 cm) cast from THF used for mechanical testing.*

From a single casting, ten strips (4.0 × 0.5 cm) were produced of which five samples were immersed in 1M TBAF/Acetone, then dried at 40 °C for 30 minutes. The stress-strain profiles for pristine polymer **2.21** and the degraded polymer (**2.22**) are shown in Figure 2.11 with numerical mechanical data summarised in Table 2.2.

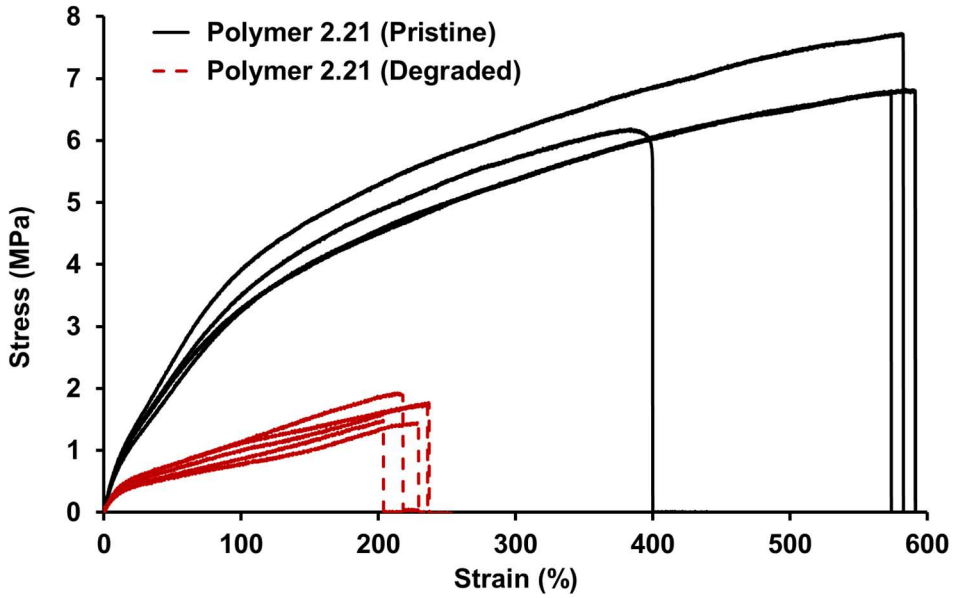

Figure 2.11 *Stress-strain curves for five samples of pristine polymer (**2.21**) and five samples of degraded polymer (**2.22**).*

	Tensile Modulus (MPa)	**Ultimate tensile Strength (MPa)**	**Elongation at break (%)**	**Toughness (MJ m^{-3})**
Polymer (2.21) Samples	2.56 (0.23)	6.90 (0.55)	531 (85)	27 (5.6)
Degraded Polymer (2.22) Samples	0.61 (0.14)	1.68 (0.20)	223 (14)	2 (0.4)

Table 2.2 *Mean (n = 5) mechanical properties of the pristine polymer (**2.21**), degraded material (**2.22**). Standard deviations are shown in brakets.*

The testing data show that the modulus of toughness of the fluoride degraded polymer (**2.22**) was just 9 % of that recorded for the pristine material **2.21**. The Young's modulus and ultimate tensile strength of the degraded polymer **2.22** both decreased by 76 % when compared to pristine polymer **2.21**. These data collectively show the dramatic effect that depolymerisation has on the physical properties of the polymer.

2.2.5. Adhesive Testing

To assess the adhesive properties of the stimuli responsive polymer, optimising the bonding conditions first had to be carried out. Adhesive tests were carried out on steel nails with 3.0 mm diameter round heads that were bonded using polymer **2.21** (Figure 2.12) for 30 minutes. Samples were bonded by heating at three different temperatures, 80, 120 and 160 °C for 30 minutes. Samples left at 80 °C showed adhesive failure as the samples fell apart as soon as the clips were removed, and hence no force to break was recorded for those samples. Samples left at 120 °C weakly bonded as the material had not completely melted after 30 minutes, however still showed adhesive failure. The strongest samples were those that were left at 160 °C for 30 minutes, which showed cohesive failure. The force to break the samples for each temperature dependant test are recorded in Figure 2.13.

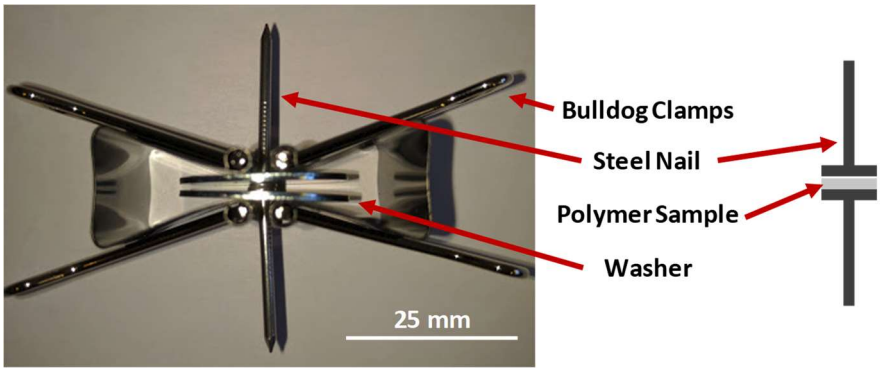

Figure 2.12 *Adhesion samples between two steel nails were prepared by clamping them head to head with 1.58 mm diameter circle sample between them. Washers were used to allow for larger surface area for the bulldog clamps to clamp onto.*

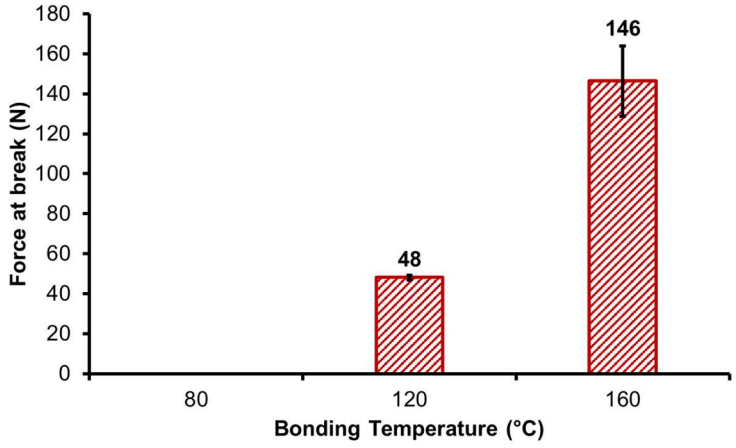

Figure 2.13 *Bond strengths as a function of bonding temperature. Errors show standard deviation from the mean (n = 5).*

Figure 2.14 shows the results of thermal re-adhesion experiments. In these tests, the samples were stressed to breaking point using a pull adhesion test. The separated surfaces were then

placed in contact and heated again for 30 minutes at 160 °C prior to re-testing. The zero cycle result corresponds to the force required to break the pristine bond, and the subsequent cycles refer to the number of times the bond has been reformed after breaking.

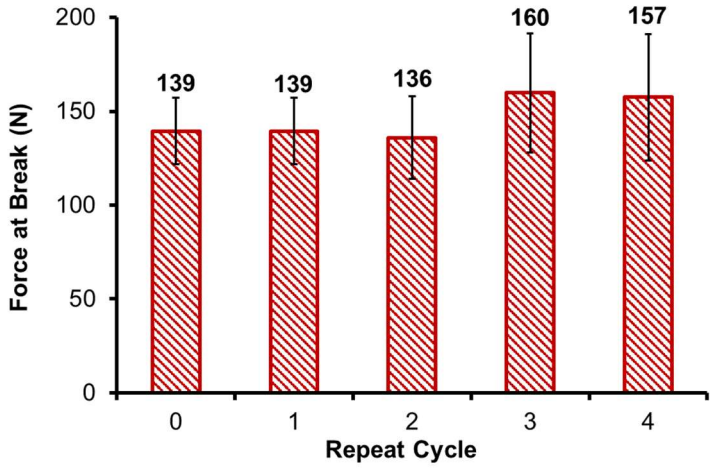

Figure 2.14 *Force at break after increasing bond/debond. Errors show standard deviation from the mean (n = 5).*

The consistency of the measured force at break as a function of the bond/debond cycle number confirms the reversible nature of the novel adhesive. Furthermore, the bond can be broken using heat, rather than force,[48] and reformed again without loss in strength.

The response of the adhesive to fluoride ions was determined by placing the bonded metal surfaces in a 0.02 M TBAF/acetone solution for 3 hours and 24 hours. A lower concentration of TBAF solution was required as permeation of fluoride ions at high concentrations was not possible. As evident from Figure 2.15, the samples that were exposed to the TBAF solution exhibited a reduction of 41% in their force at break. After the adhesion tests, the residue of one of the TBAF degraded samples was analysed by GPC (Figure 2.16) which showed an average molecular weight of ~10 $kgmol^{-1}$. The slightly higher M_n value of this degraded material compared to that observed during the solution state studies (6.2 $kgmol^{-1}$, Table 2.1) suggests that depolymerisation is hindered in the solid state, presumable as a consequence of reduced access (low rates of diffusion) of the fluoride ions through the bulk polymer to the depolymerisation units. Minimal further change was observed in the adhesive bonds strength when in sample were allowed to degrade for more than 24 hours.

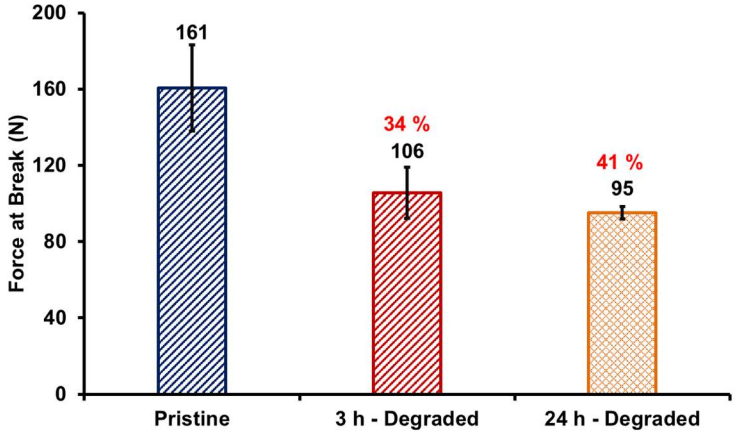

Figure 2.15 *The force at break of the bonded surfaces adhered with the pristine polymer and the polymer after exposure to TBAF after 3 and 24 hours. Errors show standard deviation from the mean (n = 5, 4 and 4 per experiment, respectively).*

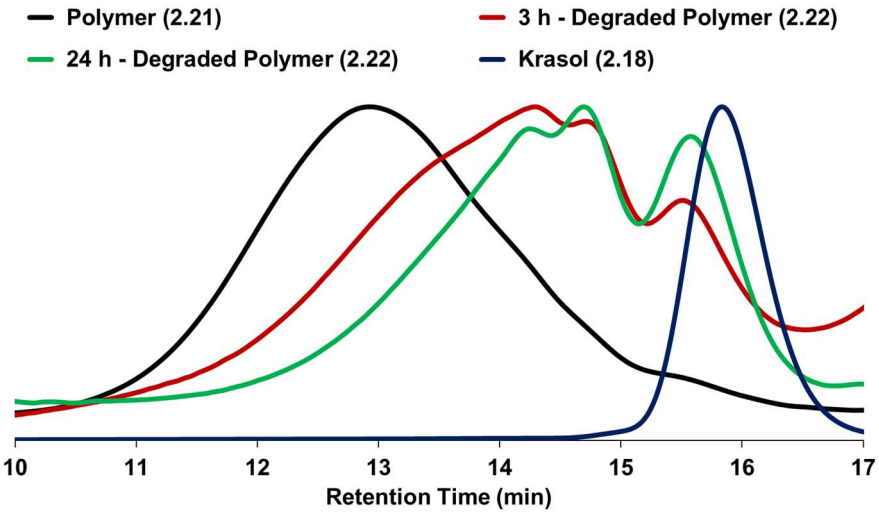

Figure 2.16 *GPC eluograms of the degraded polymer (**2.22**) from the adhesion test compared to the pristine polymer (**2.21**) and Krasol (**2.18**).*

	M_n ($gmol^{-1}$)	M_w ($gmol^{-1}$)	*Đ*
Polymer (**2.21**)	26100	71400	2.7
3 h – Degraded Polymer (**2.22**)	10400	27300	2.6
24 h – Degraded Polymer (**2.22**)	8600	19000	2.2
Krasol (**2.18**)	3300	3700	1.1

Table 2.3 *Molecular weight data from the GPC chromatographs for polymer (**2.21**), a sample of the degraded adhesive (**2.22**) and Krasol (**2.18**) (THF compared to PS).*

The irreversibility nature of the fluoride degraded adhesive was also assessed. This was investigated by thermally induced re-adhesion of the degraded polymer. Figure 2.17 shows the force at break measured during pull adhesion tests for metal samples re-bonded with either the pristine polymer, control samples that were exposed to acetone only, or samples that were exposed to an acetone solution of TBAF for 3 hours.

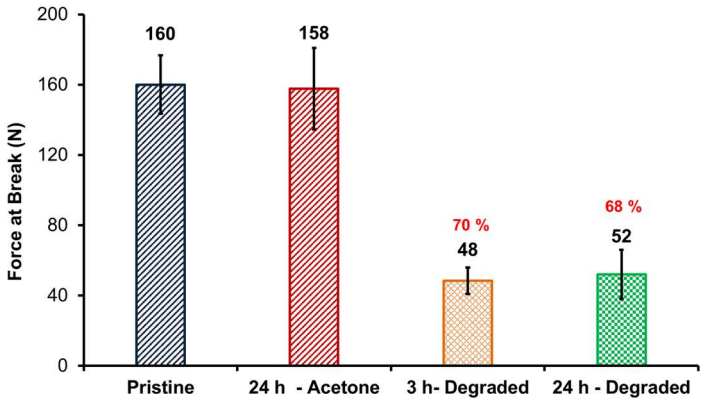

Figure 2.17 *Force separate the surfaces bonded with the pristine polymer (**2.21**), polymer **2.21** after exposure to either acetone or a solution of TBAF in acetone. Errors show standard deviation from the mean (n = 3, 3, 5, and 5 per experiment, respectively).*

These data demonstrate that exposure to acetone has essentially no impact on the strength of the re-adhered samples. In contrast, the samples that were exposed to TBAF solution prior to being re-adhered exhibited a dramatic loss (*ca*. 70%) in their force at break.

Finally, to investigate the potential utility of the new adhesive with respect to bonding different substrates, lap shear tests were carried out on samples of adhered wood, glass (soda-lime) and metal (aluminium) substrates. In these tests, pristine samples were adhered with polymer **2.21** at 160 °C for 30 minutes prior to testing. Degradation was achieved by placing the samples in a 0.02 M TBAF/acetone solution for 3 hours, prior to drying (160 °C) and testing. The maximum force before failure was recorded, and converted to lap shear stress (MPa) to account for the area of bonded polymer (Figure 2.18). During attempts to study the bonding strength on polyacetate (PA) substrates, the PA yielded before the adhesive failed.

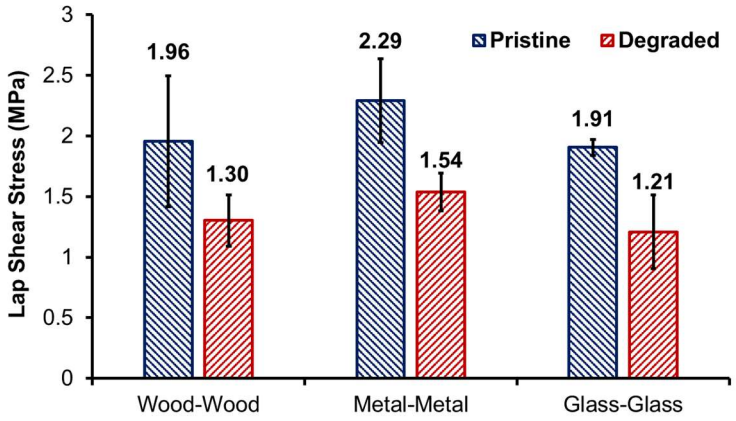

Figure 2.18 *Lap shear stress values of Polymer **2.21** between different material substrates, before and after degradation. Figures in black indicate the lap shear stress value, and red indicates the percentage of degradation in bond strength compared to the pristine material. Errors show standard deviation from the mean (n = 4 for Wood-Wood and Glass-Glass samples and n=5 for Aluminium-Aluminium samples)*

These results demonstrate that the polymer can be used to adhere several different substrate materials. Furthermore, the nature of the substrate has little effect on the loss of adhesion strength on contact with fluoride ions (*ca.* 35% loss).

2.3. Conclusions

A novel, dicarbamate containing fluoride responsive degradable group has been synthesised, which can be incorporated into a linear PU using solvent free conditions. Analysis of model compound (**2.7**) showed that the degradable group **2.7** is selectively responsive to fluoride ions (rather than other halide ions). Bond/debond tests demonstrate the linear PU behaves as a typical thermoplastic adhesive, undergoing four break/heal cycles without loss of strength. GPC and ^{1}H NMR spectroscopic studies confirm that the polymer **2.21** degrades in the both the solvent and solid state on the addition of fluoride ions. Butt tensile adhesion studies also showed bonded surfaces exhibit 40% loss of adhesion strength after the system is exposed to a fluoride source. The adhesive can be used to bond multiple different surfaces including wood, acetate and aluminium.

2.4. Experimental Section

2.4.1. Materials

Krasol HLBH-P2000 was kindly supplied by Cray Valley. 2,6-Bis(hydroxymethyl)-*p*-cresol, *tert*-butyldimethylsilyl chloride and imidazole were purchased from Alfa Aesar and used as received. All other chemicals were purchased from Sigma-Aldrich and used as received.

2.4.2. Characterisation

^{1}H NMR and ^{13}C NMR spectra were recorded on either a Bruker Nanobay 400 or a Bruker DPX 400 spectrometer operating at 400 MHz for ^{1}H NMR or 100 MHz for ^{13}C NMR, respectively. The samples for NMR spectroscopic analysis were prepared in $CDCl_3$ or d_6-DMSO, and dissolution was aided with slight heating. The data was processed using MestReNova Version 6.0.2-5475. Chemical shifts (δ) are reported in ppm relative to tetramethylsilane (δ 0.00 ppm) for $CDCl_3$ and the residual solvent peak (δ 2.50 ppm) for d_6-DMSO in ^{1}H NMR spectra. ^{13}C NMR spectroscopy was carried out using $CDCl_3$ and reported relative to chloroform (δ 77.0 ppm). ^{1}H NMR coupling constants (J) are expressed in hertz (Hz). Infrared spectroscopic analysis was carried out on a PerkinElmer 100 FT-IR spectrometer equipped with a diamond ATR sampling attachment, and samples were analysed

in neat form. The infrared spectroscopic data were processed using Microsoft Excel 2016. Ultraviolet-visible spectroscopy was conducted using a Varian Cary 300 spectrophotometer with heating attachment, using a 1 cm^3 quartz cuvette, in the wavelength range 200 – 800 nm. The UV-visible spectroscopic data were processed using Microsoft Excel 2016 Gel permeation chromatography (GPC) was conducted using an Agilent Technologies 1260 Infinity systems and the data were processed using Agilent GPC/SEC software; polystyrene was used as the calibrant. Samples for GPC analysis were dissolved in analytical grade THF (2 mg/mL) with butylated hydroxytoluene (BHT) stabiliser, and run using the same solvent as the mobile phase; eluting through two Agilent PLgel 5µm MIXED-D 300 × 7.5 mm columns in series. Differential scanning calorimetric analysis used a TA Instruments DSC Q2000, and a seven cycle process was carried out on the solid sample: heating from ambient to +100 °C at a ramp rate of 10 °C min^{-1}, followed by cooling from +100 °C to −70 °C at a ramp rate of −5 °C min^{-1} and then finally by heating from −70 °C to +200 °C at a ramp rate of +5 °C min^{-1}, with the previous two cycles repeated twice. The sample size used was 5-6 mg, and the data was processed using TA Universal Analysis Version 4.7A and Microsoft Excel 365. Thermogravimetric analysis employed a TGA Q50 instrument by heating the solid samples (sample size *ca*. 20 mg) from ambient temperature to +300 °C at a ramp rate of +10 °C min^{-1}. The data was processed using TA Universal Analysis Version 4.7A. Tensile and Adhesion tests were carried out using an AML X5-500 single column universal tester, attached with a 5 kN load cell and wedge grips. Samples were analysed at a strain rate of 100mm/min (0.0656 s^{-1}).

Rheological assessment was conducted using an Anton Paar Physica MCR 301 rheometer with a parallel plate oscillatory shear set-up. Circular samples of 25 mm diameter (0.35 mm average thickness) were cut from the polymer film using a steel punch cutter. For the single frequency temperature sweep, samples were placed into the rheometer and initialised at 150 °C and then subjected to temperature ramp cycle at a rate of 2 °C/min down to 25 °C and back up at the same rate to 150 °C. This cycle was repeated two more times to assess repeatability and any changes in properties. The frequency of oscillation was set to 5 Hz, and the shear strain amplitude to 0.1%. Dynamic shear moduli (G', G'', tan δ) were recorded to characterise the material.

The DMA employed a TA instruments Q800 DMA using a tension (film/fibre) clamp. Full calibration was performed for the clamp prior to testing according to the protocol defined by TA. The polymer sample dimensions were gauge length (defined by the clamp spacing) = 12.8 mm, width = 5.5 mm, thickness = 0.33 mm. A frequency sweep (0.5, 2, 5, 10 Hz) was

performed at 2 °C temperature steps from -75 °C to 130 °C, equilibrating for 3 minutes at each temperature step before the storage and loss moduli data (E' and E'') were recorded.

The data for both analyses were processed first using TA Universal Analysis Version 4.5A, followed by Matlab version R2016a.

Lap shear tests: The wood and metal coupons were 7 × 30 mm, with an overlap of 7 mm; and the glass coupons were 25 × 70 mm, with an overlap of 10 mm. The coupons were washed with methanol prior to use to remove any contaminants.

2.4.3. Synthesis of DU 2.6

To a solution of 2,6-bis(hydroxymethyl)-*p*-cresol (27.50 g, 0.163 mmol) in anhydrous *N*,*N*'-dimethylformamide (500 mL), imidazole (44.52 g, 0.654 mmol) and *tert*-butyldimethylsilyl chloride (98.57 g, 0.654 mmol) was added and stirred at 35 °C for 18 hours. The mixture was diluted with ethyl acetate (500 mL) and washed with deionised water (2 x 500 mL).The organic solution was dried over $MgSO_4$, filtered and concentrated to afford an orange/brown oil; which was dissolved in 50:50 methanol : diethyl ether mixture (400 mL) and *p*-toluenesulfonic acid (4.00 g, 2.32 mmol) was added and stirred at ambient temperature for 1 hour. The mixture was diluted in ethyl acetate (300 mL) and washed with saturated Na_2CO_3 solution (300 mL) followed by brine solution (300 mL), dried over $MgSO_4$, filtered and concentrated to afford a pale yellow/orange oil; which was dissolved in chloroform (100 mL) and precipitated slowly into cooled hexane (900 mL). The precipitate was filtered and allowed to dry under vacuum to afford a white powder (20.10 g, 48 %). m.p. 93 - 95 °C; ν_{max} (solid, cm^{-1}) 3220, 2961, 2926, 2881, 2857, 1453, 1221, 905, 776. δ_H (400 MHz, $CDCl_3$, ppm) 7.14 (2H, Ar-H), 4.65-4.64 (4H, d, J = 5.5 Hz, Ar-C$\underline{H}_2$OH), 2.30 (3H, Ar-CH_3), 1.57 (2H, Ar-CH_2O$\underline{H}$), 1.03 (9H, C(CH_3)$_3$), 0.19 (6H, Si(CH_3)$_2$). δ_C (100 MHz, $CDCl_3$, ppm) 147.9, 131.8, 131.7, 129.1, 61.2, 26.0, 20.6, 18.7, 0.0, -3.7. (m/z) found 305.1543 Da ($C_{15}H_{26}O_3NaSi$), calculated 305.1549 Da ($C_{15}H_{26}O_3NaSi$).

2.4.4. Synthesis of model bisurethane compound 2.7

To a solution of DU **1** (250 mg, 0.885 mmol) in anhydrous tetrahydrofuran (20 mL) was added 4-dimethylaminopyridine (10 mg, 0.09 mmol), triethylamine (0.49 mL, 3.54 mmol) and phenyl isocyanate (0.49 mL, 3.54 mmol) and allowed to stir at ambient temperature for 4 hours. The mixture was diluted into ethyl acetate (30 mL) and washed with saturated NH_4Cl (30 mL) and brine (30 mL). The organic solution was dried over $MgSO_4$, filtered and concentrated to afford

the crude product solid, which was purified by column chromatography over silica gel eluting with 20 % ethyl acetate in hexane to afford a yellow oil (331 mg, 72 %). ν_{max} (thin film, cm^{-1}) 3309, 2928, 2855, 1699, 1600, 1442, 1205, 883, 748, 690. δ_H (400 MHz, $CDCl_3$, ppm) 7.40 (4H, m, Ar-H), 7.31 (4H, m, Ar-H), 7.18 (2H, s, Ar-H), 7.07 (2H, m, Ar-H), 6.67 (2H, br, N-H), 5.20 (4H, s, Ar-CH_2), 2.30 (3H, s, Ar-CH_3), 1.05 (9H, $C(CH_3)_3$), 0.23 (6H, $Si(CH_3)_2$). δ_C (100 MHz, $CDCl_3$, ppm) 153.3, 149.1, 137.8, 131.4, 130.9, 129.1, 126.9, 123.5, 118.7, 62.5, 58.5, 25.9, 20.6, 18.7, 18.5, 0.0, -3.7. (m/z) found 543.2282 Da ($C_{29}H_{36}O_5N_2NaSi$), calculated 543.2291 Da ($C_{29}H_{36}O_5N_2NaSi$).

2.4.5. Synthesis of 2.16

2,6-Bis(hydroxymethyl)-*p*-cresol **2.5** (5.00 g, 29.73 mmol) and sodium hydroxide (1.78 g, 44.59 mmol) was dissolved in deionised water (40 mL) at 25 °C. Dimethyl sulfate (1.69 mL, 2.25 g, 17.84 mmol) was added dropwise over 1 h while keeping the reaction mixture below 40 °C, and left to stir overnight. The white precipitate was filtered off at the pump, and dimethyl sulfate (0.56 mL, 0.75 g, 5.95 mmol) was added to the filtrate, and left to stir for 5 days at 25 °C. The reaction mixture was filtered under reduced pressure to afford a cream solid product **3** (1.46 g, 27 %). m.p. 81 - 83 °C; ν_{max} (thin film, cm^{-1}) 3261, 3155, 2954, 2907, 2873, 2832, 2171, 2002, 1455, 1364, 1211, 1135, 1066, 1010, 1032, 859, 784, 693, 622. δ_H (400 MHz, $CDCl_3$, ppm) 7.13 (s, 2H, Ar-H), 4.69 (s, 4H, Ar-C$\underline{H_2}$OH), 3.82 (s, 3H, Ar-OC$\underline{H_3}$), 2.32 (s, 3H, Ar-C$\underline{H_3}$), 2.05 (s, br, 2H, Ar-CH_2O$\underline{H}$). δ_C (100 MHz, $CDCl_3$, ppm) 154.0, 134.3, 133.6, 129.5, 62.2, 61.0, 31.6, 22.7, 20.8, 14.1, 0.00. (m/z) found 205.0835 Da ($C_{10}H_{14}O_3Na$), calculated 205.0841 Da ($C_{10}H_{14}O_3Na$)

2.4.6. Synthesis of 2.17

Phenyl isocyanate (0.45 mL, 0.490 g, 4.12 mmol) was added to a stirred solution of **2.16** (0.30 g, 1.65 mmol) and 4-dimethylaminopyridine (20 mg, 0.16 mmol) in dry THF (20 mL) under a nitrogen atmosphere and left to stir for 4 h at room temperature. The mixture was diluted in ethyl acetate (30 mL), and washed with sat. ammonium chloride (30 mL) and sat. brine (30 mL). The ethyl acetate was extracted, dried over $MgSO_4$, filtered and the filtrate was concentrated under reduced pressure to give a white solid product **5** (0.47 g, 68 %). m.p. 152 -155 °C; ν_{max} (thin film, cm^{-1}) 3292, 3136, 3060 1693, 1629, 1592, 1536, 1486, 1439, 1310, 1226, 1151, 1054, 1003, 841, 753, 734. δ_H (400 MHz, $CDCl_3$, ppm) 7.38 (m, 4H, Ar-H), 7.32 (m, 4H, Ar-H), 7.24 (m, 2H, Ar-H), 7.07 (m, 2H, Ar-H), 6.71 (s, br, 2H, N-H), 5.25 (s, 4H, Ar-C$\underline{H_2}$OH), 3.85 (s, 3H, Ar-OC$\underline{H_3}$), 2.32 (s, 3H, Ar-C$\underline{H_3}$). δ_C (100 MHz, $CDCl_3$, ppm) 155.1, 153.3, 137.7,

134.2, 131.6, 129.2, 129.1, 123.6, 120.5, 118.7, 63.0, 62.1, 20.8. (m/z) found 443.1577 Da ($C_{24}H_{24}O_5Na$), calculated 443.1583 Da ($C_{24}H_{24}O_5Na$).

2.4.7. Synthesis of Polymer 2.21

Krasol HLBH-P 2000 was dried in a vacuum oven at 100 °C and 100 mbar. 4,4'-Methylene diphenyl isocyanate (5.00 g, 20.0 mmol) was added to Krasol HLBH-P2000 (21.00 g, 10.0 mmol) and stirred at 60 rpm, 80 °C for 3 hours. The reaction temperature was raised to 100 °C and DU **2.7** (2.82 g, 10.0 mmol) was added and stirred for 1 hour. The crude polymer was dissolved in chloroform (100 mL) and precipitated slowly into methanol (900 mL). The precipitate was filtered and washed with methanol (2 × 100 mL) to remove excess impurities. The precipitate was dissolved in tetrahydrofuran (100 mL) and concentrated to afford a clear white/yellow polymer (27.6 g, 96 %). ν_{max} (thin film, cm^{-1}) 3317, 2961, 2919, 2873, 2854, 2159, 1736, 1708, 1599, 1533, 1461, 1414, 1379, 1304, 1219, 1066. δ_H (400 MHz, $CDCl_3$, ppm) (n = number of chain extension) 7.38 – 7.20 (m, $8H_n$), 7.21 – 7.02 (m, $8H_n + 2H_n$), 6.55 (m, $4H_n$), 5.17 (s, $4H_n$), 4.82 – 4.59 (m, $0.3H_n$), 4.23 – 4.07 (m, $4H_n$), 3.88 (s, $4H_n$), 2.30 (m, $3H_n$), 1.93 – 0.71 (m, $350H_n$), 0.21 (s, $6H_n$). δ_C (100 MHz, $CDCl_3$, ppm) 153.7, 153.5, 149.16, 136.3, 136.2, 136.1, 135.9, 131.4, 130.8, 129.4, 126.9, 118.9, 62.5, 40.6, 38., 38.7, 38.4, 38.1, 37.9, 37.3, 36.1, 34.9, 33.5, 33.3, 30.7, 30.5, 30.2, 29.9, 29.8, 29.3, 26.8, 26.6, 26.5, 26.1, 25.9, 25.9, 20.6, 19.5, 18.7, 11.4, 10.9, 10.7, 10.66, 10.6, 9.4, 0.0, -0.9, -3.7. GPC (THF/BHT 250 ppm) M_w 71400, M_n 26100, $Đ$ 2.73. DSC T_g = -45.5 °C.

2.4.8. Sample Preparation for Mechanical Assessment.

A thin film of the polyurethane was produced for mechanical testing via a solution casting procedure. The polyurethane was dissolved in THF, and the solution was poured into a flat PTFE mold. The solvent was allowed to evaporate slowly at room temperature and pressure overnight, then at 50 °C with a pressure of approximately 800 mbar for a duration of 24 hours. Polyurethane film of uniform thickness between 200 and 500 μm was obtained at the end of this procedure without residual solvent. For tensile testing, rectangular samples of approximately 4.0 cm × 0.5 cm were cut with a blade, and paper end-tabs were used between the grips and the polymer sample. This sample assembly was found to reduce slippage and/or tearing inside the tensile grips of the tensiometer.

2.5. References

1. F. Awaja, M. Gilbert, G. Kelly, B. Fox and P. J. Pigram, *Prog. Polym. Sci*., 2009, **34**, 948–968.
2. F. Chabert, F. Tournilhac, N. Sajot, S. Tenc-Girault and L. Leibler, *Int. J. Adhes. Adhes.*, 2010, **30**, 696–705.
3. J. A. Pomposo, J. Rodrıguez and H. Grande, *Synth. Met.*, 1999, **104**, 107–111.
4. C. Galan, C. A. Sierra, J. M. Gomez Fatou and J. A. Delgado, *J. Appl. Polym. Sci.,* 1996, **62**, 1263–1275.
5. M. Fernandez, M. Landa, M. E. Munoz and A. Santamaria, *Macromol. Mater. Eng.,* 2010, **295**, 1031–1041.
6. X. Luo, K. E. Lauber and P. T. Mather, *Polymer*, 2010, **51**, 1169–1175.
7. A. Bakken, N. Boyle, B. Archambault, A. Hagen, N. Kostry, K. Fischer and R. Taleyarkhan, *Int. J. Adhes. Adhes.,* 2016, **71**, 66–73.
8. J. Canales, M. E. Muñoz, M. Fernández and A. Santamaría, *Compos. PART A*, 2016, **84**, 9–16.
9. C. W. Peak, J. J. Wilker and G. Schmidt, *Colloid Polym. Sci*., 2013, **291**, 2031–2047.
10. G. Sudre, L. Olanier, Y. Tran, D. Hourdet and C. Creton, *Soft Matter*, 2012, **8**, 8184–8193.
11. C. Ghobril and M. W. Grinstaff, *Chem. Soc. Rev.*, 2015, **44**, 1820–1835.
12. B. M. Shin, J. Kim and D. J. Chung, *Macromol. Res.*, 2013, **21**, 582–587.
13. E. M. White, J. E. Seppala, P. M. Rushworth, B. W. Ritchie, S. Sharma and J. Locklin, *Macromolecules*, 2013, **46**, 8882−8887.
14. J. H. Aubert, *J. Adhes*., 2003, **79**, 609–616.
15. S. N. Ghosh and S. Maiti, *J. Appl. Polym. Sci.*, 1997, **63**, 683–691.
16. K. Luo, T. Xie and J. Rzayev, *J. Polym. Sci. Part A Polym. Chem.*, 2013, **51**, 4992–4997.
17. Q. Zhang, M. Molenda and T. M. Reineke, *Macromolecules*, 2016, **49**, 8397–8406.
18. U. Lafont, H. Van Zeijl and S. Van Der Zwaag, *ACS Appl. Mater. Interfaces*, 2012, **4**, 6280–6288.
19. Z. Czech, *J. Adhes. Sci. Technol.*, 2007, **21**, 625–635.
20. H. Chung and R. H. Grubbs, *Macromolecules*, 2012, **45**, 9666–9673.
21. R. J. Wojtecki, M. a Meador and S. J. Rowan, *Nat. Mater.*, 2011, **10**, 14–27.
22. C. Heinzmann, S. Coulibaly, A. Roulin, G. L. Fiore and C. Weder, *ACS Appl. Mater. Interfaces,* 2014, **6**, 4713–9.
23. S. T. Phillips, W. Seo, J. S. Robbins, M. Olah, K. Schmid, A. M. DiLauro, WO2012005806 A2, 2012.
24. P. J. M. Bouten, M. Zonjee, J. Bender, S. T. K. Yauw, H. Van Goor, J. C. M. Van Hest and R. Hoogenboom, *Prog. Polym. Sci*., 2014, **39**, 1375–1405.
25. V. Delplace and J. Nicolas, *Nat. Chem*., 2015, **7**, 771–784.
26. Y. Shi, P. Zhou, R. Freitag and S. Agarwal, *ACS Biomater. Sci. Eng*., 2015, **1**, 971–977.
27. S. Ho and A. M. Young, *Eur. Polym. J.*, 2006, **42**, 1775–1785.
28. H. Mohapatra, H. Kim and S. T. Phillips, *J. Am. Chem. Soc*., 2015, **137**, 12498–12501.
29. B. T. Michal, E. J. Spencer and S. J. Rowan, *ACS Appl. Mater. Interfaces*, 2016, **8**, 11041–11049.
30. P. Pissis, G. Georgousis, C. Pandis, P. Georgiopoulos, A. Kyritsis, E. Kontou, M. Micusik, K. Czanikova and M. Omastova, *Procedia Engineering*, 2015, **114**, 590–597.
31. Z. Guo, Y. Zuo and S. Feng, *RSC Adv*., **6**, 73140–73147.
32. E. Chabert, J. Vial, J.-P. Cauchois, M. Mihalut and F. Tournilhac, *Soft Matter*, 2016, **12**, 4838–4845.

33. M. A. Ayer, Y. C. Simon and C. Weder, *Macromolecules*, 2016, **49**, 2917–2927.
34. J. Lai, J. Mei, X. Jia, C. Li and X. You, *Adv. Mater*., 2016, **28**, 8277–8282.
35. C. Heinzmann, C. Weder and L. M. de Espinosa, *Chem. Soc. Rev*., 2015, **342**, 342–358.
36. A. Faghihnejad, K. E. Feldman, J. Yu, M. V. Tirrell, J. N. Israelachvili, C. J. Hawker, E. J. Kramer and H. Zeng, *Adv. Funct. Mater*., 2014, **24**, 2322–2333.
37. K. A. Houton, G. M. Burslem and A. J. Wilson, *Chem. Sci.*, 2015, **6**, 2382–2388.
38. C. Heinzmann, U. Salz, N. Moszner, G. L. Fiore and C. Weder, *ACS Appl. Mater. Interfaces,* 2015, **7**, 13395–13404.
39. K. Yamauchi, J. R. Lizotte and T. E. Long, *Macromolecules*, 2003, **36**, 1083–1088.
40. S. Cheng, M. Zhang, N. Dixit, R. B. Moore and T. E. Long, *Macromolecules*, 2012, **45**, 805–812.
41. K. Yamauchi and A. Kanomata, *Macromolecules*, 2004, **37**, 3519–3522.
42. H. Kim, H. Mohapatra and S. T. Phillips, *Angew.Chem. Int.Ed*., 2015, **54**, 13063–13067.
43. I. S. Turan and E. U. Akkaya, *Org. Lett.*, 2014, **16**, 1680–1683.
44. M. Shamis, H. N. Lode, and D. Shabat, *J. Am. Chem. Soc.,* 2004, **126**, 1726-1731.
45. P. J. Woodward, D. Hermida Merino, B. W. Greenland, I. W. Hamley, Z. Light, A. T. Slark and W. Hayes, *Macromolecules*, 2010, **43**, 2512–2517.
46. A. Feula, X. Tang, I. Giannakopoulos, A. M. Chippindale, I. Hamley, F. Greco, C. P. Buckley, C. R. Siviour and W. Hayes, *Chem. Sci*., 2016, **7**, 4291–4300.
47. A. Feula, A. Pethybridge, I. Giannakopoulos, X. Tang, A. Chippindale, C. R. Siviour, C. P. Buckley, I. W. Hamley and W. Hayes, *Macromolecules*, 2015, **48**, 6132–6141.
48. T. S. Babra, A. Trivedi, C. N. Warriner, N. Bazin, D. Castiglione, C. Sivour, W. Hayes and B. W. Greenland, *Polym. Chem.,* 2017, **8**, 7207-7216

Chapter 3

Fluoride Responsive Debond-on-Demand Adhesives: Manipulating Hydrogen Bonding Density and Crystallinity to Modulate Adhesion Temperature

This chapter has been adapted from a submitted research article by the author entitled "Fluoride Responsive Debond-on-Demand Adhesives: Manipulating Hydrogen Bonding Density and Crystallinity to modulate Adhesion Temperature" by T. S. Babra, M. Wood, J. S. Godleman, C. N. Warriner, N. Bazin, C. Sivour, I. W. Hamley, W. Hayes and B. W. Greenland.

Note of Contribution: M. Wood helped with adhesive sample preparation and carrying out Butt-Tensile Adhesion Tests at AWE Plc. J. S. Godleman helped carry out SAXS/WAXS experimentation alongside T.S. Babra at Alba Synchrotron, Spain. T. S. Babra carried out all other work and analysis detailed below. Professor C. Sivour provided supervision at the University of Oxford for rheological analysis. Professor I. Hamley provided supervision on SAXS/WAXS experimentation and analysis. C. N. Warriner and N. Bazin were industrial supervisors from AWE Plc. Professor W. Hayes and Dr B. W. Greenland were supervisors at the University of Reading.

Abstract

This chapter reports the solvent-free synthesis of a series of novel fluoride responsive debond-on-demand adhesives, containing a silyl functionalised degradable unit (DU). The composition of the polyurethanes within this series varied according to the chemical structure of the polyol backbone or the diisocyanate linker in the main chain in order to optimise the strength and debonding nature of the adhesive. ^{1}H NMR spectroscopy was used to study the depolymerisation behaviour in solution state and showed that *tetra*-butylammonium fluoride (TBAF) triggered the breakdown of the DU unit without fragmenting the polyol backbones. GPC analysis revealed that the polyurethanes all depolymerised with reductions in M_n ranging from 64 – 90 %. The polymers behave as typical thermoplastics, and the thermal properties were characterised by rheological and SAXS/WAXS analysis to reveal reversible morphology changes of the supramolecular polymer network under thermal stimuli. Mechanical stress-strain analysis of the series of polymers showed a greater than 70 % reduction in toughness after treatment with TBAF for 30 minutes. Within the series of polyurethanes, the specimen featuring an ester based polyol demonstrated low-melt adhesion properties with strong adhesion at temperatures as low as 60 °C. This material could be thermally rebonded if broken by force without loss in adhesion strength over three debond-rebond cycles. Lap shear adhesion tests

showed a reduction of adhesive strength up to 40 % (from 11.41 MPa to 7.25 MPa) for this specimen after soaking in a fluoride solution for three hours.

3.1. Introduction

Chapter 2 reported the design and synthesis of the fluoride responsive degradable unit (DU) **2.6** and its incorporation into a polyurethane (PU) backbone which behaved as a hot-melt adhesive (**2.21**). The polymer **2.21** was constructed from a hydrogenated polybutadiene, Krasol HLBH-P 2000 **2.18** and 4,4'-methylenediphenyl diisocyanate (4,4'-MDI **2.19**) to form the polyurethane backbone that is chain extended with the bifunctional DU **2.6**. These linear chains will be chain entangled with additional strength provided by non-covalent supramolecular interactions. These supramolecular interactions allow for thermal reversibility of the polymeric network while the DU enables the polymer to depolymerise in response to fluoride ions, affording a multi stimuli-responsive adhesive.

Recently, research into stimuli-responsive adhesives has received significant attention.[1–4] These adhesives allow for the substrates to debond on application of a suitable external stimulus, and in some cases, enable multiple bonding and debonding cycles without loss of strength.[5] The drive for the optimisation of this class of adhesives is the increased focus on the whole lifecycle of a product. During the fabrication stage, adhesives can replace traditional assembly methods such as riveting or welding resulting in reduced manufacturing costs without loss of structural integrity of the desired product. For example, the adhesive Loctite® EA 9514 (Henkel) exhibits stronger adhesion to aluminium than welding and thus avoiding thermal damage to the aluminium components. In addition, at the end of a product's usable lifetime, efficient disassembly of a multi-component product (such as a laptop, mobile phone or vehicle) during disposal, can facilitate easy access to valuable materials, resulting in cost and efficiency savings during recycling processes.

Stimuli-responsive adhesives, and stimuli-responsive materials can exhibit a controlled temporary loss in tensile modulus and/or adhesion strength. This has been demonstrated in various scenarios, for example, in supramolecular materials[6] or those containing dynamic covalent bonds.[7] Progress in bottom-up material design has facilitated the emergence of new technologies[8,9] across a broad range of disciplines including biomedical applications,[10–13] sensors,[14] healable[15] and damage sensing materials[16] as well as improving product recyclability.[11,17,18]

Within the field of reversible debond-on-demand adhesive materials, dynamic covalent systems have received the most attention (Chapter 1, section 1.2.5). These systems can convert from a high to a low strength material when exposed to an external stimulus. Notable examples of such systems include polymers that contain disulfide moieties (Figure 1.12) that break and form upon exposure to high intensity UV radiation;[15] Diels-Alder adducts such as those derived from furan and maleimide precursors (Scheme 1.4), which are responsive to high temperatures (110 °C),[5] and aliphatic azo-containing polymers which weaken when exposed to heat or high intensity UV light (Scheme 1.7).[15]

An additional functionality that can be built into supramolecular, debondable adhesives is the ability to undergo a permanent reduction in tensile modulus/adhesion strength. This permanent reduction in strength can be caused by the depolymerisation of the polymer backbone,[19] which results in an irreversible reduction in molecular weight. This was demonstrated recently by Phillips and co-workers who designed an adhesive that degrades on contact with fluoride ions.[20] However, the crosslinked nature of this material meant that it could not be solvent cast or melt processed, deficiencies that could result in a loss of general utility.

In Chapter 2, the synthesis of a linear PU responsive to fluoride ions was reported.[19] This non-covalently crosslinked system exhibited the standard thermo-responsive debond-on-demand feature of a classic supramolecular hot-melt adhesive but with the added advantage of undergoing depolymerisation on demand resulting in permanent loss of adhesive properties (Scheme 3.1).

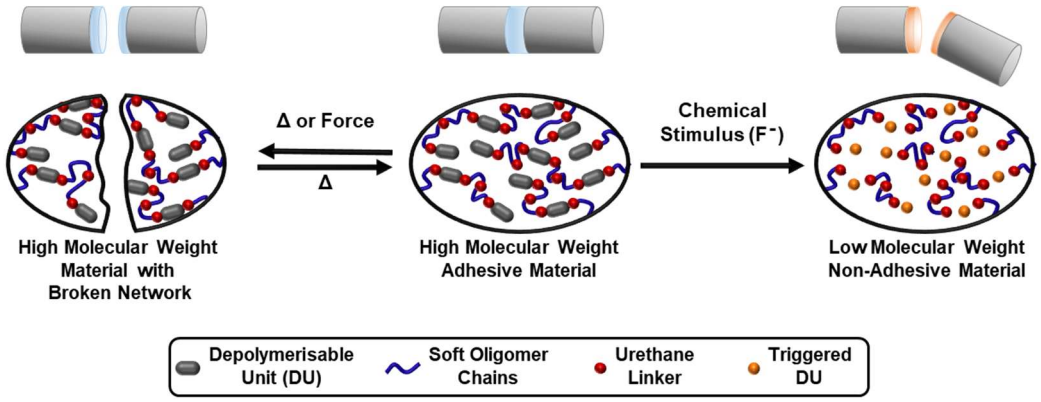

Scheme 3.1 *Schematic showing the non-reversible depolymerisation of the polymer in response to fluoride ions (right) and the rebondable nature of the adhesive in response to elevated temperatures.*

Structurally, this fluoride degradable adhesive is a phase separated polyurethane (PU)[21–24] comprising hydrogenated polybutadiene polyol **2.18** soft segments and hard segments containing an aromatic isocyanate linker ((4,4'-MDI), **2.19**) and the fluoride responsive DU

(**2.6**). This initial composition resulted in a relatively high temperature to achieve maximum adhesion (160 °C) which would be a disadvantage when bonding temperature sensitive components. Adhesion could be achieved at lower temperatures, but with much lower adhesive strength. Therefore, studies were targeted to establish the structural parameters that would facilitate a reduction in adhesion temperature without compromising adhesive performance or the ability of the material to debond on demand in response to the addition of a fluoride source.

Herein is presented the synthesis and evaluation of two series of structurally related PU materials containing the fluoride responsive DU and either different diisocyanate linkers or different polyols. In the first series of polymers, structurally distinct diisocyanates were incorporated into the PU backbone to influence phase separation between the soft and hard domains[25–29]. Within the second series of adhesives, the polyol component was varied, firstly to reduce the hard-content composition, and secondly to introduce crystallinity into the adhesive structure. It was envisaged that, in common with related healable structures,[15,30–33] the thermal properties of the crystalline regions may facilitate a dramatic reduction in tensile strength,[25] viscosity and adhesion characteristics when exceeding the melting point of the crystalline segments.[34,35]

3.2. Results and Discussion

3.2.1. Synthesis and Characterisation

Two series of polymers were synthesised to determine if the thermal and/or mechanical properties of the adhesive could be improved with respect to polymer **2.21**: (*Series 1*) polymers containing different diisocyanate linkers (**3.5** and **3.6**) and (*Series 2*) polymers containing different polyols (**3.7** and **3.8**). The polymers were synthesised by a solvent-free method as previously reported.[19] First, a pre-polymer was prepared from the polyol and diisocyanate linker, prior to the addition of the degradable unit **2.6**. The chemical structures of the polyols and diisocyanate linkers used are detailed in Scheme 3.2 and the feed ratio of each polymer are detailed in Table 3.1.

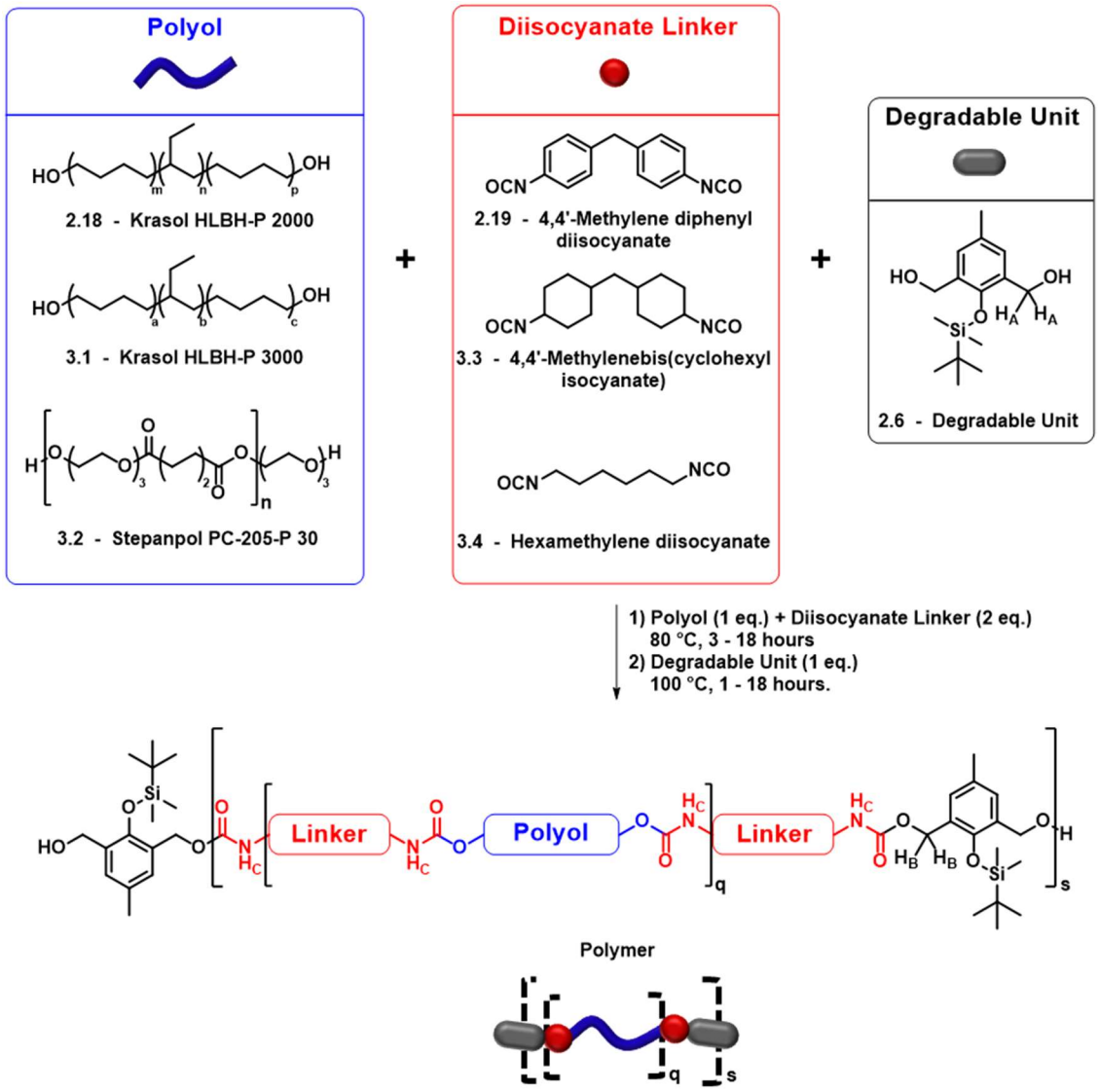

Scheme 3.2 *General synthesis of the polymers containing the degradable unit with varying polyols and diisocyanates*

Polyol		Diisocyanate Linker		Degradable Unit		Degradable adhesive (Yields)
2.18 (M_n 3.4 kDa, *Đ* 1.1)	+	**2.19**	+	**2.6**	→	**2.21** (97 %)
2.18 (M_n 3.4 kDa, *Đ* 1.1)	+	**3.3**	+	**2.6**	→	**3.5** (88 %)
2.18 (M_n 3.4 kDa, *Đ* 1.1)	+	**3.4**	+	**2.6**	→	**3.6** (87 %)
3.1 (M_n 4.6 kDa, *Đ* 1.1)	+	**2.19**	+	**2.6**	→	**3.7** (99 %)
3.2 (M_n 6.8 kDa, *Đ* 1.8)	+	**2.19**	+	**2.6**	→	**3.8** (92 %)

Table 3.1 *Chemical composition of the polymers containing different polyols or diisocyanates. Yields shown in brackets.*

The polymers were characterised by ^{1}H NMR spectroscopy where, all polymers showed a shift in resonance of the methylene protons of the degradable unit **7** (H_A) from 4.6 ppm to 5.1-5.2 ppm for the polyurethane methylene protons (H_B). A urethane (N-H_C) resonance was observed between 3.2 - 3.4 ppm in the spectra of the aliphatic isocyanate containing polymers **3.5** and **3.6**; or between 6.5 - 6.7 ppm for the aromatic isocyanate containing polymers **2.21**, **3.7**, and **3.8**. Infrared spectroscopic analysis of the polymers showed a characteristic absorbance band at approximately 1700 cm^{-1} and 3300 cm^{-1} for C=O and N-H stretches, respectively and absorbances at approximately 2200 cm^{-1} indicative of residual isocyanate were not observed.

^{1}H NMR spectroscopy was also employed to study the degradation rate on addition of fluoride ions for the new series of polymers. The fluoride source, *tetra*-butylammonium fluoride (TBAF) was added to solution of polymer in deuterated chloroform in equal molar quantities to the DU. All five polymers showed immediate degradation of the depolymerisation unit as evidenced by the loss of the methylene proton (H_B) resonances around 5.0 ppm and urethane proton (H_C) resonances. This effect is exemplified for the polymer **3.8** in Figure 3.3 (see Appendix, A.1., Figures A1-A4 for additional degradation data). In addition, the polyester backbone to polymer **3.8** was not affected by the addition of TBAF evidenced by the lack of shift in the methylene resonance at 4.1 and 2.3 ppm (Figure 3.3) demonstrating that degradation occurred exclusively at the DU as designed (Figure 3.1).

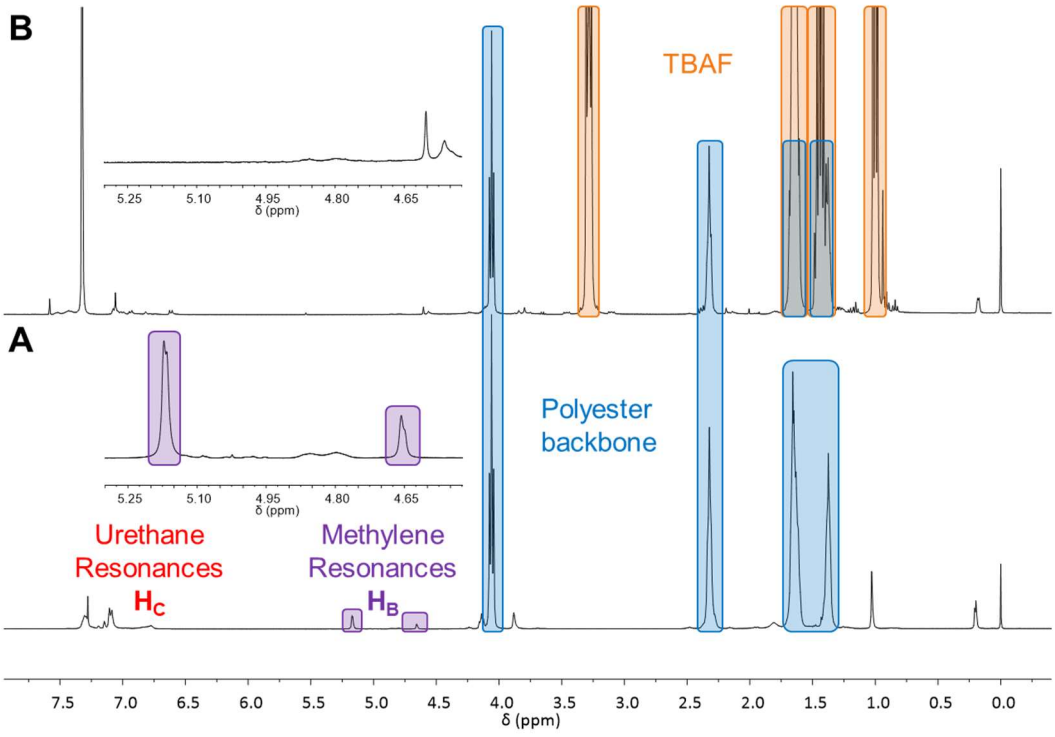

Figure 3.1 *^{1}H NMR spectra showing (A) before and (B) after addition of TBAF of polymer **3.8**. ($CDCl_3$, 400 MHz)*

The molecular weights of the two series of polymers before and after degradation with TBAF were analysed by gel permeation chromatography (GPC). The GPC eluograms are shown in Figure 3.4, with molecular weight data detailed in Table 3.2.

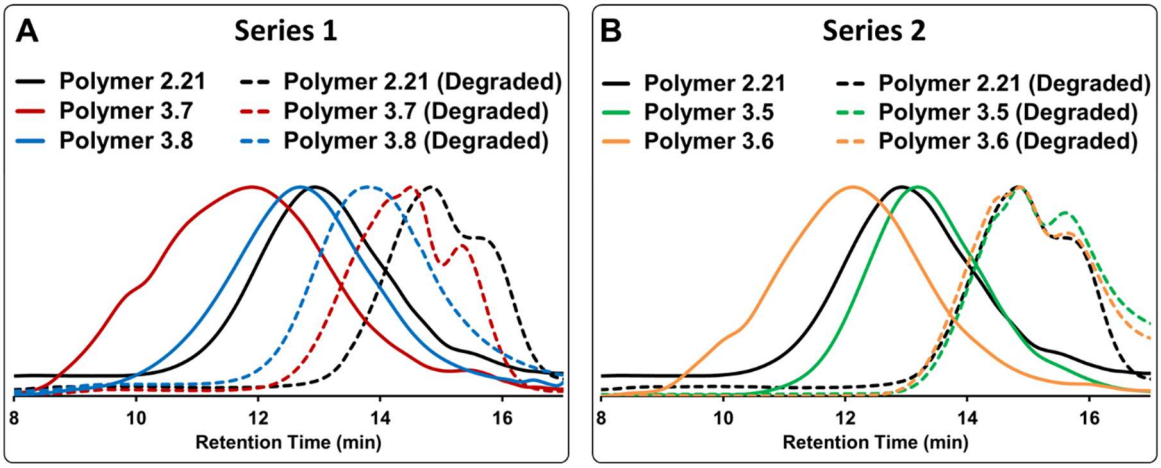

Figure 3.2 *GPC eluograms of (A) series one which vary by diisocyanate structure and (B) series two, which vary by polyol structure. (THF, PS standards).*

	Pristine			Degraded		
Polymer	**M_n (Da)**	**M_w (Da)**	***Đ***	**M_n (Da)**	**M_w (Da)**	***Đ***
2.21	26100	71480	2.74	6210 (10600)	10300 (13100)	1.65 (1.25)
3.5	20400	51800	2.54	4000 (10700)	8300 (13100)	2.08 (1.22)
3.6	56000	254000	4.54	5400 (11000)	10000 (14000)	1.85 (1.29)
3.7	77180	445000	5.77	9740 (16300)	17600 (23000)	1.81 (1.42)
3.8	35000	118000	3.37	(12400)	(27100)	(2.19)

Table 3.2 *GPC molecular weight and dispersity data for the polymers before and after degradation. Values denoted in brackets show the molecular weight calculations from the peak maxima only. Values not in brackets are calculated from the whole distribution. See Appendix A.2. for complete analysis.*

The five polymers show chain extension between the polyol, diisocyanate and DU **2.6** as evidenced by the higher molecular weights in comparison to the starting polyols. Each polymer also shows a significant reduction in molecular weight after degradation (at least by 64 %).

Inspection of the molecular weight data for series 1 (polymers **2.21**, **3.5** and **3.6**, Figure 3.4a) in which the key variable was the diisocyanate linker, show that for each material, the degraded products exhibit very similar eluograms. Each eluogram exhibits two peak maxima, corresponding to M_n ~10.7 kDa and ~ 3.0 kDa as a result of chain extension between isocyanate

and polyol (see Chapter 2). Chain extension of the pre-polymer (*q*) was seen with all five polymers and can be determined to be between 1 – 3. Furthermore, as the molecular weights of the degraded polymers were comparable to the pre-polymers (or multiples of) (Table 3.1), it was deduced that the fluoride ions do not cause the breakdown of the polyol backbone structures. This is particularly important with polymer **3.8**, containing the polyester polyol **3.2**, which is prone to break down under acidic/basic conditions, and is further evidenced by the ^{1}H NMR spectrum of the degraded polymer **3.8** (Figure 3.3) where changes were not detected for the polyester backbone resonance signals of the methylene units of the polyol.

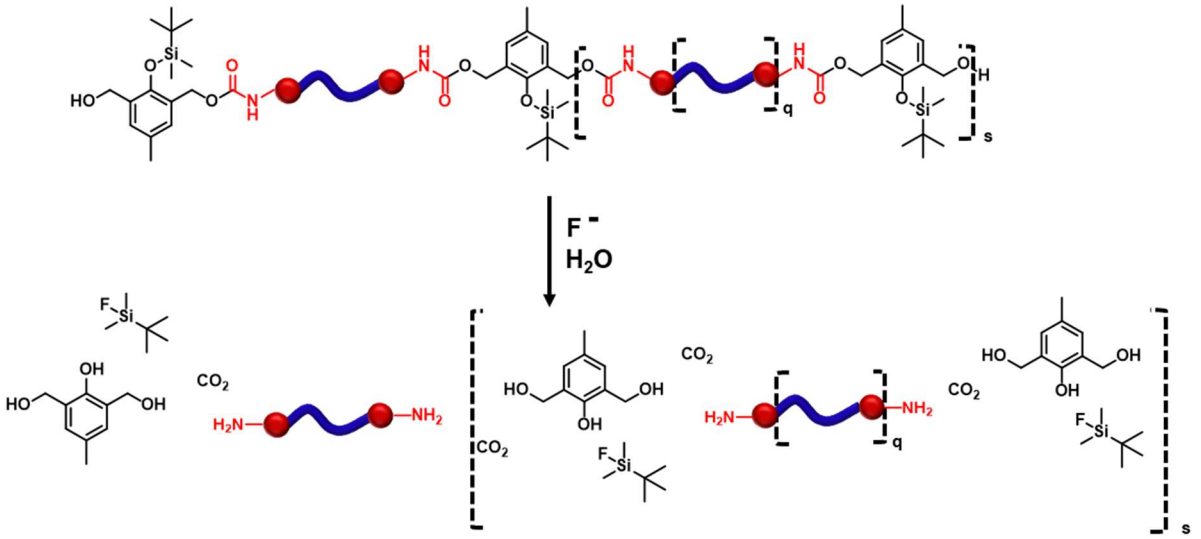

Scheme 3.3 *Schematic showing the degradation of the polymer backbone producing a smaller M_w unit which is not affected by the fluoride ions.*

With the polymers characterised and degradation properties analysed, attention moved to determining how altering the diisocyanate or the polymer affected the thermal properties.

3.2.2. Thermal Properties and Morphology of the Polymers

The thermal properties of polymers were initially determined using Differential Scanning Calorimetry (DSC). Melting temperatures (T_m) were not detected for polymers **2.21** and **3.5 - 3.7** (Figure 3.6a) which confirms the amorphous nature of the polymers. The glass transition temperatures (T_g), determined by DSC, of polymers **2.21** and **3.5 - 3.7** (Figure 3.6b), which contain the hydrogenated polybutadienes **2.18** (T_g ~ -46 °C) and **3.1** (T_g ~ -48 °C), show little variance in comparison toward the starting polyols (T_g ~ -45 ±3 °C for polymers **3.8** – **3.11**). The ester-containing polymer **3.8** exhibited a distinctive T_m at 49 °C, similar to the starting polyol **3.2** (T_m ~ 54 °C) and recrystallisation temperature, T_c at ~ 19 °C.

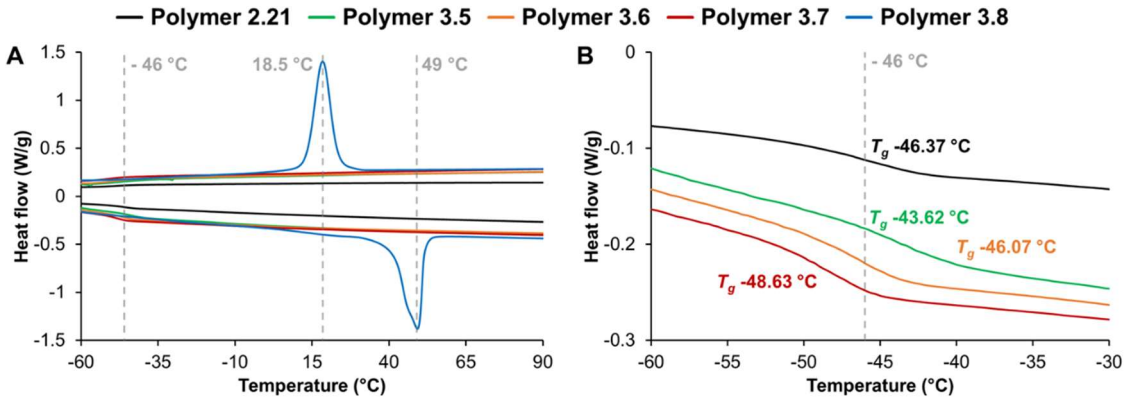

Figure 3.3 *DSC thermograms of the polymers from the second heat-cool cycle highlighting (A) the melting (T_m) and recrystallisation (T_c) temperature of polymer **3.8** and (B) the glass transition temperatures (T_g) of polymers **2.21** and **3.5 - 3.7**.*

Rheological analysis was carried out to determine the viscoelastic transition temperature (determined at the point where G'' exceeds G') which is an important factor in determining the lowest temperature that the materials are likely to adhere.[36] After an initial heat-cool temperature ramp to insure contact between the plates, three heat-cool cycles were carried out to determine the thermal reversibility of the supramolecular polymer network (see Appendix A.3. for the full data set) with the second heat cycle detailed in Figure 3.7.

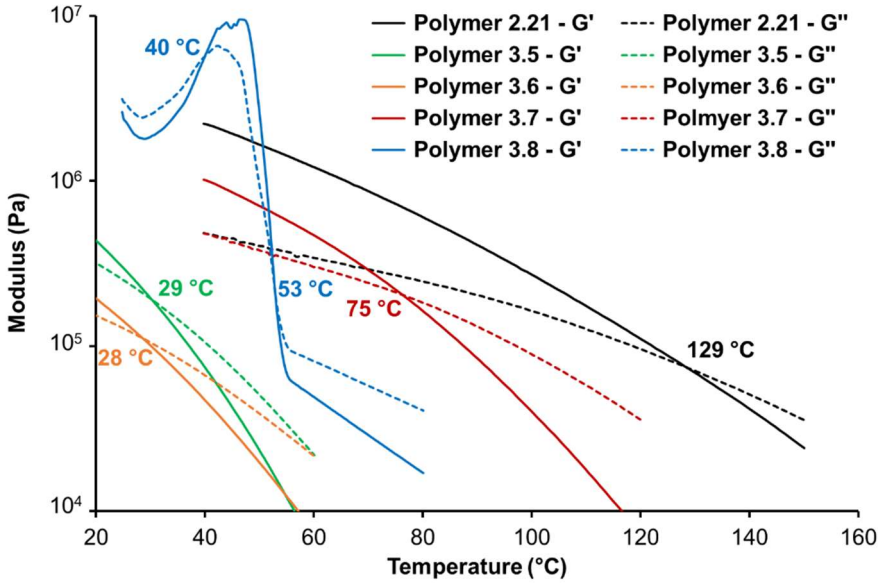

Figure 3.4 *Rheological analysis of polyurethanes **2.21** and **3.5** – **3.8**. Values indicate the viscoelastic transition temperature.*

The viscoelastic transition or flow temperature for both polymers **3.5** and **3.6** was measured to be ~28 °C, much lower than the flow temperature of polymer **2.21** (125 °C). This shows that exchange of the aromatic for aliphatic diisocyanate groups weakens the supramolecular interactions within the polymer network. This trend was evident from the physical appearance of polymers **3.5** and **3.6** at room temperature, which are very viscous liquids; not self-supporting

films that could readily be cast from polymers **2.21**, **3.7** and **3.8**. Polymer **3.7** shows a reduction in the viscoelastic temperature at 75 °C, which is a result the longer polybutadiene polyol **3.1**, thereby providing reduced hard block content within the polymer network. The rheological analysis of polymer **3.8** (Figure 3.7) exhibits two crossovers in storage and loss modulus at 40 °C and 53 °C. This temperature range is similar to the melt region determined by DSC analysis (Figure 3.6a). Complete loss in storage modulus over loss modulus occurs just above 50 °C, showing that the polymer has melted. The network does not reform exactly as the pristine materials supramolecular network upon cooling and hence changes for the different cycles. A similar effect has been reported by Tang and co-workers in the case of an hydrogen bonded telechelic supramolecular polymer.[23]

Altering the supramolecular network causes the morphology of the polymer to change. To gain an insight into the effect that the structure has on the morphology of the system, variable temperature (VT) small angle X-ray scattering (SAXS) and wide angle X-ray scattering (WAXS) were carried out on thin film samples of each of the polymers (Figure 3.8).

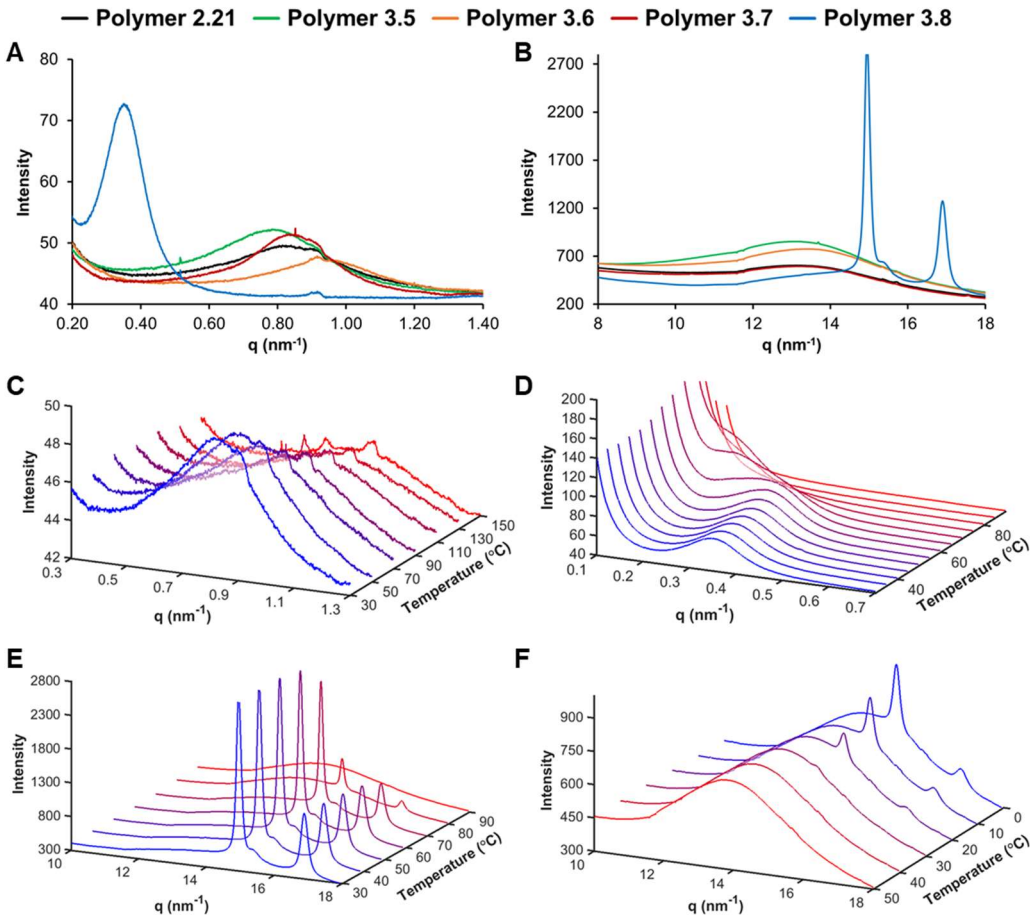

Figure 3.5 *(A) SAXS and (B) WAXS analysis of polymers **2.21** and **3.5- 3.8**; 3D spectra of (C) VT SAXS of polymer **2.21** during a heat ramp; (D) VT SAXS of polymer **3.8** during a heat ramp; VT WAXS of polymer **3.8** during (E) heating ramp and (F) cooling ramp.*

From the SAXS diffraction patterns (Figure 3.8a), polymers **2.21**, **3.5** and **3.6**, show a similar broad Bragg peak with a maximum at approximately 0.85 nm^{-1}, relating to a d-spacing of 73.9 nm, similar to that previously reported for materials using the Krasol polyols.[21,22] Polymer **3.7** shows a slightly larger d-spacing at 78.5 nm as a result of the higher molecular weight Krasol HLPH P3000 **3.1** used as the backbone. The broad diffraction pattern is characteristic of an amorphous structure[21,22] arising from the soft regions of the hydrogenated polybutadiene polyols **2.18** and **3.1**. Polymer **3.8**, consisting of the crystalline Stepanpol **3.2**, exhibited a sharper diffraction peak at 0.35 nm^{-1}, corresponding to a distance 179.5 nm. WAXS analysis (Figure 3.8b) of polymers **2.21** and **3.5** – **3.7** showed a broad diffraction peak at approximately 13 nm^{-1}, relating to a spacing of 48.3 nm (4.83 Å) and corresponding to the stacking of hydrogen bonding moieties.[37,38] Polymer **3.8** showed two sharp diffraction bands. The first band, observed at 15.0 nm^{-1}, indicates assembly via the hydrogen bonding moieties (4.19 Å) and the second band at 16.9 nm^{-1} indicates π-stacking interactions (3.72 Å) between the aromatic components of the polymer.[24]

VT-SAXS analysis was carried out on polymer **2.21** (Figure 3.8c) during a heating ramp and showed a splitting into two peaks at $q = 0.75\ nm^{-1}$ and $q = 0.92\ nm^{-1}$ as the temperature increases and the polymer begins to flow at its viscoelastic transition temperature. The development of two well-defined peaks suggests a phase separation process when the polymer starts to flow at high temperature. VT-SAXS analysis on hydrogenated polybutadiene based polymers **3.5** – **3.7** showed similar results to each other, i.e. an 8 – 12 % decrease in intensity at ~ 0.80 nm^{-1}, which is expected as a result of their similarities in overall structure. VT-SAXS on polymer **3.8** (Figure 3.8d) shows an initial sharp peak at 30 °C ($q = 0.35\ nm^{-1}$) that starts to shift to a lower *q* value at 55 °C ($q = 0.20\ nm^{-1}$), before decreasing in intensity thereafter.

VT WAXS of polymer **3.8** showed a similar thermal response, where a decrease in intensity of the two sharp peaks ($q = 15.0$ and 16.9 nm^{-1}) occurs up to 60 °C, followed by a shift to a broad diffraction pattern a lower *q* value ($q \sim 13.8\ nm^{-1}$) indicative of a weakening in hydrogen bonding with increasing temperature.[22] This initial loss in intensity is a result of the polymer melting, followed by the collapse of the supramolecular interactions at a higher temperature. The sharp signals are recovered during a cooling ramp (Figure 3.7e) at 20 °C when the polymer recrystallises. These temperatures of the thermal transitions are in agreement with both the DSC data (Figure 3.6) and trends from rheological analysis (Figure 3.7).

The thermal analysis has thus far shown that using an aliphatic diisocyanates in polymer *Series 1* lowers the flow temperature of the polymer network as a result of loss of supramolecular interactions. Changing the amorphous polyol to a crystalline polyol introduces a melting point while retaining the supramolecular interactions within the polymer network. With the above thermal properties of the materials established, attention moved towards mechanical and adhesion testing.

3.2.3. Mechanical Testing

For mechanical stress-strain testing, the polymers **2.21**, **3.7** and **3.8** were cast from THF into homogenous films (15 × 15 cm). The viscous nature of **3.5** and **3.6** at room temperature, prohibited the formation of self-supporting films that could be peeled from a surface. Five strips (4.0 × 0.5 cm) were cut from the films of polymers **2.21**, **3.7** and **3.8** and stress-strain analysis was carried out (see Appendix A.4.). The untreated polymers show different mechanical or physical properties. Analysis of polymer **2.21** (Figure A15 in the Appendix) revealed a stress-strain curve that shows an initial elastic region denoted by the sharp initial gradient up to ~ 3 MPa with a tensile modulus of 7.0 MPa. This is followed by a flexible elastomeric region denoted by the decreased gradient before breaking above 6 MPa. In comparison, polymer **3.7** (see Appendix, Figure A16) containing a higher molecular weight polyol exhibits an elastomeric nature with a low tensile modulus (3.6 MPa) and sudden drop at break above 10 MPa. In contrast, analysis of polymer **3.8** (see Appendix, Figure A17) revealed an initial sharp gradient reaching on average above 6 MPa, which is a result of the hard crystalline regions within the polymer network (Figure 3.9). As a comparison, the tensile modulus of polymer **3.8** was determined to be 203.5 MPa, which shows that the crystalline regions within the polymer network increases the stiffness of the material.

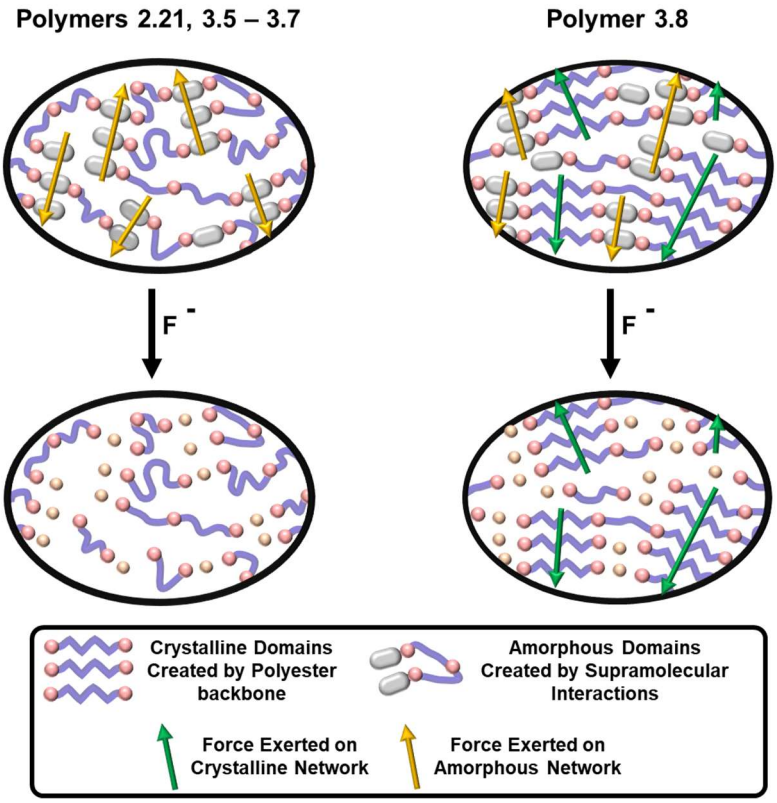

Scheme 3.4 *Schematic showing the effect of the hard crystalline structures on the strength of polymer* ***3.8*** *before and after degradation.*

Five strips of the cast films were exposed to a TBAF solution (1M; acetone for polymers **2.21** and **3.7**; and acetonitrile for polymer **3.8**) to establish the depolymerisation characteristics of these materials in the solid state. The polymer strips were each exposed for a fixed time of 30 minutes, then dried at 40 °C for 30 minutes before testing. From the stress-strain graphs (see Appendix A.4.) before and after treatment with fluoride ions, the ultimate tensile strength (Figure 3.9a) and toughness (Figure 3.9b) were calculated. All of the polymers showed a decrease in strength after depolymerisation in the TBAF solution.

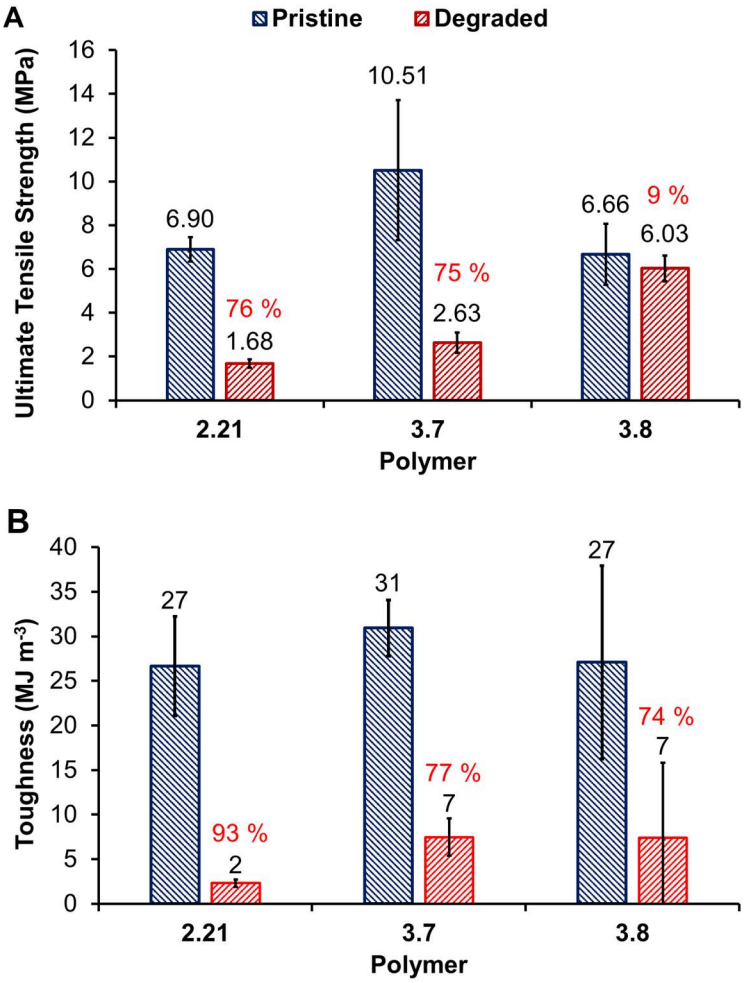

Figure 3.6 *The ultimate tensile strength (A) and toughness (B) of polymer* ***2.21****,* ***3.7*** *and* ***3.8****, before and after degradation, calculated from the stress-strain curves. Errors are calculated from the standard deviation (n = 5)*

The small loss (9 %) in ultimate tensile strength of polymer **3.8** after degradation further proves that the crystalline network provided by the polyester backbone is not compromised by the degradation process. In contrast, the reduction in ultimate tensile strength of approximately 75 % for polymers **2.21** and **3.7** show that soft domain provided by the hydrogenated polybutadiene backbone does not provide the strength of the material, but instead the strength is derived from the supramolecular interactions which are compromised by the degradation process. Regarding the materials toughness before and after degradation, both polymers **3.7** and **3.8** exhibited a similar loss in toughness (77 % and 74 %, respectively), but not as significant a loss as observed in the case of polymer **2.21** (93 %) (Figure 3.6).

3.2.4. Adhesion Testing

Although polymers **3.5** and **3.6** did not form self-supporting films, it was possible to carry out adhesion tests. Butt-tensile adhesion samples were adhered at 25 and 60 °C. The force required to break the adhesive bond was recorded (Figure 3.11).

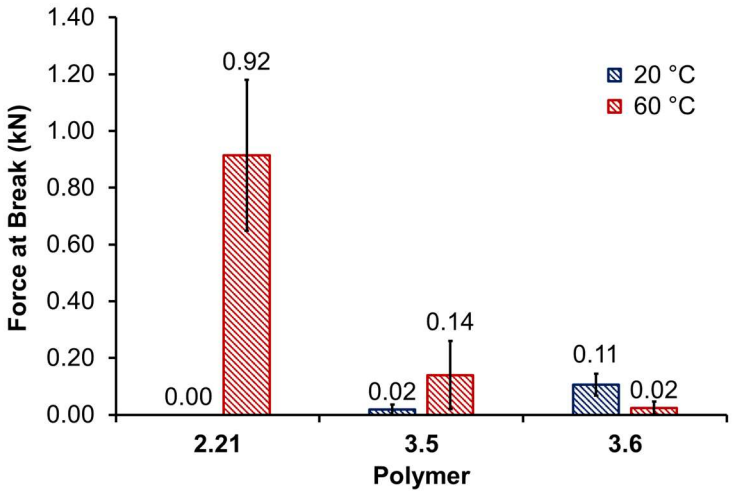

Figure 3.7 *The force required to break the adhesive bond between two butt-tensile cylinders adhered at different temperatures for the first series of polymers,* ***2.21****,* ***3.5*** *and* ***3.6*** *containing different isocyanate linkers. Errors were calculated from the standard deviation (n = 5).*

Butt-tensile adhesion tests on the viscous polymers **3.5** and **3.6** showed that they were 85 % and 98% weaker in adhesive strength, respectively, in comparison to polymer **2.21** when adhered at 60 °C (the lowest temperature that polymer **2.21** would adhere at). This data shows that loss of the phase separation within the polymer network, driven by the aromatic diisocyanate linker, results in a dramatic loss in the adhesive strengths.

In a similar fashion, polymers **2.21**, **3.7** and **3.8** were tested using lap shear and butt-tensile adhesion experiments. Lap shear adhesion tests were carried out before and after treatment with fluoride ions. Butt-tensile adhesion tests were employed to show the difference in adhesion strength at different temperatures. In addition, these samples were re-bonded to prove the reversibility of the polymeric adhesive.

Lap shear adhesion samples were carried out according to ASTM D1002,[39] where samples were compressed with a 1 kg weight at 140 °C for 18 hours. The adhered samples were pulled and the force at break was recorded and converted into the lap shear modulus which takes into account the surface area of adhered material (Figure 3.11). Samples were degraded by submerging in a 0.025 M TBAF solution in acetone (polymers **2.21** and **3.7**), or acetonitrile (polymer **3.8**), selected so that the samples did not dissolve over the timescale of the experiment.

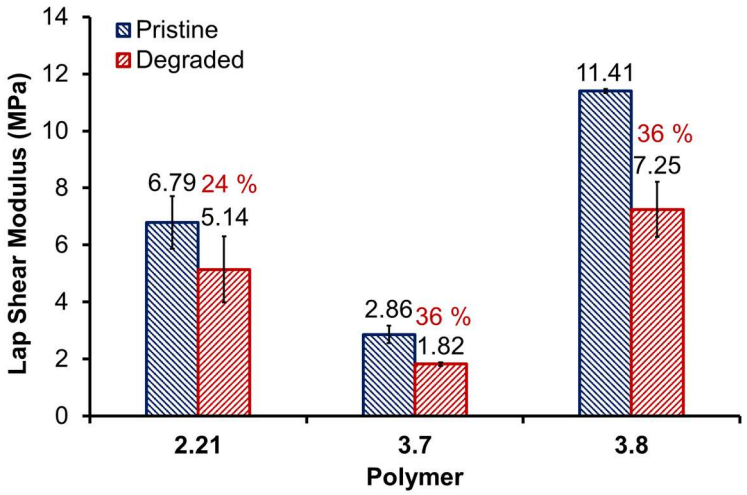

Figure 3.8 *The force at break recorded from the lap shear samples of polymer* ***2.21****,* ***3.7*** *and* ***3.8****; before and after degradation. Errors were calculated from the standard deviation of five samples. Errors were calculated from the standard deviation (n = 5)*

All three materials showed a weakening in adhesive strength of approximately 30 %; thereby proving that the degradable unit will work with a range of polymeric structures without being unaffected by the chemical compositions. Polymer **3.7** which had a marginally stronger ultimate tensile strength and toughness over polymer **2.21**, showed a much weaker adhesion strength. Polymer **3.8** shows the reverse of this trend, with a similar ultimate tensile strength and toughness to polymer **2.21**, but nearly twice as strong as an adhesive as measured by lap shear adhesion tests.

To determine the how temperature affects adhesion strengths, butt-tensile adhesion tests were carried out by placing a 16 mm diameter circle film piece between two steel cylinders. The cylinders were compressed with a 100 N force and left at the required temperature for 18 hours before testing. The force required to break the adhesive bond was recorded and detailed in Figure 3.12.

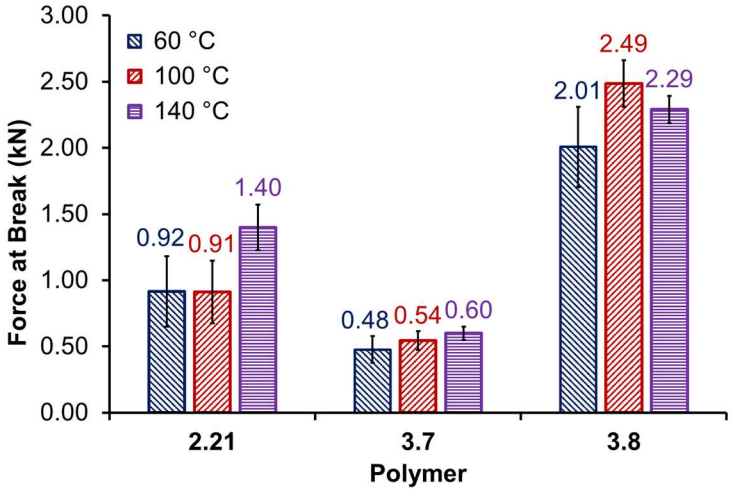

Figure 3.9 *Butt-tensile adhesion studies for polymers **2.21**, **3.7** and **3.8** adhered at different temperatures for 18 hours to determine the optimal conditions for adhesion. Errors were calculated from the standard deviation (n = 4).*

From the butt-tensile adhesion tests, a similar trend to the lap-shear adhesion results was observed. Polymer **3.7** exhibited nearly half the adhesion strength when compared to polymer **2.21**, and interestingly polymer **3.8** possesses nearly double the adhesion strength. Polymer **2.21** shows its optimum adhesion temperature is 140 °C breaking at 1.40 kN, which may be accountable as a consequence of exhibiting a viscoelastic transition or "melt" temperature at 129 °C (Figure 3.5). Polymer **3.7** shows a similarly weak adhesion (*ca.* 0.54 kN) over the range of temperatures tested. Polymer **3.8** (T_m = 49 °C (Figure 3.6)) containing the polyester **3.2** as the backbone shows the strongest bonding adhesion strengths, even at 60 °C.

The adhesion strength is close between the three temperatures tested for polymer **3.8**, thereby proving that the polymer is close to it ultimate adhesion strength at 60 °C. Even though polymers **2.21** and **3.8** show similar percentage errors (±29% and ±25%, respectively), ANOVA calculations, which determines the similarity of raw data of four samples, shows a <0.01 % chance that the force at break values for polymers **2.21** and **3.8** are the same. To assess the versatility of polymer **3.8** over **2.21**, the adhesives were adhered for 0.5 hours and compared to the results when adhered for 18 hours (Figure 3.13a).

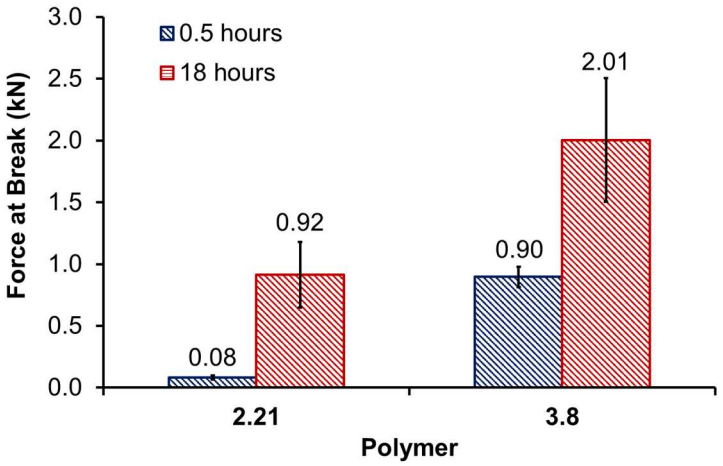

Figure 3.10 *The force required to break the adhesives from the butt-tensile adhesion test, with adhesions carried out at 60 °C for 0.5 and 18 hours. Errors were calculated from the standard deviation (n = 4).*

Polymer **2.21** shows very little adhesion strengths when adhered for 30 minutes which is a result of the polymer not being able to flow or melt during this time periods. However, polymer **3.8** does melt and flow in this time period, and hence will adhere the substrates. In fact, polymer **3.8** shows similar adhesion strengths after 30 minutes as polymer **2.21** does after 18 hours. This, therefore, proves that changing monomer backbone to a crystalline polyester increases the adhesive strength, and lowers the adhesive temperature while maintaining the degradability property of the material.

Finally, thermal debonding-rebonding experiments were carried out only on polymer **3.8** to show thermal reversibility of the adhesive (Figure 3.14).

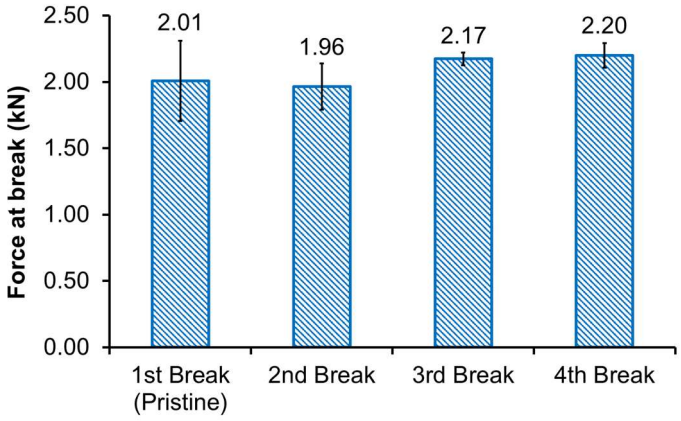

Figure 3.11 *Debonding-rebonding studies of polymer* ***3.8*** *when adhered at 60 °C for 18 hours. Errors were calculated from the standard deviation (n = 4).*

Polymer **3.7** showed weaker adhesion in comparison to polymer **3.8**, and hence re-adhesion tests were not tested; and polymer **2.21** was already shown to be thermally reversible as an

adhesive without loss of adhesive strength (Chapter 2, Figure 2.14).[19] Using butt-tensile adhesion studies with polymer **3.8** adhered at 60 °C for 18 hours, the substrates were pulled apart before re-adhering under the same thermal conditions (60 °C). The debond-rebond cycle was repeated four times, and the force to break the specimen was recorded.

These results demonstrate that polymer **3.8** containing the polyester **3.2** backbone and 4,4'-MDI diisocyanate linker **2.19** is thermally rebondable over three debond-rebond cycles. Furthermore, with strong adhesion temperatures at 60 °C and thermoplastic type properties, polymer **3.8** can be classed as a low-melt adhesive which are very desirable in the adhesives market.[40]

3.3. Conclusions

In this study, two series of polymers have been synthesised in order to determine whether changing either the diisocyanate linker or the monomer backbone would both decrease the thermal adhesion temperature and increase the mechanical/adhesive properties. Both series of polymers showed chain extension with the degradable unit, followed by reduction of molecular weight when degraded with a fluoride source. Rheological analysis was used in conjunction with differential scanning calorimetry to show that changing the diisocyanate linker reduced the viscoelastic transition temperature to near room temperature. Changing the polyol to a polyester provided a material that exhibited a melt at 49 °C. Wide-angle X-ray diffraction analysis revealed supramolecular interactions for all of the polymers, with variable temperature experiments showing the reversibility of these interactions. The polymers from the first series in which the diisocyanate linker was changed proved too weak during adhesion studies, even though they demonstrated low viscoelastomeric transition temperatures. The second series of polymers in which the polyol was changed showed good mechanical properties, and an approximately 33 % drop in strength after degradation. Adhesion tests were thus carried out on the second series of polymers. Polymer **3.8** containing the polyester **3.2** showed the greatest adhesive strengths at near 3.5 kN at 140 °C from lap shear adhesion tests and at approximately 2.0 kN at 60 °C from butt-tensile adhesion tests; nearly twice as strong as polymer **2.21** formed from a hydrogenated polybutadiene, but at a much lower bonding temperature (60 °C). This shows that polyester based debondable adhesive have promising future materials and aspects within the adhesives market.

3.4. Experimental Section

3.4.1. Materials

Krasol HLBH-P2000 and Krasol HLBH-P3000 was kindly supplied by Cray Valley. Stepanpol PC-205-P 30 was kindly supplied by Alfa Chemicals.

3.4.2. Characterisation.

Characterisation was carried out as reported in Chapter 2, page 55. Characterisation specific to this chapter are reported below.

Rheological measurements were performed using an Anton Paar Physica MCR 301 rheometer with a parallel plate oscillatory shear geometry. For polymer film samples, circular samples of 25 mm diameter (0.35 mm average thickness) were cut from the polymer film using a steel punch cutter. For the viscous polymers, the polymer was cooled to 10 °C, and a small ball of 10 mm diameter was flattened into a 25 mm disc. For the single frequency temperature sweep, samples were placed into the rheometer and initialised at a temperature above the point of polymer flow, and then subjected to temperature ramp cycle at a rate of 2 °C/min, first increasing then decreasing. This cycle was repeated twice to assess repeatability and any changes in properties. The frequency of oscillation was set to 5 Hz, and the shear strain amplitude to 0.1%. The data was processed using Microsoft Excel 365 and MATLAB R2017. SAXS and WAXS analysis was carried out at the Alba Synchrotron on the Non-Crystalline Diffraction Beamline (BL11-NCD). Samples of approximately 8 mm diameter circles were cut from the film and wrapped in aluminium foil. The sample was placed into a Linkam stage, connected to a liquid nitrogen cooling station. The beamline was equipped with an ADSC Quantum 210r CCD detector (SAXS) and Rayonix LX255-HS detector (WAXS). The data was processed using Microsoft Excel 365 and MATLAB R2017.

Tensile stress-strain experiments using an AML X5-500 single column universal tester, equipped with a 5 kN load cell and wedge grips. Specimens were cut from the film of 4.0 × 0.5 cm sizes. The samples were analysed at a strain rate of 100 mm/min.

Lap shear adhesion samples were carried out in accordance with ASTM D1002 standards using an AML X5-500 single column universal tester, equipped with a 5 kN load cell and wedge grips. The aluminium coupons were cleaned for 20 minutes in methyl ethyl ketone and dried overnight in a desiccator. The coupons were then etched using the following procedure: iron (III) sulfate (75 g) was dissolved in deionised water (500 mL), to which concentrated sulfuric

acid (100 mL) was added slowly while maintaining the temperature below 65 °C. The etching bath was placed in a water bath at 65 °C, and the coupons submerged in the etching solution for 12 minutes. Upon completion, the coupons were washed with deionised water at room temperature, followed by deionised water at 70 °C and repeating between the two temperatures three times. The coupons were placed in an oven at 70 °C for 2 hours before being used to create the lap shear samples. Samples were adhered at 140 °C for 18 hours with a 1 kg weight used as a compression source. Samples were subjected to a strain rate of 1.0 mm min^{-1}. Butt tensile adhesion samples were carried in accordance with BS EN 15870 2009 and carried out on an Instron 5500R Universal Mechanical Testing Machine equipped with a 10 kN load cell and serrated wedge grips for cylinders. Steel cylinders with a 16 mm diameter were grit blasted with Guyson fumed alumina mesh size 180/220; and cleaned sequentially with compressed air, then acetone before being stored in a desiccator prior to use. The samples were placed in a vice grip with a spacer between each substrate and compressed under a spring tension of 100 N; before being placed in an oven at specific temperatures for 18 hours. Samples were subject to a strain rate of 1.3 mm/min.

3.4.3. Synthesis of DU 2.6

The degradable unit (**2.6**) was synthesised as reported in Chapter 2, page 57.[19]

3.4.4. General method for one-pot synthesis of polymers

The polyol (15 mmol) was dried in a vacuum oven at 100 °C under 100 mbar vacuum for 1 hour. The diisocyanate (2.0 equivalents) was added to the polyol (12 mmol, 1.0 equivalent) and stirred at 80 rpm with an overhead stirrer, at 80 °C for 3 hours to form an isocyanate terminated prepolymer. The reaction temperature was raised to 105 °C and the degradable unit (1 equivalent) was added and stirred for 1 hour. The crude polymer was dissolved in chloroform (200 mL) and precipitated slowly into methanol (1.8 L). The precipitate was filtered and washed with methanol (2 × 200 mL) dried under reduced pressure to afford the adhesive polymer.

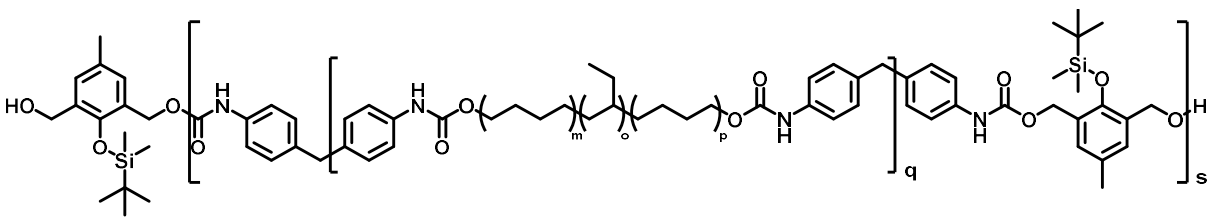

Polymer 2.21 (40.1 g, 97 %). ν_{max} (thin film, cm^{-1}) 3317, 2961, 2919, 2873, 2854, 2159, 1736, 1708, 1599, 1533, 1461, 1414, 1379, 1304, 1219, 1066. δ_H (400 MHz, $CDCl_3$, ppm) (n =

number of chain extension) 7.38 – 7.20 (m, 8H_n), 7.21 – 7.02 (m, 8H_n + 2H_n), 6.55 (m, 4H_n), 5.17 (s, 4H_n), 4.82 – 4.59 (m, 0.3H_n), 4.23 – 4.07 (m, 4H_n), 3.88 (s, 4H_n), 2.30 (m, 3H_n), 1.93 – 0.71 (m, 350H_n), 0.21 (s, 6H_n). δ_C (100 MHz, $CDCl_3$, ppm) 153.7, 153.5, 149.16, 136.3, 136.2, 136.1, 135.9, 131.4, 130.8, 129.4, 126.9, 118.9, 62.5, 40.6, 38., 38.7, 38.4, 38.1, 37.9, 37.3, 36.1, 34.9, 33.5, 33.3, 30.7, 30.5, 30.2, 29.9, 29.8, 29.3, 26.8, 26.6, 26.5, 26.1, 25.9, 25.9, 20.6, 19.5, 18.7, 11.4, 10.9, 10.7, 10.66, 10.6, 9.4, 0.0, -0.9, -3.7. GPC (THF/BHT 250 ppm) M_w 71400, M_n 26100, $Đ$ 2.73. DSC T_g = -45.5 °C.

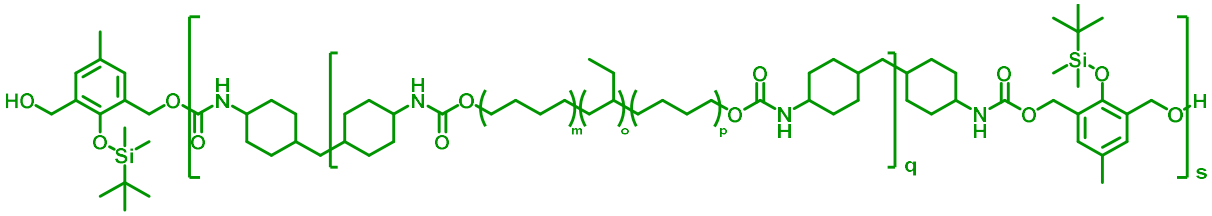

Polymer 3.5 (36.5 g, 88 %). ν_{max} (thin film, cm^{-1}) 3333, 2958, 2919, 2854, 2266, 1698, 1536, 1461, 136, 1223, 1088, 897, 778. δ_H (400 MHz, $CDCl_3$, ppm) (n = number of chain extension) 7.14 – 7.04 (m, 2H_n), 5.06 (s, 4H_n), 4.95 – 4.20 (m, 4H_n), 4.17 – 3.90 (m, 4H_n), 3.88 – 3.66 (m, 2H_n), 3.52 – 3.26 (m, 3H_n), 2.08 – 0.50 (m, 446H_n), 0.19 (s, 6H_n). δ_C (100 MHz, $CDCl_3$, ppm), 39.1, 38.9, 38.5, 38.4, 37.9, 37.6, 36.1, 36.0, 33.4, 33.2, 32.0, 30.7, 30.2, 30.1, 29.8, 28.1, 26.8, 26.6, 26.4, 26.2, 26.1, 26.0, 25.9, 20.6, 18.7, 10.9, 10.7, 0.0, -3.7. GPC (THF/BHT 250 ppm) M_w 51800, M_n 20400, $Đ$ 2.54. DSC T_g = -48.2°C.

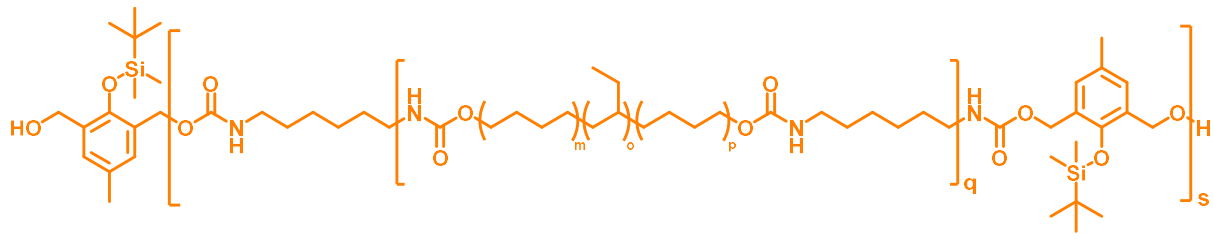

Polymer 3.6 (33.8 g, 87 %). ν_{max} (thin film, cm^{-1}) 3336, 2956, 2919, 2851, 2873, 1705, 1539, 1464, 1376, 1242, 1153, 1070, 900, 838, 778, 725. δ_H (400 MHz, $CDCl_3$, ppm) (n = number of chain extension) 7.12 – 7.06 (m, 2H_n), 5.07 (s, 4H_n), 4.92 – 4.57 (m, 4H_n), 4.14 – 3.94 (m, 4H_n), 3.31 – 2.97 (m, 10H_n), 2.30 – 2.23 (m, 3H_n), 2.04 – 1.82 (m, 4H_n) 1.71 – 0.53 (m, 413H_n), 0.19 (s, 6H_n). δ_C (100 MHz, $CDCl_3$, ppm), 62.1, 40.9, 38.9, 38.5, 38.3, 37.9, 37.6, 36.1, 33.4, 33.2, 30.7, 30.2, 29.8, 26.8, 26.6, 26.3, 26.0, 25.8, 20.6, 18.7, 10.9, 10.6, 0.0, -3.7. GPC (THF/BHT 250 ppm) M_w 254000, M_n 56000, $Đ$ 4.54. DSC T_g = -46.3°C.

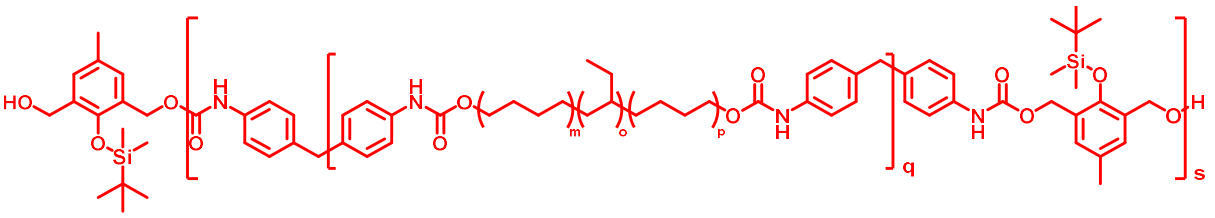

Polymer 3.7 (37.3 g, 99 %). ν_{max} (thin film, cm^{-1}) 2234, 2958, 2920, 2873, 2854, 2169, 2003, 1733, 1708, 1598, 1526, 1457, 1414, 1380, 1311, 1070, 772. δ_H (400 MHz, $CDCl_3$, ppm) (n = number of chain extension) 7.38 – 7.20 (m, $8H_n$), 7.20 – 6.97 (m, $8H_n + 2H_n$), 6.71 – 6.39 (m, $4H_n$), 5.17 (s, $4H_n$), 4.94 – 4.79 (m, $0.2H_n$), 4.23 – 4.06 (m, $4H_n$), 3.88 (s, $4H_n$), 2.28 (m, $3H_n$), 2.06 – 0.54 (m, $530H_n$), 0.21 (s, $6H_n$). δ_C (100 MHz, $CDCl_3$, ppm) 153.7, 153.4, 136.2, 135.8, 131.4, 130.8, 129.4, 126.9, 118.9, 62.5, 40.5, 38.9, 38.4, 37.8, 36.0, 34.9, 33.6, 33.2, 30.7, 30.2, 29.7, 26.7, 26.1, 25.9, 20.5, 18.6, 10.9, 10.7, 10.6, 10.0, 0.0, -3.7. GPC (THF/BHT 250 ppm) M_w 445000, M_n 77180, $Đ$ 5.77. DSC T_g = -47.9 °C.

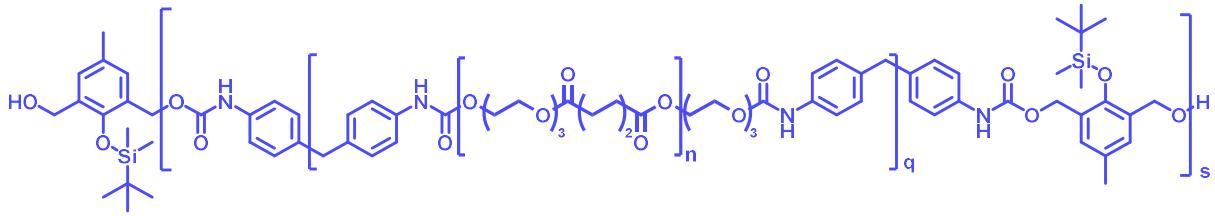

Polymer 3.8 (55.6 g, 92 %). ν_{max} (thin film, cm^{-1}) 3349, 2954, 2935, 2898, 2864, 2178, 2003, 1727, 1596, 1530, 1464,1370, 1260,1219, 1164, 1073, 1044, 969, 910, 735. δ_H (400 MHz, $CDCl_3$, ppm) (n = number of chain extension) 7.36 – 7.22 (m, $8H_n$), 7.16 – 7.03 (m, $8H_n + 2H_n$), 6.92 – 6.68 (m, $2H_n$), 5.19 – 5.14 (m, $3H_n$), 4.68 – 4.62 (m, $1H_n$), 4.17 – 4.11 (m, $4H_n$), 4.10 – 4.02 (m, $66H_n$), 3.90 – 3.85 (m, $4H_n$), 2.39 – 2.25 (m, $70H_n$), 1.86 – 1.75 (m, $4H_n$), 1.73 – 1.56 (m, $140H_n$), 1.45 – 1.31 (m, $70H_n$), 1.03 (s, $9H_n$), 0.26 – 0.14 (m, $6H_n$). δ_C (100 MHz, $CDCl_3$, ppm) 173.4, 129.4, 118.8, 64.3, 40.5, 33.9, 28.8, 28.5, 26.0, 25.6, 24.4, 18.7, 0.0, -3.7.GPC (THF/BHT 250 ppm) M_w 118000, M_n 35000, $Đ$ 3.37. DSC T_g = 1.0 °C, T_m = 48.4 °C.

3.4.5. Sample Preparation for Mechanical Assessment.

Uniform films (between 200 and 500 µm thick) suitable for mechanical testing were cast from THF (0.2 g/mL) in a PTFE mould (15 × 15 cm). The solvent was allowed to evaporate slowly at room temperature overnight, before being placed in a vacuum oven at 50 °C (800 mbar) for a further 18 hours to remove remaining solvent. DSC analysis showed that solvent was not present in the resultant cast films.

3.5. References

1. K. M. Herbert, S. Schrettl, S. J. Rowan and C. Weder, *Macromolecules*, 2017, **50**, 8845–8870.
2. M. Wei, Y. Gao, X. Li and M. J. Serpe, *Polym. Chem.*, 2017, **8**, 127–143.
3. M. A. C. Stuart, W. T. S. Huck, J. Genzer, M. Müller, C. Ober, M. Stamm, G. B. Sukhorukov, I. Szleifer, V. V Tsukruk, M. Urban, F. Winnik, S. Zauscher, I. Luzinov and S. Minko, *Nat. Mater.*, 2010, **9**, 101–113.
4. A. J. R. Amaral and G. Pasparakis, *Polym. Chem.*, 2017, 6464–6484.
5. J. H. Aubert, *J. Adhes.*, 2003, **79**, 609–616.
6. C. Heinzmann, C. Weder and L. M. de Espinosa, *Chem. Soc. Rev.*, 2015, **342**, 342–358.
7. R. J. Wojtecki, M. A. Meador and S. J. Rowan, *Nat. Mater.*, 2011, **10**, 14–27.
8. C. Heinzmann, S. Coulibaly, A. Roulin, G. L. Fiore and C. Weder, *ACS Appl. Mater. Interfaces*, 2014, **6**, 4713–9.
9. S. T. Phillips, W. Seo, J. S. Robbins, M. Olah, K. Schmid and A. M. DiLauro, .
10. P. J. M. Bouten, M. Zonjee, J. Bender, S. T. K. Yauw, H. Van Goor, J. C. M. Van Hest and R. Hoogenboom, *Prog. Polym. Sci.*, 2014, **39**, 1375–1405.
11. V. Delplace and J. Nicolas, *Nat. Chem.*, 2015, **7**, 771–784.
12. Y. Shi, P. Zhou, R. Freitag and S. Agarwal, *ACS Biomater. Sci. Eng.*, 2015, **1**, 971–977.
13. S. Ho and A. M. Young, *Eur. Polym. J.*, 2006, **42**, 1775–1785.
14. H. Mohapatra, H. Kim and S. T. Phillips, *J. Am. Chem. Soc.*, 2015, **137**, 12498–12501.
15. B. T. Michal, E. J. Spencer and S. J. Rowan, *ACS Appl. Mater. Interfaces*, 2016, **8**, 11041–11049.
16. P. Pissis, G. Georgousis, C. Pandis, P. Georgiopoulos, A. Kyritsis, E. Kontou, M. Micusik, K. Czanikova and M. Omastova, *Procedia Eng.*, 2015, **114**, 590–597.
17. Z. Guo, Y. Zuo and S. Feng, *RSC Adv.*, 2016, **6**, 73140–73147.
18. E. Chabert, J. Vial, J.-P. Cauchois, M. Mihalut and F. Tournilhac, *Soft Matter*, 2016, **12**, 4838–4845.
19. T. S. Babra, A. Trivedi, C. N. Warriner, N. Bazin, D. Castiglione, C. Sivour, W. Hayes and B. W. Greenland, *Polym. Chem.*, 2017, **8**, 7207–7216.
20. H. Kim, H. Mohapatra and S. T. Phillips, *Angew.Chem. Int.Ed.*, 2015, **54**, 13063–13067.
21. A. Feula, X. Tang, I. Giannakopoulos, A. M. Chippindale, I. Hamley, F. Greco, C. P. Buckley, C. R. Siviour and W. Hayes, *Chem. Sci.*, 2016, **7**, 4291–4300.
22. A. Feula, A. Pethybridge, I. Giannakopoulos, X. Tang, A. Chippindale, C. R. Siviour, C. P. Buckley, I. W. Hamley and W. Hayes, *Macromolecules*, 2015, **48**, 6132–6141.
23. X. Tang, A. Feula, B. C. Baker, K. Melia, D. Hermida Merino, I. W. Hamley, C. P. Buckley, W. Hayes and C. R. Siviour, *Polymer*, 2017, **133**, 143–150.
24. D. H. Merino, A. Feula, K. Melia, A. T. Slark, I. Giannakopoulos, C. R. Siviour, C. P. Buckley, B. W. Greenland, D. Liu, Y. Gan, P. J. Harris, A. M. Chippindale, I. W. Hamley and W. Hayes, *Polymer*, 2016, **107**, 368–378.
25. S. Piril Ertem, E. Yilgor, C. Kosak, G. L. Wilkes, M. Zhang and I. Yilgor, *Polymer*, 2012, **53**, 4614–4622.
26. E. Yilgör, M. Isik, C. K. Söz and I. Yilgör, *Polymer*, 2016, **83**, 138–153.
27. O. Oguz, S. A. Koutsoumpis, E. Simsek, E. Yilgor, I. Yilgor, P. Pissis and Y. Z. Menceloglu, *RSC Adv.*, 2017, **7**, 40745–40754.
28. E. Yildirim, M. Yurtsever, E. Yilgör, I. Yilgör and G. L. Wilkes, *J. Polym. Sci. Part B Polym. Phys.*, 2018, **56**, 182–192.
29. O. C. Onder, E. Yilgor and I. Yilgor, *Polymer*, 2018, **136**, 166–178.
30. P. Cordier, F. Tournilhac, C. Soulié-Ziakovic and L. Leibler, *Nature*, 2008, **451**, 977–980.

31. M. Yan, J. Tang, H.-L. Xie, B. Ni, H.-L. Zhang and E.-Q. Chen, *J. Mater. Chem. C*, 2015, **3**, 8526–8534.
32. Y. Yanagisawa, Y. Nan, K. Okuro and T. Aida, *Science*, 2018, **359**, 72–76.
33. X. Qi, D. Zhang, Z. Ma, W. Cao, Y. Hou, J. Zhu, Y. Gan and M. Yang, *ACS Nano*, 2018, **12**, 1062–1073.
34. X. Luo, R. Ou, D. E. Eberly, A. Singhal, W. Viratyaporn and P. T. Mather, *ACS Appl. Mater. Interfaces*, 2009, **1**, 612–620.
35. X. Luo and P. T. Mather, *ACS Macro Lett.*, 2013, **2**, 152–156.
36. P. Taylor, G. Marin, P. Vandermaesen and J. Komornicki, *J. Adhes.*, 1991, **35**, 23–37.
37. K. Melia, B. W. Greenland, D. Hermida-Merino, L. R. Hart, I. W. Hamley, H. M. Colquhoun, A. T. Slark and W. Hayes, *React. Funct. Polym.*, 2018, **124**, 156–161.
38. P. J. Woodward, D. Hermida Merino, B. W. Greenland, I. W. Hamley, Z. Light, A. T. Slark and W. Hayes, *Macromolecules*, 2010, **43**, 2512–2517.
39. American Society for Testing Materials, ASTM D1002-10: Standard Test Method for Apparent Shear Strength of Single-Lap-Joint Adhesively Bonded Metal Specimens by Tension Loading (Metal-to-Metal), https://www.astm.org/Standards/D1002.htm, (accessed 14 May 2018).
40. G. Habenicht, *Applied Adhesive Bonding: A Practical Guide for Flawless Results*, Wiley-VCH, Germany, 2008.

Chapter 4

Fluoride Responsive Crosslinked Debond-on-Demand Reactive Adhesives

Abstract

This chapter reports the design and synthesis of a trifunctional fluoride responsive degradable unit and its use as a crosslinker in a polyurethane network as a debond-on-demand adhesive. Model compound synthesis and degradation studies revealed that the trifunctional degradable group undergoes rapid degradation (<1 minute) when treated with TBAF. Using an *in situ* polymerisation method, the trifunctional degradable group was reacted with a diisocyanate prepolymer and applied to the adhesive surface. Crosslinked adhesives were prepared from a hydrogenated polybutadiene and a crystalline polyester, both of which showed approximately a 30 % increase in adhesive strength when compared to a linear polymeric adhesive when bonding both glass and metal substrates. On treatment with fluoride ions, the adhesive exhibited a 55 % loss in adhesive strength (from 14.6 MPa to 6.7 MPa) after 3 hours.

4.1. Introduction

The linear polymeric systems developed in Chapters 2 and 3 gain their strength from the entanglement of long chains accompanied by the non-covalent supramolecular interactions. The strength of the adhesive was increased approximately two-fold by introducing crystallinity into the network (Chapter 3). As an extension of this study, it was of interest to increase the strength of the adhesive by changing the architecture of the polymer and introducing covalent crosslinking into the polymeric network.

Crosslinked adhesive materials offer higher mechanical strengths, even at high temperatures as the polymeric network consists of one large macromolecule rather than long chains that entangle.[1] Polymers used commonly in crosslinked adhesive formulations include acrylates,[2–7] epoxy resins[8–12] and polyurethanes.[13–15] However, as a result of the larger macromolecular structure, crosslinked materials are insoluble in solvents which could be a disadvantage when the adhesive needs to be removed at the end of life of the product. Consequently, a new class of crosslinked adhesives have been developed to facilitate debonding of the adhesive.

A method used commonly for breaking a crosslinked network is to introduce reversible groups that break apart with a stimulus to allow debonding of the adhesive. For example, thermal stimulus can be used with Diels-Alder adducts which can undergo reversible [4 + 2] cycloaddition (Scheme 1.1).[16–21] Thermal stimuli has also been used with disulfide bridges (Figure 1.12).[22] UV light has been used as a stimulus with the reversible cycloaddition of anthracene based adhesives,[23–25] and with the isomerisation of azobenzene containing adhesives (Chapter 1, section 1.3.2).[26] Although these materials are crosslinked, the groups that allow for the reversibility also provide the weakest point when the material is taken to high temperatures.

Hence, a new technique has recently been employed to add covalently crosslinked regions that can only be broken by a chemical stimulus. Phillips and co-workers showed the use of a crosslinked material that contains fluoride responsive degradable units (**1.57**, Chapter 1).[27] The material showed adhesion to glass through the evaporation of solvent under vacuum. However, this material has several disadvantages. Firstly, obtaining adhesion through the evaporation of solvents results in the loss of volatile organic compounds (VOC's) which are toxic. Secondly, the degradable group requires eight synthetic steps to synthesise, increasing production costs and time. In addition, the polymer requires a ruthenium based catalyst (Grubbs' 2nd generation catalyst, Figure 1.18) for crosslinking to occur which increases toxic waste production.

Therefore, inspired with the synthesis of the bifunctional degradable unit **2.6** used in Chapters 2 and 3,[28] in this chapter is presented the design of a fluoride responsive crosslinking group (TDU) **4.1** with three benzylic groups that could be reacted with a diisocyanate prepolymer (Figure 4.1) and its incorporation into a polyurethane network as a reactive adhesive (Scheme 4.1).

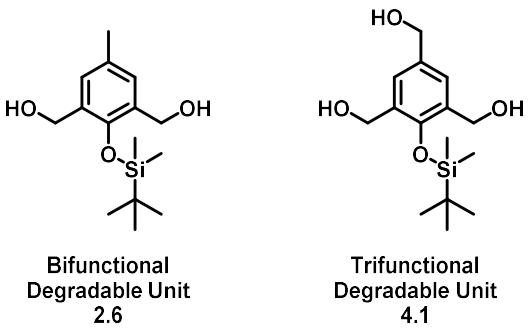

Figure 4.1 *Comparison of the chain extending and cross-linkable degradable units*

In contrast to the previous crosslinked fluoride responsive systems developed by Phillips and co-workers,[29] this proposed crosslinked adhesive requires two steps to produce the degradable group. The primary aim was for the degradable TDU group to be incorporated into a

polyurethane network without the need of catalysts or solvents and for adhesion to be achieved by the *in situ* preparation on the adhesive surface without the need of solvent evaporation. Upon treatment of fluoride ions, the resulting polyurethane network is designed to dramatically lower in molecular weight and hence reduce in adhesive strength (Scheme 4.1).

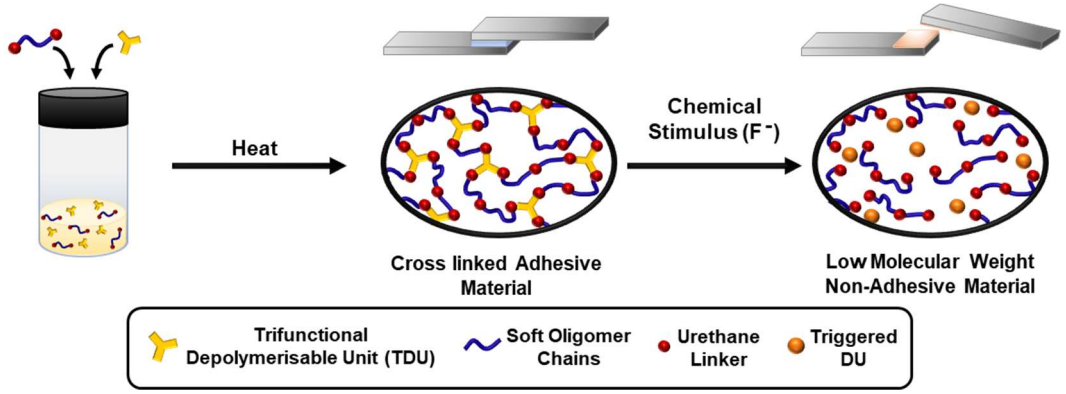

Scheme 4.1 *Schematic showing the non-reversible nature of the fluoride responsive crosslinked adhesive.*

4.2. Results and Discussion

4.2.1. Synthesis of Trifunctional Degradable unit (TDU).

To encourage crosslinking within a polymeric structure, a new fluoride responsive groups had to be designed. The bifunctional degradable unit (BDU) **2.6** had two terminal hydroxyl groups that allowed for chain extension when reacted with a diisocyanate pre-polymer (Chapter 2 and 3). Therefore, to increase crosslinking, another terminal hydroxyl group needed to be added to the aromatic ring to form a trifunctional degradable group (TDU) **4.1**. Addition of a third benzyl alcohol at the *para* position to the silyl group adds an extra site for reaction with the isocyanate terminated prepolymers facilitating the formation of the desired crosslinked materials. However, whilst this study was underway, Phillips and co-workers reported the synthesis of the TDU **4.1**.[30] This material broke down on contact with nerve agents to release pyrene groups which resulted in a colorimetric response. Phillips and co-workers reported a three-step method to synthesising the TDU **4.1** with an overall yield of 34 % (310 mg).

The bifunctional BDU **2.6** was synthesised starting from 2,6-bis(hydroxymethyl)-*p*-cresol **2.5** (Scheme 2.3, Chapter 2). However, 2,4,6-trimethylolphenol (**4.3**) required for the synthesis of **4.1** cannot be purchased and had to be synthesised. Fortunately, the synthesis of sodium 2,4,6-trimethylolphenate **4.3** has been known since the early 1950's when it was introduced by Martin during his investigations into developing multifunctional sodium phenolates.[31] Martin reports that 2,4,6-trimethlyolphenol reacts readily with itself to form dimers and trimers; whereas this

does not occur with the sodium salts. This data suggests that **4.3** was produced readily by leaving a solution of formaldehyde in sodium phenolate to stand for seven days before precipitating the red liquor into ethanol to afford **4.3** as a white powder (Scheme 4.2).

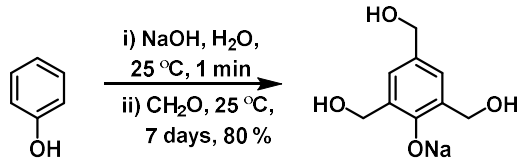

4.2 4.3

Scheme 4.2 *Martin's synthesis of sodium 2,4,6-trimethylolphenate* ***4.3***.[31]

However, when this method was attempted, on multiple occasions the white precipitate turned pink and then to red over a period of a couple of days. The red solid did not dissolve in water, DMSO or DMF as in the case of the white powder reported by Martin.[31] It was postulated that the red solid was a form of the crosslinked phenol-formaldehyde resins, which is commercially known as Bakelite™.

To avoid this occurrence, the procedure was modified so that sodium hydroxide was added to a mixture of phenol **4.3** dissolved in formalin in water at 0 °C and stirred at 25 °C for 24 hours (Scheme 4.2). The orange liquor was precipitated into *iso*-propanol at 0 °C and filtered to afford the sodiated trimethylolphenate **4.3** as a whitish pink powder in 70 % yield. The powder was dried under vacuum to remove excess formalin, and then stored under vacuum. Silyl protection of **4.4** was carried out using the same method to synthesis **2.6** (Chapter 2) with the small modification of the use of a silica plug to afford **4.1** as a white powder in 45 % yields (Scheme 4.3). The melting point was determined to be 93 °C by DSC.

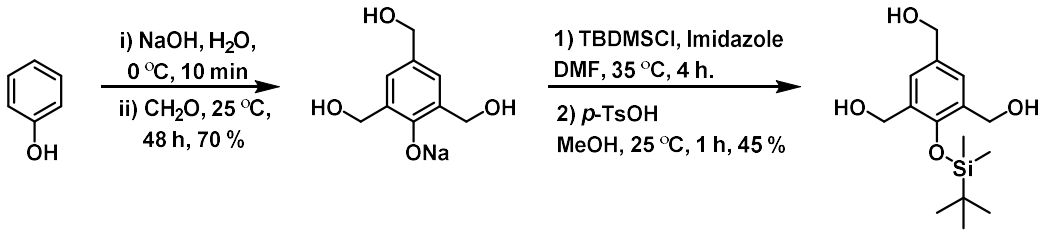

4.2 4.3 4.1

Scheme 4.3 *Synthesis of the cross linkable degradable unit* ***4.1***.

4.2.2. Synthesis and Testing of a Model Compound

In line with the studies on the degradable unit **4.1** (Chapter 2), a model compound was synthesised to determine the feasibility of degradation and potential mechanism on addition of TBAF. The model compound **4.6** was synthesised by the addition of 4-nitrophenyl isocyanate

4.4 to TDU **4.1** in THF (Scheme 4.4). ^{1}H NMR spectroscopic analysis of the crude product obtained indicated that approximately 80 % of the material generated was the desired model compound **4.5**. This mixture was used without further purification for preliminary degradation assessments.

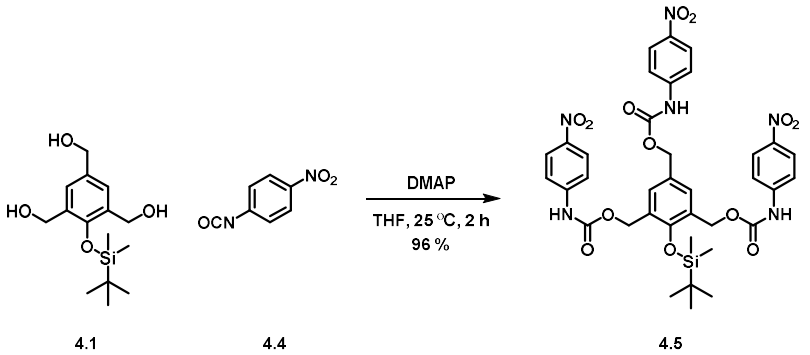

Scheme 4.4 *Synthesis of the model compound derived from TDU 2.*

Degradation of **4.5** can be achieved by the addition of a fluoride ion, with the proposed route of degradation detailed in Scheme 4.5. Addition of the fluoride ion removes the silyl detecting group to form a phenoxide ion. This then allows for the self-immolative[32] breakdown of the compound with initial release of three 4-nitrophenyl carbamic acid **4.8** groups; which in turn rapidly breakdown to form 4-nitroaniline **4.12** and carbon dioxide with water. The by-product from the breakdown of the model compound **4.5** is 2,4,6-trimethylolphenol **4.11**.

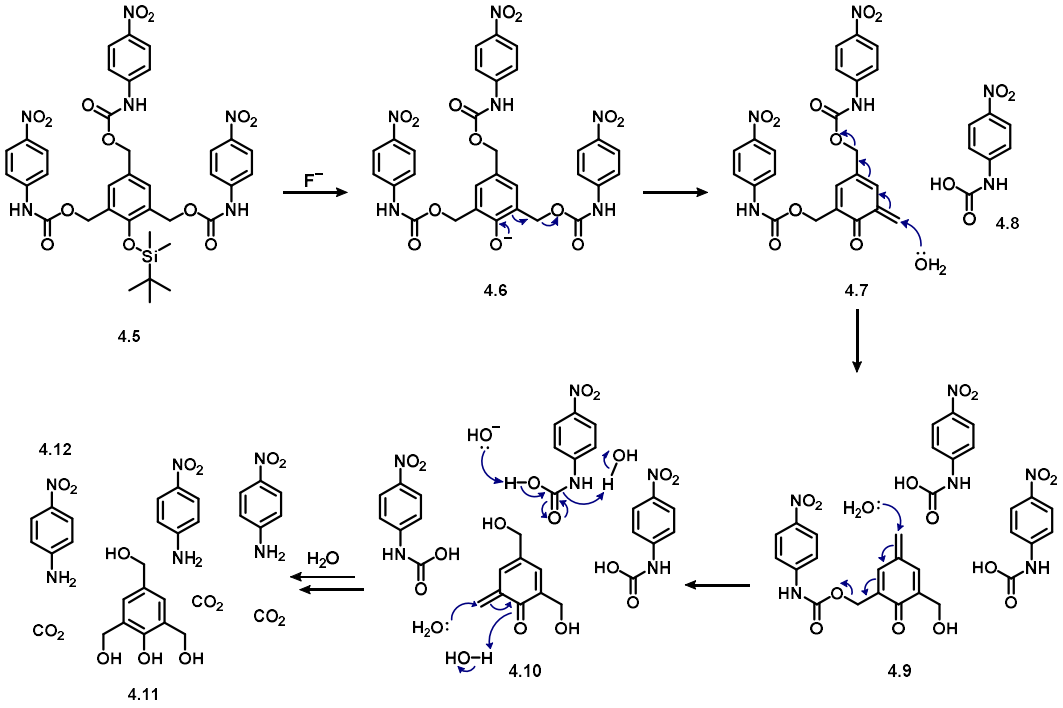

Scheme 4.5 *Mechanism showing the degradation of the model compound **4.5** upon treatment with fluoride ions*

^{1}H NMR spectroscopy was carried to observe the degradation of the model compound **4.5** upon addition of a fluoride ion - in this study *tetra*-butylammonium fluoride was used (Figure 4.2). Within a minute of the addition of fluoride ions, the intensity of the two singlet resonances at 5.18 and 5.21 ppm (H_B and H_A) corresponding to the methylene protons of the benzyl ethers decreased dramatically indicating breakdown of the model compound. Furthermore, the observed loss of aromatic resonances at 7.93 and 7.43 ppm and the appearance of two aromatic resonances at 6.58 and 7.89 ppm (H_C and H_D) after addition of TBAF revealed the release of 4-nitroaniline.

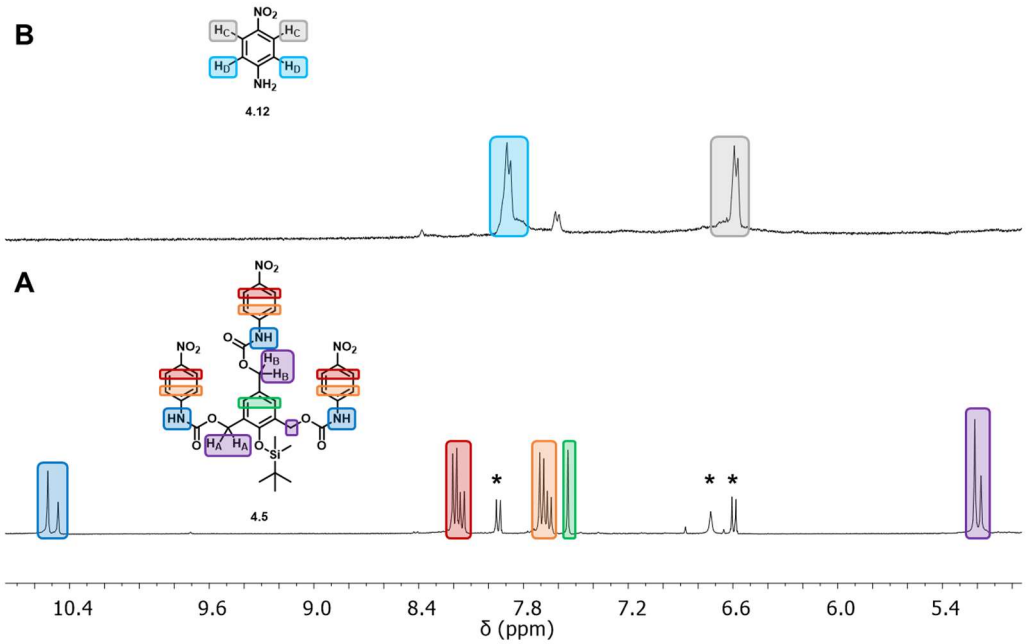

Figure 4.2 *^{1}H NMR spectra showing the model compound **4.6** (A) before degradation and (B) after degradation with TBAF. The resonances for the impurity in spectrum A, 4-nitroaniline **4.12**, is marked with an asterisk (*). (DMSO-d_6, 400 MHz).*

In agreement with the recent studies conducted by Philips,[30] the model compound **4.5** and hence the TDU **4.1** undergoes instantaneous breakdown upon addition with a fluoride source. Attention thus moved towards the synthesis of crosslinked polymers with the TDU unit **4.2**.

4.2.3. Synthesis of Crosslinked Adhesives

In Chapter 2, the non-polar hydrogenated polybutadiene (Krasol HLBH-P 2000 **2.18**) was used as the polyol backbone to facilitate phase separation between the hard aromatic regions and polyol midblock. In Chapter 3, an ester based polyol was introduced, Stepanpol PC-205P-30 **3.2** in order to introduce crystallite regions within the polymeric network to aid thermal and adhesive properties. The Krasol based polymer **2.21** produced elastomeric amorphous materials, whereas the Stepanpol based polymer **3.8** produced stiffer materials with a low

melting point. To see how crystallinity affected these crosslinked materials for the crosslinked polymers (CLP), both Krasol **2.18** and Stepanpol **3.2** were used separately to form pre-polymers which were then reacted with TDU **4.1** (Scheme 4.6). 4,4'-methylene diphenyl diisocyanate (4,4'-MDI) **2.19** was selected as the diisocyanate linker as it produced the strongest materials in Chapter 3.

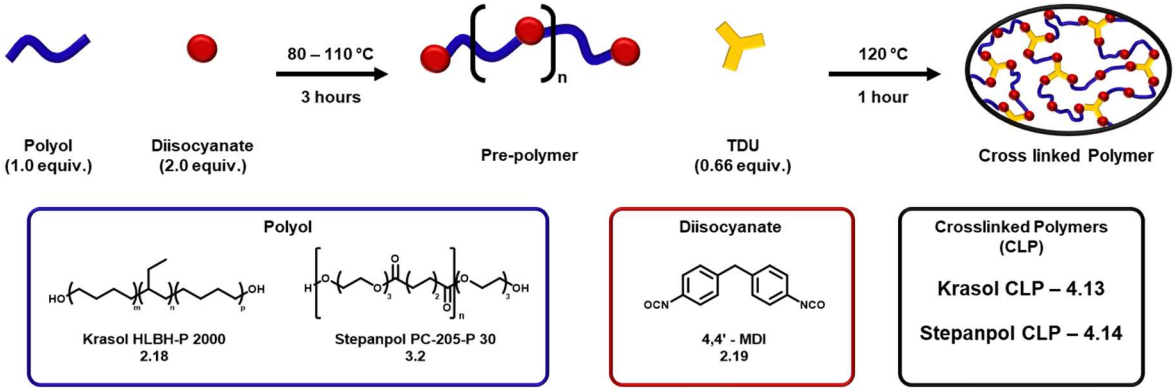

Scheme 4.6 *Synthesis of the crosslinked polymeric materials*

Synthesis of the pre-polymers were carried out using the same procedures in Chapters 2 and 3. TDU **4.1** was added to the prepolymer at 120 °C and left to stir for 1 hour at which point the material solidified to form the CLP's (Figure 4.3).

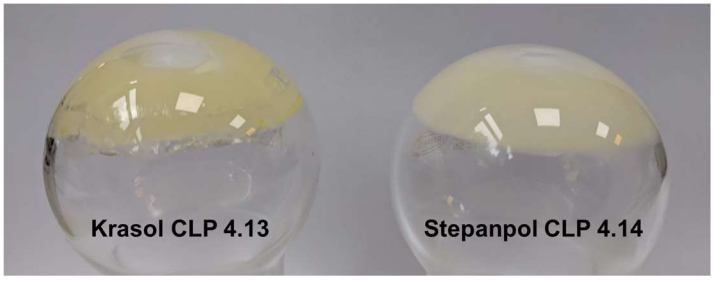

Figure 4.3 *Photographs of the Krasol CLP* ***4.13*** *(left) and Stepanpol CLP* ***4.14****. Samples were prepared on a two-gram scale.*

During the synthesis of the chain extended materials produced in Chapters 2 and 3, the mixture of pre-polymer and BDU **2.6** also solidified after 1 hour. However, in these cases, the chain extended materials dissolved easily in THF or chloroform. Therefore, to determine if the mixtures contained crosslinked materials, a variety of solvents (3 mL) were added to *ca.* 100 mg samples of the Krasol CLP **4.13** and Stepanpol CLP **4.14** and left to stir overnight at 35 °C. Figure 4.4 shows photographs of the CLP's after this time. A crosslinked material should not dissolve and at best, the material will absorb solvent causing it to the swell.

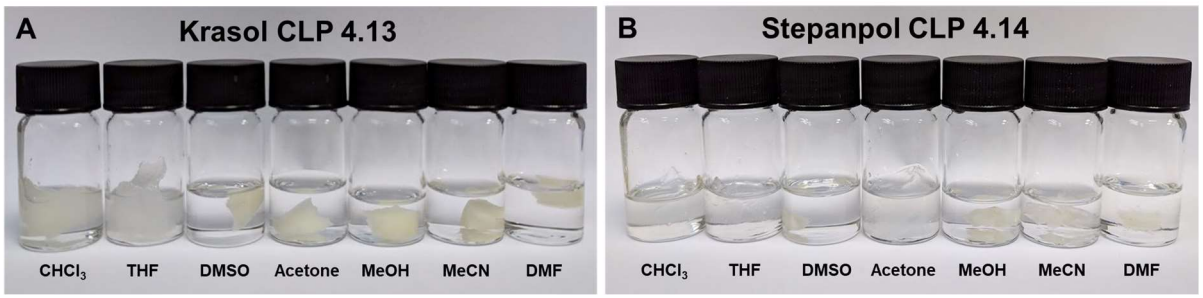

Figure 4.4 *Samples of the CLP materials soaked in various solvents for 24 hours at 35 °C to determine solubility of the polymers.*

This simple study revealed that neither the Krasol CLP **4.13** or Stepanpol CLP **4.14** dissolved in any of the solvents over the test period. The Krasol CLP showed significant swelling in both chloroform and THF, and lower levels of swelling in acetone. This may prove to be problematic for the degradation studies of the adhesive samples as acetone was used as the TBAF carrier in Chapter 2 and 3. The samples soaked in the other solvents did not exhibit any visible change to the original shape or volume of the sample. The Stepanpol CLP **4.14** showed similar results, with swelling occurring in chloroform and THF. Interestingly, the Stepanpol CLP becomes transparent when swollen which could be an effect of breaking up the crystalline regions within the network. The Stepanpol CLP also showed swelling in acetone and acetonitrile, which would be advantageous for the adhesive degradation studies. Furthermore, the Stepanpol CLP shows some swelling from DMF and DMSO. The only solvent that the Stepanpol CLP did not swell in was methanol.

To determine the thermal properties of these crosslinked materials, DSC experiments were carried out on both the Krasol CLP **4.13** and Stepanpol CLP **4.14** to determine if the material exhibited a melting transition (Figure 4.5).

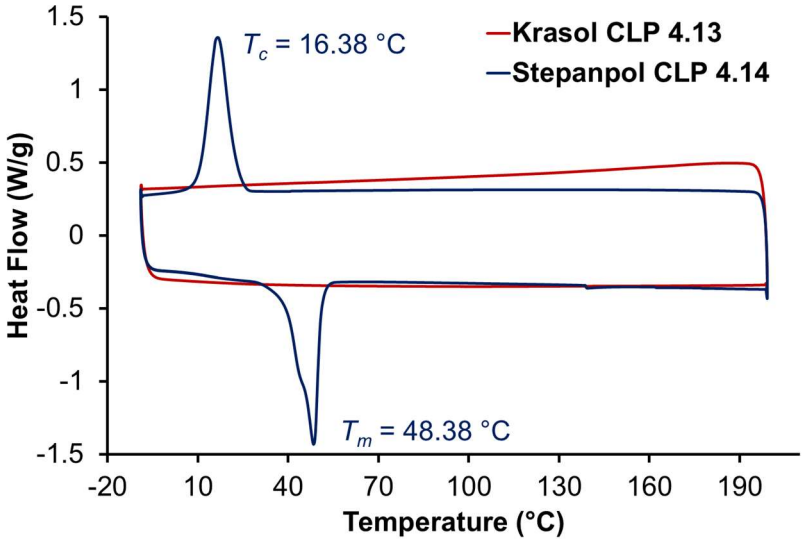

Figure 4.5 *DSC chromatogram of the Krasol CLP **4.13** and Stepanpol CLP **4.14**.*

A melt transition at ≈93 °C was not evident in the DSC thermograms of both of the CLP's indicating complete consumption of the TDU **4.1** during the crosslinking reaction. Melt and crystallisation transitions were not observed in the DSC analysis of the Krasol CLP **4.13**, similar to the linear polymer **2.12** reported in Chapter 2. In contrast, a melting transition (T_m) at 48 °C was evident for the Stepanpol-derived CLP **4.14** as well as a crystallisation transition (T_c) at 16 °C, values that are very close to those of the of the pristine Stepanpol **3.2** ($T_m \approx 54$ °C, $T_c \approx$ 36 °C). This is a result of the crystallites within the polymeric network changing upon heating (Scheme 4.7).

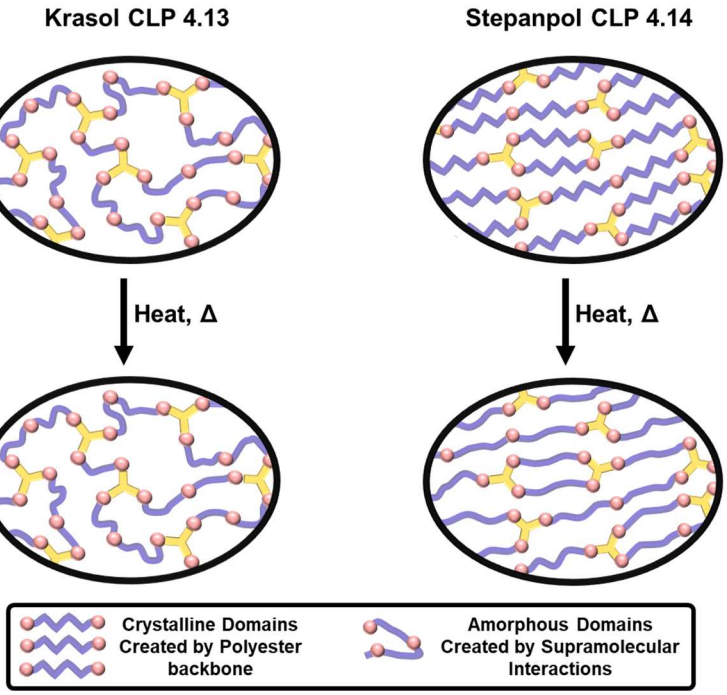

Scheme 4.7 *The effect of heating the crosslinked polymeric networks. The amorphous network is not affected by heat, whereas the crystalline regions move apart allowing the material to show a melt.*

As the CLP's do not dissolve in solvents or flow when heated, self-supporting films could not be produced as reported in Chapters 2 and 3. Hence, a new method to obtain adhesion had to be developed, as discussed below.

4.2.4. Crosslinked Adhesive Preparation and Testing

Unsurprisingly, the crosslinked polymers synthesised in section 4.2.3 were not soluble and did not flow after long (24 hours) durations at elevated temperatures (120 °C). Therefore, self-supporting films could be melt cast, and the adhesion and strength testing methods developed in Chapters 2 and 3 were not suitable for these materials.

As the degradable crosslinker could not be added to the pre-polymer prior to forming the bond, it was decided to prepare the adhesive *in situ* as a reactive adhesive. This can be achieved by mixing the isocyanate terminated prepolymer at elevated temperatures with the crosslinking group TDU **4.1** in a vial, before applying onto the site where the bond would be made (Scheme 4.8).

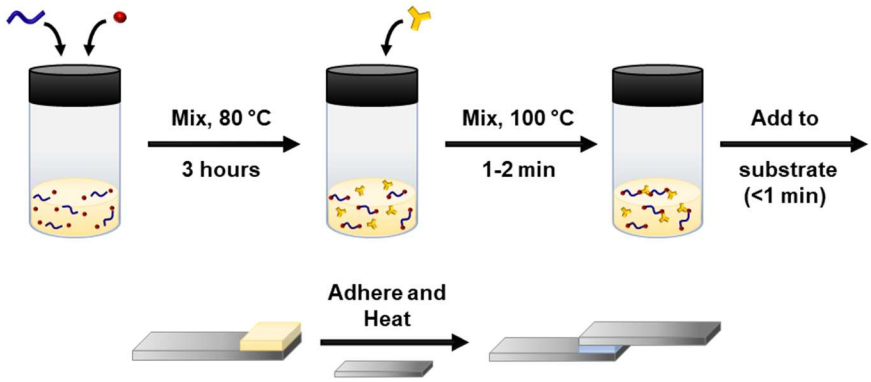

Scheme 4.8 *In situ preparation of the crosslinked materials for adhesion.*

For the first adhesives test carried out, the Krasol pre-polymer **2.20** was prepared in the bulk before being added separately to the TDU **4.1** and mixed while the pre-polymer was hot. The paste was spread over a glass slide (area: 12 × 26 mm) before the second glass slide was clamped on top with a bull dog clamp and placed in an oven at 120 °C for 1 hour to cure (the same conditions used earlier in section 4.2.1). Glass lap shear specimens were used to visually verify that all of the TDU **4.1** had melted. Lap shear adhesion tests were carried out on the prepared samples and were compared to the adhesive strength properties of linear adhesive polymer **2.21** developed in Chapter 2 (Figure 4.6).

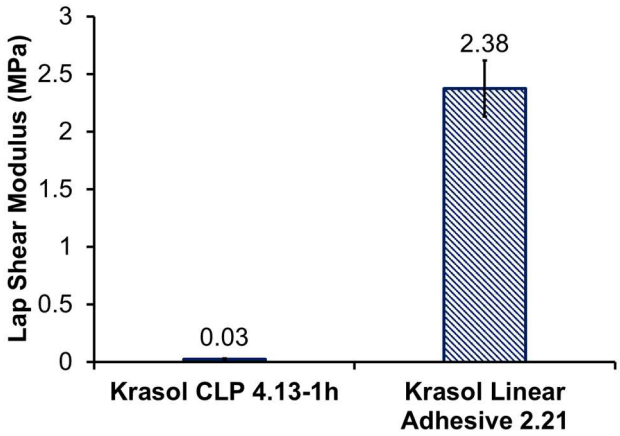

Figure 4.6 *Lap shear tests of crosslinked adhesive **4.13-1h** after 1 hour curing at 120 °C, and compared to the linear adhesive **2.21** developed in Chapter 2. The adhesives were bonded to glass substrates. Errors were calculated from the standard deviations (n = 3).*

The results in Figure 4.7 show that the crosslinked material does not form an adhesive under these conditions. On inspection of the lap shear samples after testing, the adhesive was easily scraped off with a spatula. This suggests the reaction had not gone to completion in the 1 hour time period at 120 °C. It was postulated that the lack of mixing was the possible cause for the poor adhesion strength. Therefore, to counter this problem, the cure time at 120 °C was increased to 18 hours. The lap shear adhesive results are shown in Figure 4.7.

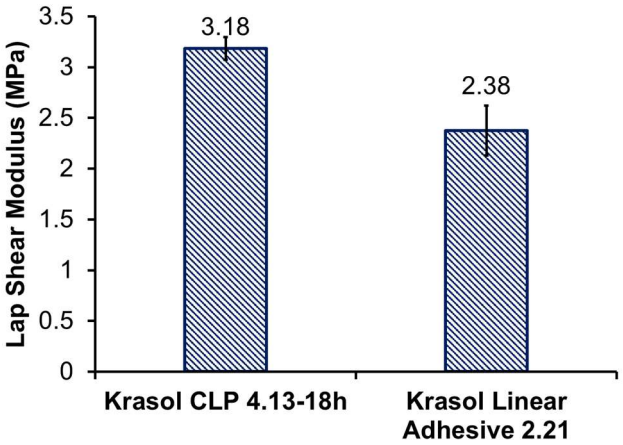

Figure 4.7 *Lap shear tests of crosslinked adhesive* ***4.13-18h*** *after 18 hours curing at 120 °C and compared to the linear adhesive* ***2.21*** *developed in Chapter 2. The adhesives were bonded to glass substrates. Errors were calculated from the standard deviations (n = 3).*

Extending the adhesive curing time shows that the crosslinker TDU **4.1** results in the formation of a crosslinked material **4.13-18h**. The crosslinking adhesive shows a 34 % increase in strength in comparison to the adhesive prepared in Chapter 2 (Figure 4.7).

For comparison, the Stepanpol prepolymer was reacted with the TDU **4.1** using the method shown in Scheme 4.7 and leaving the lap shear samples to cure for 18 hours. However, during the testing of the glass lap shear samples, the glass broke before the adhesive failed. Therefore, the lap shear substrates were changed to aluminium. Photos of the lap shear substrates are shown in Figure 4.8; with the adhesive test results shown in Figure 4.9 and compared to the linear Stepanpol adhesive **3.12** from Chapter 3.

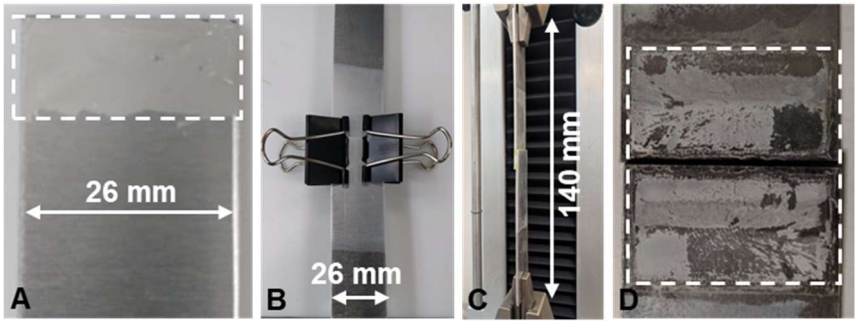

Figure 4.8 *Photos of the lap shear samples: (A) the paste spread over 12 × 27 mm area on a pre-treated aluminium coupon, (B) two aluminium coupons clamped together sandwiching the adhesive paste, (C) the aluminium lap shear sample in the tensile apparatus, and (D) the adhesive bond after breaking showing cohesive failure (adhesive remaining on both side of substrate).*

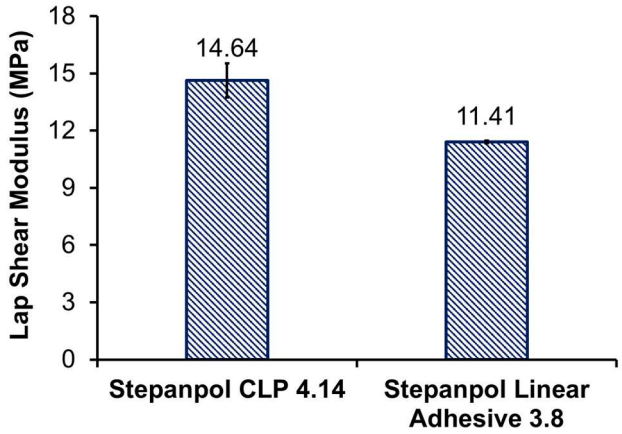

Figure 4.9 *Lap shear tests of the Stepanpol CLP **4.14** after 18 hours curing at 120 °C and compared to the linear adhesive 3.8 developed in Chapter 3. Lap shear specimens were made of aluminium. Errors were calculated from the standard deviations (n = 3).*

Before the results in Figure 4.10 are discussed, it is important to note that two of the three samples did not break on the tensile apparatus as they reached the maximum load (5 kN) of the tensiometer. As expected, the Stepanpol crosslinked adhesive **4.14** shows a much greater adhesion strength in comparison to the Krasol crosslinked adhesive **4.13**. Introducing crosslinking to the Stepanpol PU adhesives results in at least a 28 % increase in strength.

4.2.5. Fluoride responsive debonding of the crosslinked adhesive

The last experiment that was carried out was degradation studies on the Stepanpol CLP adhesive **4.13**. This was carried out by soaking the lap shear samples in 0.025 M TBAF/acetonitrile solution for 3 hours and then dried at 40 °C for 1 hour prior to adhesive testing (Figure 4.10). Acetonitrile was chosen as it does allow for swelling of the polymer (Figure 4.4b) and the degradation results of the Stepanpol CLP **4.14** can be related to the degradation results of the linear polymer **3.8** (Chapter 3, Figure 3.11).

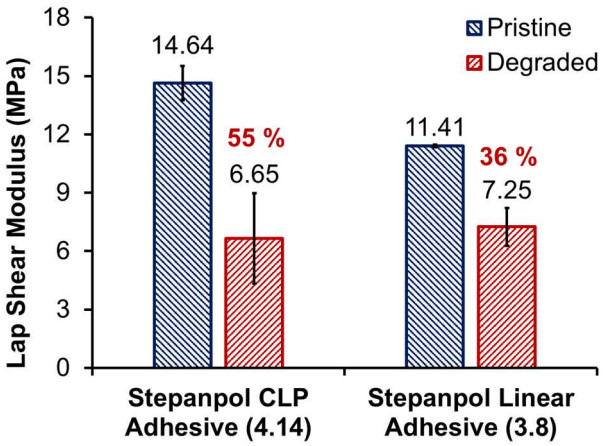

Figure 4.10 *Lap shear tests of the Stepanpol crosslinked adhesive* ***4.14*** *before and after treatment with 0.025 M TBAF in acetonitrile for 3 hours; and compared to the linear Stepanpol Adhesive* ***3.8****. Errors were calculated from the standard deviations (n = 3).*

From these tests, degradation upon treatment with the fluoride source showed a 55 % loss in adhesive strength and thereby proving the crosslinked adhesive degrades. However, as was mentioned earlier, the pristine Stepanpol CLP **4.14** adhesive would have a stronger adhesive strength than shown in Figure 4.11. Therefore, the loss in adhesive strength is greater than the 55 % loss reported. Nevertheless, the Stepanpol CLP adhesive **4.14** shows a much greater loss in adhesive strength than the linear polymer **3.8** developed in Chapter 3. In fact, as the adhesives break down to the same material, the strengths of the degraded materials are very similar (CPL **4.14** = 6.65 ± 2.32 MPa, linear adhesive **3.8** = 7.25 ± 0.97 MPa). Therefore, this data shows effectiveness of the Stepanpol CLP **4.14**.

4.3. Conclusion

In this Chapter is presented the design and synthesis of a trifunctional fluoride responsive degradable unit that can be reacted with an isocyanate terminated prepolymer to form a crosslinked adhesive. Model compound analysis showed that the crosslinking degradable group undergoes rapid degradation (<1 minute) when treated with TBAF. The crosslinked adhesives were produced *in situ* on the substrate. Both a hydrogenated polybutadiene and polyester based crosslinked adhesive were produced with the trifunctional degradable group. The two crosslinked adhesives showed approximately a 30 % increase in strength when compared to a linear polymeric adhesive with both glass and metal substrates. Finally, the adhesive exhibits a 55 % loss in strength when treated with a TBAF solution for 3 hours.

4.4. Experimental Procedures

4.4.1. Characterisation

Characterisation was carried out as reported in Chapter 2, page 55 and Chapter 3, page 81.

4.4.2. Synthesis of sodium 2,4,6-trimethylolphenate 4.3

Phenol (11.75 g, 0.13 mol) was dissolved in formaldehyde (33% in Methanol, 56 mL, 0.50 mol) at 0 °C. Water (10 mL) was added to the mixture, followed by NaOH (5.1 g, 0.13 mol) and stirred at 0 °C until all NaOH dissolved. The reaction mixture was then stirred at 25 °C for 24 h, before being poured slowly into vigorously stirred propan-2-ol (600 mL) at 0 °C. The precipitate was filtered under vacuum, washed with propan-2-ol (100 mL) before drying under high vacuum (0.1 mmbar) overnight to afford a off-white powder (14.4 g, 70 %). The product was stored under vacuum when not in use. m.p. (DSC) 142 °C; ν_{max} (thin film, cm^{-1}) 3322, 2848, 2638, 1611, 1300, 1029, 754. δ_H (400 MHz, DMSO-*d*$_6$, ppm) 6.51 (2H, br, Ar-H), 4.44 (4H, br, Ar-C$\underline{H_2}$-OH), 4.18 (2H, br, Ar-C$\underline{H_2}$-OH). δ_C (100 MHz, DMSO, ppm) 126.5, 124.1, 64.8, 63.9. (m/z) found 229.0448 Da ($C_9H_{11}O_4Na_2$), calculated 229.0453 Da ($C_9H_{11}O_4Na_2$).

4.4.3. Synthesis of TDU 4.1

Tert-butlydimethlysilyl chloride (18.27 g, 0.12 mol) was added to a mixture of sodium 2,4,6-trimethylolphenate **4.3** (5.00 g, 24.3 mmol) and imidazole (8.26 g, 0.12 mol) in anhydrous DMF (300 mL) and stirred for 4 hours at 35 °C under nitrogen. The mixture was diluted in ethyl acetate (200 mL) and washed with water (2 × 200 mL). The organic mixture was collected, dried under $MgSO_4$ and concentrated to afford the crude oil, which was dissolved in methanol (100 mL) and diethyl ether (20 mL) and *p*-toluenesulfonic acid (0.15 g, 0.87 mmol) was added and stirred at ambient temperature for 1 hour. The mixture was diluted in ethyl acetate (100 mL), washed with saturated $NaHCO_3$ solution (100 mL), followed by brine solution (100 mL). The organic mixture was collected, dried under $MgSO_4$ and concentrated *in vacuo*. The crude was purified by column chromatography eluting with ethyl acetate on silica to afford a white powder (3.56 g, 45 %). m.p. (DSC) 93 °C; ν_{max} (thin film, cm^{-1}) 3275, 2926, 2860, 1457, 1245, 886, 776. δ_H (400 MHz, DMSO-*d*$_6$, ppm) 7.26 (2H, s, Ar-H), 5.12 - 4.95 (3H, m, O$\underline{H}$), 4.51 – 4.34 (6H, m, Ar-C$\underline{H_2}$-OH), 0.98 (9H, s, Si-C-(C$\underline{H_3}$)$_3$), 0.14 (6H, s, Si-(C$\underline{H_3}$)$_2$). δ_C (100 MHz, DMSO, ppm) 156.1, 135.1, 132.1, 124.8, 63.0, 58.3, 26.0, 18.5, -3.6. (m/z) found 321.1489 Da ($C_{15}H_{26}O_4NaSi$), calculated 321.1498 Da ($C_{15}H_{26}O_4NaSi$).

4.4.4. Synthesis of model compound 4.5

To a solution of TDU **4.1** (50 mg, 0.17 mmol) and 4-dimethylaminopyridine (2.05 mg, 0.02 mmol) dissolved in anhydrous THF (10 mL) was added *p*-nitrophenyl isocyanate (0.11 mg, 0.67 mmol) under nitrogen and stirred for 4 hours at 80 °C. The mixture was diluted with ethyl acetate (20 mL), washed with saturated NH_4Cl solution (20 mL), followed by brine solution (20 mL). The organic solution was dried under $MgSO_4$ and concentrated to afford the crude product; which was used without further purification (0.159 g, 96 % yield at 80 % purity). ν_{max} (thin film, cm^{-1}) 3385, 2926, 2857, 1737, 1595, 1507, 1200, 748. δ_H (400 MHz, DMSO-d_6, ppm) 10.52 (2H, s, N-H), 10.45 (1H, s, N-H), 8.20 – 8.14 (6H, m, Ar-H), 7.71 – 7.64 (6H, m, Ar-H), 7.55 (2H, br, Ar-H), 5.21 (4H, s, Ar-C$\underline{H}_2$), 5.18 (2H, s, Ar-C$\underline{H}_2$), 1.00 (9H, s, Si-C(C$\underline{H}_3$)$_3$), 0.24 (6H, s, Si-(C$\underline{H}_3$)$_2$). δ_C (100 MHz, DMSO, ppm) 152.9, 145.5, 126.4, 125.0, 117.7, 112.3, 65.8, 25.6, -3.9. (m/z) found 813.2169 Da ($C_{36}H_{38}O_{13}N_6NaSi$), calculated 813.2164 Da ($C_{36}H_{38}O_{13}N_6NaSi$).

4.5. References

1. G. Habenicht, *Applied Adhesive Bonding: A Practical Guide for Flawless Results*, Wiley-VCH, Germany, 2008.
2. J. H. Lee, T. H. Lee, K. S. Shim, J. W. Park, H. J. Kim, Y. Kim and S. Jung, *J. Adhes. Sci. Technol.*, 2016, **30**, 2316–2328.
3. J. H. Lee, T. H. Lee, K. S. Shim, J. W. Park, H. J. Kim, Y. Kim and S. Jung, *Int. J. Adhes. Adhes.*, 2017, **74**, 137–143.
4. Z. Czech, *J. Adhes. Sci. Technol.*, 2007, **21**, 625–635.
5. H. S. Do, Y. J. Park and H. J. Kim, *J. Adhes. Sci. Technol.*, 2006, **20**, 1529–1545.
6. Y. J. Park, D. H. Lim, H. J. Kim, D. S. Park and I. K. Sung, *Int. J. Adhes. Adhes.*, 2009, **29**, 710–717.
7. J. Asahara, A. Sano, N. Hori, A. Takemura and H. Ono, *J. Appl. Polym. Sci.*, 2003, **89**, 3039–3045.
8. B. U. Kang, J. Y. Jho, J. Kim, S. S. Lee, M. Park, S. Lim and C. R. Choe, *J. Appl. Polym. Sci.*, 2001, **79**, 38–48.
9. A. Murakami, D. Saunders, K. Ooishi, T. Yoshiki, M. Saitoo, O. Watanabe and M. Takezawa, *J. Adhes.*, 1992, **39**, 227–242.
10. K. P. Unnikrishnan and E. T. Thachil, *Int. J. Polym. Mater. Polym. Biomater.*, 2006, **55**, 323–338.
11. R. J. C. Carbas, E. A. S. Marques, L. F. M. da Silva and A. M. Lopes, *J. Adhes.*, 2014, **90**, 104–119.
12. G. G. Buonocore, L. Schiavo, I. Attianese and A. Borriello, *Compos. Part B Eng.*, 2013, **53**, 187–192.
13. D. Kim, D. G. Lee, J. C. Kim, C. S. Lim, N. S. Kong, J. H. Kim, H. W. Jung, S. M. Noh and Y. Il Park, *Int. J. Adhes. Adhes.*, 2017, **74**, 21–27.
14. E. Orgilés-Calpena, F. Arán-Aís, A. M. Torró-Palau and C. Orgilés-Barceló, *Int. J. Adhes. Adhes.*, 2016, **70**, 218–224.
15. M. M. Rahman, H. Do Kim and W. K. Lee, *Fibers Polym.*, 2009, **10**, 6–13.

16. K. Luo, T. Xie and J. Rzayev, *J. Polym. Sci. Part A Polym. Chem.*, 2013, **51**, 4992–4997.
17. O. Ursache, C. Gaina and V. Gaina, *Express Polym. Lett.*, 2017, **11**, 467–478.
18. K. Ishida and N. Yoshie, *Macromolecules*, 2008, **41**, 4753–4757.
19. V. Gaina, O. Ursache, C. Gaina and E. Buruiana, *Des. Monomers Polym.*, 2012, **15**, 63–73.
20. S. A. Canary and M. P. Stevens, *J. Polym. Sci. Part A Polym. Chem.*, 1992, **30**, 1755–1760.
21. A. J. Inglis, L. Nebhani, O. Altintas, F. G. Schmidt and C. Barner-Kowollik, *Macromolecules*, 2010, **43**, 5515–5520.
22. B. T. Michal, E. J. Spencer and S. J. Rowan, *ACS Appl. Mater. Interfaces*, 2016, **8**, 11041–11049.
23. T. Harper, R. Slegeris, I. Pramudya and H. Chung, *ACS Appl. Mater. Interfaces*, 2017, **9**, 1830–1839.
24. S. Saito, S. Nobusue, E. Tsuzaka, C. Yuan, C. Mori, M. Hara, T. Seki, C. Camacho, S. Irle and S. Yamaguchi, *Nat. Commun.*, 2016, **7**, 1–7.
25. H. Akiyama, Y. Okuyama, T. Fukata and H. Kihara, *J. Adhes.*, 2018, 1–15.
26. E. Kizilkan, J. Strueben, A. Staubitz and S. N. Gorb, *Sci. Robot.*, 2017, **2**, eaak9454.
27. H. Kim, H. Mohapatra and S. T. Phillips, *Angew. Chemie - Int. Ed.*, 2015, **54**, 13063–13067.
28. T. S. Babra, A. Trivedi, C. N. Warriner, N. Bazin, D. Castiglione, C. Sivour, W. Hayes and B. W. Greenland, *Polym. Chem.*, 2017, **8**, 7207–7216.
29. H. Kim, H. Mohapatra and S. T. Phillips, *Angew.Chem. Int.Ed.*, 2015, **54**, 13063–13067.
30. X. Sun, J. F. Reuther, S. T. Phillips and E. V. Anslyn, *Chem. - A Eur. J.*, 2017, **23**, 3903–3909.
31. R. W. Martin, *J. Am. Chem. Soc.*, 1951, **73**, 3952–3954.
32. R. J. Amir, N. Pessah, M. Shamis and D. Shabat, *Angew. Chem. Int. Ed. Engl.*, 2003, **42**, 4494–9.

Chapter 5

Branched Polycaprolactones as soft segments in Fluoride Responsive Reactive Hot-Melt Debondable Adhesives

Abstract

This chapter reports studies towards the production of a star shaped polycaprolactone with a fluoride responsive centre group to develop a new chemical architecture for debondable adhesives. Addition of TDU **4.1** to ε-caprolactone using the catalyst, tin(II) octanoate, produced a branched polyester contained terminal hydroxyl groups as determined by ^{1}H NMR spectroscopy. Studies of the degradation of the polymer in solution revealed that the system degraded rapidly from 16.7 kgmol^{-1} to 6 kgmol^{-1} upon contact with fluoride ions. The branched polyester was then crosslinked at 60 °C in the bulk with an aromatic diisocyanate to increase the strength of the adhesive. Lap shear studies were carried out, with the crosslinked material showing a 12 % increase in adhesive strength over the uncrosslinked, branched polyester. When treated with a TBAF solution for 3 hours, the adhesive exhibited a loss of up to 23 % in bonding strength.

5.1. Introduction

In Chapter 2, adhesion using polymer **2.21** was achieved by placing a film of the material between the two adherents and heating the joint at 120 °C for 18 hours.[1] Chapter 3 showed how the chemical structure of the adhesive was optimised to deliver in a hot-melt film that allowed for adhesion to occur at significantly lower temperatures (60 °C), while the adhesive strength of the material was increased by approximately two-fold. Chapter 4 outlined how the introduction of crosslinking groups could be used to further increase adhesion strength by ≈30 %. The crosslinked adhesive was obtained by mixing an isocyanate terminated pre-polymer with the trifunctional crosslinker (**4.1**) at 120 °C between the surfaces to be bonded.

These polymeric adhesives relied on the reaction of an isocyanate and benzylic alcohol of the degradable groups in the bulk to form polyurethanes. In both the linear and crosslinked adhesives, an isocyanate terminated prepolymer had to be synthesised prior to addition of the degradable group. In general, prepolymers have short life times (<1 year) as the isocyanates decompose with moisture. Therefore, an alternative approach was sought to design a new polyol containing a fluoride responsive group that would possess an enhanced shelf life. This could be

achieved by attaching the polymer onto the degradable group (DU) group directly rather than through a diisocyanate linker. The resultant polyol could be reacted with a commercially available diisocyanate to form a chain extended or crosslinked network. As the crosslinking material in Chapter 4 showed higher adhesive strengths, the trifunctional degradable group (TDU) **4.1** (Chapter 4, Figure 4.1) was chosen as the DU for the proposed new polyol.

The results from Chapter 3 showed that incorporating a polyester into the polymeric network increased mechanical strengths while lowering the adhesive curing temperatures. Attaching polyesters to the TDU **4.1** would result in branched or star shaped polymers. Two methods exist to attach the bulk polymer centre groups of star shaped polymers: (i) reacting low molecular weight polymers with the DU; or (ii) "growing" polymers from the DU terminal hydroxyl groups from monomeric units.[2]

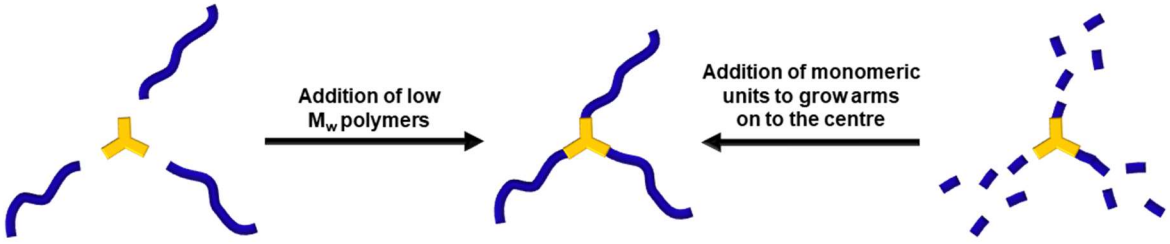

Scheme 5.1 *Two methods used to create star shaped polymers.*

Although the first method would produce the desired material, either the TDU **4.1** or the low molecular polymer would require pre-functionalisation prior to attaching the two substituents. Whereas, in contrast, "growing" polyester chains or arms from a hydroxyl terminated centre group has been reported in the literature using the ring opening polymerisation (ROP) of lactone rings and its derivatives.[2–7]

The two star shaped polyesters produced commonly from multi-hydroxyl-functionalised centres are polymers **5.4-O** and **5.5-O**; synthesised from the tri-armed 2-tetramethylolpropane **5.2** and tetra-armed pentaerythritol **5.3** and lactone ring **5.1-O** (Scheme 5.2).[3,8,9] These materials are synthesised in the bulk with the use of a tin catalyst. Varying the chain length (*m*) on the branches or using different size lactone rings (*n*) allow for modifications to the thermal and/or mechanical properties.[8,9] Alternative chemical structures that have been produced, for example, using caprolactams (**5.1-NH**) which result in amide functionalised arms on the stars. Furthermore, using lactides (dicyclic esters) has further improved the mechanical and thermal properties.[5,10,11]

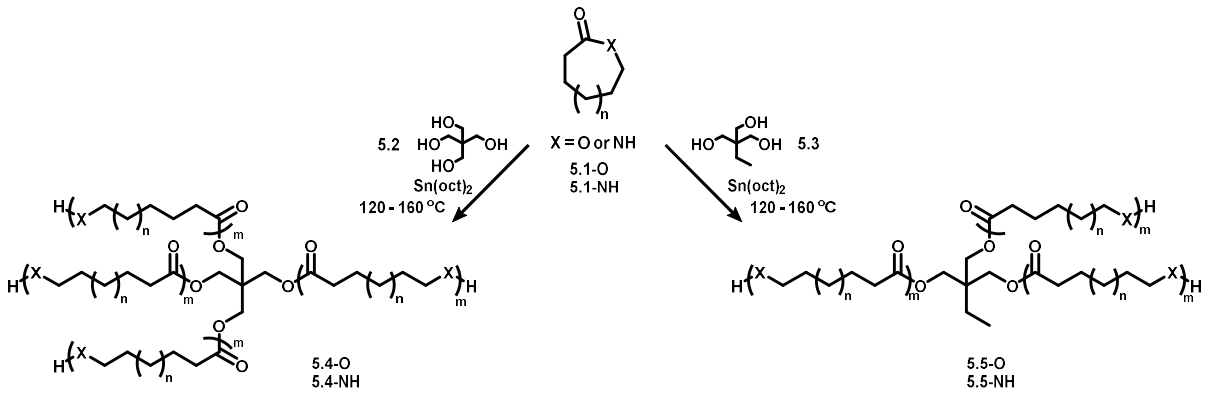

Scheme 5.2 *Synthesis of star shaped polyesters with multi-hydroxyl-functionalised centres.*

These materials have been used in drug delivery applications and tissue engineering as they are generally biocompatible and biodegradable;[12–14] with the latter property being of most interest to this study on degradable adhesives.

Post-polymerisation of the terminal OH groups has been studied by various groups to enhance the mechanical properties of the polymers. For example, Sijbesma and co-workers attached ureidopyrimidinone groups via an isocyanate as terminal groups on the stars, which allows for the formation of reversible supramolecular crosslinking.[15] Schubert and co-workers terminated polycaprolactone stars with poly(ethylene glycol) methacrylates, which form block copolymeric microcapsules which can trap/release dye molecules in aqueous environments.[16] Additionally, crosslinking polyester stars have been reported with diisocyanates to form flexible materials with high thermal stability.[6,17]

Polyester based materials are biodegradable by ester cleavage[4,18–21] and this property has been utilised with star shaped polyesters for biomedical uses.[4,22] Polyesters stars have also been shown to degrade through hydrolysis.[6,23] However, chemo-selective degradation at the centre of the star material has not been reported to date. This concept allows for material breakdown without degrading the bulk of the material.

Herein is presented the design and synthesis of a tris-hydroxy terminated polyester incorporating a fluoride responsive degradable centre. When reacted with a diisocyanate in the melt, the mixture can be applied to a substrate and allowed to react at easily accessible temperatures for strong adhesion (Scheme 5.3). Furthermore, utilising this method for crosslinking moves the aromatic urethane groups away from the degradable group and hence reduces the areas of high aromatic density, resulting in a different phase separated material that may provide advantageous mechanical and thermal properties. Application of a fluoride source results in degradation at the centre of the star, hence facilitating debonding.

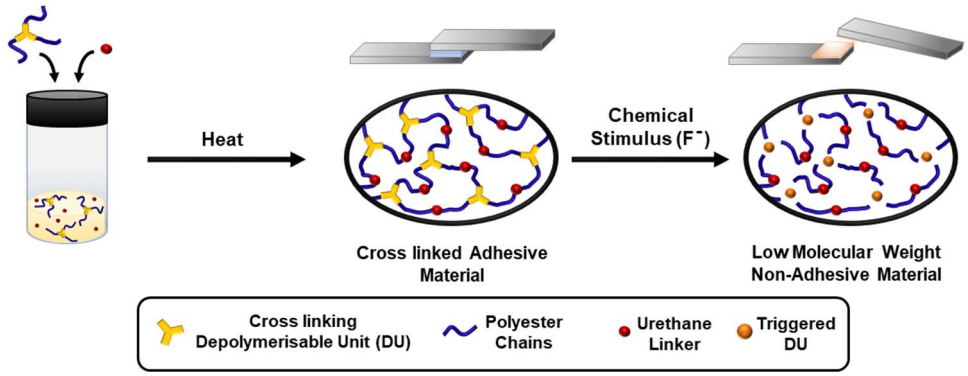

Scheme 5.3 *Schematic showing the debond-on-demand properties of a cross linker polyester based adhesive.*

In comparison to the work described in Chapter 4, the advantages to this method include: (i) lower hot-melt reactive adhesion temperatures as the star shaped polyester melts at a considerably lower temperature than the depolymerisable unit in Chapter 4; (ii) the star shaped polymers contain a lower weight percentage of the synthetically costly TDU **4.1** as the bulk of the material is polymer; and finally (iii) the star shaped polymer can be stored under ambient conditions whereas the isocyanate terminated prepolymer used in Chapter 4 requires preparation prior to use and can degrade if left under ambient conditions.

5.2. Results and Discussion

5.2.1. Synthesis of Fluoride Responsive Branched Polycaprolactone

The polymer designed would incorporate the TDU **4.1** designed in Chapter 4, with polyester arms "grown" from the centre and would have terminal hydroxyl groups that could be crosslinked with a commercially available diisocyanate to form the adhesive (Scheme 5.2). 4,4'-MDI **2.19** was chosen as it provides strong mechanical properties (as demonstrated in Chapters 2, 3 and 4) and has a low melting point at *ca*. 43 °C. This is extremely important as this will allow for a low-melt adhesive (i.e. adhesion at temperatures lower than 100 °C). Furthermore, the solid 4,4'-MDI has a longer shelf life when compared to liquid state diisocyanate counterparts.[24]

To synthesise the star shaped polycaprolactone, the trifunctional depolymerisable unit (TDU) **4.1** developed in Chapter 4 was dissolved in ε-caprolactone **5.1** at 120 °C before addition of the tin catalyst and raising the temperature to 180 °C for 18 hours (Scheme 5.4). Thirty equivalents of the caprolactone was used to create a star shaped material with a theoretical average of 10 repeat units per arm. The crude was dissolved in minimum amounts of chloroform before

precipitating into methanol to afford *ca.* 18 g of polymer **5.6** as a white powder (Figure 5.1) in high yields (93 %).

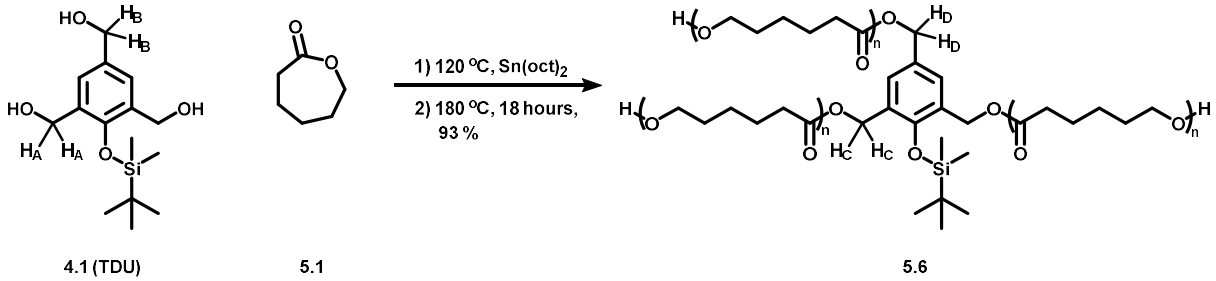

Scheme 5.4 *Synthesis of the star shaped polymer* ***5.6***

Figure 5.1 *Approximately 18 g of polymer* ***5.3*** *produced in one reaction with minimal purification.*

Infrared spectroscopic characterisation showed a strong absorption at 1720 cm^{-1} indicative of ester-carbonyl stretches. Thermal analysis of the star polymer revealed a melting temperature (T_m) at 49 °C and a crystallisation temperature (T_c) at 20 °C. ^{1}H NMR spectroscopic analysis showed a downfield shift in the methylene singlet resonances of the core trigger group from 4.6 ppm (H_A) to 5.1 ppm (H_C) for the *ortho*-methylene groups and from 4.5 ppm (H_B) to 5.0 ppm (H_D) for the *para*-methylene group. Appearance of a broad triplet at 3.6 ppm shows the presence of terminal hydroxyl groups at the end of the polycaprolactone branches (Figure 5.2). However, when integrated with respect to H_C and H_D (six protons), the resonance at 3.6 ppm revealed an integral of four protons. If the star had formed with perfect structural integrity, the integral for polymer **5.6** should correlate to three protons.

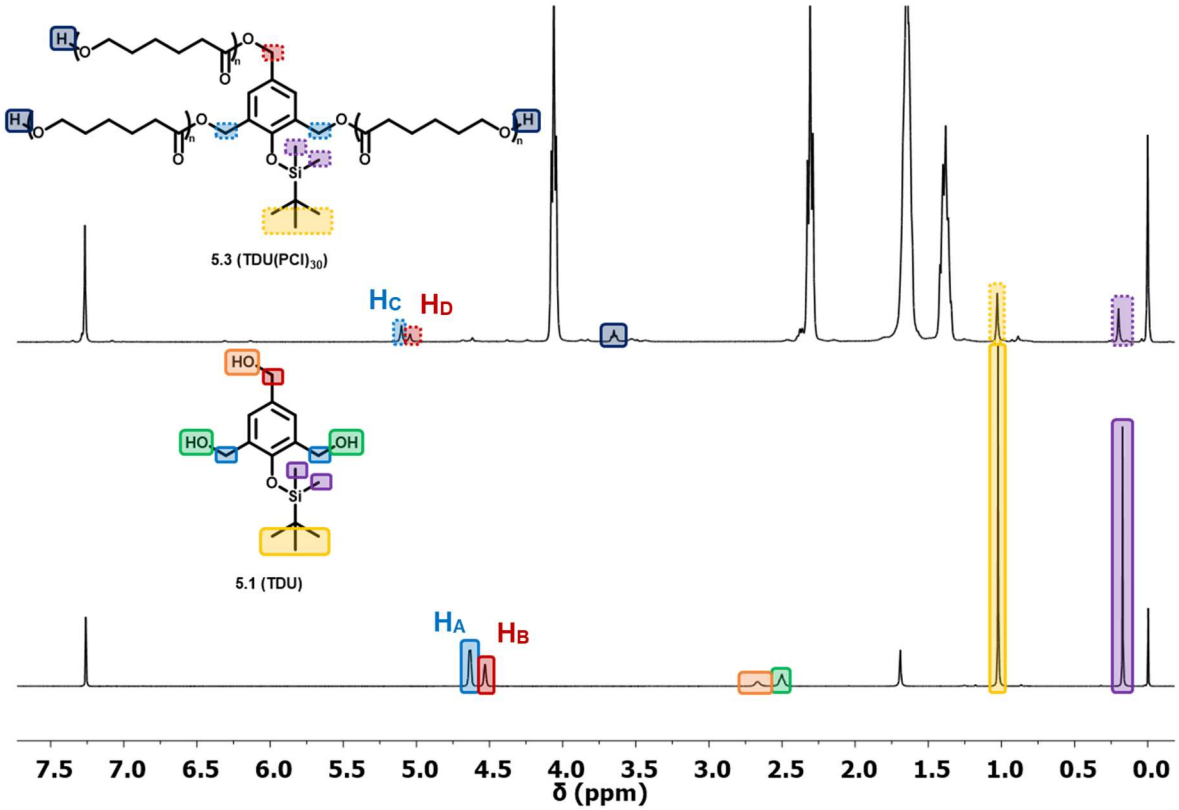

Figure 5.2 *^{1}H NMR spectra of the TDU (**5.1**) and polymer **5.3**.*

To understand this further, GPC analysis was carried out. Assuming formation of a perfect star with each arm containing 10 repeat units, the theoretical molecular weight should be 3.7 kgmol^{-1}. GPC analysis of polymer **5.6** reported a partially bimodal distribution with M_w 45.2 kgmol^{-1}, M_n 16.7 kgmol^{-1} and $Đ$ 2.70.

This relatively high molecular weight and dispersity may be as a consequence of transesterification occurring in the presence of the organotin catalyst.[25,26] Transesterification is the process were an alcohol can react with an ester to form a new ester (as exemplified in step 3 of Scheme 5.5). In the scheme, the red dot represents the star molecule **5.6**. The first two steps show the formation of the tin species bound to the star polymer. The third step of the process results in the formation of a new ester, with two of the star shaped molecules covalently bound together. As the molecular weight of the material produced is 16.7 kgmol^{-1}, this would suggest that the process of transesterification is occurring multiple times, with an average of transesterification occurring four times. One possible method to reduce the amount of transesterification occurring is to reduce the reaction time, or change the catalyst.[26]

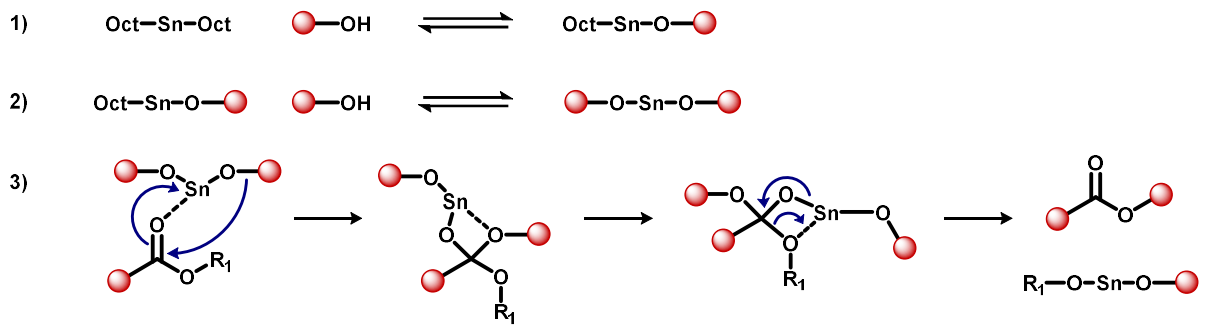

Scheme 5.5 *Process of transesterification occurring during the synthesis of polymer* ***5.6****.*

Therefore, the structure of the polymer synthesised (**5.7**) may be better represented as shown in Figure 5.3. However, even if transesterification is occurring during the synthesis of the material, the polymer still contains the fluoride responsive group and terminal hydroxyl groups as determined by ^{1}H NMR spectroscopy (Figure 5.2). With a proposed molecular weight for the star polymer **5.3** of 3.7 kgmol^{-1} and the actual molecular weight of polymer **5.7** at 16.7 kgmol^{-1}, this branched material contains 4 – 5 fluoride degradable units, which still have the desired degradation features required for the adhesive. Hence, attention moved towards the degradation studies of the material when exposed to fluoride ions.

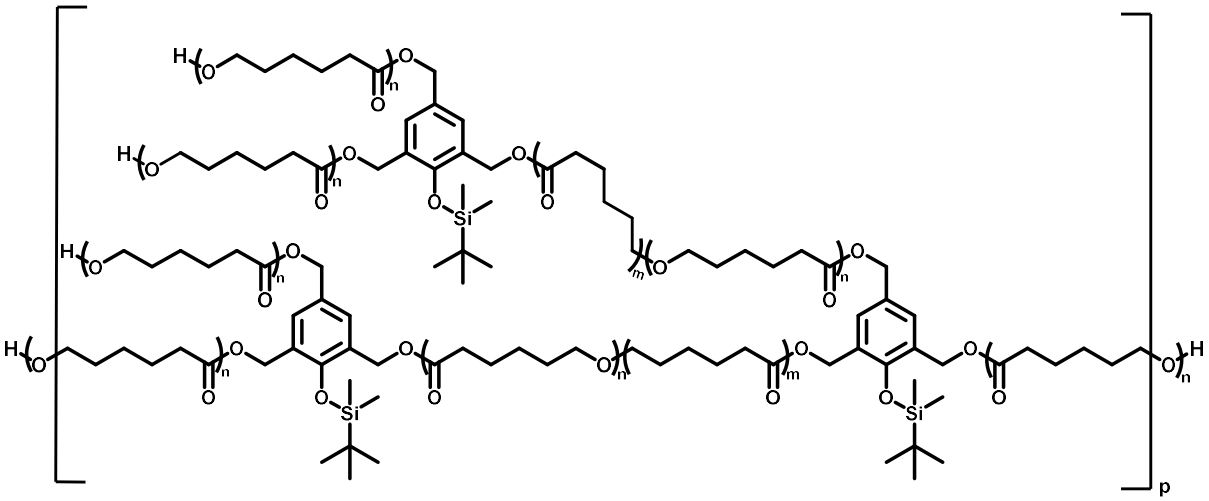

Figure 5.3 *The synthesised hyperbranched fluoride responsive polyester.*

5.2.2. Solution State Degradation Studies

Although, esters have been attached to the cresol core groups in small molecule self-immolative systems,[27,28] esters have not been attached to either the bifunctional **2.6** or trifunctional degradable **4.1** groups. Hence, initial degradation studies were carried out in the solutions state to determine reaction of polyester **5.7** with fluoride ions.

Scheme 5.6 shows the proposed mechanism of breakdown upon addition of a fluoride source. As observed for the Stepanpol polymer **3.8** detailed in Chapter 3, the polyester branches on polymer **5.7** should not breakdown and are released as the carboxylic acid **5.9**.

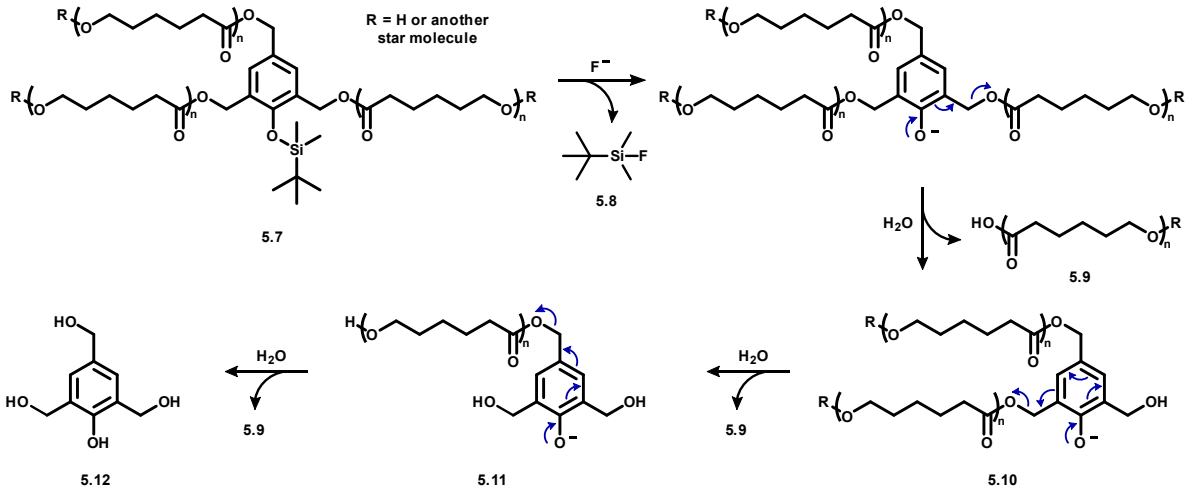

Scheme 5.6 *Synthesis of the star shaped polymer* ***3.3***

Depolymerisation studies were carried out by addition of *tetra*-butylammonium fluoride (TBAF) to a solution of polymer **5.7**. In conjunction with the solution state studies in Chapters 2 - 4, the solution of polymer **5.7** turned yellow on addition of TBAF, indicating formation of the cresol **5.12**. Initial degradation studies were analysed by GPC. The resulting eluograms for polymer **5.7** before and after addition of *tetra*-butylammonium fluoride shown in Figure 5.4 with the molecular weight data presented in Table 5.1. The eluograms shows that the material after depolymerisation is essentially monomodal, with molecular weights calculated at *ca.* M_n 6.0 kgmol^{-1} and $Đ$ 1.65. This proves that the polymer **5.7** does break down as desired when treated with TBAF.

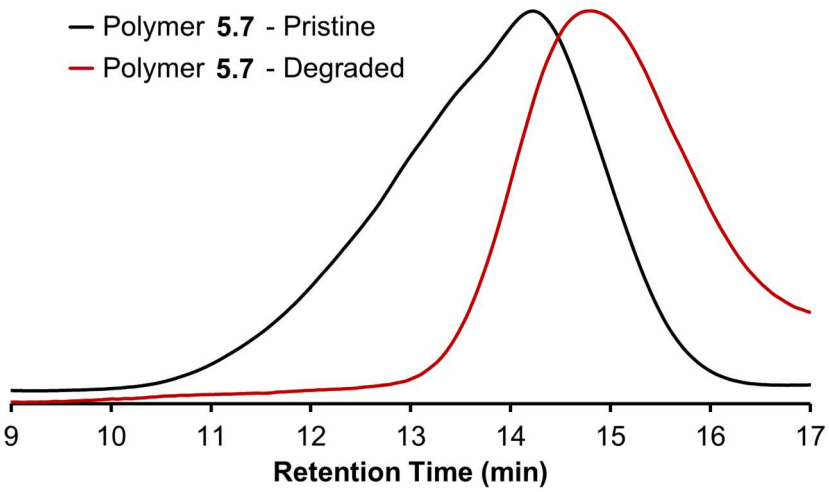

Figure 5.4 *GPC eluograms of the polymer* ***5.7*** *before (black) and after (red) addition of the fluoride source. (THF, PS standards)*

	M_w (gmol^{-1})	M_n (gmol^{-1})	*Đ*
Polymer **5.7** - Pristine	45200	16700	2.70
Polymer **5.7** - Degraded	9800	5980	1.65

Table 5.1 *Molecular weight estimation from the GPC chromatographs for polymer 5.7 before and after degradation; (THF, PS standards).*

However, as a side effect of the randomised transesterification process, the actual degree of polymerisation of the polyester arms cannot be determined. Therefore, clarifying if the polyester chains were degraded with the fluoride ions could was not possible. Hence, ^{1}H NMR spectroscopy was carried out to determine if polymer **5.7** was breaking down from the fluoride responsive centre and not at the polyester arms. The ^{1}H NMR spectra before and after addition of TBAF to a solution of polymer **5.7** in $CDCl_3$ (Figure 5.5). The spectra show loss of the methylene resonances of the TDU core at 5.0 ppm and silyl methyl groups at 1.0 and 0.2 ppm; indicating breakdown of the TDU centres within the hyperbranched polymer. The appearance of a singlet resonance at 0.17 ppm shows the presence of **5.8**, the by-product from the degradation process. No change in chemical shift was detected with the methylene polyether branch resonances, and thereby proving that the fluoride does not affect the polyether branches.

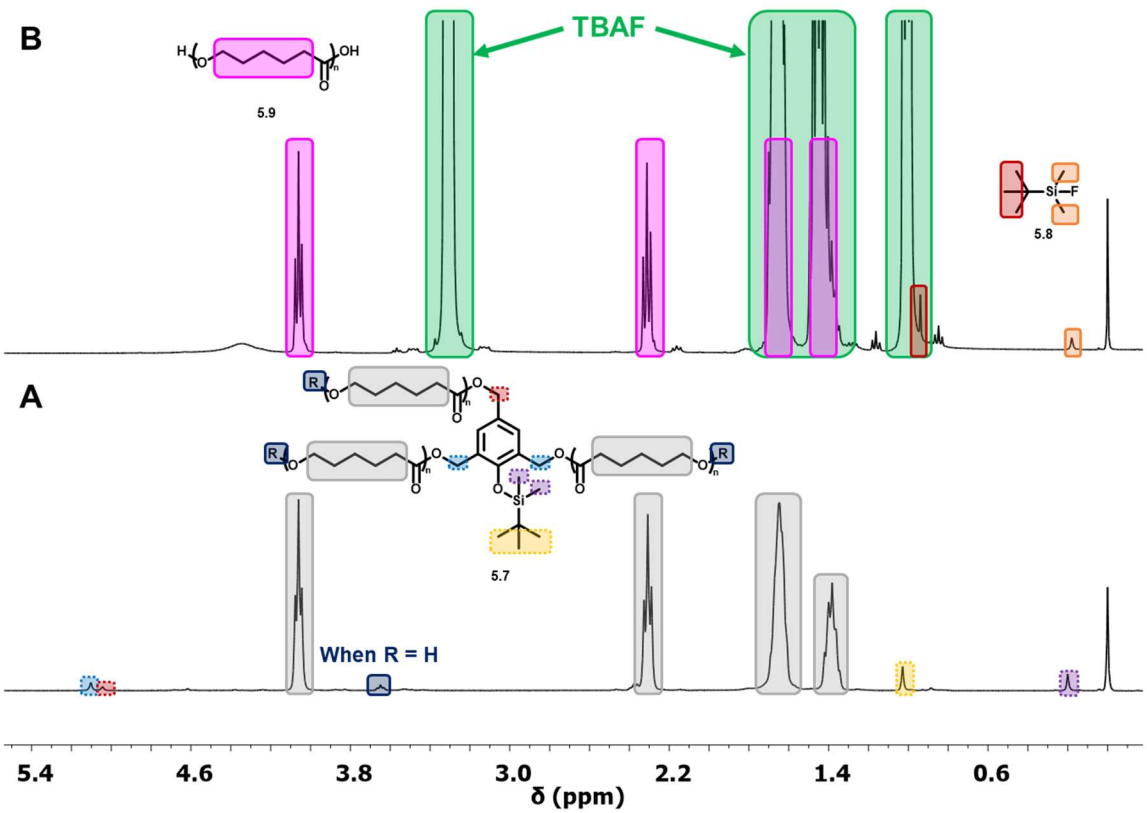

Figure 5.5 *^{1}H NMR spectra of polymer **5.3** (A) before and (B) after addition of TBAF. ($CDCl_3$, 400 MHz)*

These experiments confirmed the synthesis and degradation polymer **5.7**. Attention then turned towards the crosslinking reaction with a diisocyanate with strength testing carried out by lap shear adhesion studies.

5.2.3. Crosslinking with diisocyanates

For crosslinking reactions, 4,4'-methylenediphenyl diisocyanate (4,4'-MDI) **2.19** was selected as the diisocyanate linker as it provides stronger mechanical properties in comparison to other diisocyanates (see Chapter 3). As 4,4'-MDI is solid at room temperature, it is less prone to moisture degradation than its liquid counterparts.[24] Additionally, its low melting point (*ca.* 42 °C) allows it to be reacted with the star polymer at the low temperatures that adhesion would be carried out.

The first attempt at crosslinking the two components was carried out using a similar method as optimised in Chapter 4. In this instance, 4,4'-MDI **2.19** was added to molten polymer **5.7** at 60 °C with mechanical stirring to afford the crosslinked polymer (CLP) **5.13a** (Scheme 5.7). The mixture quickly (<2 minutes) stopped stirring as it solidified to a yellow material and could not be melted again, presumably as a consequence of crosslinking, and hence could not be transferred to the adhesive substrate.

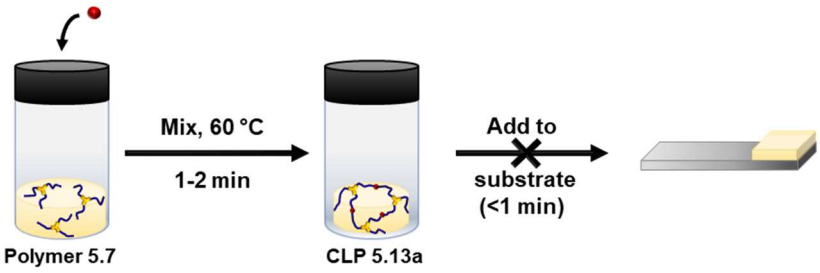

Scheme 5.7 *In situ preparation of the crosslinked polymer (CLP)* ***5.13a*** *which could not be transferred to the adhesive substrate*

Therefore, a melt casting method was used where 4,4'-MDI **2.19** and polymer **5.7** were ground together in a mortar and pestle to form a fine white powder. The powder was then spread into a PTFE mould (5 × 5 cm) and placed into an oven at 60 °C for three hours to afford CLP **5.13b** (Scheme 5.8). As a comparison, polymer **5.7** was also finely ground before placing into a PTFE mould to determine how addition of 4,4'-MDI affected the material.

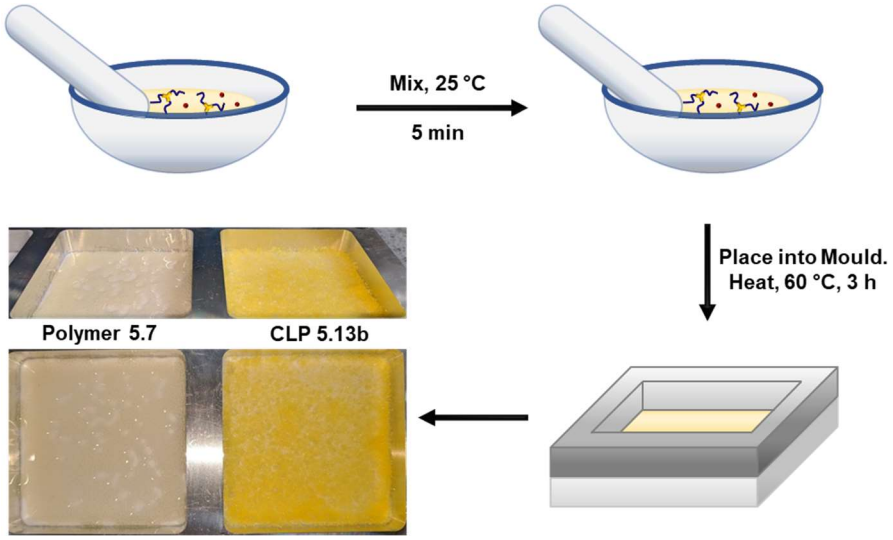

Scheme 5.8 *Crosslinking reaction of polymer* ***5.7*** *and 4,4'-MDI* ***2.19****, which were ground into a fine powder before casting into a PTFE mould. Polymer* ***5.7*** *was also ground into a fine powder as a comparison.*

The CLP **5.13b** material obtained after heat treating at 60 °C for 3 hours was a granular film that easily broke apart when held. In comparison, heat casting uncrosslinked polymer **5.7** under the same conditions resulted in a self-supporting material, even though holes had formed within the film. The CLP **5.13b** did not dissolve or swell in THF, chloroform, acetone, acetonitrile or DMSO suggesting that crosslinking had occurred, whereas, in contrast the Stepanpol-derived CLP **4.14** did exhibit swelling in these solvents. This could lead to problems when tested as an adhesive as the lack of swelling may result in poor degradation throughout the material.

DSC experiments were carried out to determine the thermal properties of the CLP **5.13b**, with the sample cycled from 0 °C to 200 °C to 0 °C (Figure 5.6).

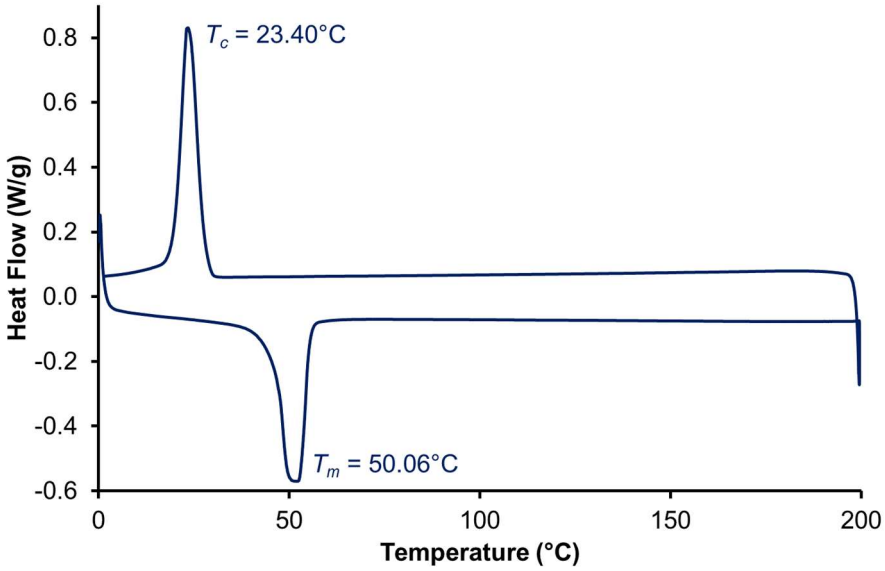

Figure 5.6 *DSC thermogram of the CLP* ***5.13b*** *produced by heat treating at 60 °C for three hours.*

DSC analysis showed that the material exhibits a melting transition (T_m) at 50 °C and a crystallisation transition (T_c) at 23 °C; both similar to polymer **5.7** before crosslinking ($T_m \approx 49$ °C and $T_c \approx 20$ °C). This is a result of the crystallites within the polymeric network melting, which was also seen with the Stepanpol CLP **4.14** (Chapter 4). However, CLP **5.13b** does not show visual evidence of flowing, nor can it be manipulated by mechanical force like the Stepanpol CLP **4.14** can above its melting temperature.

These experiments thereby show that addition of 4,4'-MDI **2.19** to polymer **5.7** does cause crosslinking. Attention moved towards testing the materials adhesive properties using lap shear studies.

5.2.4. Adhesion Testing

For adhesive strength testing of uncrosslinked polymer **5.7**, lap shear specimens were prepared by spreading a fine powder of polymer over a 12 × 26 mm area before clamping and placing in an oven at 60 °C for 18 hours. The crosslinked samples **5.13** were prepared as shown in Scheme 5.8, with a fine powder spread on aluminium lap shears. The lap shear modulus was recorded before and after crosslinking with 4,4'-MDI (Figure 5.7).

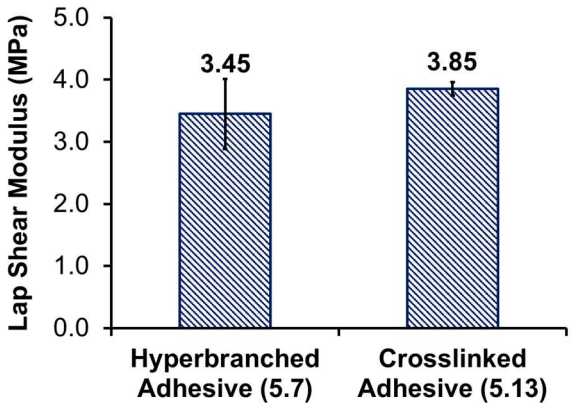

Figure 5.7 *Lap shear testing of polymer **5.7** and the crosslinked adhesive **5.13** after addition of 4,4'-MDI **2.19**. Adhesive samples were prepared from powders (Scheme 5.7). Errors were calculated from the standard deviation (n = 3).*

The adhesive strength of the crosslinked material is marginally stronger (12 %) than the pristine adhesive. However, error calculations show that the adhesive strengths of the two materials are very similar. This may be a result of the poor flow of the crosslinked adhesive during the heating stage of the lap shear sample preparation that is evident in the photographs of the lap shear samples after testing (Figure 5.8).

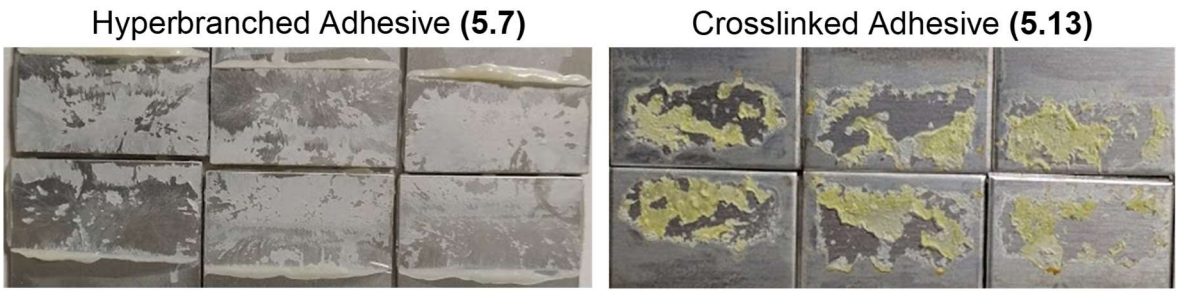

Figure 5.8 *Photographs of the lap shear samples after testing of the pristine (left) and crosslinked (right) adhesives.*

Nevertheless, the crosslinked material **5.13** did behave as an adhesive as it was able to bond the two aluminium samples. Hence three new samples of the crosslinked polymer were prepared, and degradation tests were carried out. The samples were degraded in 0.025 M TBAF in acetonitrile for three hours before drying at 40 °C for 30 minutes. The lap shear modulus was calculated from the force at break (Figure 5.9).

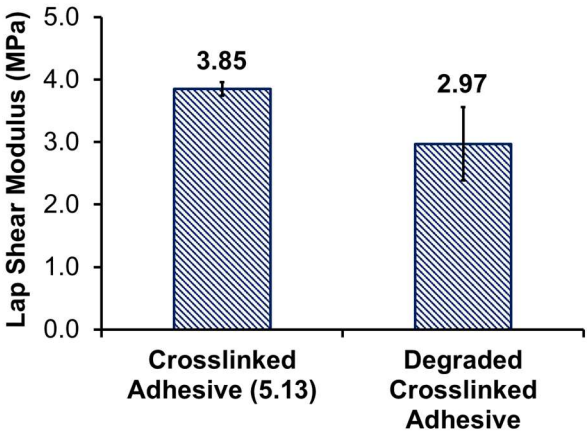

Figure 5.9 *Lap shear testing of the crosslinked polymer **5.13** before and after degradation with 0.025 M TBAF in acetonitrile. Errors were calculated from the standard deviation (n = 3).*

Upon treatment of fluoride, the adhesive showed a reduction in lap shear modulus from 3.85 MPa to 2.97 MPa, which is a 23 % reduction in adhesive strength. However, the crosslinked samples exhibited poor contact between the two aluminium plates from poor flow of material when heated (60 °C) and compressed. Furthermore, the degraded adhesive samples demonstrated little swelling after 3 hours soaking, which would reduce the amount of degradation occurring throughout the polymer. Nevertheless, the degraded crosslinked material **5.13** did show a reduction in adhesive strength.

5.3. Conclusions

A hyperbranched polyester **5.7** containing fluoride responsive degradable units was synthesised in this chapter. The polyester demonstrated a drop in molecular weight when treated with TBAF

(*ca.* 17 $kgmol^{-1}$ to 6 $kgmol^{-1}$), with ^{1}H NMR spectroscopy proving that degradation was occurring at the degradable unit rather than at the ester groups in the polymeric arms. The branched polyester has multiple terminal hydroxyl groups, which when reacted with a diisocyanate without solvent, results in crosslinking at 60 °C. The crosslinked material was used as a reactive hot-melt adhesive. After treating with a 0.025 M TBAF solution for three hours, the adhesive shows a 23 % reduction in adhesive strength.

5.4. Experimental Procedures

5.4.1. Characterisation

Characterisation was carried out as reported in Chapter 2, page 55 and Chapter 3, page 81.

5.4.2. Synthesis of TDU 4.1

TDU **4.1** was synthesised as reported in Chapter 4, Page 100.

5.4.3. Synthesis of Polymer 5.7

TDU **4.1** (1.55 g, 5.19 mmol) was dissolved in ε-caprolactone **5.1** (17.27 mL, 0.156 mol) at 120 °C under vacuum (~0.1 mbar) before equalising pressure under an N_2 atmosphere. Tin (II) octanoate (0.017 mmol) dissolved in toluene (1 mL) was added before evacuating the vessel under vacuum. The pressure was equalised under N_2 before heating to 180 °C for 18 hours. The solution was cooled to ~50 °C before dissolving in chloroform (50 mL). The mixture was precipitated into methanol (500 mL) and left to stand overnight. The precipitate was filtered and dried under vacuum to afford a white powder (17.9 g, 93 %). T_m (DSC) = 47.7 °C, ν_{max} (thin film, cm^{-1}) 2942, 2896, 2865, 1720, 1470, 1369, 1295, 1162, 1107, 1045, 959, 841.25. δ_H (400 MHz, $CDCl_3$, ppm) 7.28 (2H, m, Ar-H), 5.10 (4H, s, br, Ar-C$\underline{H}_2$), 5.04 (2H, s, br, Ar-C$\underline{H}_2$), 4.05 (135H, m, nC$\underline{H}_2$), 3.65 (3H, m, O$\underline{H}$), 2.31 (135H, m, nC$\underline{H}_2$), 1.65 (300H, m, nC$\underline{H}_2$), 1.38 (135H, m, nC$\underline{H}_2$), 1.03 (9H, s, SiC(C$\underline{H}_3$)$_3$), 0.20 (6H, s, Si(C$\underline{H}_3$)$_2$). δ_C (100 MHz, $CDCl_3$, ppm) 173.6, 64.2, 34.1, 28.4, 25.5, 24.6, 0.0. GPC (THF/BHT 250 ppm) M_w 16700, M_n 45200, $Đ$ 2.70.

5.4.4. Lap Shear Adhesion Preparation

Lap shear samples were prepared as following: Polymer **5.7** (1.0 g) and 4,4'-MDI **2.19** (0.101 g) were ground in a mortar and pestle before being spread on an aluminium lap shear coupon in a 12 × 26 mm area and sandwiched with another aluminium lap shear coupon. The samples were clamped and placed in an oven at 60 °C for 18 hours.

5.5. References

1. T. S. Babra, A. Trivedi, C. N. Warriner, N. Bazin, D. Castiglione, C. Sivour, W. Hayes and B. W. Greenland, *Polym. Chem.*, 2017, **8**, 7207–7216.
2. J. M. Ren, T. G. McKenzie, Q. Fu, E. H. H. Wong, J. Xu, Z. An, S. Shanmugam, T. P. Davis, C. Boyer and G. G. Qiao, *Chem. Rev.*, 2016, **116**, 6743–6836.
3. J. Choi, I. K. Kim and S. Y. Kwak, *Polymer*, 2005, **46**, 9725–9735.
4. D. J. A. Cameron and M. P. Shaver, *Chem. Soc. Rev.*, 2011, **40**, 1761–1776.
5. C.-M. Dong, K.-Y. Qiu, Z.-W. Gu and X.-D. Feng, *Macromolecules*, 2001, **34**, 4691–4696.
6. J. Yi, C. Huang, H. Zhuang, H. Gong, C. Zhang, R. Ren and Y. Ma, *Prog. Org. Coatings*, 2015, **87**, 161–170.
7. A. L. Sisson, D. Ekinci and A. Lendlein, *Polymer*, 2013, **54**, 4333–4350.
8. J. L. Wang and C. M. Dong, *Polymer*, 2006, **47**, 3218–3228.
9. W. Xie, N. Jiang and Z. Gan, *Macromol. Biosci.*, 2008, **8**, 775–784.
10. J. P. Brutman, P. A. Delgado and M. A. Hillmyer, *ACS Macro Lett.*, 2014, **3**, 607–610.
11. Y. Nakayama, K. Aihara, H. Yamanishi, H. Fukuoka, R. Tanaka, Z. Cai and T. Shiono, *J. Polym. Sci. Part A Polym. Chem.*, 2015, **53**, 489–495.
12. A. C. Albertsson and I. K. Varma, *Biomacromolecules*, 2003, **4**, 1466–1486.
13. Y. C. Wang, Y. Y. Yuan, J. Z. Du, X. Z. Yang and J. Wang, *Macromol. Biosci.*, 2009, **9**, 1154–1164.
14. H. Tian, Z. Tang, X. Zhuang, X. Chen and X. Jing, *Prog. Polym. Sci.*, 2012, **37**, 237–280.
15. J. L. Wietor, D. J. M. Van Beek, G. W. Peters, E. Mendes and R. P. Sijbesma, *Macromolecules*, 2011, **44**, 1211–1219.
16. O. G. Schramm, G. M. Pavlov, H. P. Van Erp, M. A. R. Meier, R. Hoogenboom and U. S. Schubert, *Macromolecules*, 2009, **42**, 1808–1816.
17. J. Zotzmann, M. Behl, D. Hofmann and A. Lendlein, *Adv. Mater.*, 2010, **22**, 3424–3429.
18. L. S. Nair and C. T. Laurencin, *Prog. Polym. Sci.*, 2007, **32**, 762–798.
19. A. K. Mohanty, M. Misra and G. Hinrichsen, *Macromol. Mater. Eng.*, 2000, **276**–**277**, 1–24.
20. F. Sinclair, L. Chen, B. W. Greenland and M. P. Shaver, *Macromolecules*, 2016, **49**, 6826–6834.
21. F. Faÿ, I. Linossier, V. Langlois, E. Renard and K. Vallée-Réhel, *Biomacromolecules*, 2006, **7**, 851–857.
22. K. M. Stridsberg, M. Ryner and A.-C. Albertson, in *Degradable Aliphatic Polyesters*, 2002, pp. 41–65.
23. J. T. Wiltshire and G. G. Qiao, *Macromolecules*, 2006, **39**, 9018–9027.
24. Y. Yakabe, K. M. Henderson, W. C. Thompson, D. Pemberton, B. Tury and R. E. Bailey, *Environ. Sci. Technol.*, 1999, **33**, 2579–2583.
25. R. F. Storey and J. W. Sherman, *Macromolecules*, 2002, **35**, 1504–1512.
26. A. B. Ferreira, A. Lemos Cardoso and M. J. da Silva, *ISRN Renew. Energy*, 2012, **2012**, 1–13.
27. N. Fomina, C. L. McFearin, M. Sermsakdi, J. M. Morachis and A. Almutairi, *Macromolecules*, 2011, **44**, 8590–8597.
28. N. Fomina, C. McFearin, M. Sermsakdi, O. Edigin and A. Almutairi, *J. Am. Chem. Soc.*, 2010, **132**, 9540–2.

Chapter 6

Designing a Novel UV Responsive Degradable Group for Debondable Polyurethane based Adhesives

Abstract

This chapter reports the design and synthesis of a novel UV responsive degradable group (UVDU) which incorporates an *o*-nitrobenzyl alcohol (ONB) group. It was synthesised through a three-step procedure with an overall yield of 56 %. A model bisurethane compound was synthesised containing the UVDU to determine the degradation properties of the system. Time dependant degradation experiments followed by UV/vis and ^{1}H NMR spectroscopies revealed degradation within 30 minutes of irradiation at 365 nm. The UVDU was incorporated into a polyurethane (PU) backbone, with solution state studies showing degradation within 2 hours by ^{1}H NMR spectroscopies with a 36 W UV lamp. GPC analysis indicated a breakdown of the polymer with a decrease in molecular weight from 21 to 14 kgmol^{-1} observed over the same time period. The PU was cast into a homogenous film (*ca.* 330 μm thickness). On exposure to UV radiation from a 200 W UV lamp, the film changed colour from yellow to deep red within 10 minutes with a concomitant of loss surface tackiness. However, tensile stress-strain tests showed no weakening in mechanical properties, which was determined to be a result of incomplete degradation throughout the film as a result of the film thickness. Nevertheless, as the polymer exhibited reduced tackiness after 10 minutes of UV light, the film was used to adhere two glass slides at 120 °C for 8 hours. The adhered samples displayed a yellow to red colour change after 10 minutes UV exposure, and lap shear studies resulted in an 86 % drop in adhesive strength after 5 minutes. Accurate molecular weight data for the irradiated adhesive could not be obtained as a consequence of incomplete degradation throughout the sample and competing crosslinking reaction. Even so, the loss in adhesive strength was a result of UV irradiation and not heat induced degradation, and therefore proves the potential for this UVDU in UV debondable adhesives.

6.1. Introduction

In Chapter 1, the use of thermal and chemical stimuli as a method to cause debonding of polymeric adhesives was discussed.[1] These stimuli were further explored with hot-melt and reactive adhesives within in this project in Chapters 2 – 5. An alternative stimulus to produce a

responsive stimulus us to use UV light to induce debonding. UV light would be advantageous when the substrate is sensitive to heat and/or chemical stimuli.

Three types of UV responsive adhesives have been reported in the literature: (i) light induced heating for debondable adhesives;[2,3] (ii) reversible adhesives which can rebond after being broken with UV light;[4–7] and (iii) non-reversible adhesives which cannot rebond after being broken by UV light (Chapter 1).[8] Light induced heating is an approach where high powered light sources have been used to activate photophores within the polymeric network which radiate heat to cause adhesive failure. This method was shown by Weder and co-workers, where a benzotriazole **1.38** was blended into a telechelic supramolecular polymers which exhibited rapid debonding (<1 minute) on exposure to a 200 W UV light source.[3] Another example of using light as a source of thermal energy was reported by Rowan and co-workers, where a high powered UV light source (200 W) was used to induce heating to melt the crystallites within the polymeric network.[2] However, UV light was then used to break disulfide bridges which further reduced bonding strength.

Examples of reversible adhesives include polymers containing anthracene residues which photo-cyclise at 365 nm and break at 264 nm or under heat (Scheme 1.2).[4,7] Similarly, coumarin based adhesives undergo [2+2] cycloaddition at 300 nm for strong adhesion and can debond at 290 nm (Scheme 1.8).[9] Consequently, mechanistically distinct UV debondable systems have been created that harness the reversible isomerism to switch between *cis*- and *trans*- isomers of azobenzenes (Scheme 1.6).[5,6,10]

Non-reversible adhesives that respond to UV light are less common in the literature. Weder and co-workers reported an aliphatic azo containing polymer **1.42** that breaks down to carbon radicals and molecular nitrogen when exposed to UV light in the range of 320 – 390 nm (Scheme 1.7). *o*-Nitrobenzyl alcohols (ONB's **1.49**) have been used within adhesive polymers to facilitate debonding by causing a large drop in molecular weight of the polymer; without the possibility of allowing for adhesive strength recovery. Examples of the use of ONB's within polymeric adhesives include a linear polymeric chained polyester based adhesive[11] and as a crosslinker in a polymethacrylate based adhesive.[12]

However, the original reports of the use of ONB's by Barltrop and co-workers described the application as an alcohol protecting group that could be triggered by UV light.[13] This paper described how the ONB units were attached to alcohols through an ester link (Chapter 1, Scheme 1.9). Upon treatment with a UV light (365 nm), the ONB undergoes degradation to

form an *o*-nitrosoaldehyde **1.53** and the adjoining hydroxyl anion. However, since its introduction in 1966, ONB's have been reported as a protecting group for phenols through an ester linkage.[14] Therefore, following on from the simple design of the fluoride degradable group **2.6** in Chapter 2, the UV degradable unit (UVDU) **6.1** shown in Figure 6.1 was proposed.

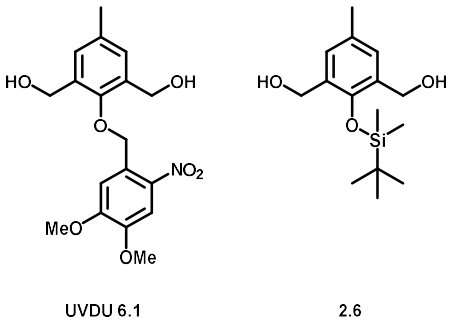

Figure 6.1 *The UV responsive group* ***6.1*** *proposed for this study and its comparison to the fluoride responsive group* ***2.6*** *(Chapter 2).*

Upon cleavage of the ONB, a cresol anion will form allowing for same route of degradation to occur to the polymer as reported with the fluoride responsive group in Chapter 2 (Scheme 2.8).

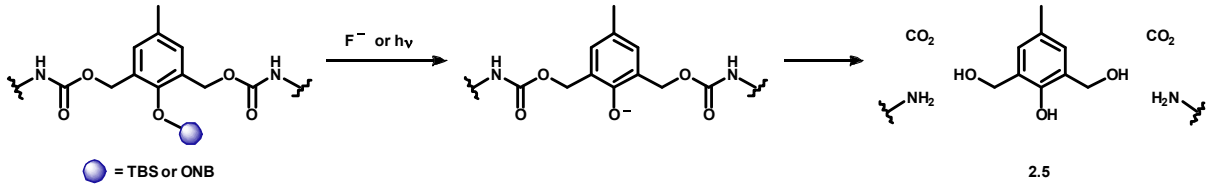

Scheme 6.1 *Degradation of the stimuli responsive degradable groups* ***2.5*** *and* ***6.1*** *forming the cresol anion.*

An extensive search into the literature showed that the UVDU **6.1** had not been synthesised. The closest UV responsive group in chemical structure was reported by Shabat and co-workers, which was used to form self-immolative dendrimers[15] and later used in UV responsive microcapsules by Fomina and co-workers.[16] Shabat's UV responsive group **6.10** required seven steps to synthesise, with an overall yield of 23 % (Scheme 6.2). Four synthetic steps are required to add the *N,N*-dimethylurethane linker between the core cresol group (**2.5**) and the ONB (**6.2**). The proposed UVDU **6.1** does not require a *N,N*-dimethylurethane linker and hence four steps can be eliminated from the proposed synthesis thus saving labour time and costs.

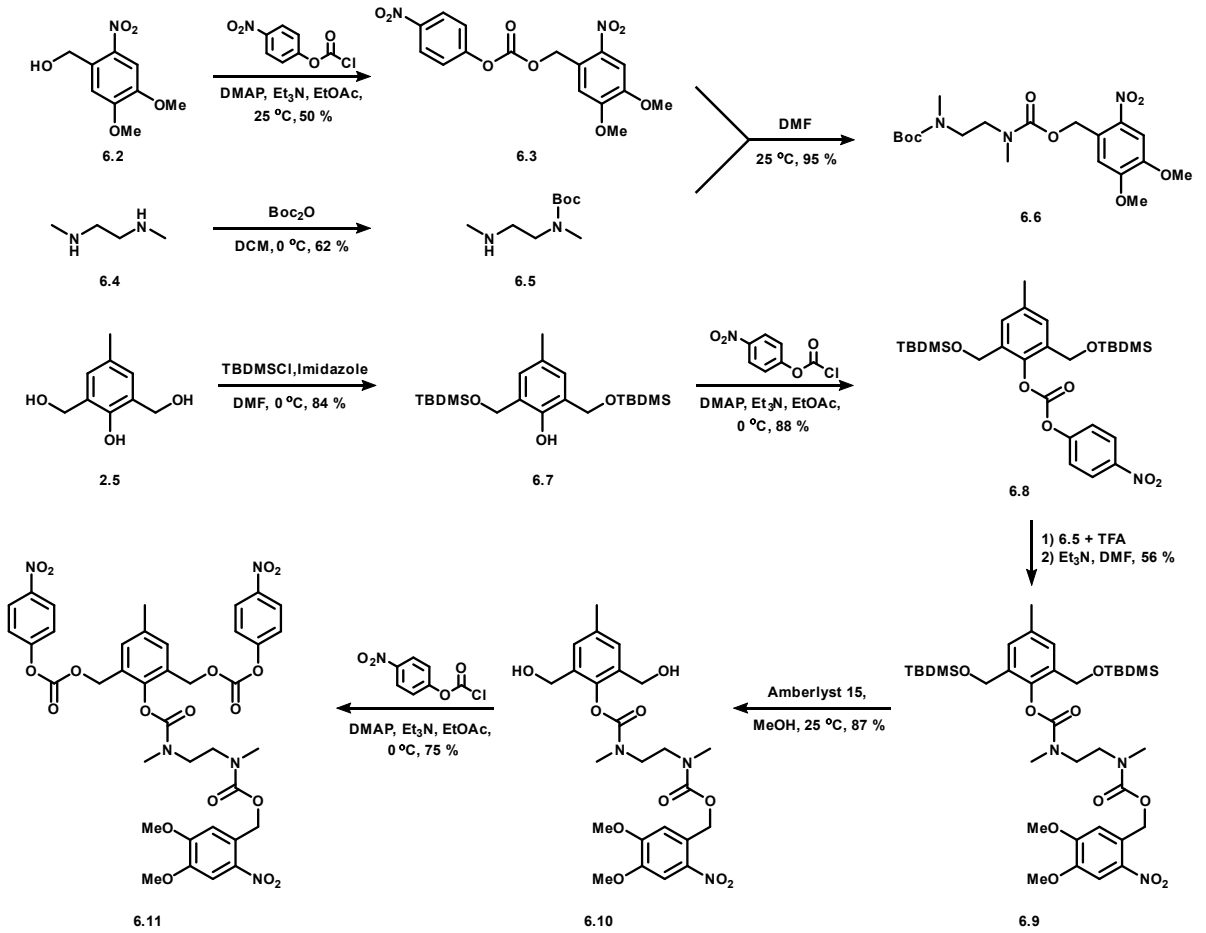

Scheme 6.2 *Synthesis of the Shabat UV responsive group* ***6.10*** *used for making dendrimers, and later used in a microcapsule wall.*

Herein is presented the design and synthesis of a novel UVDU **6.1**, which is activated at 365 nm. The UVDU **6.1** has an ether linkage directly between the core cresol group **2.5** and the ONB **6.2**. The UVDU is incorporated into a model compound to determine the efficiency of degradation when irradiated with a UV light. Furthermore, the synthesis of chain extended polyurethane (PU) adhesive incorporating the UVDU is reported. Irradiation with UV light resulted in 84 % loss in bonding strengths as determined by lap shear tests.

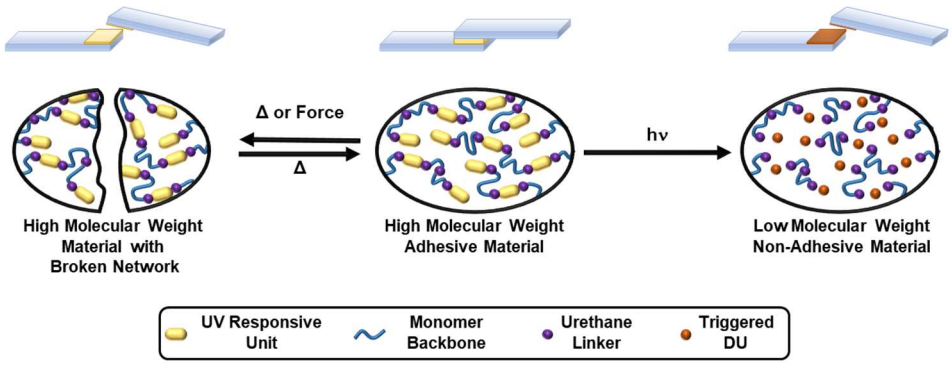

Scheme 6.3 *Schematic showing the proposed depolymerisation on exposure to UV light resulting in debonding of the adhesive, and the additional rebondable nature of the adhesive in response to temperature.*

6.2. Results and Discussion

6.2.1. Synthesis of UV Responsive Degradable Group

The UV degradable group **6.10** reported by Shabat and co-workers used a *N,N*-dimethyleneurethane linker between the core cresol (**2.5**) group and ONB **6.2**. This was synthesised from the carbonate **6.8** and Boc-protected amine **6.6**. However, as the proposed UVDU **6.1** used an ester linkage between the cresol **2.5** and ONB **6.2**, a new synthetic approach had to be taken. Forming benzyl ethers have been reported from different starting materials, with the phenol and benzyl bromide being used the most frequently.[14,17–20] Benzyl ethers can be synthesised directly from the phenol and benzyl alcohol, but require toxic catalysts and hence were not attempted.[21,22] Prior to synthesising the UVDU **6.1**, the benzyl bromide **6.12** had to synthesised. Fortunately, the bromide **6.12** has been previously reported using phosphorous bromide in chloroform (Scheme 6.4).[23] The bromide **6.12** was obtained as a yellow powder without the need of purification with 82 % yields.

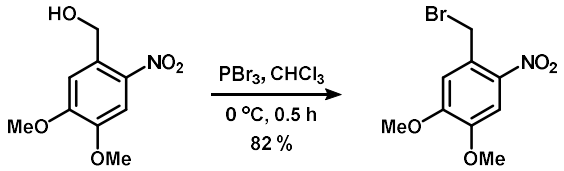

6.2 6.12

Scheme 6.4 *Synthesis of the brominated ONB* ***6.12****.*

With the synthesis of the benzyl bromide **6.12** complete, attention moved towards synthesising the UVDU. To avoid unwanted reactions occurring, the *tert*-butyldimethylsilyl (TBDMS) protected cresol **6.13** was synthesised first,[15] before reacting with the benzyl bromide **6.12** (Scheme 6.5) achieving the TBDMS-protected UVDU **6.14** in 32 % yield (1.45 g). Attempting to remove the TBDMS protecting groups with either amberlyst-15 as Shabat had reported,[15] or with TBAF resulted in the breakdown of the compound.

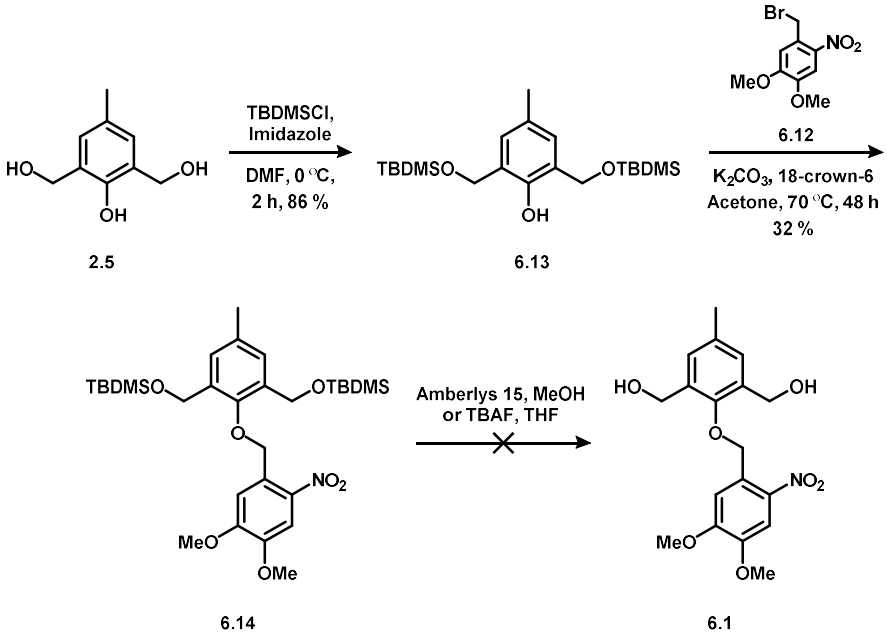

Scheme 6.5 *Unsuccessful synthesis of the UVDU* ***6.1*** *using a TBDMS-protected cresol* ***6.13****.*

Therefore, the next attempts at synthesising the UVDU **6.1** were carried out from the commercially available cresol **2.5** and reacting it with the benzyl bromide **6.12** under different conditions (Table 6.1). The pK_a of the phenols are approximately 10,[24,25] whereas benzyl alcohols pK_a are approximately 15.[25] Potassium and caesium carbonates were chosen as the base as their pK_a's are approximately 10,[26] resulting in deprotonation of the phenol only.

Reagents	Solvent	Reaction time (hours)	Temperature (°C)	Yield of UVDU 6.1 (%)
18-crown-6, K_2CO_3	Acetone	48	70	0
K_2CO_3	Acetone	48	70	0
K_2CO_3	Acetone	48	25	10
Cs_2CO_3	Acetone	48	25	13
Cs_2CO_3	MeCN	48	25	32
Cs_2CO_3	MeCN	2	25	68

Table 6.1 *Reaction conditions used to optimise the synthesis of the UVDU* ***6.1****. Solvents were anhydrous prior to use. Carbonates were dried at 110 °C for 24 hours prior to use.*

It was found through the series of different reactions that the optimal reaction conditions to produce the UVDU **6.1** were using anhydrous acetonitrile with addition of dried caesium carbonate, and stirring for 2 hours at 25 °C. After this duration, the salts were filtered off, and the solvent was removed to give the yellow crude product, which was triturated with cooled

(0 – 5 °C) chloroform to afford the UVDU **6.3** in respectable 68 % yields (6.00 g) as yellow powder (Scheme 6.6). The UVDU **6.3** was characterised by ^{1}H NMR spectroscopy (Figure 6.2). The upfield shift for the methylene protons from 4.9 ppm for the benzyl bromide **6.2** to 5.4 ppm for the UVDU indicates formation of the desired ether link.

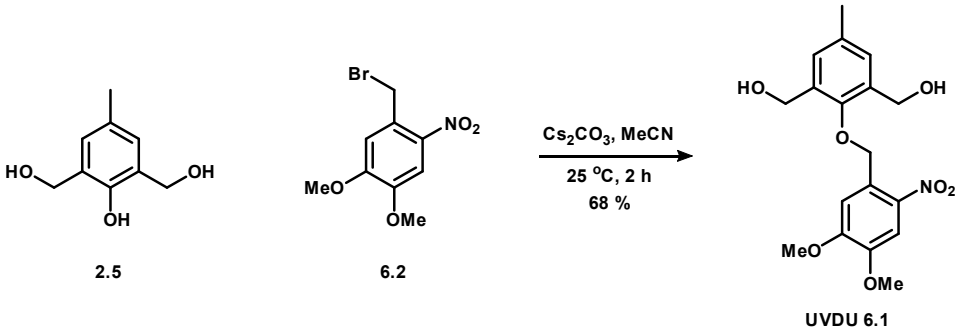

Scheme 6.6 *Synthesis of the UVDU* ***6.1****.*

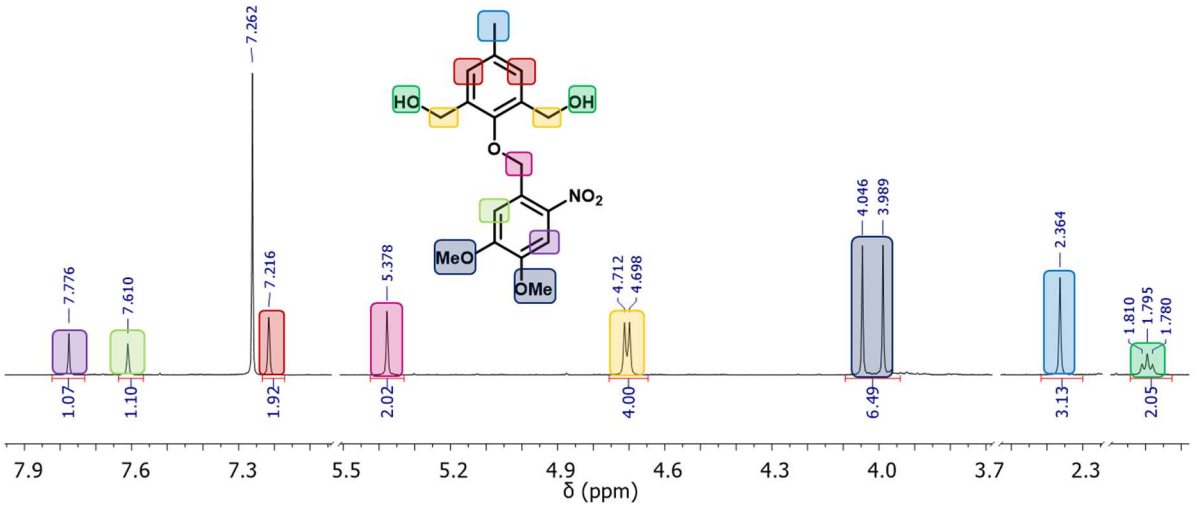

Figure 6.2 *^{1}H NMR spectrum of the UVDU* ***6.1*** *($CDCl_3$, 400 MHz). See Appendix A.6. for full spectrum.*

6.2.2. Model Compound Synthesis and Degradation Studies

To determine if the UVDU **6.1** would breakdown with UV light, a model compound **6.15** was synthesised by reacting phenyl isocyanate with UVDU in THF (Scheme 6.7). The model compound **6.15** was afforded as a pale brown powder in 72 % yield. The model compound **6.15** did not dissolve in chloroform and hence was characterised by ^{1}H NMR spectroscopy in DMSO-d_6 (Figure 6.3). A shift in the methylene resonances of UVDU **6.1** from 4.5 ppm to 5.2 ppm, and the appearance of a broad resonance at 9.7 ppm indicated the formation of the desired urethane.

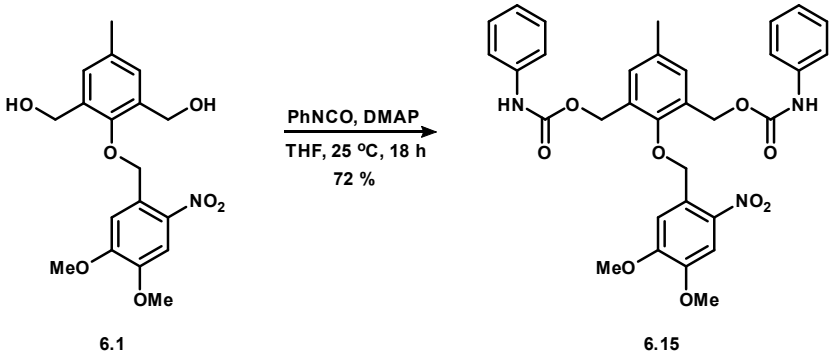

Scheme 6.7 *Synthesis of the UV responsive model compound* ***6.15****.*

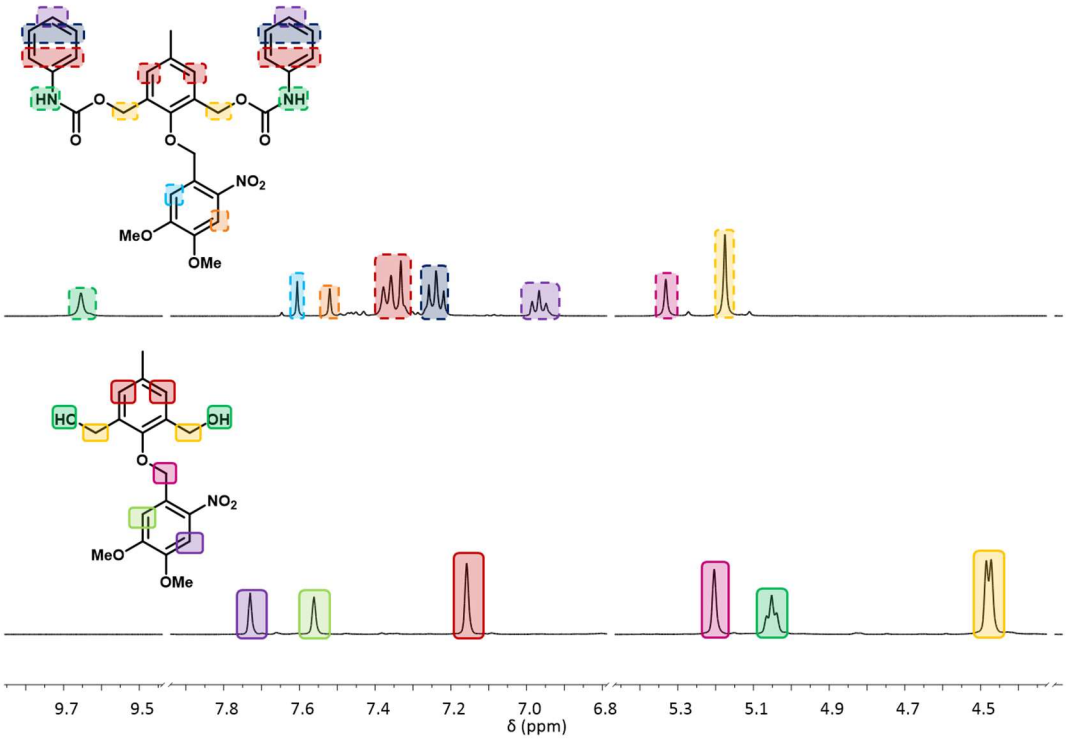

Figure 6.3 *^{1}H NMR spectra of the model compound* ***6.15*** *in comparison to the UVDU* ***6.1****. (DMSO-d$_6$, 400 MHz). See Appendix A.7. for full spectrum.*

The mechanism of degradation of ONB's has been known since its introduction in 1966 by Barltrop and co-workers,[13] who showed that the ONB breaks down to a nitroso-aldehyde **1.53** with the release of a hydroxyl anion (Chapter 1, Scheme 1.9). The same degradation pathway is possible in this model system (Scheme 6.8).

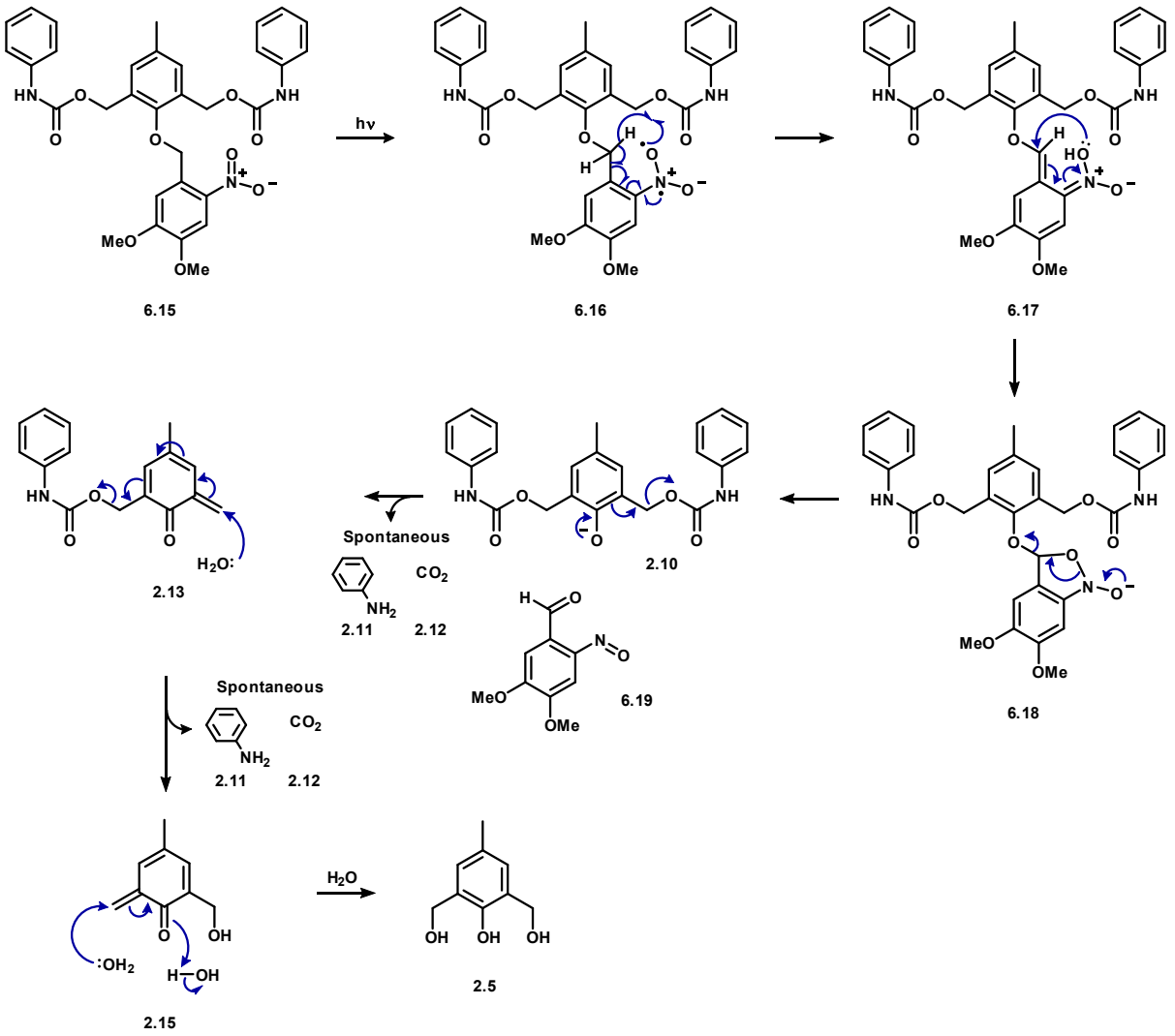

Scheme 6.8 *Proposed mechanism of degradation of the UV responsive model compound* ***6.15****.*

For degradation studies, UV/visible spectroscopy was initially employed to determine if degradation was occurring. The absorption spectra were carried out at two concentrations: (A) 10 µg/mL and (B) 1 µg/mL in acetonitrile; the spectra obtained are shown in Figure 6.4. Samples were irradiated with a 36 W UV lamp in a quartz cuvette for up to 120 minutes.

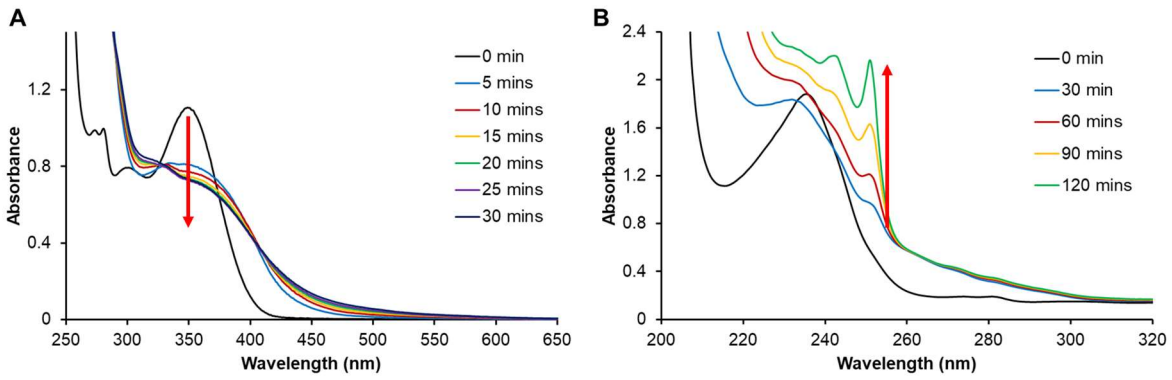

Figure 6.4 *UV/visible spectroscopic analysis of the model compound* ***6.15*** *at (A) 10 µg/mL and (B) 1 µg/mL after irradiating with a 36 W UV lamp.*

Analysis of the UV/visible spectra at 10 µg/mL (Figure 6.4a) showed a rapid decrease in absorbance at 365 nm after 5 minutes indicating rapid cleavage of the ONB group in the UVDU **6.1**. Thereafter, the absorbance at 365 nm decreased slowly. At lower concentrations (Figure 6.4b), the spectra showed that self-immolative breakdown of the model compound was occurring with loss of the absorbance at 236 nm indicative of the phenyl groups of the UVDU **6.1**. An increase in absorbance at 251 nm indicated the release of the aniline **2.11** leaving group as the degradation time increased.

To further investigate that the mechanism of breakdown of the UVDU **6.1**, ^{1}H NMR spectroscopy was carried out (Figure 6.5) on the model compound **6.15** dissolved in acetonitrile, which was irradiated with UV light through a quartz NMR tube. A decrease in intensity of the benzyl ether of the ONB (pink) at 5.4 ppm and the methylene groups of the core cresol (yellow) at 5.2 ppm showed both cleavage of the ONB and self-immolative breakdown of the core group. The appearance of a broad resonance at 7.9 ppm indicated the appearance of an aldehyde **6.12**. Finally, loss of the broad urethane resonance at 7.7 ppm and shifts in the aromatic region showed release of the phenyl carbamic acid **6.14** which rapidly breaks down to aniline **6.16** as observed during degradation of the fluoride responsive model compound **2.7** in Chapter 2.

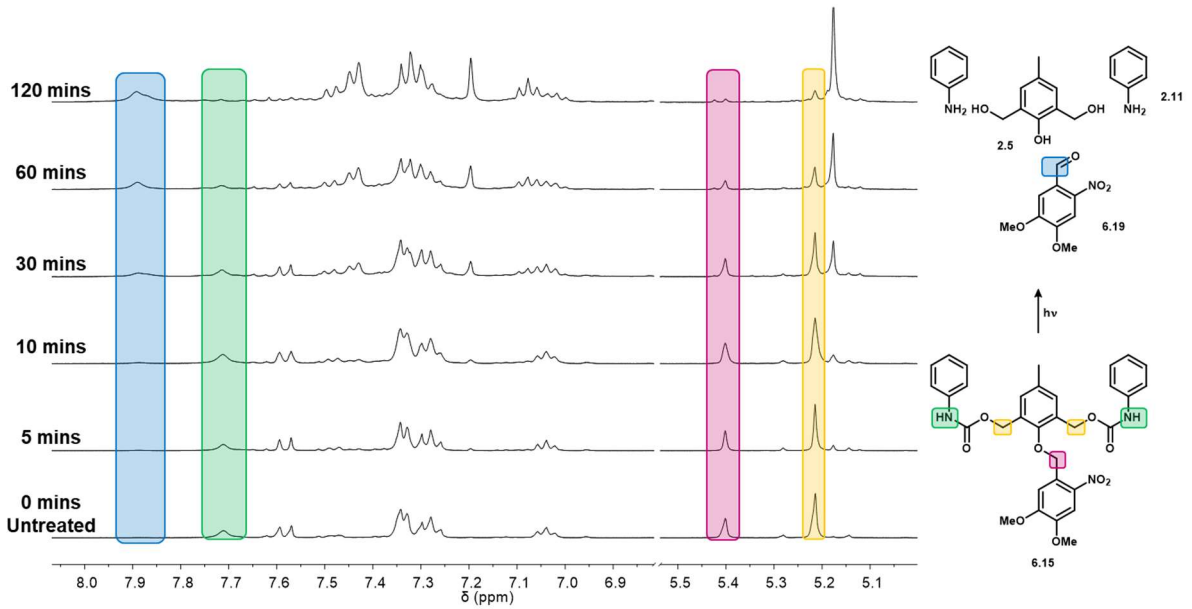

Figure 6.5 *^{1}H NMR spectra showing the degradation of the model compound* ***6.15*** *with UV light. (CD_3CN, 400 MHz).*

The model compound degradation experiments demonstrated the UV responsive nature of the novel UVDU **6.1**, and attention moved to implementing it into a polymer backbone.

6.2.3. Synthesis of UV Responsive Polyurethane

With the synthesis and mechanism of degradation determined, the UVDU **6.1** was incorporated into a polyurethane (PU) backbone in similar fashion to the synthesis of polymer **2.21** (Chapter 2). For polymer **2.21**, the fluoride degradable group **2.6** was added to the prepolymer **2.20** at 100 °C and stirred for 1 hour until it solidified. This was possible as the fluoride responsive degradable group **2.21** melted at *ca.* 94 °C. However, DSC reported a melt at 198 °C for UVDU **6.1**.

Nevertheless, the first attempt at synthesising a UV responsive polymer was carried out using the similar conditions as polymer **2.21** to determine if the UVDU would "dissolve" into the prepolymer to allow for a reaction to occur; rather than acting through the melt of UVDU. The prepolymer **2.20** was prepared from Krasol HLBH-P 2000 (Krasol) **2.18** and 4,4'-methylene diphenyl diisocyanate (4,4'-MDI) **6.18** (Scheme 6.9). The UVDU **6.1** was added to the prepolymer **2.20** at 110 °C and allowed to stir for 1 hour. The mixture did not solidify after this period, and after cooling, the mixture visibly showed small aggregates of yellow powder indicating that the UVDU **6.1** did not react with the prepolymer.

Therefore, the reaction was modified with the addition of THF to the prepolymer **2.20** at room temperature followed by the addition of the UVDU **6.1** before refluxing for 24 hours. ^{1}H NMR spectroscopic analysis of the crude mixture showed no change to the UVDU resonances after either 24 hours or 48 hours thereafter.

Hence, the reaction procedure was further changed. Dibutyltin dilaurate (DBTDL), a catalyst used in the synthesis of many polyurethanes,[27] was added to the mixture of prepolymer **2.20** and UVDU **6.1** in THF at room temperature before being held under reflux for 1 hour. ^{1}H NMR spectroscopic analysis of the crude mixture showed a shift in resonance from 4.7 ppm to 5.2 ppm of the methylene protons indicative of the formation of a urethane linkage between the UVDU and prepolymer. However, the majority (>80 %) of the UVDU was still unreacted. The reaction was left under reflux for 18 hours, after which no resonance was detected for any unreacted UVDU, and hence the reaction was cooled to room temperature. Slow precipitation into methanol was required to remove any metal salts, before drying to afford polymer **6.20** in 86 % yield (Scheme 6.9).

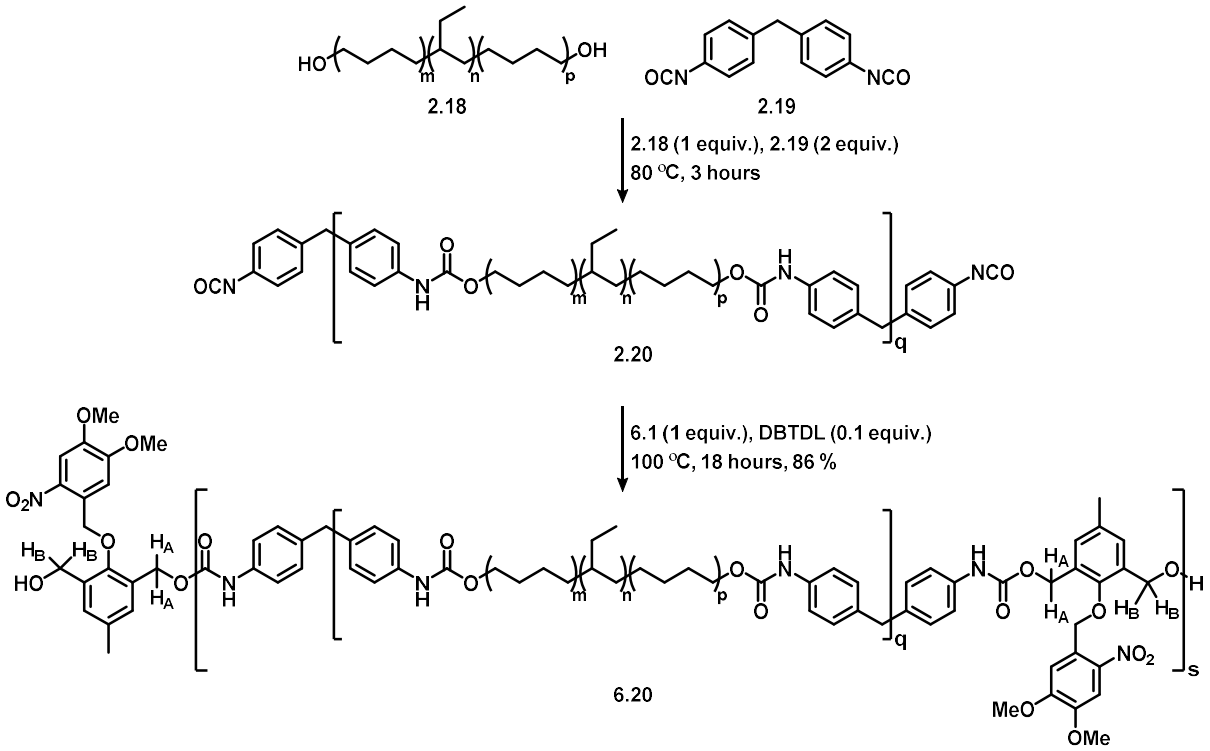

Scheme 6.9 *Synthesis of the UV responsive polymer* ***6.20****.*

Characterisation by ^{1}H NMR spectroscopy showed a downfield shift in resonance for H_A from 4.7 ppm to 5.2 ppm. A low intensity resonance at 4.7 ppm for H_B indicated terminal UVDU groups at the ends of the polymer chain. A broad resonance was observed at 6.5 ppm indicating the presence of urethane N-H group. Integral analysis of the Krasol methylene resonance and MDI methylene resonance indicated that chain extension of the prepolymer backbone was $q \approx 2$. GPC analysis of polymer **6.20** showed a broad monomodal dispersion with M_n 21 kgmol^{-1}, M_w 96 kgmol^{-1} and $Đ$ 4.60, indicating chain extension had occurred between the prepolymer **6.19** and UVDU **6.3**, with $s \approx 9 – 10$ repeat units.

The thermal properties of polymer **6.20** were determined by DSC and thermogravimetric analysis (TGA) followed by rheological analysis. TGA of the polymer **6.20** showed initial onset degradation at 185 °C, with rapid degradation occurring at 230 °C (Figure 6.6a). The DSC of polymer **6.20** revealed no characteristic melting or crystallisation transitions, in similar fashion to polymer **2.21** (Chapter 2), indicating an amorphous material. The glass transition temperature (T_g) was observed at *ca.* -46 °C (Figure 6.6b), which is the same as the starting Krasol **2.18** (T_g *ca. -46 °C),* and indicative of a phase separated material. The T_g of polymer **6.20** did not change over three heat/cool cycles, showing that the material has thermo-reversible properties.

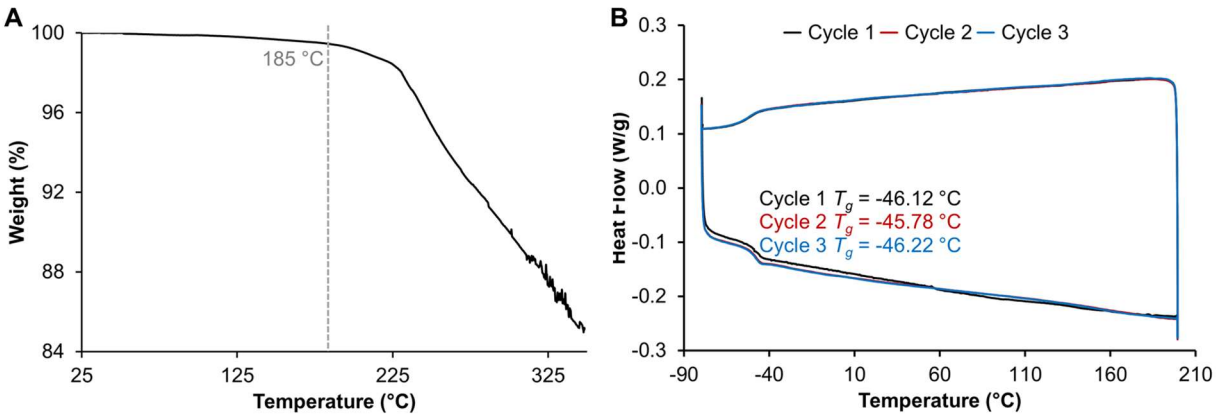

Figure 6.6 *(A) The TGA and (B) DSC thermograms of polymer* ***6.20****.*

Polymer **6.20** was subjected to rheological analysis between 80 °C and 180 °C (Figure 6.7). In comparison to the polymers synthesised in Chapters 2 and 3, polymer **6.20** does not show a viscoelastic transition point where G'' > G', indicating the material does not flow below its degradation temperature.

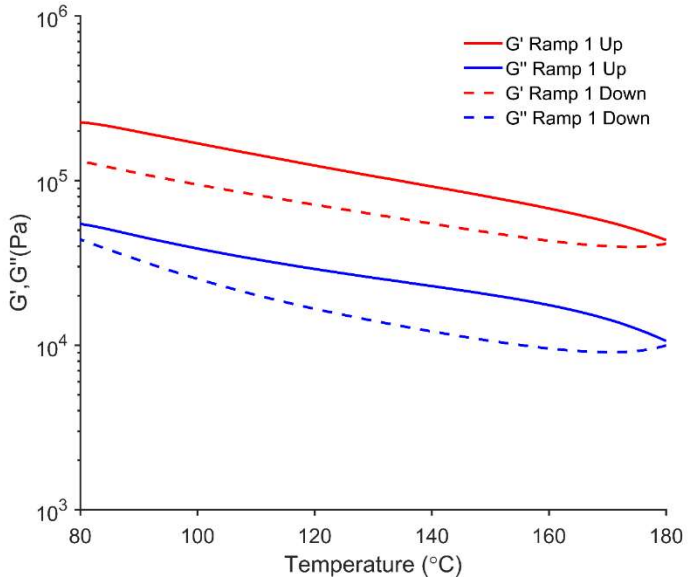

Figure 6.7 *Rheological analysis of the polymer* ***6.20*** *during a heat-cool cycle.*

With the synthesis and thermal properties of polymer **6.20** determined, the material was taken forward for degradation studies under UV light in the solution and solid states.

6.2.4. Solution State UV Depolymerisation Studies

To determine how polymer **6.20** responds to UV light (365 nm), solution state degradation studies were initially carried out using ^{1}H NMR spectroscopy (Figure 6.8) followed by GPC analysis (Figure 6.9 and Table 6.2).

For ^{1}H NMR spectroscopic analysis, polymer **6.20** dissolved in $CDCl_3$ was irradiated over different time periods with a 36 W UV lamp through a quartz glass NMR tube. Gradual loss of

the resonance at 5.2 ppm and 5.4 ppm indicated breakdown of the UVDU group within the PU backbone. Sharpening of the resonance at 6.5 ppm indicated loss of one of the N-H urethane moieties closest to the UVDU in the PU backbone. Finally, the presence of the released aldehyde at 8.0 ppm further proves degradation of the UVDU and hence polymer **6.20** (Scheme 6.10).

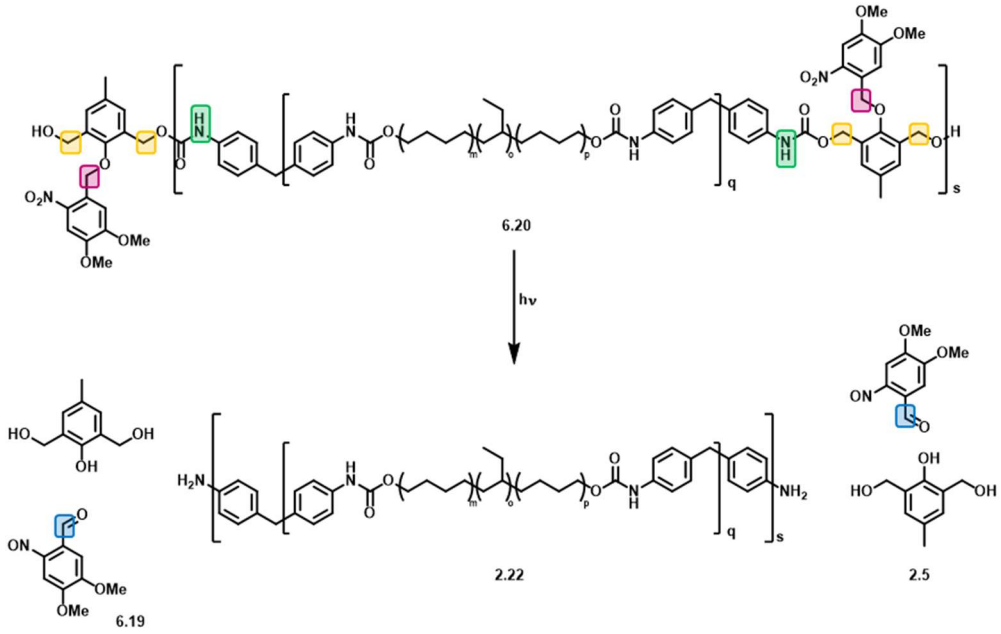

Scheme 6.10 *Degradation products after treatment of the UV responsive adhesive* ***6.20****.*

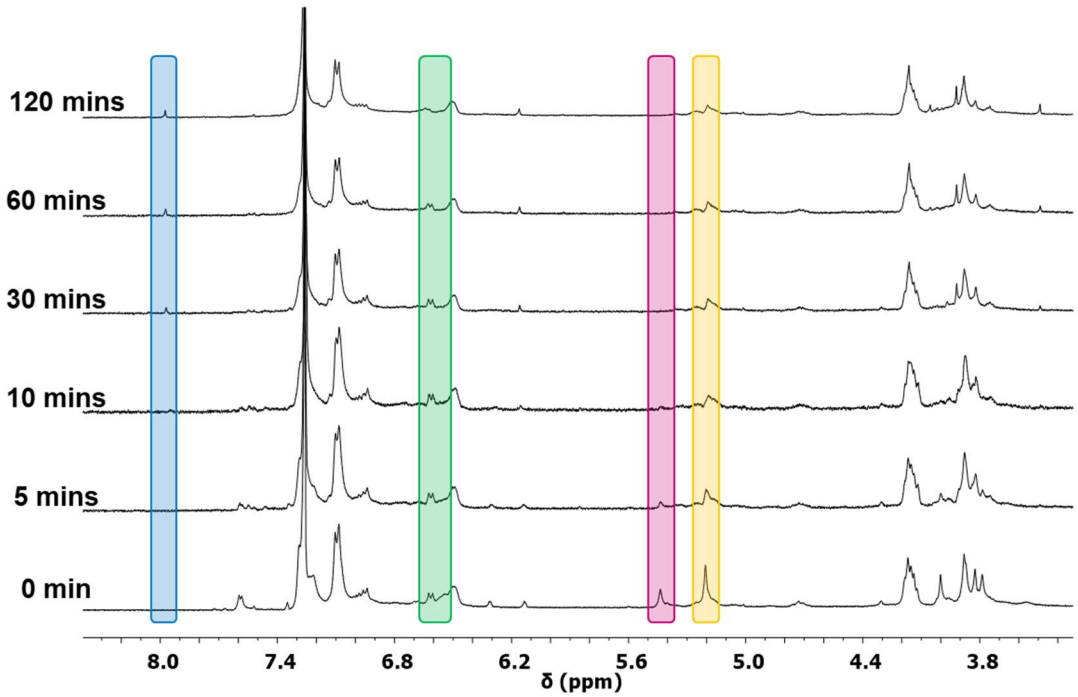

Figure 6.8 *^{1}H NMR spectroscopic analysis showing the degradation of polymer* ***6.20*** *with UV light. ($CDCl_3$, 400 MHz).*

GPC analysis was carried in THF (Figure 6.9a), after the sample had been irradiated in a quartz cuvette. The A plot of Mn and Mw as a function of degradation time are shown in Figure 6.9b. From the GPC results, depolymerisation of the PU **6.20** started occurring in the first 5 minutes with a drop in M_n from 21 kgmol^{-1} to 18 kgmol^{-1}. Thereafter, the rate of depolymerisation in the first 30 minutes started to slow down, going down to M_n 15 kgmol^{-1} before nearly plateauing near 2 hours at M_n of 14 kgmol^{-1}. Both M_n and M_w show the similar trends over time, with GPC eluograms shifting to longer retention times as degradation times increase. Furthermore, as degradation time increases, the peak maxima observed at 15.5 minutes increased corresponding to the appearance of the degraded polymeric material.

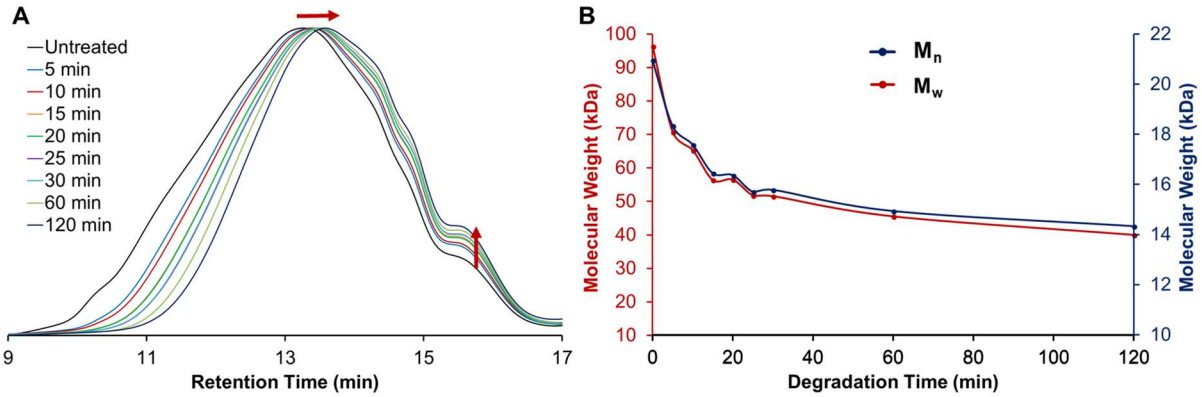

Figure 6.9 *(A) GPC eluograms of the UV responsive polymer* ***6.20*** *after UV treatment. (B) The change in averaged molecular weight calculated from the GPC eluograms against time. (THF, PS standards).*

Degradation time (min)	M_n	M_w	*Đ*
0 (untreated)	21000	96000	4.60
5	18000	70800	3.86
10	17600	65000	3.71
15	16000	56000	3.43
20	16000	56500	3.45
25	15700	52000	3.30
30	15800	52000	3.27
60	15000	46000	3.05
120	14000	40000	2.79

Table 6.2 *Averaged molecular weight estimation from the GPC eluograms for polymer* ***6.20*** *before and after UV irradiation treatment. (THF, PS Standards).*

6.2.5. Solid state mechanical testing

Attention moved towards mechanical testing of a homogeneous polymer film cast from THF. From a film (15 × 15 cm) with an average thickness of 336 µm, four pieces of 4 × 5 cm were irradiated for up to 10 minutes with a 200 W fibre optic UV lamp source (Omnicure S2000) fitted with a 365 – 500 nm filter (Figure 6.10a) (carried out by J. Godleman at Domino Printing Sciences). A higher powered light source than was used in the solution state studies was used in an effort to increase the rate of depolymerisation within the solid film. Polymer films were irradiated on both front and reverse sides of the film to increase penetration of UV light and to maximise degradation throughout the film.

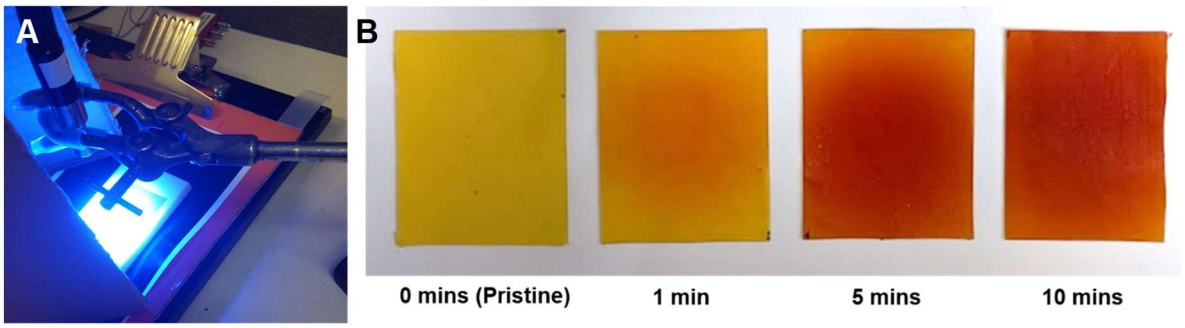

Figure 6.10 *(A) Fibre optic UV light source used for solid state degradation studies on (B) polymer films over different degradation periods.*

Visually, as the degradation time increases, the polymer shows begins to turn red, even after 1 minute of UV irradiation. The material also feels less tacky with increased irradiation, which is an encouraging result for a debondable adhesive. From the four film pieces, five strips (4.0 × 0.5 cm) were cut and mechanical stress-strain experiments were carried out. The stress-strain graphs are shown in Figure 6.11, with mechanical properties detailed in Table 6.3. The graph clearly shows that UV irradiation has very little effect on the mechanical properties of polymer **6.20**, with all five strips of each degraded film showing similar trends.

Degradation time (min)	Tensile Modulus (MPa)	Ultimate Tensile Strength (MPa)	Modulus of Toughness (MJ m^{-3})
0 (untreated)	5.01 (0.33)	6.66 (0.22)	17 (2.7)
1	5.01 (0.32)	7.26 (0.35)	21 (2.0)
5	4.71 (0.24)	7.75 (0.36)	19 (1.3)
10	5.23 (0.11)	7.73 (0.19)	18 (1.3)

Table 6.3 *Mean (n = 5) mechanical properties of the polymer **6.20** before and after irradiation with UV light. Standard deviations are shown in brackets.*

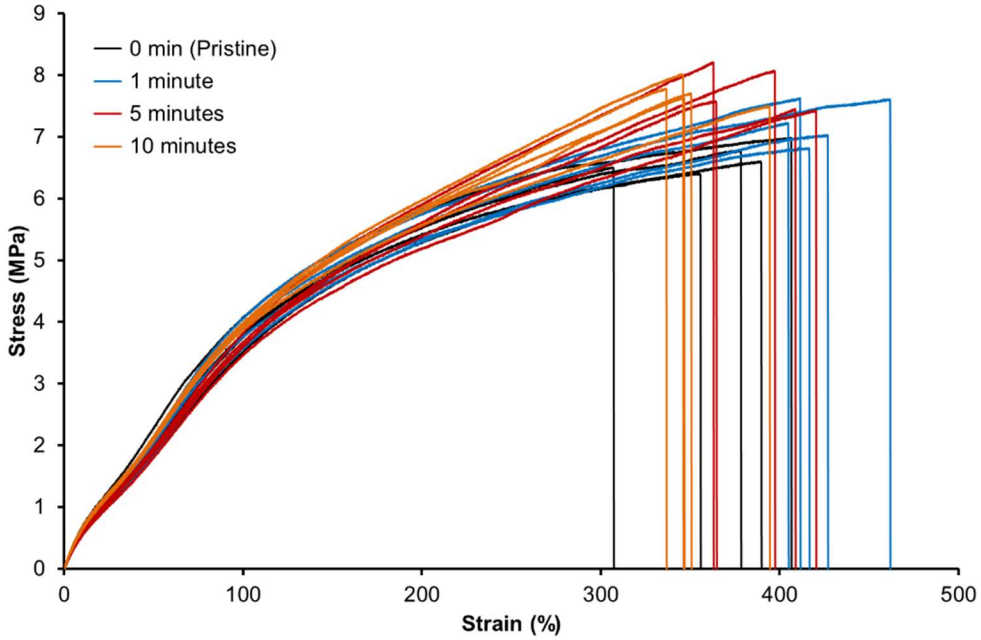

Figure 6.11 *Stress-strain curves for five samples of each UV irradiated sample of polymer* ***6.20****.*

This was believed to be a result improper degradation occurring throughout the film, with UV light only acting on the surface of the film (Figure 6.12). Thinner films could provide better strength loss results after degradation. However, the hydrogenated polybutadiene based UV responsive PU **6.20** forms weak films (*ca.* 80-90 µm) which tear when peeled from the PTFE casting plate.

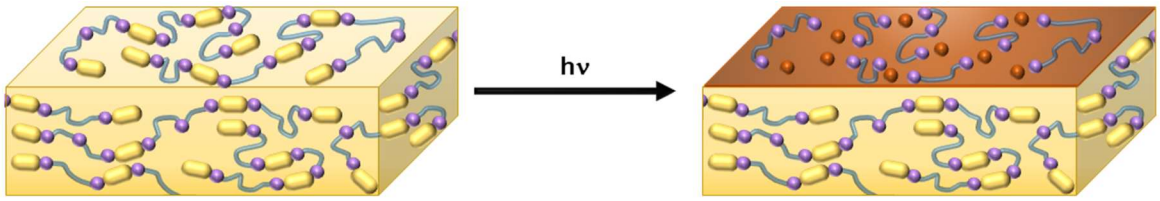

Figure 6.12 *Improper degradation of the UV responsive film as a result of poor penetration of UV light into the bulk of the film.*

To determine the extent of degradation on the films, GPC analysis was carried out. On preparation of the samples in THF, some of the material did not dissolve and therefore the data does not represent the whole sample. The GPC eluograms in Figure 6.13 show the results for the material that did dissolve.

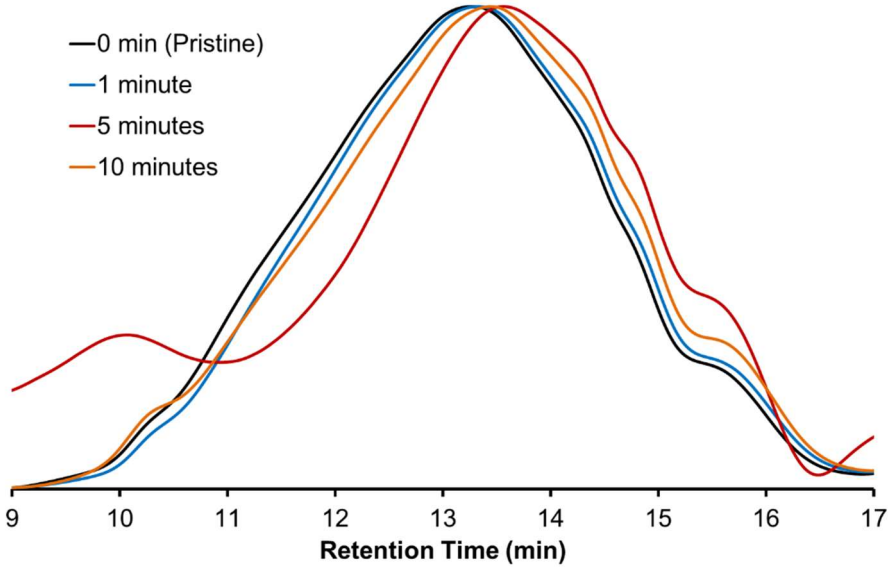

Figure 6.13 *GPC eluograms for the solid-state degradation samples of polymer* ***6.20****. (THF, PS standards).*

	M_n	M_w	*Đ*
0 min (Pristine)	21000	96000	4.60
1 minute	19000	90000	4.68
5 minutes	16000	57000	3.30
10 minutes	17000	94000	5.31

Table 6.4 *Molecular weight estimations from the GPC eluograms of the solid-state degraded films of polymer* ***6.20****. (THF, PS standards).*

GPC analysis showed very little change in molecular weight for the degraded samples, which suggests that the UV light has very little effect on the degradation of the solid-state samples. However, a colour change is seen after degradation; which also occurred with the model compound samples during the UV/visible spectroscopic analysis. Inspection of the insoluble parts of the samples revealed that the darker part to the film did not dissolve. This suggests that a secondary reaction (e.g. a crosslinking reaction) may be occurring. The use of a UV light to photo-cure an adhesive has been known for decades, especially with polyurethanes.[28,29] It is also possible that the red colour appearing after degradation is blocking UV light passing through the material, and hence degradation would only be occurring at the surface of the film. Thinner films may provide the degradation results wanted. In an attempt to cast thinner films (*ca.* < 100 nm), the film tore while peeling away from the PTFE mould and hence could not be tested.

Nevertheless, a small drop in molecular weight and loss in tackiness of the samples after UV irradiation in the solid state was a positive result. Therefore, attention moved towards testing the adhesive properties of polymer **6.20**, before and after degradation.

6.2.6. Adhesion Testing

For adhesive testing, pieces of polymer 12 × 25 mm in dimension were cut from the pristine film and adhered between two glass (soda-lime) slides. The pieces were clamped and placed in an oven at 120 °C for 8 hours. After cooling, samples were then irradiated on both sides for the same durations used in the mechanical tests in Section 6.2.5. (Figure 6.14). Lap shear adhesion tests were carried out on the specimens to determine their adhesive strengths, with the results shown in Figure 6.15.

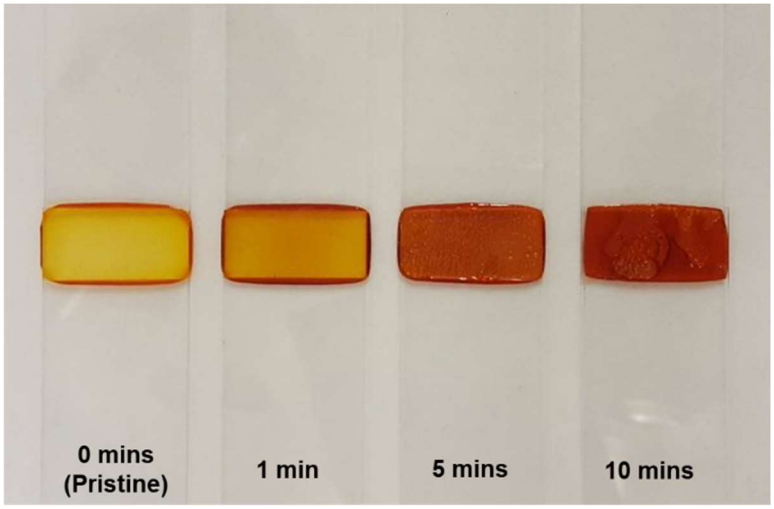

Figure 6.14 *Photographs of the lap shear samples bonded to glass after set periods of degradation time with a 200 W fibre optic UV light source.*

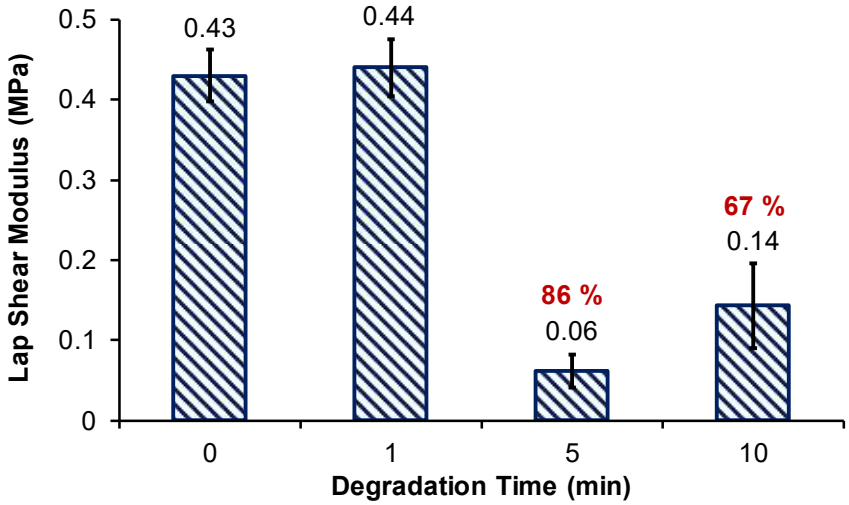

Figure 6.15 *Lap shear testing of polymer **6.20** before and after degradation with a 200 W fibre optic UV light source. Errors were calculated from the standard deviation (n = 5).*

Comparison of the dimensions of the untreated adhesive film and the thickness of the lap shear sample between the two glass slides decreases from the original film thickness (*ca.* 335 nm) to approximately 100 nm. Even though the material showed no viscoelastic transition by rheology (Figure 6.8), the polymer is still above its T_g (*ca.* -46 °C) and will still flow at temperatures when compressed. Visual inspection of the lap shear samples also developed a red colour after UV irradiation indicating a reaction had occurred through the glass slides. The samples also showed adhesion failure between the adhesive material and glass substrate with both the 5 and 10 minute degraded samples with the latter showing more prominent adhesive failure. Lap shear adhesion studies showed little to no change in adhesive strength after 1 minute of UV irradiation. However, after 5 minutes of UV irradiation, the adhesive strength dropped by 86 % (0.43 MPa to 0.06 MPa). The samples irradiated for 10 minutes showed a slightly lower drop in adhesive strength at 67 % decrease, which maybe evidence for any secondary crosslinked reactions occurring.

To study the depolymerisation of the PU **6.20** when used as an adhesive, infrared (IR) spectroscopy carried out (Figure 6.16) on polymer samples scratched off the glass slides. As the Krasol backbone is not affected by UV irradiation and is mainly C-H bonds, the spectra were normalised to at 2920 cm^{-1}. In conjunction with the lap shear adhesion tests, very little change is detected between the untreated sample (0 mins) and the sample irradiated for 1 minutes. Analysis of the IR spectra showed a decrease in absorbance at 1707 cm^{-1}, indicative of loss of urethane moieties. Complete loss of absorbance is not seen as the urethane moieties between the Krasol backbone and diisocyanate linker would not be affected by degradation (Chapter 2, Scheme 2.8). A decrease in absorbance at 1520 cm^{-1} shows loss of N-O groups,[30] indicative of breakdown of the ONB group of the UVDU within the PU backbone.

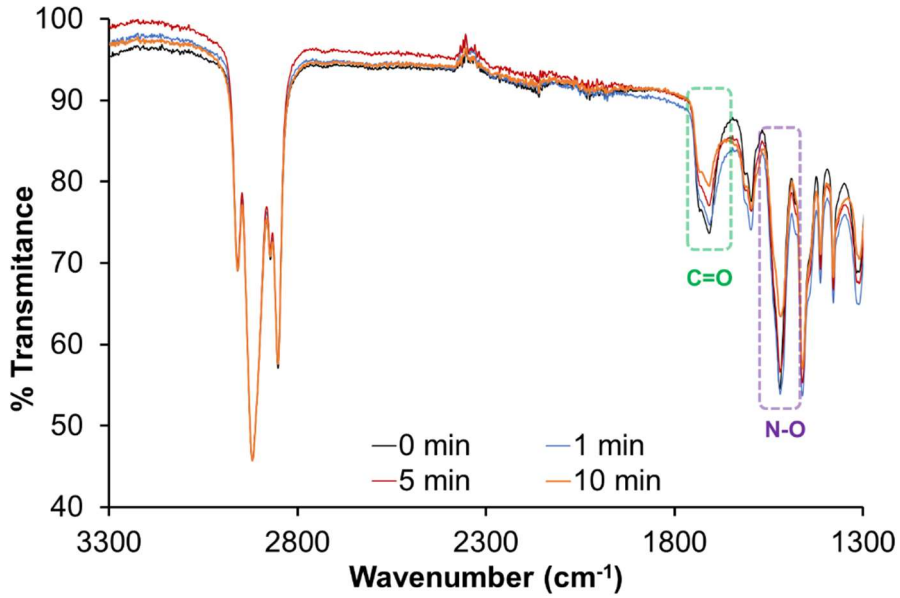

Figure 6.16 *Infrared spectroscopic analysis of polymer* ***6.20*** *from the lap shear samples before and after degradation. Spectra have been normalised to at 2920 cm^{-1}.*

Further analysis of the UV degraded lap shear specimens was carried out using GPC. The polymer was scratched off the glass slides and dissolved in THF for analysis. Similarly to the material analysed during mechanical testing, the samples showed poor dissolution in THF, even after gentle heating or stirring overnight. However, the soluble fraction was submitted for GPC analysis and the GPC eluograms are shown in Figure 6.17, with molecular weight data provided in Table 6.4. The GPC analysis shows that the samples that were irradiated with UV light degraded, with drops in M_n from 21 kgmol^{-1} to *ca*. 8 kgmol^{-1}. The multimodal nature of the eluogram indicated that the PU degrades uniformly no matter the extent of chain extension (see Chapter 3, section 3.2.1), with the last peak appearing at 16 minutes showing similar retentions times to the Krasol starting material (**2.18**). However, GPC analysis of the lap shear sample that was not irradiated and irradiated for 1 minute also exhibited the same drop in molecular weight, even though lap shear adhesion tests and IR spectroscopy showed very little change.

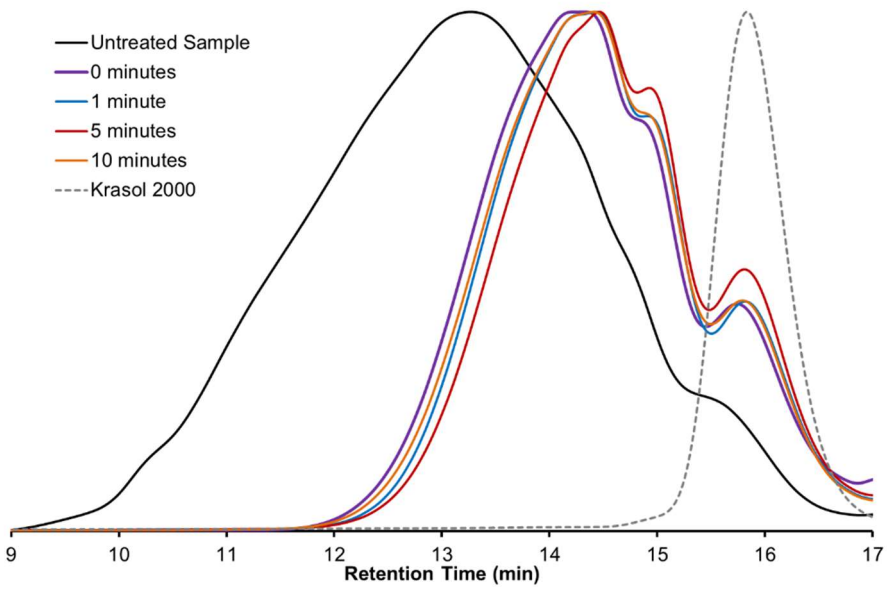

Figure 6.17 *GPC eluograms of the lap shear samples after degradation with a 200 W UV light source. Samples were compared to Krasol* ***6.17****. (THF, PS standards).*

	M_n	M_w	*Đ*
0 min (Untreated)	21000	96000	4.60
0 minutes	9000	19000	2.10
1 minute	8800	17000	1.94
5 minutes	8000	15500	1.95
10 minutes	8700	17600	2.03
Krasol HLBH-P 2000	3400	3700	1.10

Table 6.5 *Molecular weight estimations from the GPC eluograms of the lap shear adhesion samples. (THF, PS standards).*

In comparison to the polymers in Chapters 2 – 5, the chemoresponsive adhesives showed breakdown and hence loss of adhesion as a result of treatment with fluoride ions only. With this UV responsive polymer, the material possibly breaks down with heat prior to irradiating with UV light. To determine if heating was causing additional breakdown of the PU, untreated PU **6.20** was placed into an oven at 120 °C for 8 hours. GPC analysis was carried out on the sample, which showed the same decrease in molecular weight (M_w 17 $kgmol^{-1}$, M_n 8 $kgmol^{-1}$ and *Đ* 2.1). This result thereby proves that the adhesive is not thermally stable at this temperature over this time period. However, the polymer may be stable at lower temperatures and/or over shorter time durations. Nevertheless, the polymer films exhibited reduced tackiness and lap shear adhesion studies demonstrated that the polymer loses adhesive strength (86 %) when irradiated with UV light for 5 minutes. Hence, further optimisation of the bonding conditions is required.

6.3. Conclusions

In this chapter the synthesis of a novel UV degradable unit was reported that required only three synthetic steps using simple purification procedures with overall yields at 56 %. The UV degradable unit was first incorporated into a model bisurethane compound. UV/visible and ^{1}H NMR spectroscopic analysis both presented rapid degradation (>5 minutes) when irradiated with a 36 W UV light source. When incorporated into the backbone of a polyurethane as a chain extender, the degradation characteristics of this material was first analysed by ^{1}H NMR spectroscopy resulting in degradation of the degradable unit within 120 minutes. GPC analysis of the polymer after UV irradiation exhibited a drop in molecular weight by 33 % (from 21 kgmol^{-1} to 14 kgmol^{-1}) after the same time periods. During solid state degradation studies with a 200 W UV light source, the material displayed no weakening in mechanical strength determined by stress-strain analysis. Furthermore, when used as a hot-melt adhesive, the adhesive showed breakdown by thermal stimuli which was analysed by GPC (from 21 kgmol^{-1} to 8 kgmol^{-1}). However, irradiating the thermally degraded adhesive further decreased the adhesives strength by 86 % after 5 minutes irradiation.

6.4. Experimental Procedures

6.4.1. Characterisation

Characterisation was carried out as reported in Chapter 2, page 55. Characterisation specific to this chapter are reported below.

Rheological assessment was conducted using an Anton Paar Physica MCR 301 rheometer with a parallel plate oscillatory shear set-up. Circular samples of 8 mm diameter (0.33 mm average thickness) were cut from the polymer film using a steel punch cutter. For the single frequency temperature sweep, samples were placed into the rheometer and initialised at 150 °C and then subjected to temperature ramp cycle at a rate of 2 °C/min down to 25 °C and back up at the same rate to 150 °C. This cycle was repeated two more times to assess repeatability and any changes in properties. The frequency of oscillation was set to 5 Hz, and the shear strain amplitude to 0.1%. Dynamic shear moduli (G', G'') were recorded to characterise the material. The data was analysed using MATLAB R2017a.

Lap shear tests were carried out using soda lime glass microscope slides (26 mm × 76 mm × 1 mm) which were washed with methanol prior to use. Film samples (26 mm × 12 mm) were

placed on the edge of the sample and sandwiched with another glass slide. The two slides were clamped together and adhered at 120 °C for 18 hours.

6.4.2. Synthesis of 4,5-dimethoxy-2-nitrobenzyl bromide 6.6

To a solution of 4,5-dimethoxy-2-nitrobenzyl alcohol (10.0 g, 46.91 mmol) in anhydrous chloroform (200 mL, distilled over CaH_2) at 0 °C was added potassium bromide (2.88 mL, 93.81 mmol) dropwise under inert atmosphere. The mixture was stirred for 30 minutes, before allowing to equilibrate to ambient conditions. The mixture was washed with cool water (2 × 200 mL), and the organic solution was dried over $MgSO_4$ before concentrating *in vacuo* to afford a yellow powder (10.7 g, 82 %). m.p. (DSC) = 145 °C ν_{max} (thin film, cm^{-1}) 2969, 2935, 2841, 1520, 1511, 1270, 796, 607. δ_H (400 MHz, $CDCl_3$, ppm) 7.68 (s, 1H, Ar-H), 6.95 (s, 1H, Ar-H), 4.88 (s, 2H, Ar-C$\underline{H}_2$), 3.99 (d, J = 14.5 Hz, 6H, Ar-OC$\underline{H}_3$). δ_C (100 MHz, $CDCl_3$, ppm) 153.2, 148.9, 140.2, 127.5, 113.6, 108.5, 56.6, 30.1. m/z found 300.0239 ($C_9H_{10}NO_2BrNa$), calc. 299.0758 ($C_9H_{10}NO_2BrNa$).

6.4.3. Synthesis of UVDU 6.3

To a solution of 2,6-bis(hydroxymethyl)-*p*-cresol (4.06 g, 24.15 mmol) in acetonitrile (200 mL) was added Cs_2CO_3 (8.00 g, 28.98 mmol) and stirred under inert conditions. Upon colour change from orange to brown (*ca.* 10 minutes), 4,5-dimethoxy-2-nitrobenzyl bromide was added and stirred for 2 hours at 25 °C. The mixture was filtered, and the solute was concentrated *in vacuo* to afford a yellow powder, which was triturated with chloroform (3 × 50 mL) and allowed to dry under vacuum to afford a yellow powder (6.00 g, 68 %). m.p. (DSC) = 195 °C ν_{max} (thin film, cm^{-1}) 8, 2933, 2842, 1615, 1578, 1521, 1272, 797, 605. δ_H (400 MHz, DMSO-*d*$_6$, ppm) 7.73 (m, 1H, Ar-H), 7.56 (m, 1H, Ar-H), 7.16 (m, 2H, Ar-H), 5.20 (s, 2H, Ar-C$\underline{H}_2$-O-Ar), 5.07 – 5.04 (m, 2H, Ar-CH_2-O$\underline{H}$), 4.48 – 4.47 (m, 4H, Ar-C$\underline{H}_2$-OH), 3.94 (s, 3H, Ar-OC$\underline{H}_3$), 3.89 (s, 3H, Ar-OC$\underline{H}_3$), 2.29 (s, 3H, Ar-C$\underline{H}_3$). δ_C (100 MHz, DMSO-*d*$_6$, ppm) 153.5, 151.1, 147.5, 138.6, 134.7, 132.9, 129.1, 128.1, 109,8, 107.9, 72.1, 58.1, 56.2, 56.1, 20.7. m/z found 386.1201 ($C_{18}H_{21}NO_7Na$), calc. 386.3558 ($C_{18}H_{21}NO_7Na$).

6.4.4. Synthesis of UV responsive model compound 6.7

To a solution of UVDU (0.50 g, 1.38 mmol) and 4-dimethylaminopyridine (0.017 g, 0.138 mmol) in anhydrous tetrahydrofuran (10 mL) was added phenyl isocyanate (0.38 mL, 3.44 mmol) dropwise at room temperature. The mixture was allowed to stir at room temperature for 18 hours, before being diluted with ethyl acetate (20 mL). The mixture was washed with

saturated NH_4Cl solution (2 × 20 mL) and brine solution (2 × 20 mL) before drying over $MgSO_4$. The mixture was concentrated *in vacuo* to afford the crude material, which was purified by column chromatography eluting in 30 % ethyl acetate in hexanes over silica to afford a brown powder (596 mg, 72 %). m.p. (DSC) = 211 °C ν_{max} (thin film, cm^{-1}) 3285, 2953, 1698, 1601, 1526, 1278, 1221, 1063, 754. δ_H (400 MHz, DMSO-*d*$_6$, ppm) 9.65 (s, 2H, N-H), 7.61 (m, 1H, Ar-H), 7.52 (m, 1H, Ar-H), 7.38 – 7.33 (m, 4H + 2H, Ar-H), 7.26-7.22 (m, 4H, Ar-H), 6.99 – 6.95 (m, 2H, Ar-H), 5.33 (s, 2H, Ar-C$\underline{H_2}$-O-Ar), 5.18 (s, 4H, Ar-C$\underline{H_2}$-O-C(O)), 3.86 (s, 3H, Ar-OCH_3), 3.76 (s, 3H, Ar-OCH_3), 2.32 (s, 3H, Ar-C$\underline{H_3}$). δ_C (100 MHz, DMSO-*d*$_6$, ppm) 153.5, 153.1, 147.5, 138.9, 138.4, 133.9, 131.1, 129.8, 128.7, 128.6, 128.5, 122.4, 118.1, 109.5, 107.9, 73.0, 61.3, 55.9, 55.8, 20.4. m/z found 624.1954 ($C_{32}H_{31}N_3O_9Na$), calc. 624.1958 ($C_{32}H_{31}N_3O_9Na$).

6.4.5. Synthesis of UV responsive polymer 6.20

4,4'-methylene bis(phenyl isocyanate) (1.51 g, 6.04 mmol) was added to Krasol HLBH P-2000 (6.36 g, 3.03 mmol) at 80 °C under nitrogen and stirred for 3 hours. Anhydrous THF (70 mL) was added to the pre-polymer before cooling to room temperature. UVDU **6.7** (1.10 g, 3.03 mmol) was added to the mixture prior to addition of dibutyltin dilaurate (0.19 mg, 0.30 mmol). The mixture was refluxed for 18 hours, before cooling to room temperature. The mixture was slowly precipitated into methanol from THF twice. The precipitate was dissolved in THF, before drying *in vacuo* to afford pure polymer (7.7 g, 86 %). The polymer was cast into a 15 × 15 cm film from THF using the same methods described in Chapter 2, page 55. ν_{max} (thin film, cm^{-1}) 3334, 2959, 2919, 2853, 1710, 1598, 1524, 1378, 1221, 1069, 763. δ_H (400 MHz, $CDCl_3$, ppm) (n = number of chain extension) 7.60 – 7.58 (m, $1H_n$), 7.35 – 6.86 (m, $8H_n + 2H_n + 1H_n$), 6.59 – 6.41 (m, $4H_n$), 5.44 (m, $2H_n$), 5.21 (m, $4H_n$), 4.77 – 4.63 (m, $1H_n$), 4.22 – 4.10 (m, $8H_n$), 4.00 (m, $4H_n$), 3.92 – 3.74 (m, $6H_n + 6H_n$), 2.40 – 1.80 (m, $20H_n$), 1.74 – 0.55 (m, $700H_n$). δ_C (100 MHz, $CDCl_3$, ppm) 153.7, 129.4, 38.9, 36.1, 33.4, 30.7, 30.2, 29.8, 26.7, 25.9, 10.9, 10.7. GPC (THF/BHT 250 ppm) M_w 96000, M_n 21000, *Đ* 4.60. DSC T_g = -46.0 °C.

6.5. References

1. T. S. Babra, A. Trivedi, C. N. Warriner, N. Bazin, D. Castiglione, C. Sivour, W. Hayes and B. W. Greenland, *Polym. Chem.*, 2017, **8**, 7207–7216.
2. B. T. Michal, E. J. Spencer and S. J. Rowan, *ACS Appl. Mater. Interfaces*, 2016, **8**, 11041–11049.
3. C. Heinzmann, S. Coulibaly, A. Roulin, G. L. Fiore and C. Weder, *ACS Appl. Mater. Interfaces*, 2014, **6**, 4713–4719.
4. H. Akiyama, Y. Okuyama, T. Fukata and H. Kihara, *J. Adhes.*, 2018, 1–15.

5. H. Akiyama, T. Fukata, A. Yamashita, M. Yoshida and H. Kihara, *J. Adhes.*, 2017, **93**, 823–830.
6. H. Akiyama, M. Yoshida, H. Kihara, Y. Norikane and R. Azumi, *J. Photopolym. Sci. Technol.*, 2014, **27**, 301–305.
7. S. Saito, S. Nobusue, E. Tsuzaka, C. Yuan, C. Mori, M. Hara, T. Seki, C. Camacho, S. Irle and S. Yamaguchi, *Nat. Commun.*, 2016, **7**, 1–7.
8. M. A. Ayer, Y. C. Simon and C. Weder, *Macromolecules*, 2016, **49**, 2917–2927.
9. S. R. Trenor, T. E. Long and B. J. Love, *J. Adhes.*, 2005, **81**, 213–229.
10. H. Akiyama, S. Kanazawa, Y. Okuyama, M. Yoshida, H. Kihara, H. Nagai, Y. Norikane and R. Azumi, *ACS Appl. Mater. Interfaces*, 2014, **6**, 7933–7941.
11. S. M. June, T. Suga, W. H. Heath, Q. Lin, R. Puligadda, L. Yan, D. Dillard and T. E. Long, *J. Adhes.*, 2013, **89**, 548–558.
12. M. Kim and H. Chung, *Polym. Chem.*, 2017, **8**, 6300–6308.
13. J. A. Barltrop, P. J. Plant and P. Schofield, *Chem. Commun.*, 1966, **22**, 822–823.
14. T. Kobayashi, T. Komatsu, M. Kamiya, C. Campos, M. González-Gaitán, T. Terai, K. Hanaoka, T. Nagano and Y. Urano, *J. Am. Chem. Soc.*, 2012, **134**, 11153–11160.
15. R. J. Amir, N. Pessah, M. Shamis and D. Shabat, *Angew. Chem. Int. Ed. Engl.*, 2003, **42**, 4494–4499.
16. N. Fomina, C. McFearin, M. Sermsakdi, O. Edigin and A. Almutairi, *J. Am. Chem. Soc.*, 2010, **132**, 9540–9542.
17. H. Taniguchi and E. Nomura, *Chem. Lett.*, 1988, 1773–1776.
18. J. C. Lee, J. Y. Yuk and S. H. Cho, *Synth. Commun.*, 2001, **25**, 1367–1370.
19. G. Keglevich, E. Bálint, É. Karsai, J. Varga, A. Grün and M. Bálint, *Lett. Org. Chem.*, 2009, **6**, 535–539.
20. P. Srivastava and R. Srivastava, *Tetrahedron Lett.*, 2007, **48**, 4489–4493.
21. J. Nithyanandhan and N. Jayaraman, *Tetrahedron*, 2005, **61**, 11184–11191.
22. M. E. Lanning and S. Fletcher, *Tetrahedron Lett.*, 2013, **54**, 4624–4628.
23. L. Feng, K. Lv, M. Liu, S. Wang, J. Zhao, X. You, S. Li, J. Cao and H. Guo, *Eur. J. Med. Chem.*, 2012, **55**, 125–136.
24. M. D. Liptak, K. C. Gross, P. G. Seybold, S. Feldgus and G. C. Shields, *J. Am. Chem. Soc.*, 2002, **124**, 6421–6427.
25. F. G. Bordwell, *Acc. Chem. Res.*, 1988, **21**, 456–463.
26. D. Gimenez, A. Dose, N. L. Robson, G. Sandford, S. L. Cobb and C. R. Coxon, *Org. Biomol. Chem.*, 2017, **15**, 4081–4085.
27. D. K. Chattopadhyay and K. V. S. N. Raju, *Prog. Polym. Sci.*, 2007, **32**, 352–418.
28. D. Randall and S. Lee, *The Polyurethanes Book*, John Wiley & Sons, 2003.
29. G. Habenicht, *Applied Adhesive Bonding: A Practical Guide for Flawless Results*, Wiley-VCH, Germany, 2008.
30. D. R. White and R. L. White, *J. Appl. Polym. Sci.*, 2005, **95**, 351–357.

Chapter 7

Conclusions and Future Work

7.1. Conclusions

Stimuli responsive debond-on-demand adhesives is a growing field of research with advances in these materials transitioning towards industrial situations. Within this study, new chemical, thermal and UV responsive adhesives have been designed and developed.

Chapter 2 described the design and synthesis of a fluoride responsive degradable unit[1,2] which was incorporated into a polyurethane backbone resulting in the production a new hot-melt adhesive. Solution state degradation studies showed rapid (<1 minute) depolymerisation of the polyurethane material by ^{1}H NMR spectroscopy. GPC analysis displayed a reduction in molecular weight by 76 % (from 26.1 kgmol^{-1} to 6.2 kgmol^{-1}) when treated with *tetra*-butylammonium fluoride (TBAF). Using mechanical stress-strain testing on a polymeric film, the material shows a 91 % loss in toughness (27 MJ m^{-3} to 2 MJ m^{-3}) when treated with a fluoride source for 30 minutes. Butt-tensile adhesion testing demonstrated loss in adhesive strength by 34 % after 3 hours of degradation. Lap shear adhesion testing revealed that the material was able to bond to wood, metal and glass materials. Utilising the urethanes as supramolecular hydrogen bonding motifs, the polyurethane acts as a traditional thermoplastic and could be used a thermally reversible adhesive showing no loss in adhesive strength over four debond-rebond cycles.

The fluoride responsive degradable unit (**2.6**) was then incorporated into polyurethanes with carrying chemical structures to determine if the thermal and/or adhesive properties could be improved (Chapter 3). Two series of polymers were developed, the first containing different diisocyanate residues and the second containing different polyols. Rheological analysis showed the first series of polymers with aliphatic diisocyanate linkers exhibited a low (*ca*. 28 °C) viscoelastic transition temperature. The second series of polyurethanes, one of which contained a polyester based polyol, exhibited a viscoelastic temperature at 49 °C, significantly less than the original polymer (**2.21** at 129 °C). To improve the understanding of the morphology of the materials, SAXS and WAXS analysis was carried out at the Alba Synchrotron, which showed the thermoreversible nature of the supramolecular interactions. The second series of polymers were able to form self-supporting films, whereas the first series did not. When mechanical

stress-strain testing was carried out, the polyester based material displayed a 74 % decrease in toughness (27 MJ m^{-3} to 7 MJ m^{-3}) after 30 minutes in contact with fluoride ions. Butt-tensile adhesive testing showed that the polymers exhibited approximately a 30 % loss in adhesive strength after 3 hours of degradation time. The polyester based adhesive also demonstrated strong adhesion (0.9 MPa) after 30 minutes at 60 °C; whereas, the original adhesive required much longer times (18 hours) to achieve the same adhesive strength. This low temperature hot-melt adhesive also exhibited thermoreversibility through four debond-rebond cycles.

To further increase the adhesive strength of the fluoride responsive adhesive, a new crosslinking group was designed (Chapter 4). Model compound studies revealed rapid degradation with a fluoride source as measured by ^{1}H NMR spectroscopic analysis. When reacted with a diisocyanate prepolymer, a crosslinked material was formed that did not dissolve in range of solvents or flow at high temperatures. Consequently, solvent and hot-melt cast films could not be produced, and adhesion had to be studied by a new method of a hot-melt reactive adhesive; where the adhesive was prepared *in situ* on the substrate before heat curing at 110 °C. Under lap shear testing conditions, the crosslinked adhesive showed a 28 % increase in strength over the linear polymeric adhesives. Degradation studies were carried out by soaking the lap shear samples in 0.025 M TBAF solution for 3 hours, which resulted in a weakening in adhesive strength of 55 %, a much a greater loss in strength than the linear chain extended materials showed (33 %).

The fluoride responsive crosslinking group was also used as a core in efforts to make star shaped polymers by the ring opening polymerisation of ε-caprolactone (Chapter 5). However, GPC analysis showed that transesterification had occurred resulting in a branched polymer, as proven by the higher than expected molecular weight (16.7 $kgmol^{-1}$, predicted 3.7 $kgmol^{-1}$). Nevertheless, ^{1}H NMR spectroscopy showed the polymer had terminal hydroxyl groups, and GPC analysis resulted in a reduction of molecular weight from 16.7 $kgmol^{-1}$ to 6 $kgmol^{-1}$ after treatment with TBAF. The powdered polymer exhibited a melting point of 49 °C. Reactions of the polyester with an aromatic diisocyanate at 60 °C produced a crosslinked material. Comparison of lap shear adhesion test results for the crosslinked material showed only a 12 % increase in adhesive strength over the branched polymer (3.45 MPa to 3.85 MPa). This difference may be accounted for by the poor flow of material at this bonding temperatures. Degradation studies on the adhesive resulted in a 23 % weakening in adhesive strength after 3 hours. Although the material did not show as great adhesion properties as the previous crosslinked material **4.14** (Chapter 4), there are many aspects of the structure that could be

changed to further increase the materials mechanical and adhesive properties. The main advantage to this adhesive material over the crosslinked material in Chapter 3 is that the polyester based star polymer can be stored for long durations without degradation occurring; whereas, an isocyanate prepolymer will slowly degrade on contact with moisture.

In Chapter 6, a novel UV responsive degradable unit (**6.1**) was designed and developed. The UV degradable unit was synthesised successfully using only three steps in comparison to the seven steps required for UV responsive group **6.10** reported by Shabat and co-workers.[3] Degradation studies were carried on a model compound by ^{1}H NMR and UV/visible spectroscopic analysis. Both methods showed degradation of the UV responsive group within 5 minutes of irradiation with a 36 W UV light source. The UV responsive group was then incorporated into a polyurethane backbone. ^{1}H NMR spectroscopy and GPC analysis showed breakdown of the polyurethane within 2 hours; with the later presenting a reduction in molecular weight from 21 kgmol^{-1} to 14 kgmol^{-1}. The polyurethane was cast into a homogenous film, which was irradiated with a 200 W UV light source. Disappointingly, tensile stress-strain tests did not reveal any dramatic changes in the material properties, even though the polymer changed colour (yellow to red) and was less tacky when touched. This result was thought to be a result of the thickness of the film and the UV light was only degrading the surface of the film, and a thinner film may provide the loss in mechanical strength after UV irradiation. Lap shear adhesion tests were also carried out, with adhesion carried out at 120 °C for 8 hours. The samples were irradiated with UV light (200 W) before testing. Samples that were irradiated for 1 minute did not change in terms of adhesive strength. However, when irradiated with UV light for 5 minutes, the samples exhibited a decrease in adhesive strength by 86 % (0.43 MPa to 0.06 MPa). Further analysis by IR spectroscopy presented a reduction in intensity of the signals for urethane and nitro groups consistent with the expected degradation path of the UV responsive PU. GPC analysis showed a significant decrease in molecular weight to *ca.* 8 kgmol^{-1}. Unfortunately, the 1 minute UV irradiated sample (which did not change in strength) also showed similar molecular weights indicating that initial degradation was a result heat curing the adhesive. Nevertheless, the polymer displayed an 86 % reduction in adhesive strength after 5 minutes. Therefore, further optimisation would be required with this polymer to ensure that degradation is solely caused by UV irradiation.

Finally, to show the commercial aspect of the adhesives designed and produced in this thesis, the strength of reported adhesives is detailed in Table 7.1 and compared to the materials produced during this work. However, an important note to make is that not all adhesive

strengths detailed in Table 7.1 come from the same adhesive test method and hence the strengths of the adhesives cannot be compared completely.

Adhesive Type	Adhesive Bond Strength (MPa)	Reference
Reactive Adhesives	5 – 8 (LSS – Glass fibre resin) 15.1 (LSS – Aluminium) 2 – 11 (LSS - Aluminium) 8 – 35 (LSS – Titanium)	[4–7]
Hot melt adhesives: film adhesives	0.52 (LSS – Aluminium)	[8]
Hot melt adhesives: hot glue gun adhesives	0.82 (LSS – glass)	[9]
Solvent based adhesives	10 – 11 (LSS – aluminium)	[10]
Pressure-sensitive adhesives	1.75 N/mm (PTS – tape to steel) 0.17 (LSS – Duct tape)	[11]
Thesis – Reactive Adhesives	14.64 (LSS – Aluminium)	Chapters 4
Thesis – Hot Melt Film adhesives	2.86 – 11.41 (LSS – Aluminium)	Chapter 2 and 3

Table 7.1 *Comparison of reported adhesives and the adhesives produced in this thesis. The adhesive test method and substrate material are detailed in brackets. (Abbreviations – LSS: lap shear strength, PTS: peel test strength).*

As detailed in Table 7.1, the range of adhesives produced in this thesis range from the weaker hot melt adhesives to mid-range reactive adhesives. This, therefore, shows that these adhesives would be suitable for the current adhesive market. Furthermore, the added functionality of debonding on demand with an external stimulus provides a unique selling point for each of these adhesives in the market.

7.2. Future Work

There are many future avenues of research that could be initiated within the field of debond-on-demand adhesives. Within this study, we reported the use of two methods of initiating degradation, chemical and photo-initiated degradation. Other stimuli that could be used to initiate degradation include thermal stimuli (which was briefly mentioned in the Chapter 6), and mechanical stimuli; both of which have been utilised in stimuli responsive debond-on-demand adhesives.[12–14] Specific areas of future work stemming from each chapter are discussed

in the following sections. Thereafter, other future concepts relating to the work carried out in this thesis are also discussed.

7.2.1. Changing the Structure of the Degradable group.

In Chapter 2, a fluoride responsive degradable unit **7.1** was incorporated into a polyurethane backbone to form a hot-melt adhesive.[2] The material consists of three main parts: (i) the polyol backbone, (ii) the diisocyanate linker and (iii) the degradable group. Varying the structure of (i) and (ii) were further explored in Chapter 3. The chemical structure of the fluoride responsive group **2.5**, however, was not changed after this work was completed. The group relies on the silyl protecting group for degradation with a fluoride source. The silyl protecting group is attached to a bis-hydroxyl functionalised phenol (which was later changed to a tris-hydroxyl functionalised phenol to induce crosslinking in Chapter 4). Alternative alcohol protective groups could be used instead of the silyl group; many of which respond to different chemical stimuli. Therefore, a series of polymeric adhesives could be designed which respond to different chemical stimuli. For example, the methoxy protected degradable unit **2.16** was synthesised as part of the selectivity tests of this study. Methyl ether protecting groups are labile to nucleophiles such as thiols or Lewis acids such as *tetra*-methylsilyl iodide.[15] The group was incorporated into a polyurethane backbone; however, no degradations studies were not carried out on the material. Another protecting group that was experimented on was acetyl protected phenols **7.1** which has previously been synthesised in the laboratory for alternative projects.

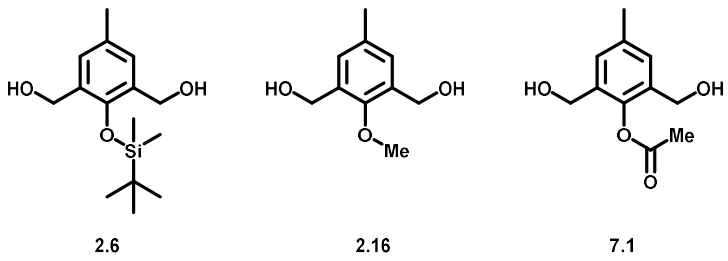

2.6 2.16 7.1

Figure 7.1 *Chemoresponsive degradable units designed as part of this study.*

7.2.2. Alternative polyols and diisocyanate linkers

Chapter 3 investigated altering the chemical structure of the polyol backbone and diisocyanate to improve the thermal and adhesive properties of the fluoride responsive adhesive. Changing the diisocyanate improved the thermal properties but resulted in diminished adhesive properties. However, other diisocyanates exist other than the three tested, and they may show better adhesive results. For example, polymers utilising 2,4-toluenediisocyanate, 1,4-phenylene

diisocyanate and 1,3-phenylene diisocyanate could provide interesting properties. Furthermore, using ureas or isothiocyanates could provide different mechanical properties over urethanes.

The introduction of a polyester backbone afforded improved results for both thermal and adhesive properties in contrast to the hydrogenated polybutadiene. Alternative polyester systems could provide different thermal and mechanical properties for the adhesive. The use of different polyols could also afford materials to better suite the needs of the end user. For example, a polyethylene glycol or polyglycerol based polyols could provide water soluble adhesives for biocompatible substrates or needs.

Copolymer systems could also provide different mechanical and thermal properties by altering the phase separation within the polymeric network. Different ratios of the polyester and polybutadiene polyols were mixed prior to adding the diisocyanate and bifunctional degradable group **2.6**. This resulted in block copolymers with both crystalline and amorphous regions within the network.

7.2.3. Crosslinked Materials

The crosslinked adhesive polymers in Chapters 4 showed an increase in adhesive strengths when compared to the linear polymeric adhesives developed in Chapters 2 and 3. Although reacting the prepolymer and crosslinking group resulted in strong adhesion, a more user-friendly method of adhesion would be to use hot-melt films like those produced in Chapters 2 and 3. The Stepanpol® based crosslinking polymer (CLP) **4.14** showed a melt at *ca.* 48 °C as a result of the crystallites within the polymeric network. The material did not flow when inverted but could be manipulated with a spatula. Therefore, in theory, if a film could be produced, adhesion could be achieved through a hot melt with compression to provide a user-friendly strong adhesive.

7.2.4. Star shaped polymers

The star shaped polymer design was a new approach to crosslinked stimuli responsive adhesives described in Chapter 5. However, during the synthesis, the star polymers underwent transesterification as determined by ^{1}H NMR spectroscopy and GPC analysis. Therefore, initial further work would be to optimise the reaction conditions to afford star shaped polymers without transesterification occurring. For example, the reaction time could be reduced.

The other advantage of star shaped polymers over the polymers in Chapters 2 - 4 lies in the modifications that could lead to a series of polymeric adhesives with different thermal and

mechanical properties. The four different modifications that could be applied to star shaped polymers to optimise the adhesive properties include: (i) altering the arm length of the star[16] (ii) using different esters or changing to amides or lactides;[16,17] (iii) using different diisocyanates to allow better phase separation (e.g. hexamethylene diisocyanate); and (iv) using dynamic covalent bonding residues for crosslinking (Diels-Alder adducts or anthracene moieties).[18–20] Each of these on its own are completely new projects and could provide very promising results. Furthermore, linear materials could also be made using the bifunctional material as the core group and incorporated into the star shaped materials.

7.2.5. UV responsive adhesives

The last project reported showed the design and synthesis of a UV responsive degradable unit (Chapter 6). Model compound tests showed rapid degradation within five minutes. Furthermore, the adhesive showed an 86 % decrease in adhesive strength after five minutes of UV irradiation. However, the adhesive was not thermally stable under the tested conditions, and the polyurethane broke down prior to UV testing. Therefore, the first step to counteract this would be to lower the adhesion temperature and increase clamping pressure. Additionally, the hydrogenated polybutadiene **2.21** could be changed for the polyester **3.2** which would introduce a melting transition to the material. The polyester material **7.2** was synthesised with DSC showing a melting temperature at 49 °C. Furthermore, polymer **7.2** forms self-supporting films at *ca.* 80 μm thick. Degradation studies are still to be carried out.

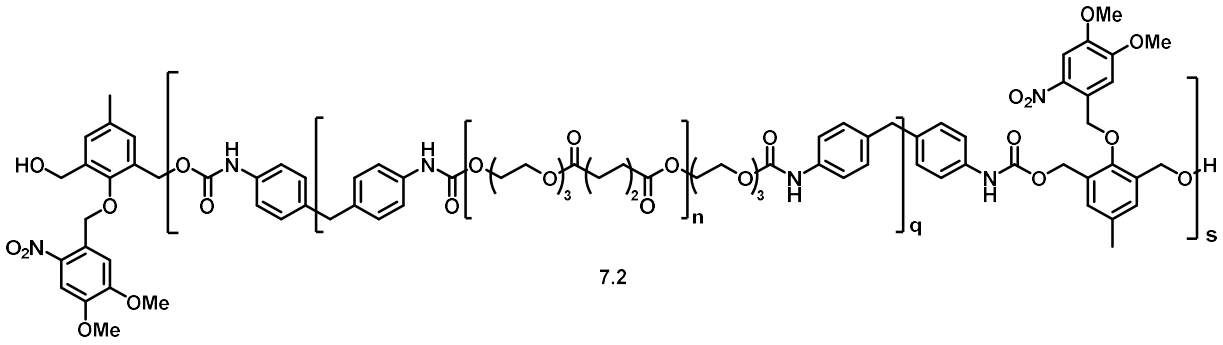

Figure 7.2 *The polyester based UV responsive polymer* ***7.2****.*

Another possible alternative to form UV responsive adhesives would be to form polyester diols or even stars if the core group is changed to a trifunctionalised group.

7.2.6. Fluoride responsive Telechelic and Hyperbranched materials

Although crosslinking materials showed promising results with an increase in adhesive strength over linear systems, self-supporting films could not be produced. One method to counter

solubility issues was to develop hyperbranched materials with the trifunctional degradable group **4.1** and supramolecular hydrogen bonding end groups. Three monofunctional fluoride responsive groups were designed to be used as supramolecular end groups. The proposed reaction scheme is outlined in Scheme 7.1.

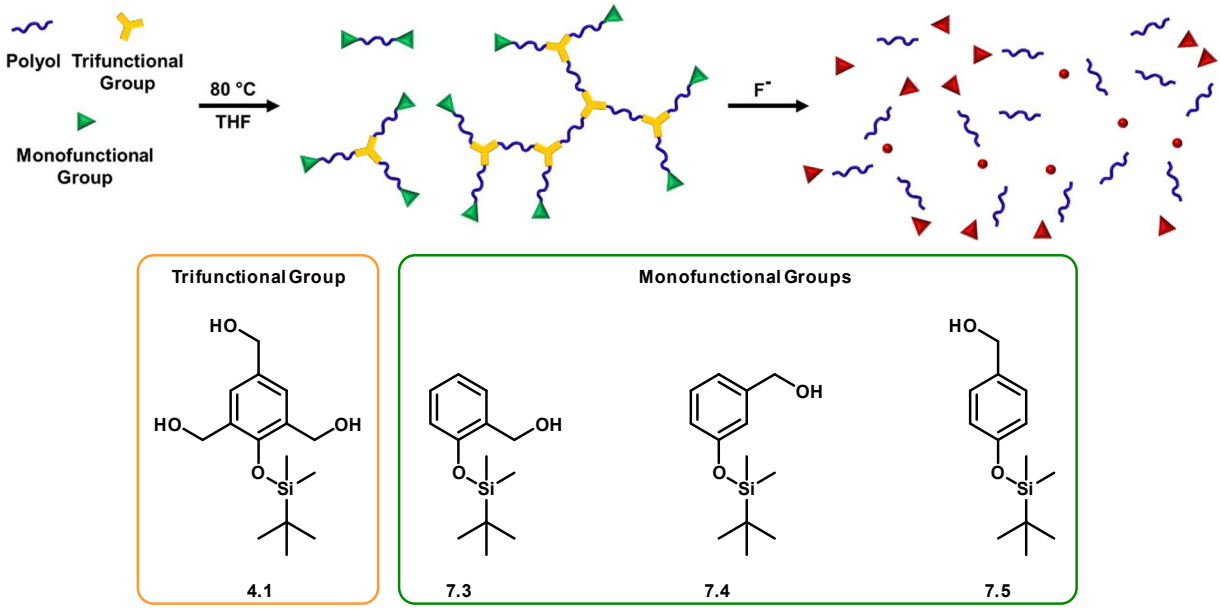

***Scheme** 7.1 Hyperbranched fluoride responsive polymer.*

7.2.7. UV responsive Telechelic materials

Hayes and co-workers have developed a telechelic supramolecular polymer **7.6**, which utilised a nitro-methoxy functionalised dibenzylamine end group.[21] The material showed some interesting adhesive properties. These two functional groups were chosen to alter the electron density around the aromatic diisocyanate linker to enhance π-stacking supramolecular interactions. As *o*-nitrobenzyl (ONB) groups could be used for UV responsive materials, the end group could be modified to include the ONB group as shown with polymer **7.7**. UV degradation of polymer **7.7** would result in cleavage of the ONB and alter the electron density of the end group and hence alter the mechanical property of the polymeric material.

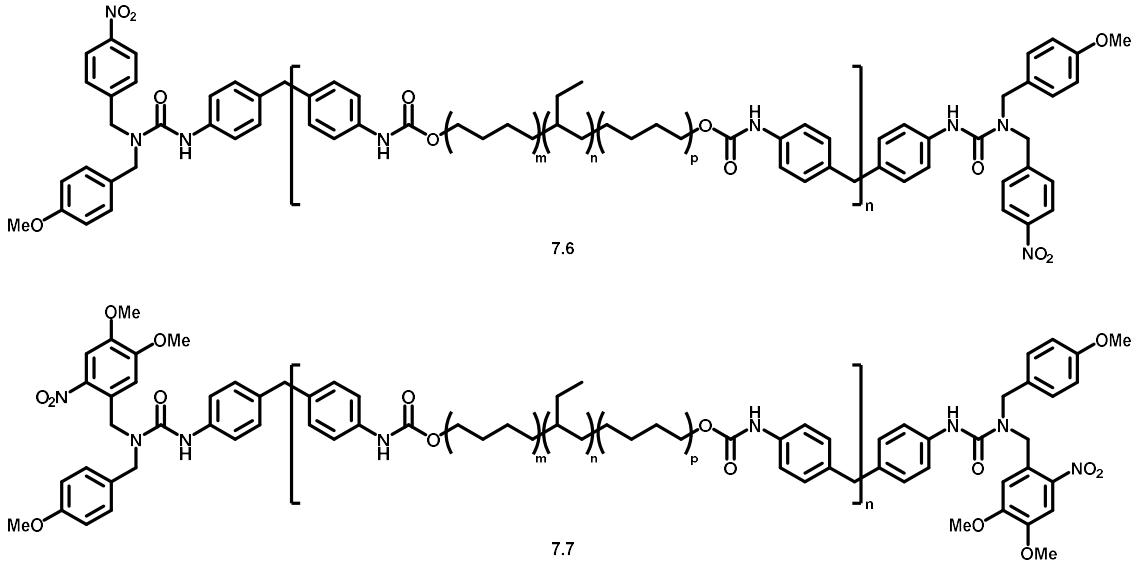

Figure 7.3 *A UV responsive telechelic supramolecular polymer **7.7** inspired by the supramolecular polymer **7.6** developed by Hayes and co-workers.*

7.2.8. Carbon based Composite Materials

An interesting idea was proposed during the course of this project which involved the use an electrical current as a form of inducing heat within a thermally reversible adhesive material.[22] This theory was based on the fact that any material that is able to conduct electricity would generate thermal energy. However, the materials developed in this project are insulators and do not conduct electricity. Therefore, to increase conductivity of the polymers, carbon based particles (graphite, carbon nanotubes and graphene) could be blended into the polymer. This would lead to a series of electronically responsive adhesives.

7.2.9. Fluoride responsive light-melt debond-on-demand adhesives

Cray Valley, who kindly supplied the hydrogenated polybutadiene Krasol HLBH-P 2000 **2.18** and HLBH-P 3000 **3.1** polyols used in Chapters 2 and 3 of this project, also provided the polybutadiene Krasol LBH-P 2000. This was used to synthesise polymer **7.8** (Figure 7.5) but was not used for further testing.

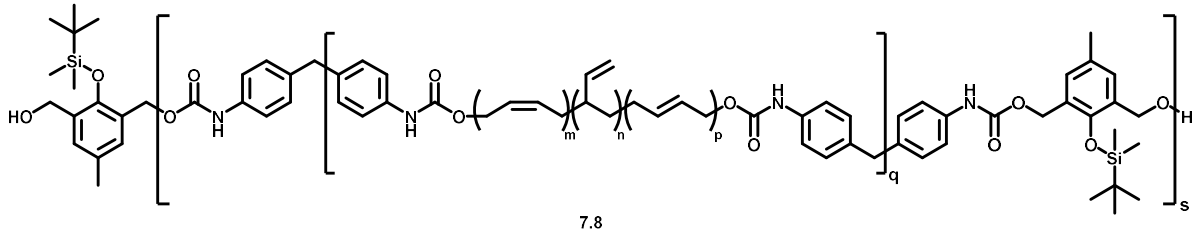

Figure 7.4 *A polybutadiene based fluoride responsive adhesive that could be used for light-melt curable adhesives.*

The material contains terminal alkene groups on the main chain of the polyurethane. Upon irradiation of UV light, the material could crosslink with other chains in the network and thereby increase the strength of the material. The material would still contain the fluoride responsive units which will allow for the degradation of the polymeric network, and hence debond from its substrates when used as an adhesive. Therefore, this material could be used as a UV curable and fluoride degradable adhesive.

7.3. References

1. I. S. Turan and E. U. Akkaya, *Org. Lett.*, 2014, **16**, 1680–1683.
2. T. S. Babra, A. Trivedi, C. N. Warriner, N. Bazin, D. Castiglione, C. Sivour, W. Hayes and B. W. Greenland, *Polym. Chem.*, 2017, **8**, 7207–7216.
3. R. J. Amir, N. Pessah, M. Shamis and D. Shabat, *Angew. Chem. Int. Ed. Engl.*, 2003, **42**, 4494–4499.
4. U. Kemiklioglu, O. Sayman, T. Batar, I. F. Soykok, T. Akderya and E. Akan, *Appl. Adhes. Sci.*, , DOI:10.1186/s40563-015-0042-4.
5. F. C. Amorim, J. M. L. Reis, J. F. B. Souza and H. S. da Costa Mattos, *Appl. Adhes. Sci.*, , DOI:10.1186/s40563-018-0103-6.
6. Henkel, Loctite Super Glue Profesional : Technical Data Sheet, http://www.loctiteproducts.com/tds/SG_BOTTLE_PRO_tds.pdf, (accessed 20 August 2018).
7. Masterbond, Lap Shear Strenght of Adhesives for Titanium, https://www.masterbond.com/articles/lap-shear-strength-adhesives-titanium, (accessed 20 August 2018).
8. D. C. Moreira and L. C. Nunes, *Appl. Adhes. Sci.*, 2014, **2**, 1–8.
9. S. Salimi, T. S. Babra, J. Nightingale, W. Hayes and B. W. Greenland, *Induction Heating as an Effiecient Stimulus to Activate a Rebondable Nanocomposite Adhesive*, 2018.
10. M. R. Ayatollahi, A. Nemati Giv, S. M. J. Razavi and H. Khoramishad, *J. Adhes.*, 2017, **93**, 896–913.
11. Hilltop Products Ltd, Adhesive-Lined Crosslinked Polyolefin Tape, https://www.hilltop-products.co.uk/media/Adhesive Lined Heat Shrink Tape - HDV.pdf, (accessed 21 August 2018).
12. M. W. Urban, *Stimuli-Responsive Materials: From Molecules to Nature Mimicking Materials Design*, Royal Society of Chemistry, Cambridge, UK, 1st edn., 2016.
13. M. Wei, Y. Gao, X. Li and M. J. Serpe, *Polym. Chem.*, 2017, **8**, 127–143.
14. A. J. R. Amaral and G. Pasparakis, *Polym. Chem.*, 2017, 6464–6484.
15. P. G. M. Wuts and T. W. Greene, *Greene's Protective Groups in Organic Synthesis*, John Wiley & Sons, 4th Editio., 2007.
16. D. J. A. Cameron and M. P. Shaver, *Chem. Soc. Rev.*, 2011, **40**, 1761–1776.
17. S. Ho and A. M. Young, *Eur. Polym. J.*, 2006, **42**, 1775–1785.
18. J. H. Aubert, *J. Adhes.*, 2003, **79**, 609–616.
19. H. Akiyama, Y. Okuyama, T. Fukata and H. Kihara, *J. Adhes.*, 2018, 1–15.
20. H. Akiyama, S. Kanazawa, Y. Okuyama, M. Yoshida, H. Kihara, H. Nagai, Y. Norikane and R. Azumi, *ACS Appl. Mater. Interfaces*, 2014, **6**, 7933–7941.
21. A. Feula, A. Pethybridge, I. Giannakopoulos, X. Tang, A. Chippindale, C. R. Siviour, C. P. Buckley, I. W. Hamley and W. Hayes, *Macromolecules*, 2015, **48**, 6132–6141.
22. B. C. K. Tee, C. Wang, R. Allen and Z. Bao, *Nat. Nanotechnol.*, 2012, **7**, 825–832.

Appendix

Chapter 3

A.1. ^{1}H NMR Spectroscopy: Degradation Studies for Chapter 3

Polymer 3.5

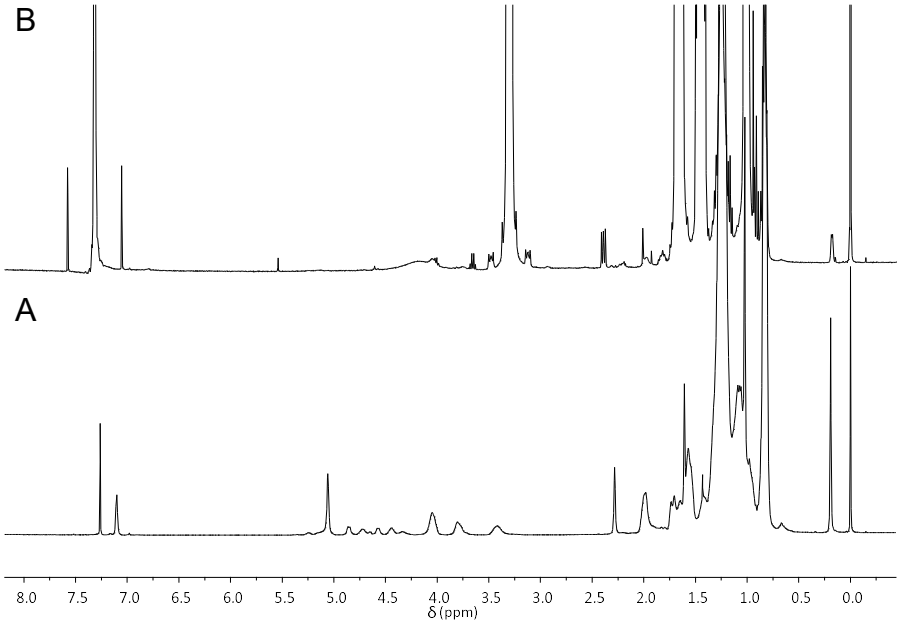

Figure A1 *^{1}H NMR spectra showing (A) before and (B) after degradation of polymer* ***3.5****. ($CDCl_3$, 400 MHz)*

Polymer 3.6

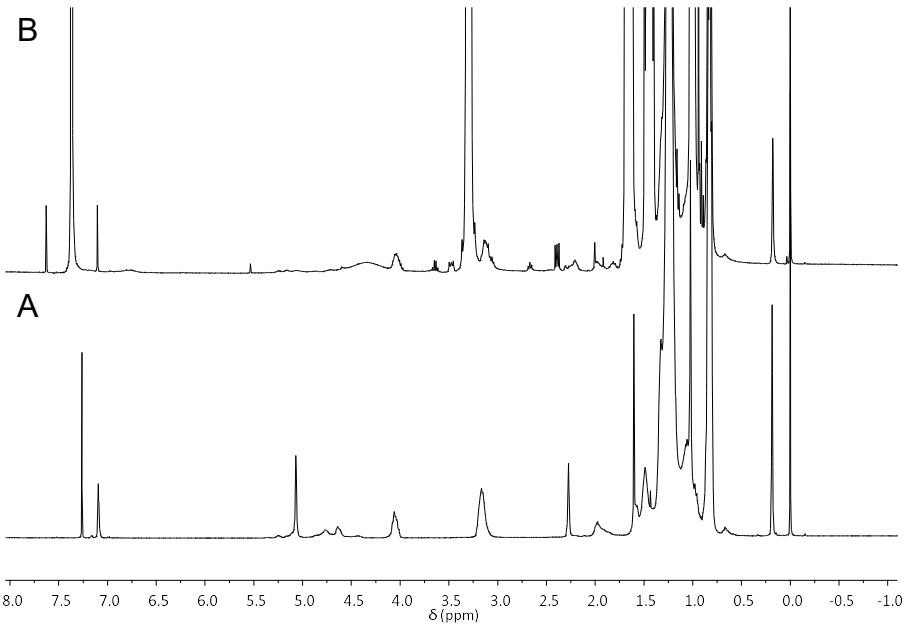

Figure A2 *^{1}H NMR spectra showing (A) before and (B) after degradation of polymer* ***3.6****. ($CDCl_3$, 400 MHz)*

Polymer 3.7

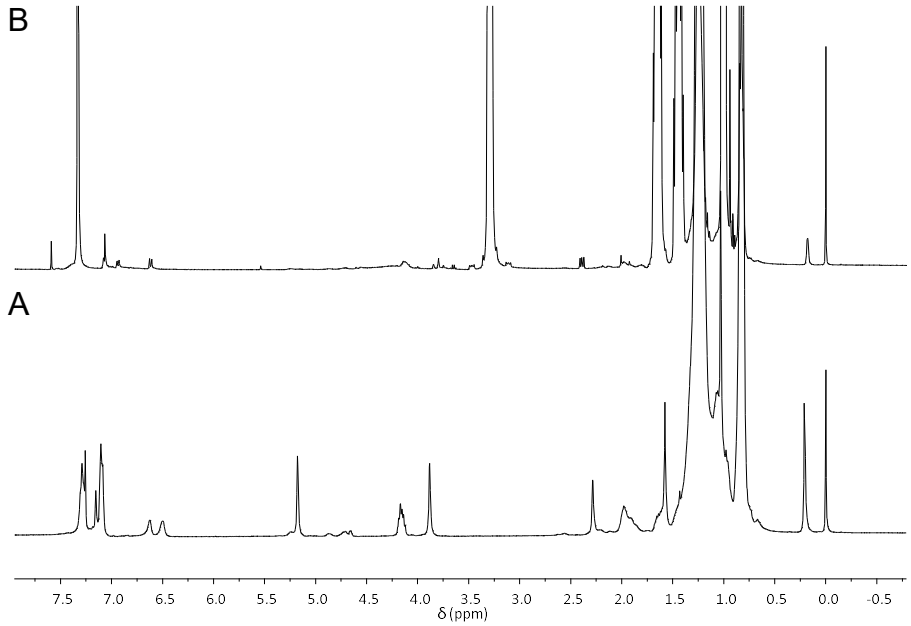

Figure A3 *^{1}H NMR spectra showing (A) before and (B) after degradation of polymer* ***3.7****. (CDCl$_3$, 400 MHz)*

Polymer 3.8

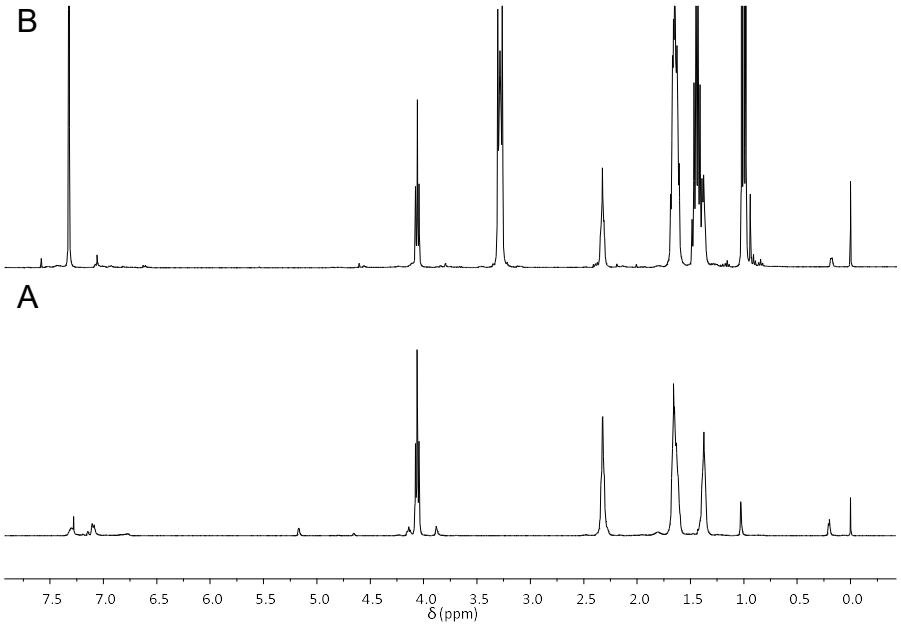

Figure A4 *^{1}H NMR spectra showing (A) before and (B) after degradation of polymer* ***3.8****. (CDCl$_3$, 400 MHz)*

A.2. GPC Peak Maxima Calculations for Chapter 3

Polymer 2.21

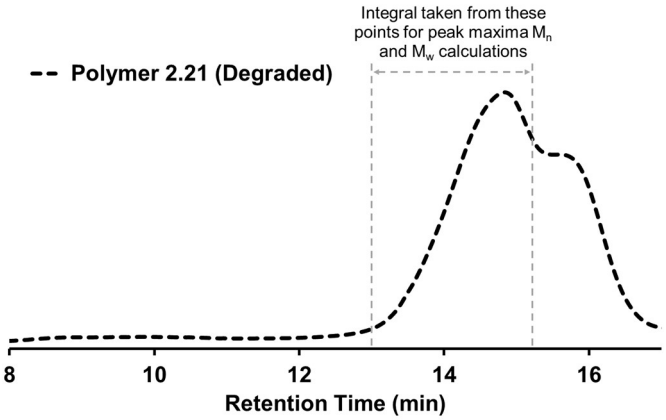

Figure A5 *GPC eluogram of Polymer* ***2.21*** *after degradation, showing the region used to determine the molecular weight of the peak maxima. (THF, PS standard).*

Polymer 3.5

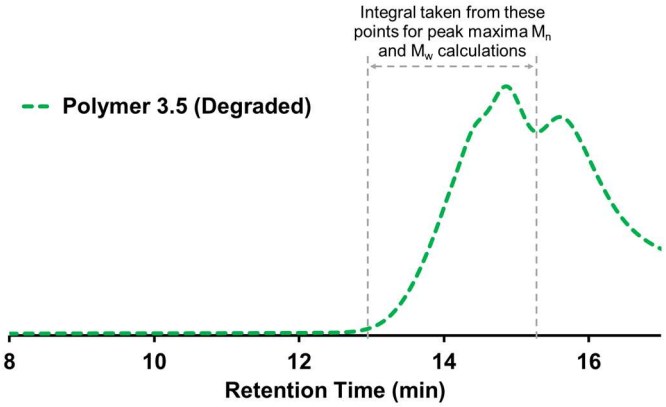

Figure A6 *GPC eluogram of Polymer* ***3.5*** *after degradation, showing the region used to determine the molecular weight of the peak maxima. (THF, PS standard).*

Polymer 3.6

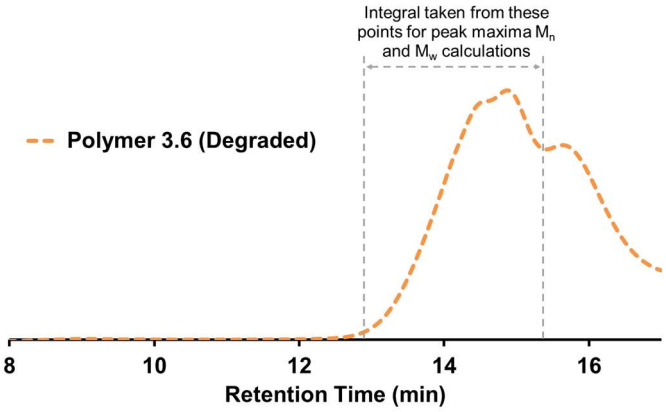

Figure A7 *GPC eluogram of Polymer* ***3.6*** *after degradation, showing the region used to determine the molecular weight of the peak maxima. (THF, PS standard)*

Polymer 3.7

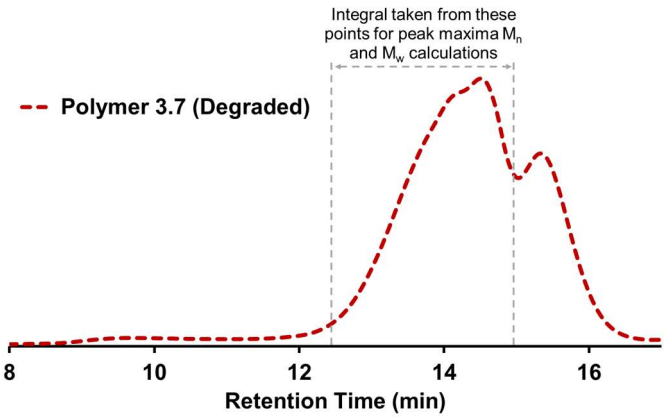

Figure A8 *GPC eluogram of Polymer* ***3.7*** *after degradation, showing the region used to determine the molecular weight of the peak maxima. (THF, PS standard).*

Polymer 3.8

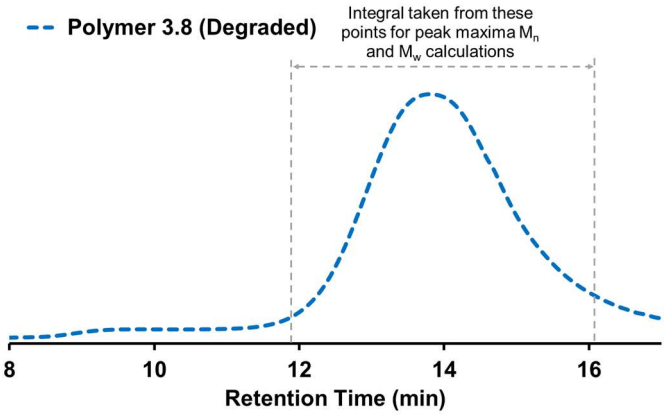

Figure A9 *GPC eluogram of Polymer* ***3.8*** *after degradation, showing the region used to determine the molecular weight of the peak maxima. (THF, PS standard).*

A.3. Rheological Analysis Full Dataset

Temperature ramps used for rheometry analysis:

Polymer **2.21** - 40 °C – 140 °C

Polymer **3.5** - 10 °C – 60 °C

Polymer **3.6** - 10 °C – 50 °C

Polymer **3.7** - 40 °C – 100 °C

Polymer **3.8** - 25 °C – 80 °C

Polymer 2.21

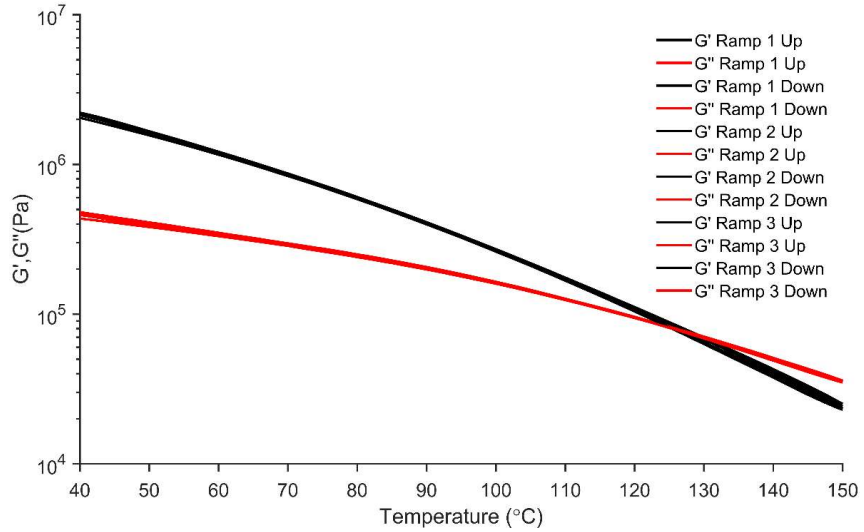

Figure A10 *Rheological Data from three heat-cool cycles for Polymer* ***2.21****.*

Polymer 3.5

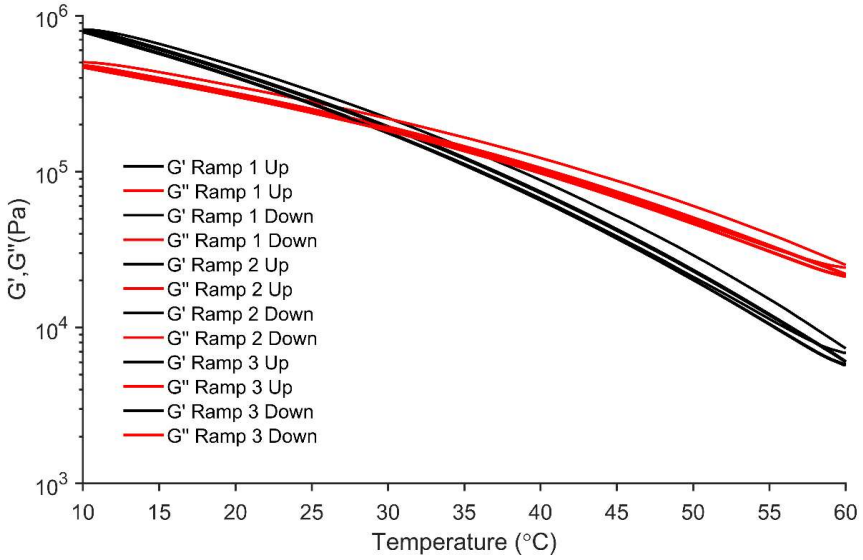

Figure A11 *Rheological Data from three heat-cool cycles for Polymer* ***3.5****.*

Polymer 3.6

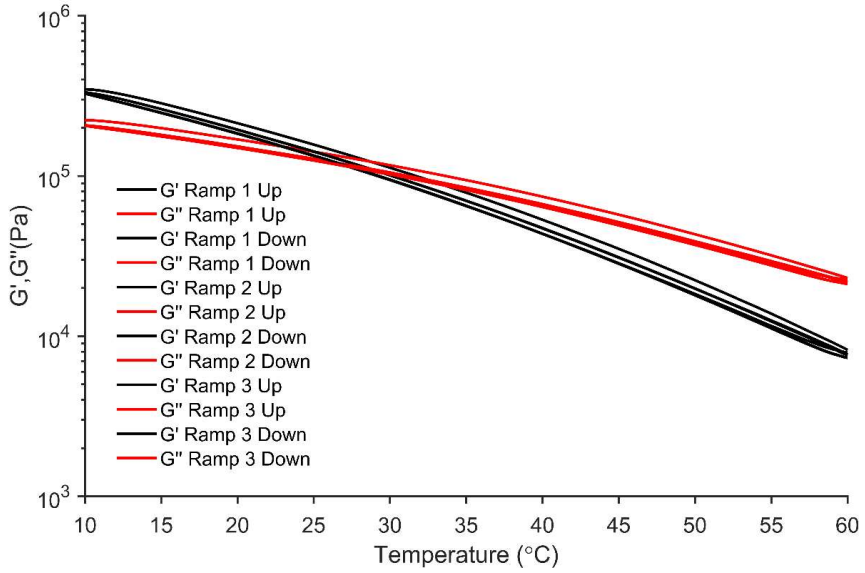

Figure A12 *Rheological Data from three heat-cool cycles for Polymer* ***3.6****.*

Polymer 3.7

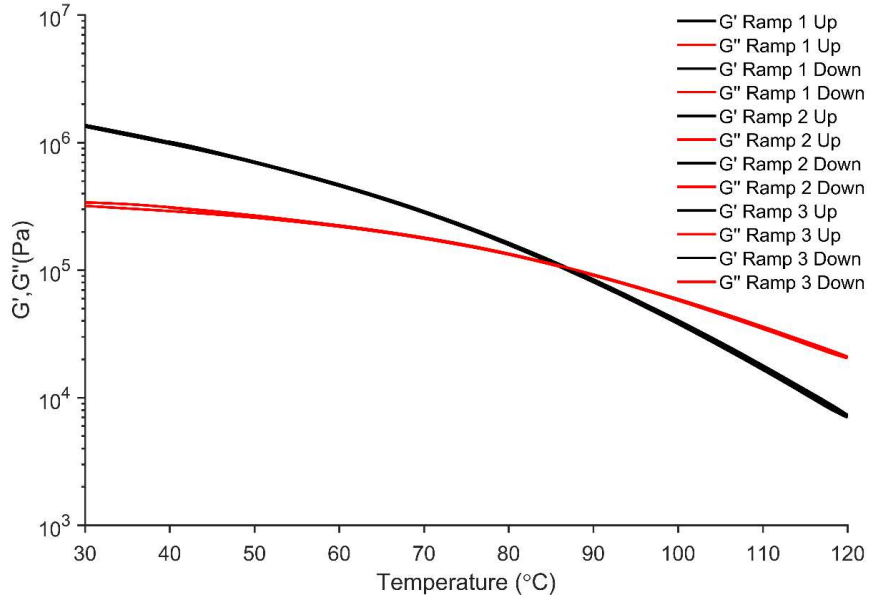

Figure A13 *Rheological Data from three heat-cool cycles for Polymer* ***3.7***

Polymer 3.8

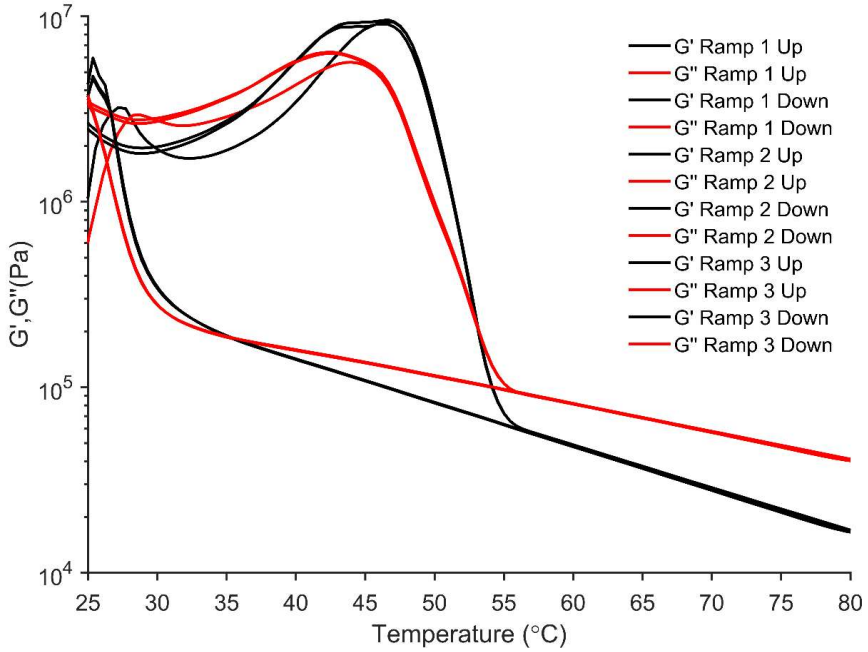

Figure A14 *Rheological Data from three heat-cool cycles for Polymer* ***3.8****.*

A.4. Stress Strain Curves for Chapter 3

Polymer 2.21

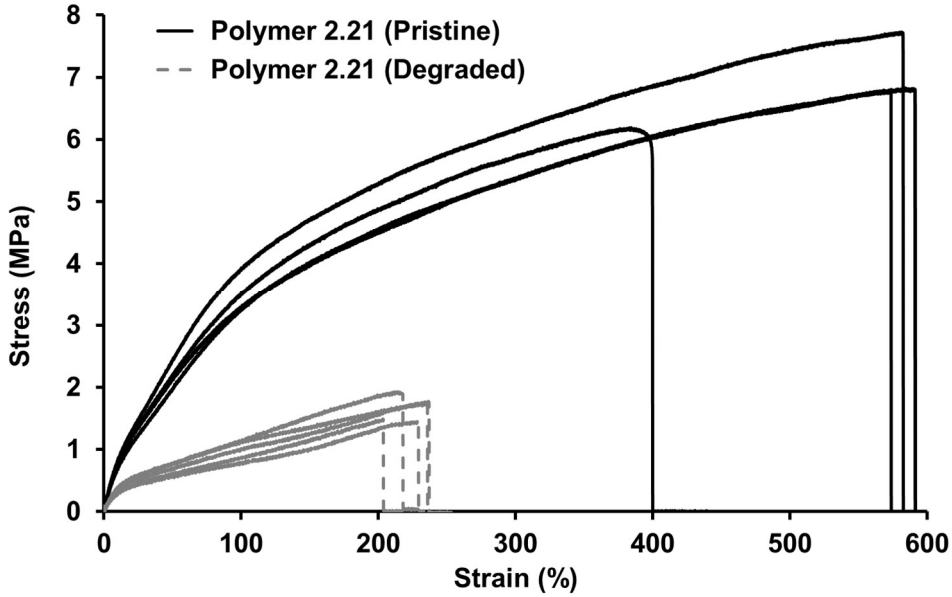

Figure A15 *Five Stress-Strain curves of polymer* ***2.21*** *before (solid) and after (dashed) degradation in 1M TBAF/Acetone for 30 minutes.*

Polymer 3.7

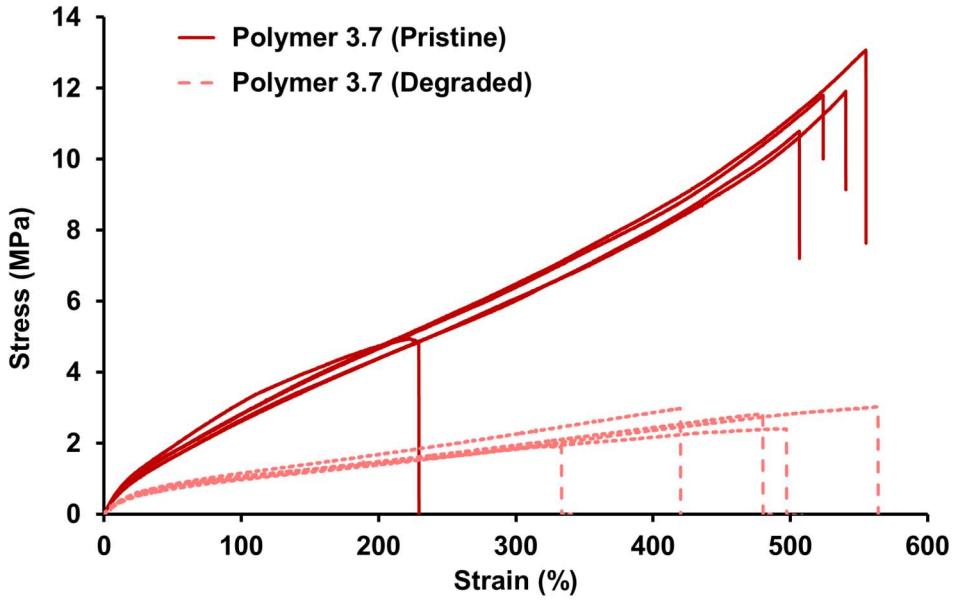

Figure A16 *Five Stress-Strain curves of polymer* ***3.7*** *before (solid) and after (dashed) degradation in 1M TBAF/Acetone for 30 minutes.*

Polymer 3.8

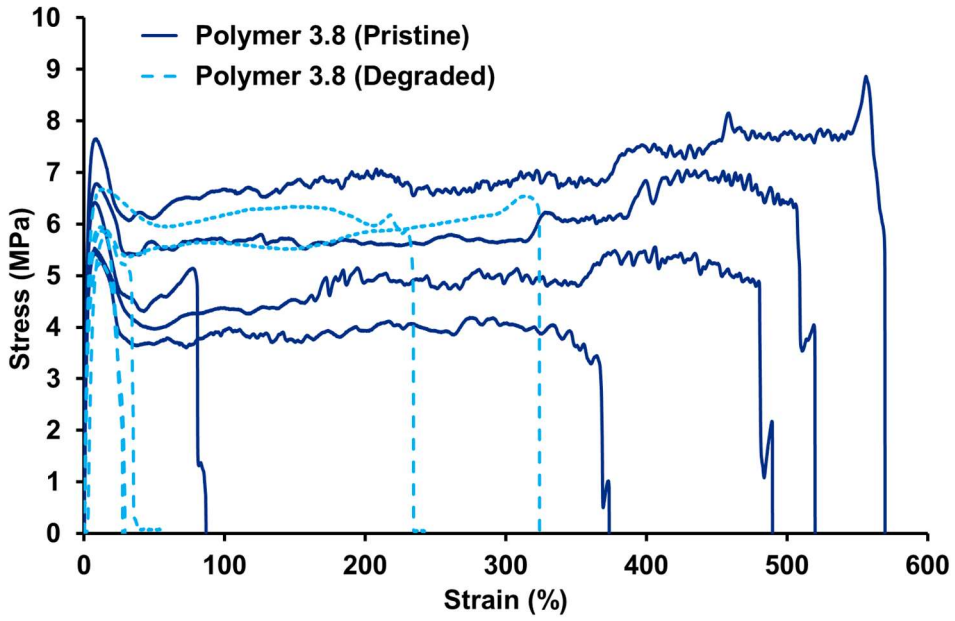

Figure A17 *Five Stress-Strain curves of polymer* ***3.8*** *before (solid) and after (dashed) degradation in 1M TBAF/Acetonitrile for 30 minutes.*

A.5. Full DSC Thermograms

Polymer 2.21

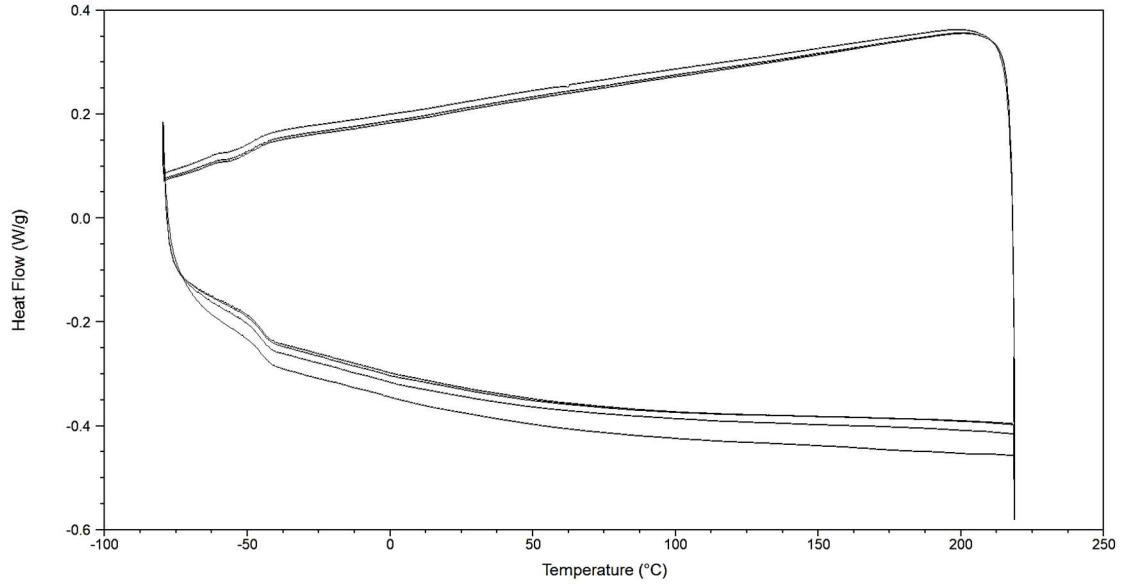

Figure A18 *DSC thermogram showing the three heat-cool cycles of polymer* ***2.21****.*

Polymer 3.5

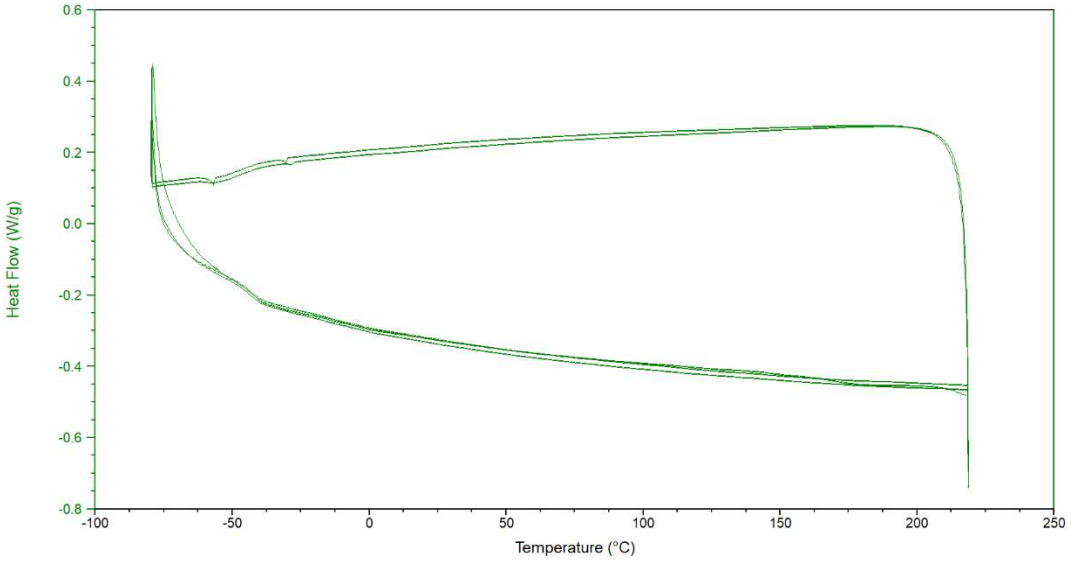

Figure A19 *DSC thermogram showing the three heat-cool cycles of polymer* ***3.5****.*

Polymer 3.6

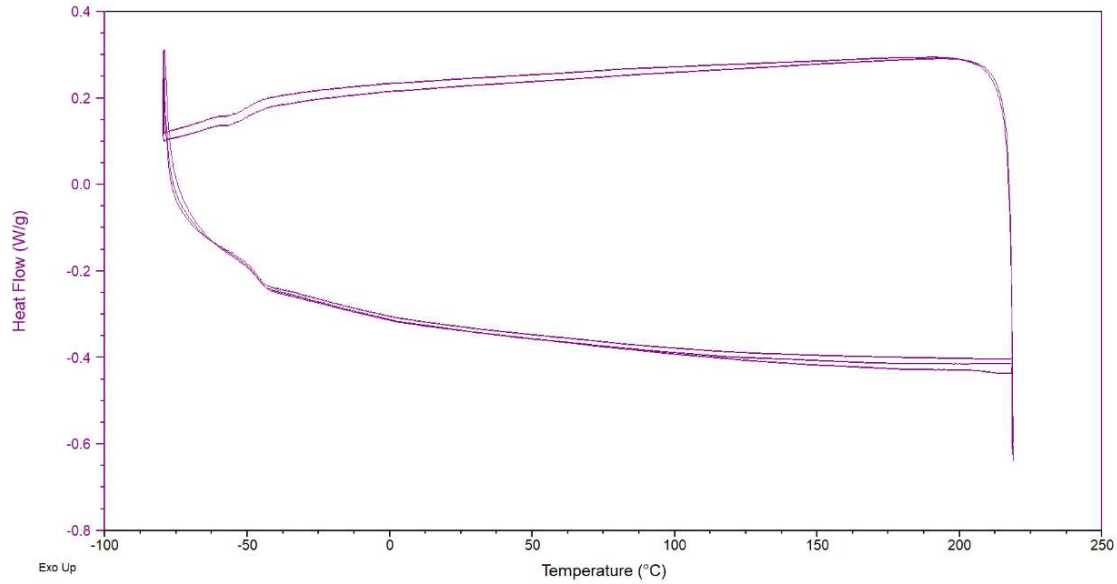

Figure A20 *DSC thermogram showing the three heat-cool cycles of polymer* ***3.6****.*

Polymer 3.7

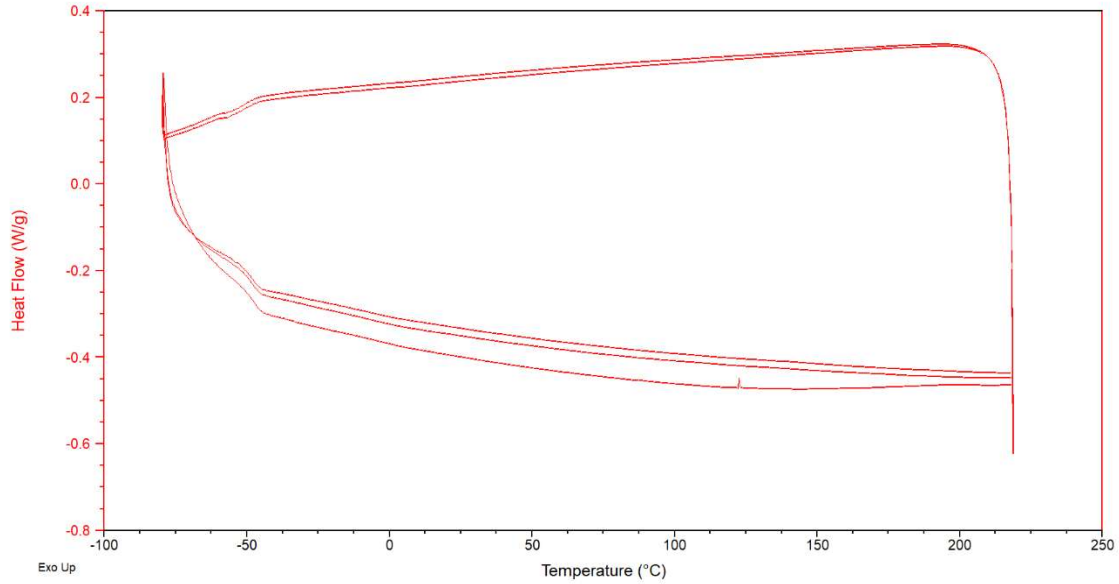

Figure A21 *DSC thermogram showing the three heat-cool cycles of polymer* ***3.7****.*

Polymer 3.8

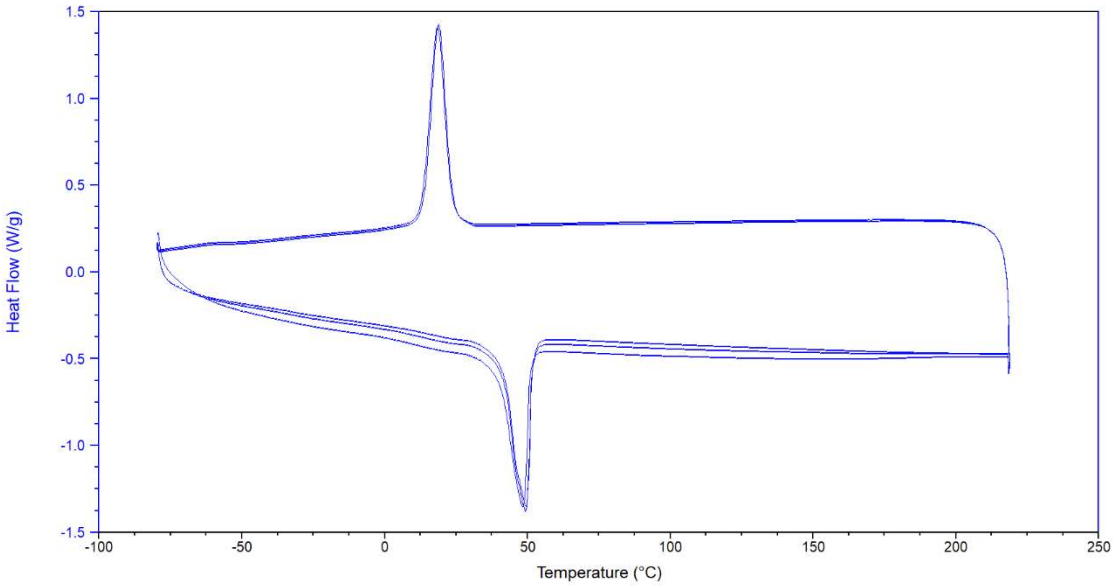

Figure A22 *DSC thermogram showing the three heat-cool cycles of polymer* ***3.8****.*

Chapter 6

A.6. Full ^{1}H NMR spectra for UVDU 6.1

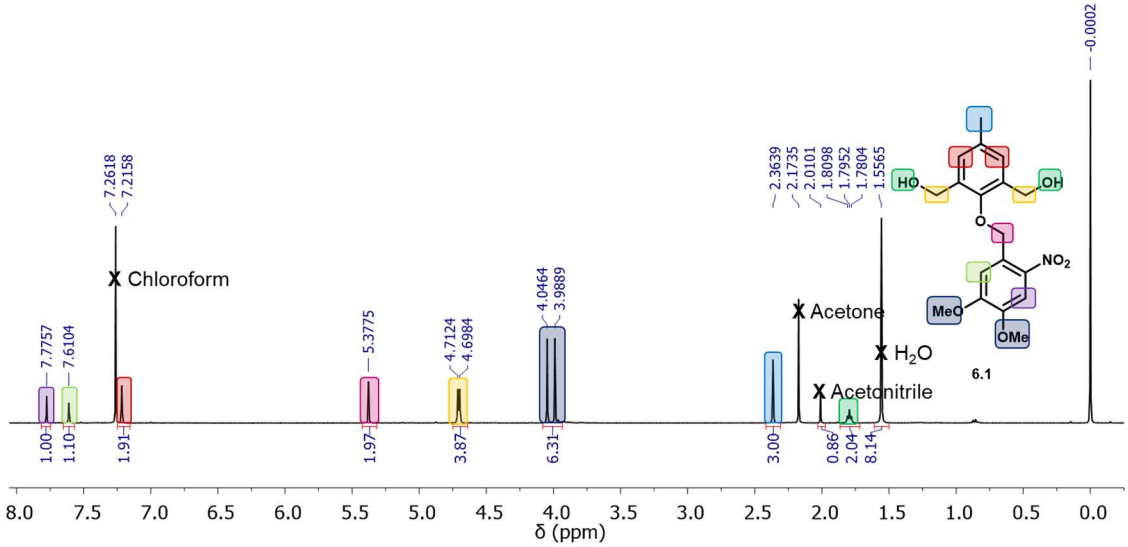

Figure A23 *Full ^{1}H NMR spectra for UVDU **6.1**. (400 MHz, $CDCl_3$)*

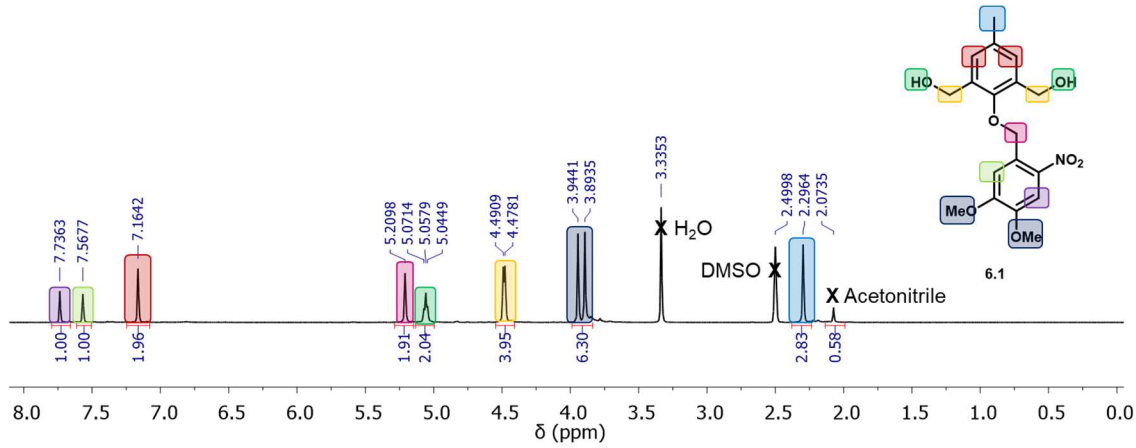

Figure A24 *Full ^{1}H NMR spectra for UVDU **6.1**. (400 MHz, DMSO-d_6)*

A.7. Full ^{1}H NMR spectrum of UV responsive model compound 6.10

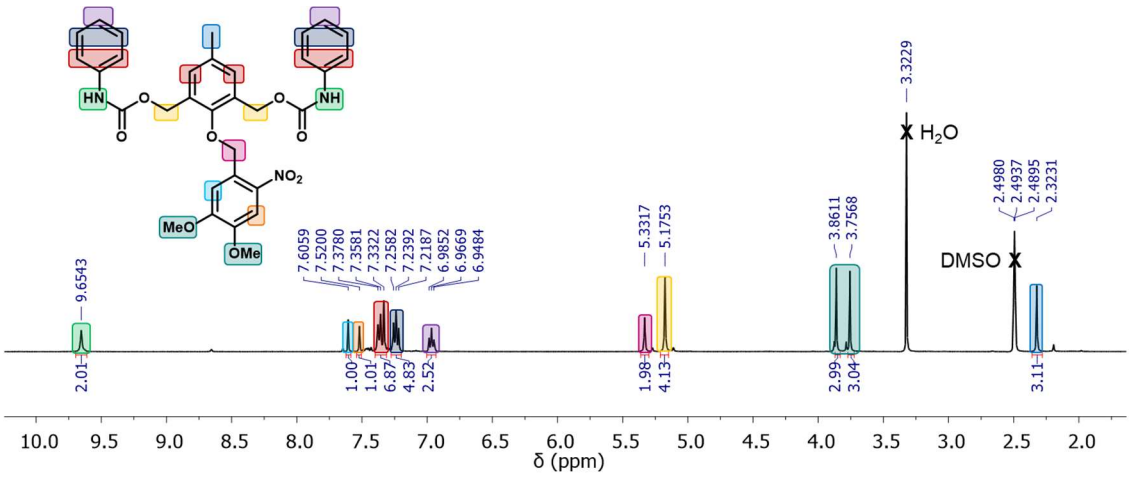

Figure A25 *Full ^{1}H NMR spectra for UV responsive model compound* ***6.10****. (400 MHz, DMSO-d_6)*